STUDY OF BASIC REQUIREMENTS
FOR
A NAVIGATION, GUIDANCE, AND CONTROL SYSTEM
FOR
AN UNMANNED LUNAR LANDING VEHICLE

Final Summary Report

NAS8-11254

15 June 1965

Prepared for

George C. Marshall Space Flight Center

NATIONAL AERONAUTICS AND SPACE ADMINISTRATION

Huntsville, Alabama

by

WESTINGHOUSE DEFENSE AND SPACE CENTER

Aerospace Division

Baltimore, Maryland

AUTHORS:

E. J. Bowers
R. L. Taylor
E. H. Thompson
J. W. Knight, Gr. Leader

ABSTRACT

This document is a Final Summary Report for a study to establish basic sensor requirements for a spaceborne navigation, guidance, and control system capable of performing unmanned lunar landings from a point in the earth-lunar midcourse trajectory to touchdown on the lunar surface. A determination of candidate systems and an exposition of possible tradeoffs is performed and, based on these results, a recommended system is derived. Sensor requirements, in the main, are found to be well within the state-of-the-art, the most severe requirement being that on measurement of vehicle-beacon line-of-sight rate during the main braking phase.

PROBLEM STATUS

This document is a final summary report of the study performed and completes the present contract.

AUTHORIZATION

NASA/MSFC Contract NAS 8-11254
Westinghouse G.O. No. 51256

SUMMARY

This report examines the basic sensor requirements for the onboard navigation, guidance, and control of an unmanned lunar landing vehicle from a time after first midcourse correction (to be determined by the study) to touchdown on the lunar surface. General mission profile and trajectories, earth-based tracking accuracy, thrust control accuracy, and vehicle configuration are assumed through agreement with NASA. A transponder beacon is assumed at the landing site. A 72-hour earth-lunar trajectory terminating in an orbital descent to the lunar surface is examined, and a similar direct descent is examined for comparison. The mission is examined by phases, and candidate navigation and guidance systems are determined. Based on assumed earth-based tracking by Deep Space Instrumentation Facility (DSIF) prior to initiation of onboard navigation and guidance, assumed thrust control accuracy and specified allowable terminal error, onboard navigation, guidance, and sensor requirements are determined.

A primary result of the study is the determination of a system configuration utilizing the minimum onboard complexity consistent with minimum reliance on earth-based tracking. For this system, DSIF tracking is assumed until second midcourse correction, which is made 66 hours after injection into earth-lunar trajectory. The inertial platform and a horizon scanner provide knowledge of the orbital plane and local vertical directions via gyrocompassing mode initiated approximately 1-hour prior to retrothrust into lunar orbit to provide initial condition information for retrothrust. Other than this, no midcourse approach navigation and guidance is required for the assumed DSIF accuracy. Retrothrust is initiated at the nominal time, and retrothrust guidance utilizes initial condition information and linear

acceleration and attitude information obtained from the inertial measurement unit to place the vehicle in a 185-km circular orbit. The inertial platform and horizon scanner are used in the gyrocompassing mode to provide coordinate information for the descent kick which is nominal in magnitude, direction, and time of implementation. The lunar beacon is acquired during the latter portion of the descent coast, and main braking is initiated at nominal measured range. Line-of-sight range, range rate, angle, and angle rate furnish guidance for main braking. Touchdown is completed utilizing inertial measurement unit information. A more detailed summary of the primary results of the study is given in section 3.1, pages 3-1 through 3-8.

TABLE OF CONTENTS

LIST OF ILLUSTRATIONS

LIST OF TABLES

1. INTRODUCTION

The presently estimated capability of earth-based tracking networks together with improvements contemplated for the near future tend to make earth-based vehicle guidance competitive with local or onboard guidance even in the immediate lunar vicinity. Nevertheless, there exists a continuing need, with advancing state of the art, to determine the ultimate capability of onboard vehicle guidance in order to obtain the optimum tradeoff between earth-based and vehicle-based guidance for any given set of mission conditions. The purpose of the study documented in this report, then, is to establish the capability, in terms of basic sensor requirements of an onboard vehicle navigation, guidance, and control system, which will supersede assumed earth-based guidance at the earliest feasible time after first midcourse correction and which will then guide an unmanned lunar landing vehicle to a successful soft landing within 500 meters of a specified location on the lunar surface. The study assumes the desirability of a minimum dependence on earth-based equipment consistent with simplicity and feasibility of onboard navigation and guidance and assumes a light transportable beacon, easily carried by two men, as the only allowable guidance equipment to be assumed on the lunar surface. A summary of study guidelines, in brief, is: (1) that the mission profile will begin after first midcourse correction and end at touchdown near a lunar surface beacon to be located at a specific site in the Lansberg-Copernicas-Kepler Triangle, (2) that the vehicle is required to land within 500 meters of a 500-meter offset from the beacon with a velocity of less than 5 meters per second vertical and 1 meter per second horizontal and with a vehicle attitude of less than 0.18 radian from vertical, (3) that assumed vehicle configuration will be as defined in reference 1, and

(4) that the principal study effort will be devoted to a nominal 72-hour midcourse, parking orbit descent-type of trajectory as defined in references 2, 3, 4, and 5, with a secondary effort devoted to a direct-descent-type of trajectory, primarily for comparison with the parking orbit descent.

The lunar landing vehicle, as defined in reference 1, consists of an L-I and an L-II stage, each stage possessing three similar independent propulsion systems: a primary thrust system, a vernier thrust system, and an attitude control system. The primary thrust system for each stage, consisting of two gimbaled RL-10 type engines, throttleable from 100 to 12.5 percent of maximum rated value, is used for braking and attitude control during lunar parking orbit injection (or preliminary braking for direct descent), main braking, and final touchdown. The vernier thrust system for each stage, consisting of four fixed vernier engines, is used for midcourse corrections and for the descent kick from lunar orbit. The attitude system is used for attitude control when required except during primary thrusting. Total initial mass for the L-I stage is 12,200 kg and for the L-II stage, 30,400 kg. The primary propulsion system for each stage is rated at 133,500 newtons maximum thrust; the vernier system is rated at 17,800 newtons. The L-I stage provides the required thrust and attitude control through the midcourse trajectory and injection into lunar orbit phases after which it is jettisoned; the L-II provides control for the remainder of the mission until touchdown on the lunar surface.

The nominal mission profile for orbital descent, as defined for the study, consists of a Saturn V launch into a 185-km earth parking orbit, injection into a ballistic earth-lunar trajectory resulting in a 185-km altitude at periselenum, and retrothrust into a 185-km lunar orbit. A first midcourse correction is assumed at 10 hours after injection, a second at 50 hours after injection, or shortly thereafter. After retrothrust, the vehicle coasts approximately one-half of a 185-km circular orbit, or until about 70 degrees of lunar central angle from the target area. Based on information contained in reference 5, a 67-meter-per-second descent kick is implemented at this

point to send the vehicle into a 60-degree coasting arc, during the latter portion of which the lunar surface beacon becomes visible to the spacecraft. Shortly after beacon visibility, when the spacecraft has reached an altitude of 100 km, main braking is initiated. Main braking terminates at an altitude of some 300 meters vertically over the target. The assumed trajectory profile, and guidance and control system, are based on information contained in references 4 and 5. The final vertical descent or touchdown terminates the study profile.

The assumed mission profile for direct descent is similar to that outlined above with regard to midcourse approach, main braking, and touchdown phases and is outlined in section 2.2 of this report.

Limiting assumptions upon which the results of this report are based are: 1) the assumed earth-based tracking accuracy (assumed to be performed by DSIF) prior to initiation of onboard navigation and guidance outlined in sections 2.1.1.3.1 and 5.4 of this report; 2) the assumed thrust control accuracy listed in the appropriate sections of this report; 3) the allowable terminal error as specified above.

Utilizing the ground rules and assumptions outlined above, the following sections consider the unmanned lunar mission by successive phases. The appropriate navigation and guidance systems for midcourse approach and subsequent phases are determined, and their capabilities examined. Based on possible tradeoffs resulting in the required terminal accuracy, necessary onboard sensor requirements are determined.

2. DISCUSSION

2.1 PARKING ORBIT MISSION

The principal effort in this study is devoted to an examination of the parking orbit mission, a sketch of which is shown in figure 2-1. Times shown are approximate. Powered phases are shown in heavy lines. The nominal mission is assumed as a ground rule for the study, and was arrived at by agreement with MSFC based on references 2, 3, 4, and 5, subject to modification during the course of the study as required. The first midcourse correction is made at 10 hours. The second correction is made at 50 hours primarily because this allows sufficient time for redetermination of vehicle state by DSIF after correction. The assumption of onboard navigation instead of DSIF tracking after this point allows modification of second correction time, if advantageous. The 60-degree descent coast followed by the approximately 10-degree main braking phase is based on prior studies, reference 6, and enables landing site beacon acquisition by the vehicle prior to initiation of main braking.

The following paragraphs of 2.1 examine successively the various phases of this mission in terms of onboard navigation, guidance, and control and resulting sensor requirements. The general approach taken for each phase is to determine possible candidate navigation and guidance systems and then to determine the relation between initial conditions, end conditions, and sensor requirements based on tentative accuracy requirements for the mission phase. An overall integrated examination of the mission allows the apportionment of firm requirements for each phase based on the allowable terminal error at touchdown, a defined input to the study. Based on these apportioned requirements, a recommended system is selected.

The study begins with an examination of midcourse approach.

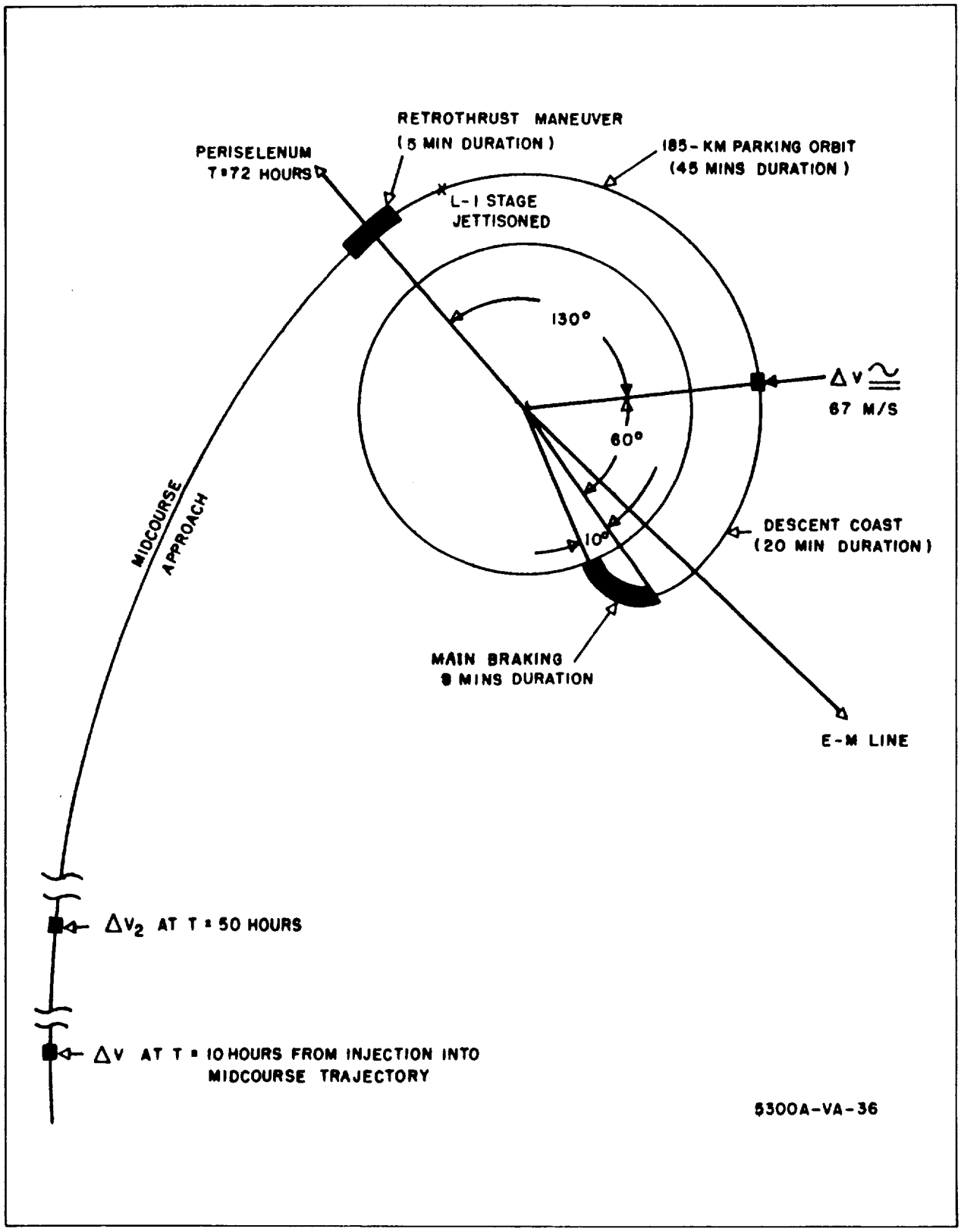

Figure 2-1. Parking Orbit Mission

2.1.1 Midcourse Approach to Lunar Orbit

The midcourse approach to lunar orbit portion of this study examines the unmanned lunar mission from post first midcourse correction to injection into lunar orbit in order to specify onboard navigation, guidance and control, the point in the mission at which it should be initiated, and the required sensor accuracies. The midcourse trajectory is assumed as a nominally 72-hour trajectory with two corrections, the first at 10 hours after departure from earth orbit, the second in the vicinity of 50 hours. DSIF tracking is assumed prior to onboard navigation and guidance.

A glossary of symbols as used in paragraph 2.1.1 is as follows:

$X, Y, Z, \dot{X}, \dot{Y}, \dot{Z}$	Cartesian position and velocity components
$x, y, z, \dot{x}, \dot{y}, \dot{z}$	Deviations from the nominal trajectory
$\tilde{x}, \tilde{y}, \tilde{z}, \dot{\tilde{x}}, \dot{\tilde{y}}, \dot{\tilde{z}}$	Errors in estimating the deviations
$\tilde{a}, \tilde{d}, \tilde{c}, \dot{\tilde{a}}, \dot{\tilde{d}}, \dot{\tilde{c}}$	Altitude, downrange and crossrange estimation errors
$\underline{p}$	6-vector of deviations $x, y, \ldots \dot{z}$
$\underline{\tilde{p}}$	6-vector of estimation errors $\tilde{x}, \tilde{y} \ldots \dot{\tilde{z}}$
$[P]$	Covariance matrix of trajectory deviations
$[\tilde{P}]$	Covariance matrix of estimation errors
R	Range from spececraft to moon center
R_o	Mean lunar radius
V	Spacecraft velocity
v	rms velocity deviation at periselenum
$\tilde{v}$	rms velocity estimation error at periselenum
$\lvert\Delta v_2\rvert$	rms correction velocity magnitude
θ	Central angle
β	Flightpath angle
$[\Phi]$	Transition matrix
μ	Lunar gravitational constant

2.1.1.1 Trajectory Model and Geometry

The two trajectory models are utilized in this analysis. The first is a 72.88-hour flight from a 185-km earth parking orbit to a 185-km periselenum at a point 175 degrees east longitude from the earth-moon line and nearly in the plane of the moon's equator. This trajectory was generated by integrating the equations of motion including gravitational forces due the earth, sun, moon, and earth oblateness. The pertinent characteristics of this trajectory are listed in table 5-1, section 5.7.

An approximate trajectory was also generated using hyperbolic equations to achieve the same nominal periselenum conditions for use in analyzing midcourse navigation after the second connection. Characteristics of this trajectory are also listed in table 5-1 of section 5.7. A plot of the hyperbolic trajectory for the last 7 hours before periselenum is shown in figure 2-2.

2.1.1.2 Candidate Navigation, Guidance, and Control Systems

Control for this phase consists only in the implementation of second midcourse correction and is considered impulsive with assumed control accuracies of 1/4 degree in direction and 0.1 m/sec in magnitude (rms) as specified by the ground rules of this study.

Guidance for the second midcourse correction is assumed to be based on fixed time of arrival at periselenum which entails no complications and is not a subject of this study. The necessity for guidance for initiation of retrothrust is examined in section 2.1.6, and it is shown that initiation based on nominal time from second midcourse correction is sufficient.

Thus, primary emphasis in this study portion is on the navigation function to provide initial condition estimation for retrothrust and subsequent phases. Candidate navigation systems analyzed in this study are summarized as follows.

2.1.1.2.1 No Navigation - This method would require no sensor information during the approach phase. In other words, the estimate of the vehicle's state, $\underline{p}_t$, at some time t would be given by:

$$\underline{p}_t = \lfloor \Phi \rfloor_t \, \underline{p}_o \qquad (2\text{-}1)$$

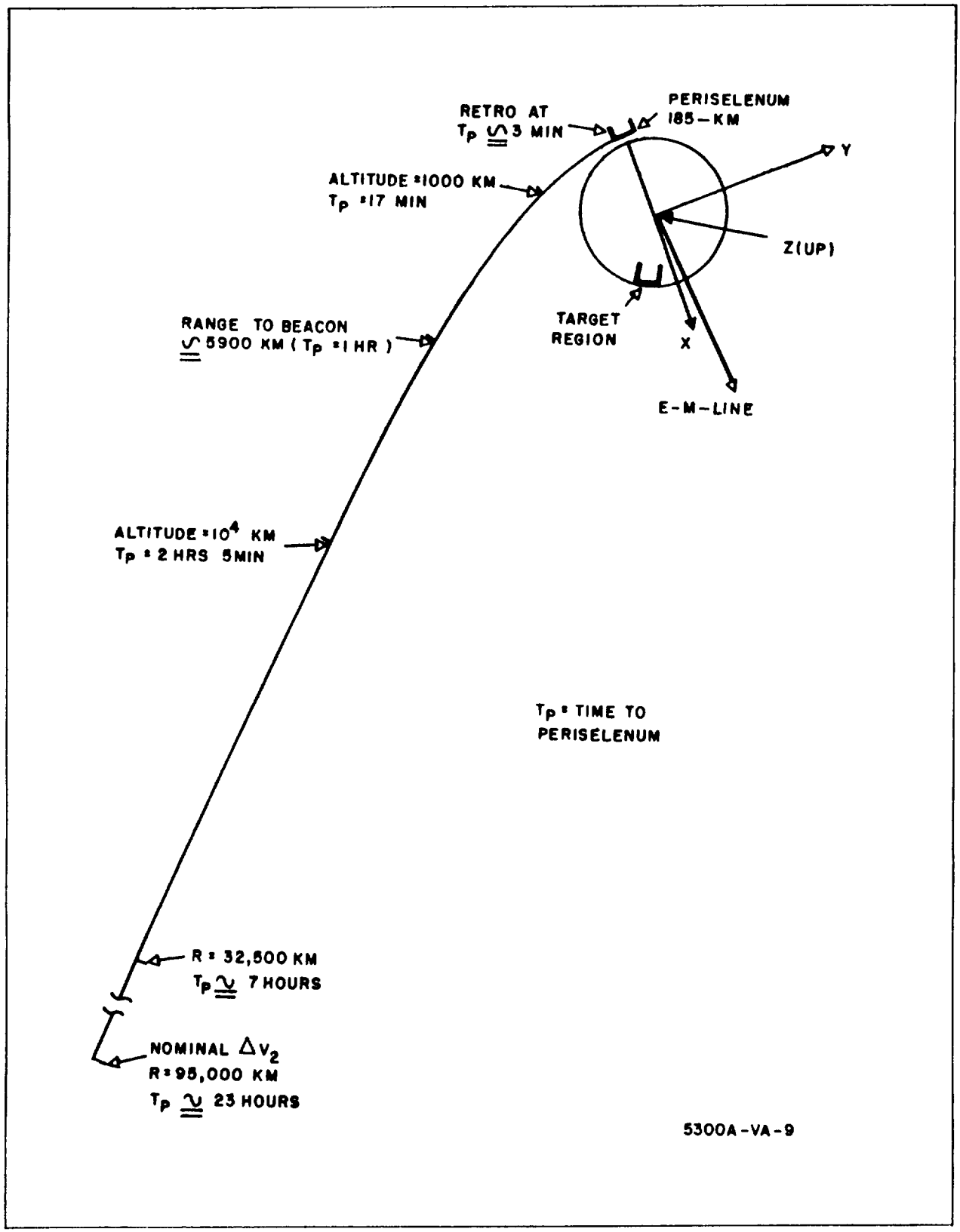

Figure 2-2. Midcourse Orbital Approach

where $\underline{p}_o$ is the state estimate obtained from the DSIF at the termination of earth tracking, and $[\Phi]_t$ is the transition matrix relating trajectory deviations at t_o to deviations at t. This analysis was performed initially to provide a basis for comparison for the onboard navigation systems considered. Both nominal and degraded initial conditions resulting from DSIF control are examined, and the effect of postponing the second midcourse correction, nominally at 50 hours, to 66 hours was examined. Postponement is feasible at negligible fuel penalty, and DSIF tracking time, normally the determining consideration for time of second correction, is, of course, not a factor here. DSIF tracking is, in general, assumed until implementation of second midcourse correction on the basis of analyses showing the impracticality of onboard navigation for an unmanned vehicle at the distances encountered in the 50- to 66-hour portion of the trajectory; DSIF tracking is assumed to terminate at the initiation of the second correction.

The advantages of this system are obvious and the computations required (equation 2-1) are simple. The primary disadvantage is that system accuracy is totally dependent on the initial estimate obtained from DSIF.

2.1.1.2.2 Altimeter Measurements - A radar altimeter may be used for midcourse navigation by taking range measurements to the lunar surface during the approach, and updating the state estimate with new measurements. Thus:

$$\underline{p}\,(\text{updated}) = \underline{p} + K\left[R - R_p\right] \qquad (2\text{-}2)$$

shows how the estimated state deviations, $\underline{p}$, are updated by adding $K\left[R - R_p\right]$, which is a weighting vector times the difference between the measured range R and the predicted range R_p.

The primary advantages of using an altimeter as compared to other onboard navigation methods are that accurate pointing is not necessarily required, that timing is not difficult, and that an altimeter is especially adaptable to automatic, unmanned operation. Disadvantages of an altimeter

are that the range is limited by power considerations and a large antenna may be required. In addition, measurements are available only in the radial direction; thus, deviations out of the nominal trajectory plane go undetected.

2.1.1.2.3 Horizon Scanner Measurements - Angular information about the approach trajectory may be obtained by measuring the angle between lunar local vertical and some inertial direction. This can be accomplished by measuring the angle between the horizon scanner axis and a stellar-referenced stable platform. The difference between the predicted and measured angles can then be incorporated into the new trajectory estimate as in equation 2-2. An advantage of using this type of measurement is that the maximum range of operation is not limited as in the case for an altimeter. In addition, measurements may be made with respect to any inertial axis, so that information about out-of-plane deviations is available. Possible disadvantages of this system are that an accurate inertial reference must be maintained, and that the accuracy of local vertical determination around the moon by horizon scanner must be demonstrated, especially when the local horizon is near the lunar terminator.

2.1.1.2.4 Beacon Navigation - A basic assumption of the LLV study is that a transponder radar is available at the target site for use in the landing operation. However, it was also considered desirable to investigate the use of this beacon as a method of midcourse navigation. Range or angle measurements to the beacon are equivalent to the altimeter or horizon scanner measurements from a data-processing standpoint except that the beacon is now the reference point rather than the center of the moon.

An advantage of this type of measurement is that some measurement difficulties due to lunar surface irregularities are avoided. In addition, the one-way radar mode extends the feasible range for a given power and antenna size. A serious drawback to the use of the beacon for midcourse navigation is that the beacon will not always be visible during the latter part of the approach phase. Thus, tracking may have to be terminated prematurely.

2.1.1.2.5 Other Navigation Systems - Two other navigation systems which were considered briefly at the outset of this study were not considered further after preliminary analyses showed the difficulty in using these concepts. These methods are (1) ranging by horizon scanner measurements and (2) doppler measurements to the lunar surface. More details on these analyses are given in sections 2.1.1.4 and 5.1. Briefly, it was found that horizon-scanner ranging is inaccurate at the large ranges encountered during the mid-course phase, while doppler measurements require precise pointing to the lunar local vertical. Thus, these methods of navigation were not treated in greater detail.

2.1.1.3 Methods of Analysis and Error Sources

To obtain maximum flexibility and generality of results, ensemble statistical methods were used where possible in the error analysis and much use was made of computer programs developed during the NASw-460 studies (reference 7, Volume V, Section B6) for analysis of random errors. Bias errors were also considered where applicable and their effects determined by hand calculation or simulation as required. Inputs for the random error analysis of the various navigation sensor schemes considered are:

- Number and timing of measurements
- Measurement accuracy
- Timing and accuracy of velocity corrections
- Initial estimation error
- Initial actual deviation error

The program outputs for the inputs listed above are the covariance matrices of trajectory deviations, $\lfloor P \rfloor$, and of estimation errors, $\lfloor \tilde{P} \rfloor$, at various time points along the trajectory, including nominal time of periselenum. Equations are given in reference 7, Volume V, Section B6.

Bias errors, such as altimeter bias error, were examined for the sensors considered. Another type of bias error is that caused by uncertainty in the astrodynamic constants of the earth and moon. However, tracking of recent

Ranger flights has resulted in considerable reduction in these uncertainties such that is felt that by the post-Apollo time period, they will be relatively insignificant. Thus, astrodynamic uncertainties were not considered in this study except for uncertainty in position of the moon.

In addition to $\lfloor P_o \rfloor$, the covariance matrix of trajectory deviations, and $\lfloor \tilde{P}_o \rfloor$, the covariance matrix of estimation errors at periselenum, various operations were performed on these results to determine the altitude deviations from the nominal trajectory (a) at the start of main braking caused by estimation errors and also the cross-track miss ($\delta\epsilon$) which results if no out-of-plane guidance is performed after the second velocity corrections. The equations relating to these quantities to $\lfloor P_o \rfloor$ and $\lfloor \tilde{P}_o \rfloor$ are shown in paragraph 5.3.

2.1.1.3.1 DSIF Errors - The practicable point for termination of DSIF tracking and initiation of onboard navigation is taken as the time of second midcourse correction, primarily because errors in midcourse correction show up directly as a significant fuel penalty for the mission, and onboard navigation prior to this point entails considerable system complexity at no increase of accuracy. For any reasonable division of labor between DSIF and onboard navigation and guidance, initial condition trajectory deviations $\lfloor P_o \rfloor$ and estimation errors $\lfloor \tilde{P}_o \rfloor$ for the onboard system as determined at DSIF termination must have a significant effect on resulting onboard navigation performance for any feasible set of onboard sensor accuracies. Study groundrules specified DSIF capability on the order of that given in reference 3. However, the data actually required for input to this study is not available as such in the reference.

Since it was beyond the scope of the contract to analyze DSIF performance, approximate methods had to be used to generate $\lfloor P_o \rfloor$ and $\lfloor \tilde{P}_o \rfloor$. In paragraph 5.4, the analysis used to generate these matrices are detailed. A check analysis has shown these to be consistent in order of magnitude

with the standard assumptions of reference 3, figure 4-32. The results of this comparison are shown in paragraph 5.4.

Two initial covariance matrices are generated in paragraph 5.4, one being the best estimate of projected DSIF capability that could be obtained based on reference 8 and the other being larger by approximately one order of magnitude. These matrices are:

$$\text{Standard } \left[\tilde{P}_{T_o}\right] = \begin{bmatrix} \overbrace{\begin{matrix} 6.447 & .618 & 0 \\ .618 & 1.90 & 0 \\ 0 & 0 & 1.667 \end{matrix}}^{km^2} & 0_{33} \\ 0_{33} & \underbrace{\begin{matrix} 2.447\,(10^{-10}) & 0.618\,(10^{-10}) & 0 \\ 0.618\,(10^{-10}) & 0.9\,(10^{-10}) & 0 \\ 0 & 0 & .667\,(10^{-10}) \end{matrix}}_{(km/sec)^2} \end{bmatrix}$$

$$\text{Large } \left[\tilde{P}_{T_o}\right] = \begin{bmatrix} \overbrace{\begin{matrix} 311 & & \\ & 311 & \\ & & 311 \end{matrix}}^{km^2} & - 0 - \\ - 0 - & \underbrace{\begin{matrix} 1.083\,(10^{-8}) & & \\ & 1.083\,(10^{-8}) & \\ & & 1.083\,(10^{-8}) \end{matrix}}_{(km/sec)^2} \end{bmatrix}$$

where the coordinate system and the initial conditions are as described in table 5-1, section 5.7, for the hyperbolic trajectory.

Both matrices include an uncertainty in position of the moon (in earth coordinates) of 2 km in the radial direction and 1 km cross-track. The rms position and velocity uncertainties are 3.16 and 0.02 m/sec for the standard

errors, and 30.5 km and 0.18 m/sec for the larger errors. Note that the uncertainties perpendicular to the trajectory plane (Z and $\dot{Z}$) are assumed uncorrelated with the inplane errors.

The deviations affect the analysis primarily by determining the magnitude of the required correction. It was assumed that $\lfloor P_o \rfloor = (10^3) \lfloor \tilde{P}_o \rfloor$. This gave a correction velocity of $\Delta V_2 = 1.34$ m/sec for the standard errors and $\Delta V_2 = 12.9$ m/sec for the large errors.

The error matrices described above were used for both the standard case, on which the second correction was made at $t_o = 50$ hours from translunar injection, as well as for the cases in which $t_o = 66$ hours was used.

2.1.1.3.2 Horizon Scanner Errors - A horizon scanner is postulated as one of the methods of measuring angles to the moon. A brief analysis of horizon scanner errors is given in section 5.5, in which it is assumed that errors in the determination of local vertical are caused by both lunar terrain irregularities and instrument errors. Using the assumption of a 1.355-km rms horizon fluctuation due to terrain, the rms error in determination of local vertical, σ_θ, is found to be:

$$\sigma_\theta = \frac{1}{\sqrt{2R}} \left(\sigma_h\right) = \frac{0.986}{R} \text{ rads} \qquad (2\text{-}3)$$

where σ_h is the rms altitude error and R is the radius to the center of the moon. Figure 2-3 shows a plot of σ_θ as a function of time on the hyperbolic approach trajectory assuming no instrument errors. It can be seen that horizon irregularities cause appreciable errors in defining the local vertical only in the last hour or so of the midcourse approach. If the instrument errors are on the order of 2 milliradians, the horizon uncertainties have an insignificant effect throughout.

2.1.1.3.3 Altimeter Errors - A brief analysis of the errors expected in using an altimeter is given in paragraph 5.6. Since the object of using an altimeter is to estimate the range from the spacecraft to the moon's center

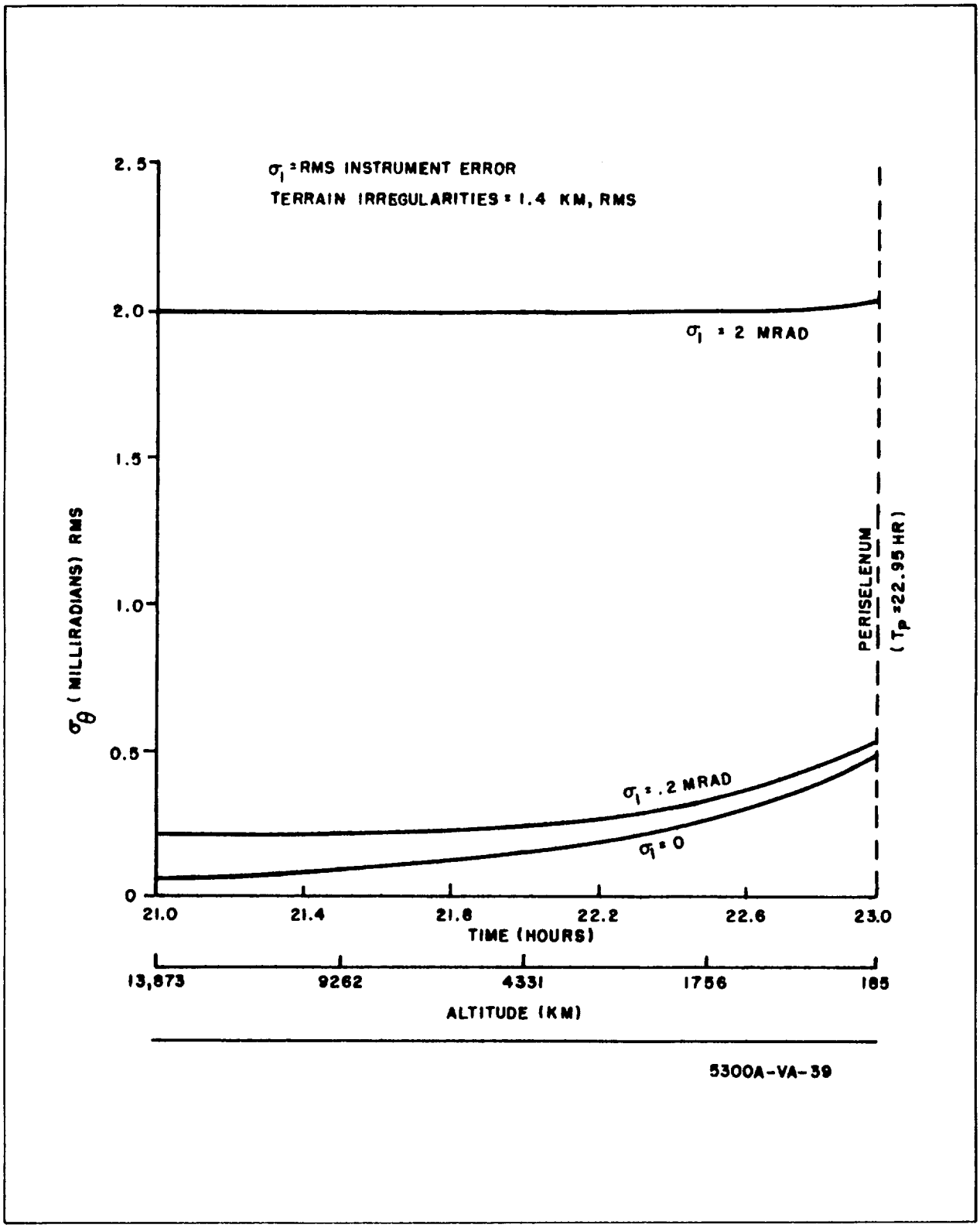

Figure 2-3. Errors in Determination of Local Vertical Angle Due to Instrument Errors and Horizon Irregularities

of gravity, any deviation of the moon's surface from a perfect sphere of known radius will cause an error in the range estimate. Thus, in addition to the (radar) altimeter error, there are errors due to uncertainty in the mean lunar radius, out-of-roundness of the moon, and local terrain (mountains, craters, etc). The rms values for these errors used in this study are as follows:

a. Radar Noise	0.3 km	random
b. Lunar Terrain	1.355 km	
c. Lunar Oblateness	1.08 km	bias
d. Lunar Radius	1.0 km	

Considering all these errors as independent, the overall rms error on each measurement is 2.04 km. This was used as a nominal value for altimeter errors in this study, independently of measurement range.

2.1.1.4 Results

Most of the numerical results in this study were generated using the digital computer program described in paragraph 2.1.1.3 (and reference 7). The main program outputs which will be utilized in discussing the midcourse results are as follows:

a. rms estimation errors in altitude, downrange and crosstrack position and velocity at nominal time of periselenum

b. rms velocity deviation at periselenum

c. rms errors in cross-track deviations (at the target)

d. magnitude of second velocity correction

e. rms velocity estimation error at periselenum

2.1.1.4.1 No-Navigation Runs - Several computer runs were made using both the standard and large initial errors described in paragraph 2.1.1.3. These runs were made to determine the feasibility of using no navigation measurements at all during the midcourse approach. Results of these runs are shown in table 2-1.

TABLE 2-1

RESULTS OF NO-NAVIGATION RUNS

Run No.	Description	$\tilde{a}$ (km)	$\tilde{d}$ (km)	$\tilde{c}$ (km)
*126	Standard errors	4.89	10.5	1.17
125	Large errors	16.0	56.3	6.62
*108	Standard errors, t_o = 66 hr	2.37	4.56	0.59
*146	Large errors, t_o = 66 hr	15.1	47.0	6.32
104	Standard errors, σ_ϵ = 0.01 m/sec	2.05	4.43	0.50
103	Large errors, σ_ϵ = 0.01 m/sec	15.6	55.7	6.46

* Complete covariance matrices of periselenum results for these runs are listed in paragraph 5.2.

The quantities shown in table 2-1 for system comparison are the position estimation errors in the altitude, downrange, and crossrange directions at nominal time of periselenum. Other quantities could be included, but it was found that the components $\tilde{a}$, $\tilde{d}$, $\tilde{c}$ can be used as accurate indicators of midcourse navigation system performance.

Run 126 is considered the standard case for the study. Input conditions include the standard initial error matrix $\lfloor P \rfloor_{to}$ described in paragraph 2.1.1.3, second velocity correction at t_o = 50 hours from translunar injection, and velocity correction errors of 0.1 m/sec in magnitude and 1/4 degree in direction (both in application and measurement). The periselenum estimation errors obtained using the standard conditions are seen to be reasonable. The altitude estimation error, for instance, is less than 5 km. Although the effect of midcourse guidance errors on overall system performance will not be treated extensively here, it was found that rms estimation errors of 5 km in altitude and 20 km in downrange at periselenum do not cause intolerable errors in the initial conditions at main braking, assuming

no further navigation is done. This is due to the fact that for a target location approximately 180 degrees from periselenum, both altitude and crossrange errors tend to reach a minimum, while downrange errors increase. But since downrange errors are nearly nulled out by initiating main braking on range rather than time, the choice of target location made in this study tends to reduce the effect of midcourse guidance errors.

Run 125 shows the effect of assuming the large initial errors described in paragraph 2.1.1.3. Although these errors are nearly an order of magnitude larger than the standard errors, the final estimation errors are increased by a factor of only about 5. This is because the errors in measuring the second velocity correction are quite important in the standard case, while these uncertainties are swamped by the initial estimation errors in Run 125. However, it can be seen that the estimation errors at periselenum are considerably above the figures of 5 km altitude and 20 km downrange. Thus, it may be concluded that in the case of the large DSIF errors, no navigation during the midcourse approach gives unacceptable results.

The standard case assumed that the second velocity correction (ΔV_2) occurs at t_o = 50 hours after translunar injection, since this was an input from a previous study (reference 3) which assumed DSIF tracking after ΔV_2. Since it is assumed here that no tracking is done after ΔV_2, there is no reason why ΔV_2 cannot be postponed. Table 2-2 presents velocity comparisons of Run 126 and Run 108. Run 108 is identical to 126, except that ΔV_2 is at t_o = 66 hours instead of 50 hours.

TABLE 2-2

COMPARISON OF VELOCITY REQUIREMENTS FOR ΔV_2 AT t_o = 50 HOURS AND t_o = 66 HOURS

No.	Description	$\lvert\Delta V_2\rvert$ (m/sec)	v (m/sec)	$\tilde{v}$ (m/sec)	a (km)
126	Standard case	1.34	7.08	6.75	4.89
108	t_o = 66 hours	3.89	7.01	3.08	2.37

The quantities shown include $|\Delta V_2|$, the rms correction velocity magnitude, v, the rms velocity deviation at periselenum, a, the rms altitude miss at periselenum, and $\tilde{v}$, the rms velocity estimation error at periselenum. The results show that the altitude miss (and correspondingly, the altitude estimation error) can be cut in half by postponing ΔV_2 until t_o = 66 hours. This is done at a nominal fuel cost, as can be seen by comparing $\Sigma \Delta V = |\Delta V_2| + v$ for each of the cases; i.e., $\Sigma \Delta V$ = 8.42 m/sec for the standard case compared to $\Sigma \Delta V$ = 10.9 m/sec for the 66-hour case. In other runs not presented here, it was found that postponing ΔV_2 much past 66 hours gave poor results due to the rapid rise in both $|\Delta V_2|$ and v as t_o is made closer to periselenum. Thus, 66 hours (or approximately 7 hours prior to periselenum) appears to be near-optimum timing for ΔV_2.

Another useful result that can be inferred from the results in table 2-2 is that fixed-time-of-arrival guidance (FTOA) is sufficient for the computation of ΔV_2. This can be seen by comparing v and $\tilde{v}$ for the standard case. An FTOA scheme corrects only the final position, not final velocity, which is left unconstrained. Thus v, the final velocity deviation, results from two sources: the initial uncertainties (at t_o) and the FTOA guidance law. But the close agreement between v and $\tilde{v}$ in Run 126 indicates that almost all the velocity miss has been caused by initial uncertainties rather than the FTOA guidance. Even in the 66-hour case, v is only increased over $\tilde{v}$ by 4 m/sec, thus indicating that FTOA is a reasonable method of guidance for the second velocity correction.

Referring again to table 2-2, it can be seen by comparing Runs 108 and 126 that postponing ΔV_2 is an effective method of reducing the estimation errors at periselenum when standard DSIF errors are considered. However, when the larger errors are present, postponing ΔV_2 accomplishes little, as can be seen by comparing Runs 125 and 146, and performance is still unacceptable. This is because the large initial errors are more important in these cases than the propagation of ΔV_2 errors.

Another method of reducing the standard errors of Run 126 is to measure ΔV_2 more accurately. In Run 126 (the standard case) it is assumed that an rms resolution error (cutoff) of 0.1 m/sec exists on both the applied and measured ΔV_2. Although this is a state-of-the-art accuracy for implementing the velocity correction, it is reasonable to assume that the velocity pulse could be measured to 0.01 m/sec rms. Assuming this measurement accuracy results in a reduction of estimation errors about equivalent to postponing ΔV_2, as can be seen by comparing Runs 104 and 108 with Run 126. Also, Run 103 shows that measuring ΔV_2 more accurately on the large error case accomplishes little. Finally, results of several computer runs not shown here, using similar initial conditions, showed that system performance obtained by <u>both</u> ΔV_2 postponement and 0.01 m/sec correction monitoring is only slightly better than doing one or the other.

In general, if no navigation is performed during the approach phase, and correction monitoring accuracy is equivalent to application accuracy, the estimation errors and deviations at periselenum are equal. Thus, the results obtained for $\tilde{a}$, $\tilde{d}$, $\tilde{c}$ in table 2-2 also equal the deviations a, d, c. From this, it can be seen that the standard error cases give acceptable results as far as altitude and crossrange miss are concerned, ranging from 2 to 5 km in altitude and 0.5 to 1.2 km in crossrange. However the large errors give miss distances which may be greater than the ability of the retrothrust (into lunar orbit) guidance system to handle. For instance, for a 16-km rms altitude miss, a 3σ deviation of 48 km on an intended 185-km orbit might require more complicated retrothrust guidance methods than those considered in this study.

In summary, the conclusions drawn from the no-navigation runs are as follows:

- The standard initial errors give acceptable results in both estimation and miss with no navigation.
- If no navigation is done during the midcourse approach, then a factor of two improvement in system performance may be obtained by either postponing ΔV_2 until t_o = 66 hours, or measuring σ_ϵ to 0.01 m/sec in magnitude.

The large initial errors give periselenum estimation errors which would require some midcourse navigation and a miss distance which might require a complex retro guidance system.

FTOA guidance is sufficient for ΔV_2.

2.1.1.4.2 Horizon Scanner Runs - This paragraph discusses the requirements on angle-measurement accuracy for the horizon-scanner navigation system. Since the results of the previous paragraph showed that no navigation is required when the standard initial errors are used, only cases in which the large errors are present are considered here and in other paragraphs discussing onboard navigation. In addition, only navigation will be discussed since the periselenum deviations are strictly a function of the accuracy of ΔV_2.

Table 2-3 presents the periselenum results of angle-measurement navigation together with Run 125, the no-navigation large error case shown for comparison. Since all angle measurements were assumed to be made in the trajectory plane, no reduction of $\tilde{c}$ (cross-track estimation errors) was obtained. However the value of 6.62 km rms is reasonable as will be shown later.

TABLE 2-3

HORIZON SCANNER RESULTS

Run	Description	$\tilde{a}$ (km)	$\tilde{d}$ (km)	$\tilde{c}$ (km)
125	No navigation (large initial errors)	16.0	56.3	6.62**
109	σ = 0.2 mrad	.79	1.42	6.62
111*	σ = 2 mrad	3.21	6.15	6.62
112	σ = 1 mrad	1.75	3.31	6.62
121*	σ = 2 mrad, t_o = 66 hours	3.39	6.26	6.31
122	σ = 2 mrad, 1/2 measurements of Run 109	3.85	6.86	6.62

σ = instrument accuracy

*Complete covariance matrices are listed in paragraph 5.2.
**No cross-track navigation

All measurements include an additional angle error due to 1.4 km lunar horizon irregularities.

In general, the results of table 2-3 show that the degraded no-navigation results can be improved considerably by measuring angles. Run 109, assuming σ = 0.2 mrad instrument accuracy and measurements starting when the vehicle reaches within 10,000 km of the moon, gives excellent results. Run 111, assuming 2-mrad accuracy and the same measurement schedule, also gives acceptable results. (All these runs include a 1.4-km horizon fluctuation in addition to the instrument errors). Comparison of Runs 111 and 112 show a nearly linear relationship between the final estimation errors and the measurement accuracy. Run 121 shows that postponement of ΔV_2 is not necessary to reduce estimation errors when navigation measurements are taken. Run 122, compared to 111 (both have σ = 2 mrad) shows that data rate is not a prime factor in determining system performance using angle measurements so long as measurements are made over a large enough central angle.

In summary, these computer runs show that several angle measurements during the midcourse approach, accurate to 2 mrad rms, reduce the large estimation errors to acceptable values.

2.1.1.4.3 Altimeter Runs - Before going into a discussion of results obtained using the altimeter, it should be mentioned that although a radar altimeter may be accurate to tens of meters, lunar surface roughness and lunar radial uncertainty may well limit the use of an altimeter for lunar navigation. In addition, since an altimeter is an active device, its range is limited by considerations of power and antenna size. For the purposes of this study, 10,000-km and 1,000-km altimeter ranges have been considered.

In paragraph 2.1.1.3, a value of σ_R = 2 km was estimated as the rms error in determining spacecraft radius to the center of lunar gravity. Although this figure was composed of random and bias-type components, in the computer program the altimeter errors were considered to be purely random, and a nominal value of σ_R = 2 km was used as a standard. However it will be shown later in this paragraph that this assumption is reasonable, and typical bias errors will not greatly affect the results obtained.

In table 2-4, the periselenum results obtained by varying the range-measurement accuracy and altimeter range are included with Run 125 again included as a comparison case. Large initial errors were assumed on all runs.

TABLE 2-4

ALTIMETER RUNS

Run	Description	$\tilde{a}$ (km)	$\tilde{d}$ (km)	$\tilde{c}$ (km)
125	No navigation (large errors)	16.0	56.3	6.62
127	σ_R = 2 km (10,000-km range)	1.37	1.10	6.62
128	σ_R = 4 km (10,000-km range)	2.61	2.13	6.62
135*	σ_R = 2 km (1,000-km range)	2.41	5.01	6.62
136*	σ_R = 4 km (1,000-km range)	4.47	9.40	6.62
138	σ_R = 0.5 km (1,000-km range)	0.63	1.31	6.62

σ_R = rms range (to center of moon) measurement error, in km.

*Complete covariance matrices are listed in paragraph 5.2.

Runs 127 and 128 show the excellent results obtained when using a 10,000-km altimeter. This is primarily due to the effect on random errors of taking measurements in many different directions. However, restricting altimeter measurements to times at which the spacecraft is less than 1000 km from the moon also gives acceptable results, at least for Run 135, in which σ_R = 2 km. Increasing σ_R to 4 km yields acceptable, though possibly marginal results, as shown in Run 136. Finally, since there is some uncertainty in just how large range measurement errors will be, σ_R = 0.5 km was tried in the final run and gave excellent results.

The preceding data was computed assuming that the error quantity σ_R is completely random. Actually, however, the range measurement errors

might include some bias due to deviations of the lunar surface from a sphere of known radius. Assuming a 2-km bias error in the range measurement, the following estimation errors result at periselenum from this bias:

$\tilde{a}$ = 1.9 km

$\tilde{d}$ = 1.2 km

$\tilde{\dot{a}}$ = 1.1 m/sec

$\tilde{\dot{d}}$ = 0.18 m/sec

Comparing the above results with Run 135 in table 2-4, where random errors of 2 km are used, it can be seen that bias errors of this magnitude are tolerable, and that the assumption of purely random errors in the computer runs is reasonable.

In summary, the results of the altimeter runs show that using range measurements accurate to 2 km, and out to a range of 1000 km from the moon, is sufficient to reduce the estimation errors to an acceptable level before periselenum.

2.1.1.4.4 Angle-Beacon Measurements - The next navigation system considered involves tracking an optical signal at the target beacon and measuring the angle with respect to inertial space. One of the limitations of this scheme is that eventually the spacecraft will go below the beacon horizon and no further information can be obtained.

Figure 2-4 shows the range at which the LLV goes below 10 degrees above the target horizon for various target longitudes on the lunar equator. (It is assumed that tracking cannot be relied on below this elevation angle.) For the target area of interest in this study, the range at which this occurs varies from 3900 km (at 40°W longitude) to 5900 km (at 20°W longitude). Thus, a minimum range of operation of 5900 km is required for beacon tracking. Actually, the range must be considerably greater if sufficient data is to be obtained.

The LLV-beacon range of 5900 km corresponds to a LLV-lunar center range of 6420 km which occurs at t = 72 hours (0.95 hour before periselenum)

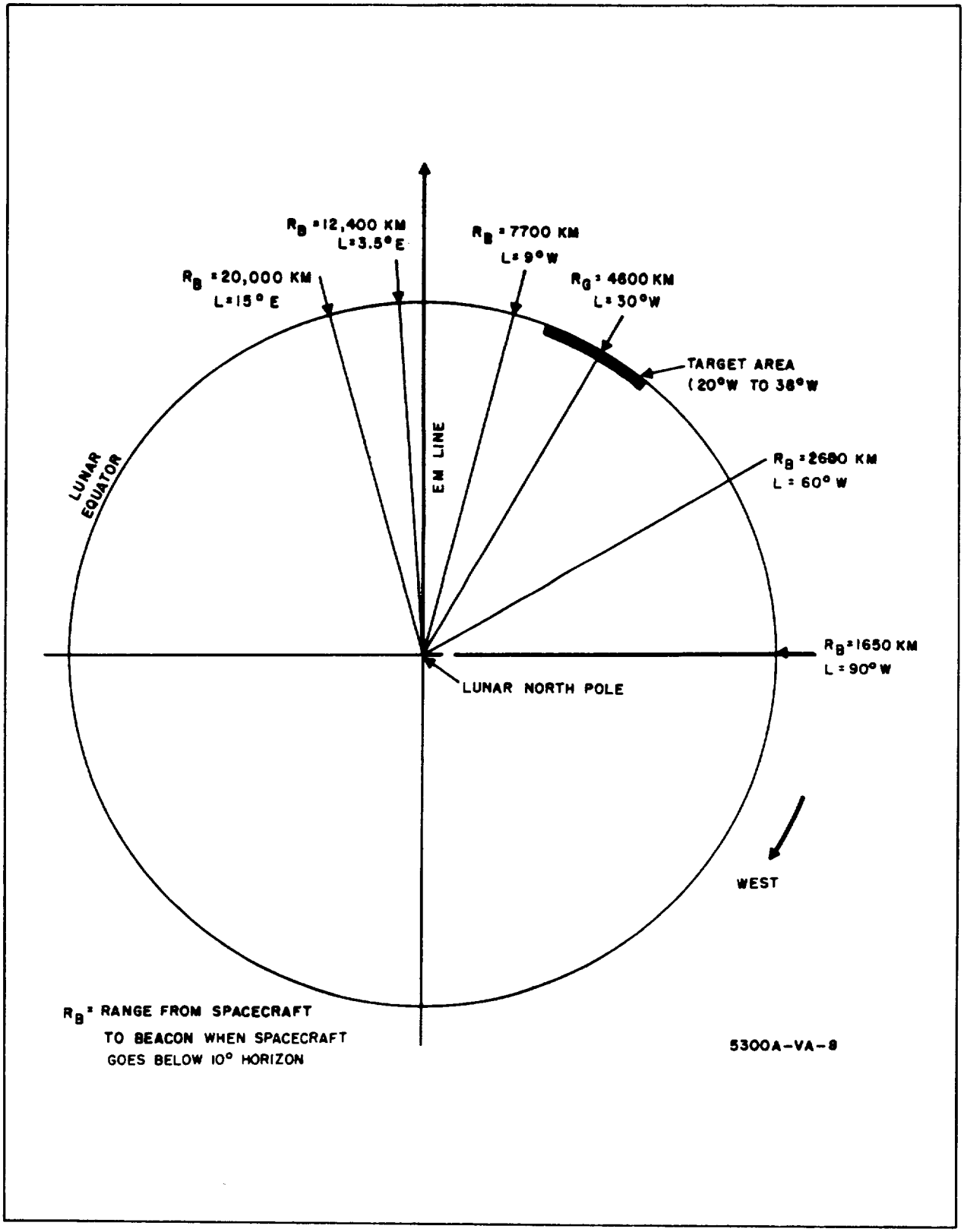

Figure 2-4. Range at Which Spacecraft Goes Below 10-Degree Horizon for Various Target Locations on Lunar Equator

on the hyperbolic trajectory. Thus, in the computer runs using beacon-angle measurements, no measurements were assumed during the last hour before periselenum.

Table 2-5 shows the results of two computer runs using beacon-angle measurement navigation, together with the no-navigation case with large errors and the horizon scanner run with 2-mrad instrument accuracy.

TABLE 2-5

BEACON ANGLE RUNS

Run	Description	$\tilde{a}$ (km)	$\tilde{d}$ (km)	$\tilde{c}$ (km)
125	No-navigation (large errors)	16.0	56.3	6.62
**147	Beacon σ = 0.1 mrad	1.66	5.46	6.62
**148	Beacon σ = 1 mr	6.04	24.6	6.62
111	Horizon Scanner σ = 2 mrad	3.21	6.15	6.62

σ Angle Measurement Accuracy

**Results include 1-km uncertainty in beacon location

Beacon measurements are taken over the interval from t = 70.8 hours (10,000 km range) until t = 72.0 hours. A comparison of Runs 125 and 148 shows that some navigation capability is obtained with measurements accurate to σ = 1 mrad, but system performance is marginal. A comparison with the 2-mrad horizon scanner navigation (Run 111) shows the latter to be significantly better, especially in estimation of the downrange errors. This is due to the beacon-angle measurements being made the last hour before periselenum, when information useful in defining downrange uncertainties is available to the horizon scanner system. Reduction of beacon-angle measurements to 0.1 mrad yields useful results, but it is felt that such accuracy might be difficult to achieve. Thus, the use of beacon-angle measurements are considered inferior to altimeter or horizon scanner measurements because of line-of-sight limitations; consequently, this system is not recommended.

2.1.1.4.5 Cross-Track and Altitude Errors - In most of the preceding discussion, only inplane (XY) errors have been considered, thus essentially reducing the guidance and navigation problem to two dimensions. Cross-track (Z) errors will be considered in greater detail here.

The cross-track quantity used for analysis here is $\delta\epsilon$ which is defined as the shortest distance between the target point and the trace of the trajectory plane on the lunar surface, as shown in figure 2-5a. If no crosstrack velocities are applied (either intentional or otherwise), then $\delta\epsilon$ can be determined directly from the covariance of deviations at the end of midcourse, as shown in Section 5-3. The rms value of $\delta\epsilon$ for several cases of interest is indicated in table 2-6.

TABLE 2-6

RMS VALUES OF $\delta\epsilon$

Run	Description	Target at 20° W. Longitude		Target at 40° W. Longitude	
		$\delta\epsilon$ (km)	$\delta\phi$(degs)	$\delta\epsilon$ (km)	$\delta\phi$(degs)
126	Standard Error, no navigation	0.81	0.61	0.66	0.49
108	Standard Error, no navigation(t_o = 66 hours)	0.82	0.62	1.61	1.21
125	Large Errors, no navigation	5.58	4.20	8.13	6.09

The results shown in table 2-6 include the rms cross-track error for both extremes of the target region. In addition, the quantity $\delta\phi$ is shown (as calculated using equation (5.8-10) derived in paragraph 5.8) which is the out-of-plane angle required of the descent kick to make up for the indicated cross-track error. Three no-navigation runs are shown in the table, including the standard error cases from 50 and 66 hours and the large error case from 50 hours.

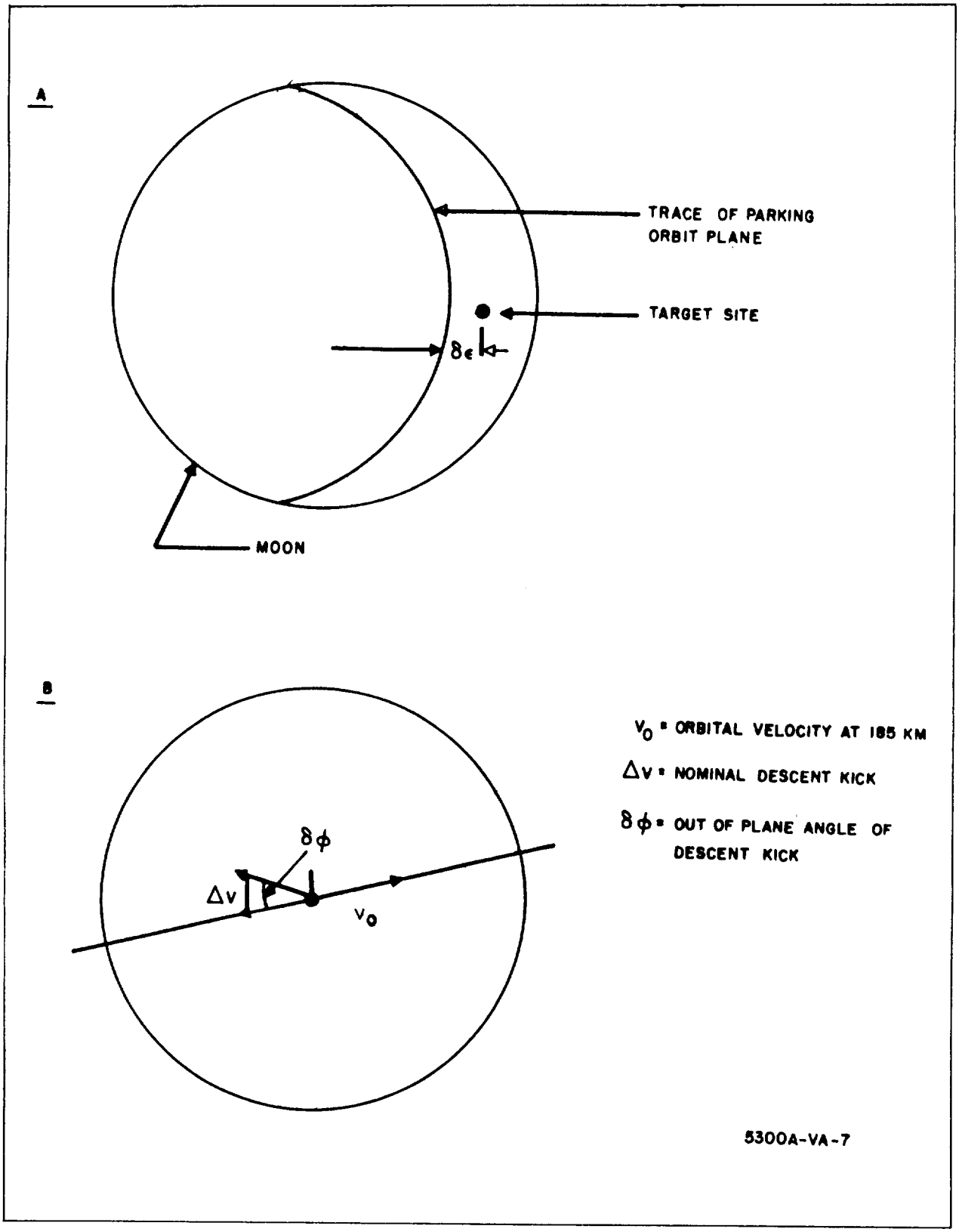

Figure 2-5. Definition of Cross-Track Error Quantities

The first question to consider is whether or not two-dimensional guidance at retrothrust is sufficient. It can be seen that the cross-track deviations on the standard cases are on the order of 1 km. Since main braking starts at a range of about 300 km, it is clear that such a cross-track error will not heavily penalize the main braking operation. Next, consider the possibility of correcting the out-of-plane errors at the descent kick into elliptical orbit. This would be quite economical from a fuel standpoint, but it can be seen that the indicated out-of-plane correction angle ranges on the order of 0.5 to 1.2 degrees. Since the control accuracy is expected to be on the order of 0.25 to 1 degree, even very precise navigation information at this point would not guarantee reduction of the cross-track errors due to control errors in the descent kick. Thus, in the case of the standard errors, no cross-track navigation or guidance is required before main braking.

In the large error case, $\delta\epsilon$ is larger, so that some reduction in these errors would be possible at the descent kick if navigation information is available. It was found in other parts of this study that crossrange errors on the order of 6 km at the start of main braking caused significant but not intolerable increase in fuel cost. Thus, even in the case of the large errors, it is reasonable to leave out-of-plane errors uncorrected until main braking.

In summary, the results of the out-of-plane analysis indicate that two-dimensional navigation and guidance is sufficient prior to main braking. In the case of large errors, some fuel could be saved by correcting the out-of-plane errors at the descent kick, but only at the cost of considerably complicating the guidance and navigation system.

2.1.1.4.6 Effect of Target Location - Figure 2-6 shows the propagation of errors from the standard case (Run 126) as a function of central angle from periselenum. It can be seen that the choice of target area is a good one from a guidance standpoint, since the cross-track and altitude deviations, which are the critical factors in determining initial errors, tend to a minimum in this region.

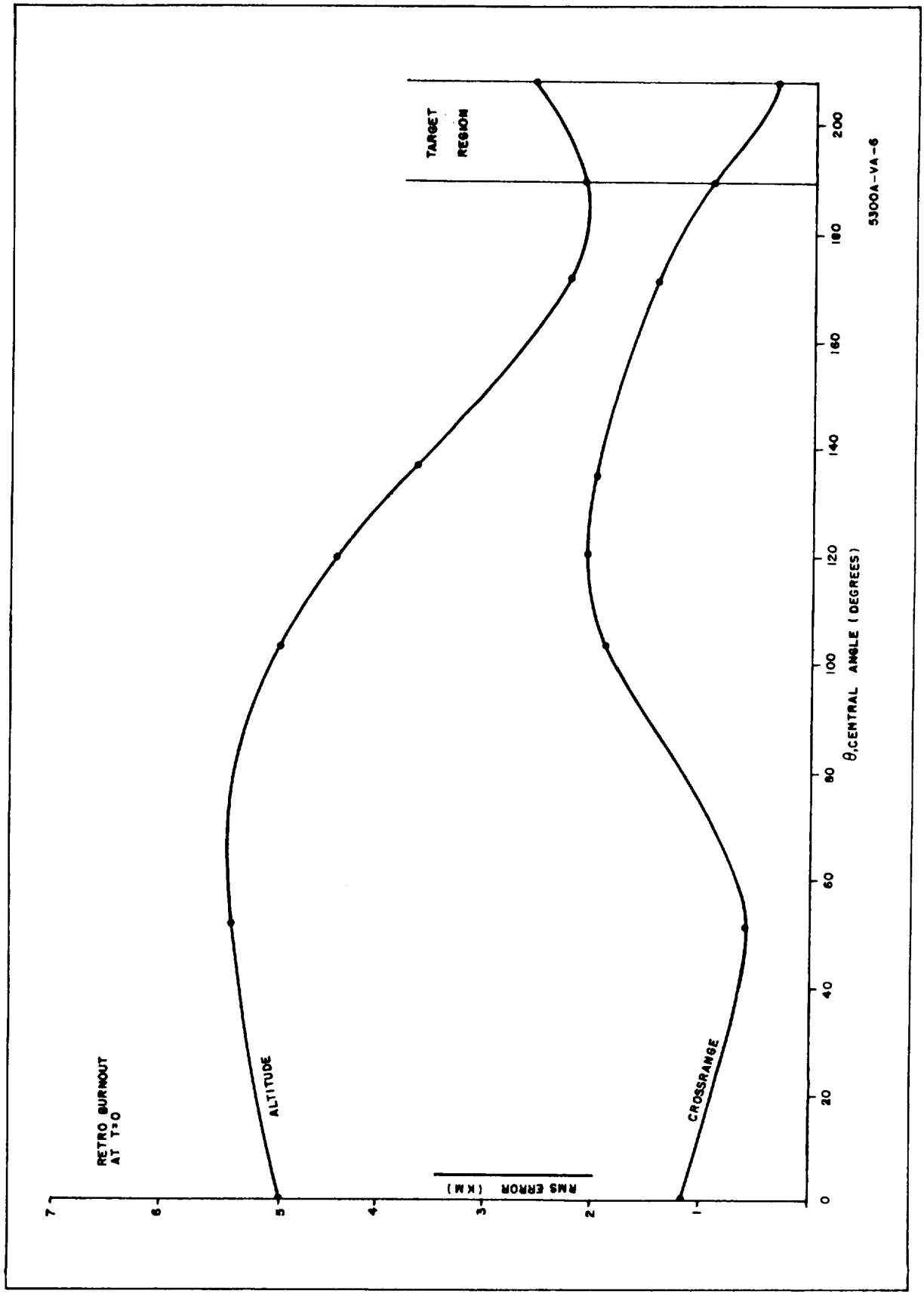

Figure 2-6. Propagation of Standard Errors From Retro Burnout to Main Breaking

2.1.1.4.7 Control Accuracy - Although the control accuracies specified for this study were specified as 0.1 m/sec in magnitude (due to cutoff inaccuracy) and 1/4 degree in pointing error, it was desired to determine the effect of relaxing the pointing angle requirements. It was found that increasing the pointing error of the second correction at t_o = 50 hours from 1/4 degree to 1 degree (rms) has a nearly negligible effect on miss distance. This is due to the fact that for the small second correction assumed (1.29 m/sec for t_o = 50 hours), the dominant error is the 0.1 m/sec cutoff error.

2.1.1.4.8 Other Navigation Systems - Two other midcourse navigation system possibilities were considered briefly during this study. These were (1) the use of the horizon scanner to measure range and (2) the use of doppler measurements to the lunar surface. The results of the analyses done in paragraph 5.1 are presented here.

Figure 2-7 shows the results of an analysis of the range accuracy which can be obtained with a horizon scanner. It can be seen that this is not an attractive method of navigation since even with an assumed instrument accuracy of σ_I = 1 mrad, range errors increase rapidly with range. For instance, only 1 hour prior to periselenum, the range to the moon center is approximately 6400 km, giving an altitude error of approximately 23 km. Thus, this method of midcourse navigation was not investigated further.

A problem with the use of doppler navigation is that if a single beam system is used, it must be accurately pointed. In addition, the finite beamwidth tends to smear the returned doppler frequencies over a considerable band. The results of an analysis of this problem are presented in table 2-7.

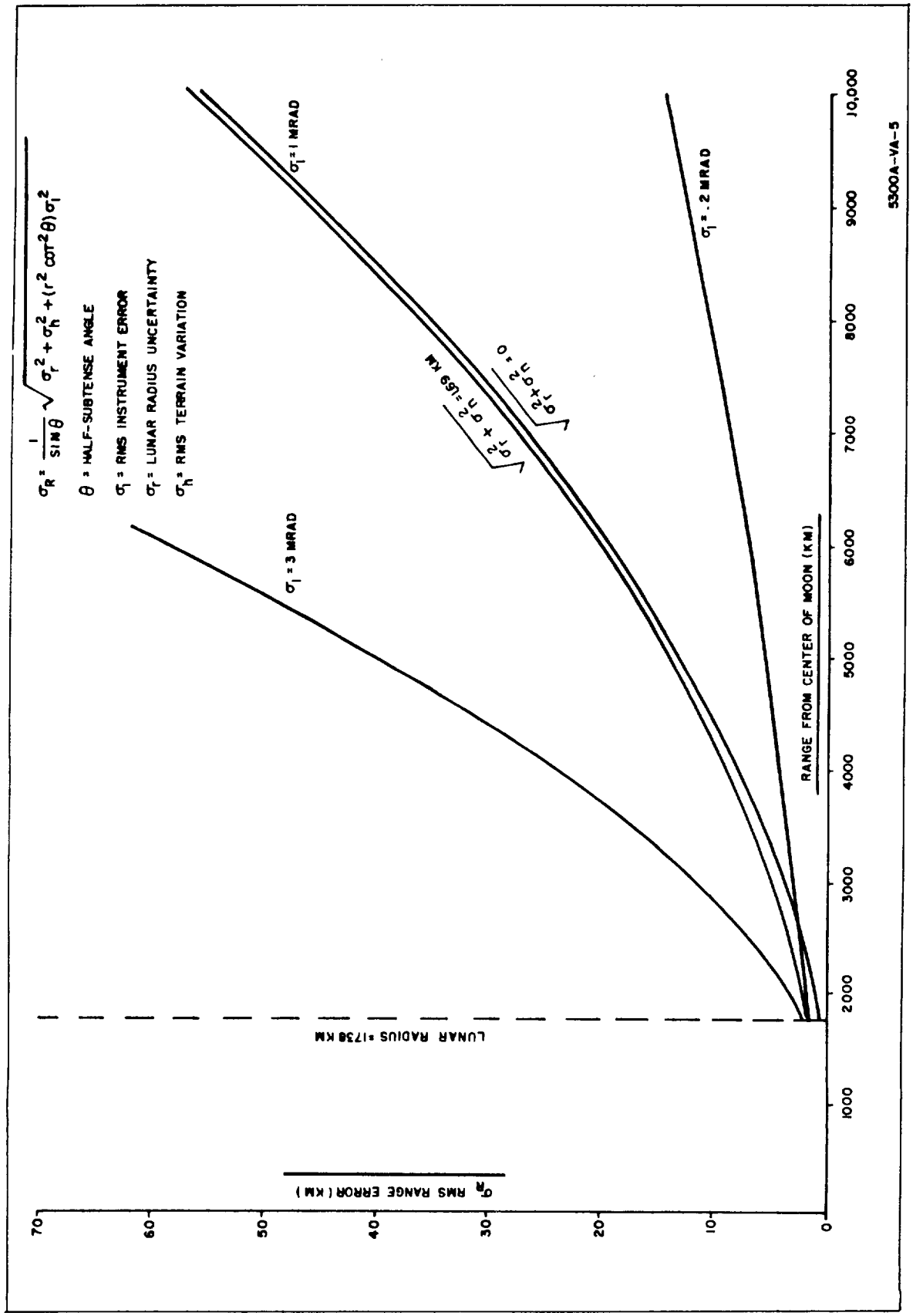

Figure 2-7. Error in Range Estimation by Disc Measurement With Various Values of Instrument Error

TABLE 2-7
VELOCITY ESTIMATION ERRORS DUE
TO POINTING AND BEAMWIDTH

t(hr)	V(m/sec)	$\delta\zeta$ = 0.5 deg. δV(m/sec)	$\delta\zeta$ = .05 deg. δV(m/sec)
72.6	2168	15.5	1.55
72.7	2314	18.3	1.83
72.8	2439	20.6	2.06
72.88	2476	21.6	2.16

As shown in figure 2-8, $\delta\zeta$ is the angular difference between the direction of local vertical and the direction of the returned doppler energy. In table 2-7 it can be seen that in order to obtain useful navigation results, $\delta\zeta$ must be on the order of 0.05 degree. In other words, only energy within a 0.05-degree cone of local vertical will give useful information. Thus, the use of doppler radar to the lunar surface for midcourse does not appear to give useful results.

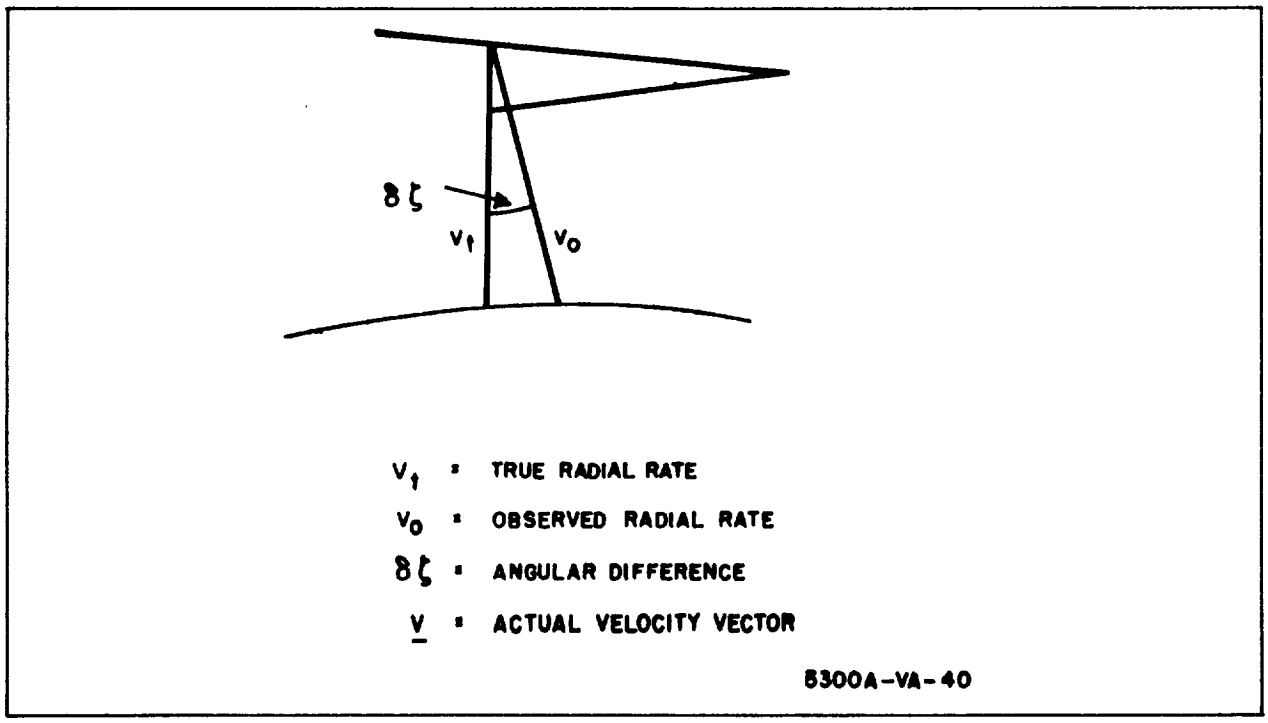

Figure 2-8. Pointing and Beamwidth Errors in Doppler Navigation System

2.1.2 Retrothrust Into Lunar Orbit

A list of symbols used in this paragraph is as follows:

$[K_B]$	a matrix of sensitivity coefficients which relate actual initial state deviations from nominal to final state deviations from nominal
$[K_{\tilde{p}}]$	a matrix of sensitivity coefficients which relate initial state estimation errors to final state deviations from nominal
$[K_{\tilde{q}}]$	a matrix of sensitivity coefficients which relate navigation and control sensor bias errors to final state deviations from nominal
F	the applied thrust vector
V_θ	the magnitude of the horizontal component of vehicle velocity
R	the range of the vehicle from the center of the moon
Θ	the angular displacement of the vehicle (lunar central angle)
h	the altitude of the vehicle above the actual lunar surface
A_C	the commanded thrust vector angle measured from the estimated local horizontal
T_B	the time required to execute the retrothrust maneuver
t	time, referenced to initiation of retrothrust
$\lvert\Delta\underline{V}\rvert$	the estimated value of the incremental velocity change required by an impulsive correction
$\tilde{f}_c$	a constant error in measuring the applied thrust
$\tilde{\alpha}_C$	a constant error in measuring the applied thrust vector angle
$\tilde{\gamma}_i$	an initial, misalignment of the inertial measurement unit (IMU) platform to the estimated local horizontal
$\tilde{a}_{FR}$	an accelerometer bias error
$\tilde{a}_{F\theta}$	an accelerometer bias error
$\tilde{r}_h$	a constant error in measuring range to the center of the moon

SUBSCRIPTS

i	an initial value, referenced to initiation of retrothrust
T	a final value, referenced to the completion of retrothrust

c	a commanded value (value commanded by guidance logic subsystem)
R	a component along the radius vector to the vehicle from the center of the moon
θ	a component along the local horizontal and in the plane of the retrothrust maneuver
h	quantities pertaining to the altimeter measurements.

OPERATORS

[ ]	a vector in column matrix form
cov[ ]	a covariance matrix

2.1.2.1 Requirements, Trajectory Model and Geometry

Retrothrust into lunar orbit is a powered maneuver occurring approximately at periselenum, which transfers the vehicle from its 72.9-hour midcourse approach trajectory, into a retrograde, circular parking orbit, nominally 185 km above the lunar surface. The maneuver profile geometry is shown in figure 2-9. A preliminary analysis utilizing the characteristics of the L-I stage, reference 1; shows that the required change in velocity must occupy some 4 or 5 minutes during which the vehicle will cover approximately 16 degrees of lunar central angle. Analysis assuming an impulsive correction was found to be inadequate, as shown in paragraph 2.1.2.4., and a non-impulsive analysis is therefore performed for this phase. For this reason a guidance law must be established and candidate navigation systems postulated. A nominal trajectory is generated utilizing the guidance law assuming error-free inputs to the system.

General analytical assumptions utilized for this analysis are that vehicle motion is adequately described by the dynamics of a restricted two-body system, and that perturbation effects such as lunar oblatness and lunar motion have a second order effect on analysis of errors.

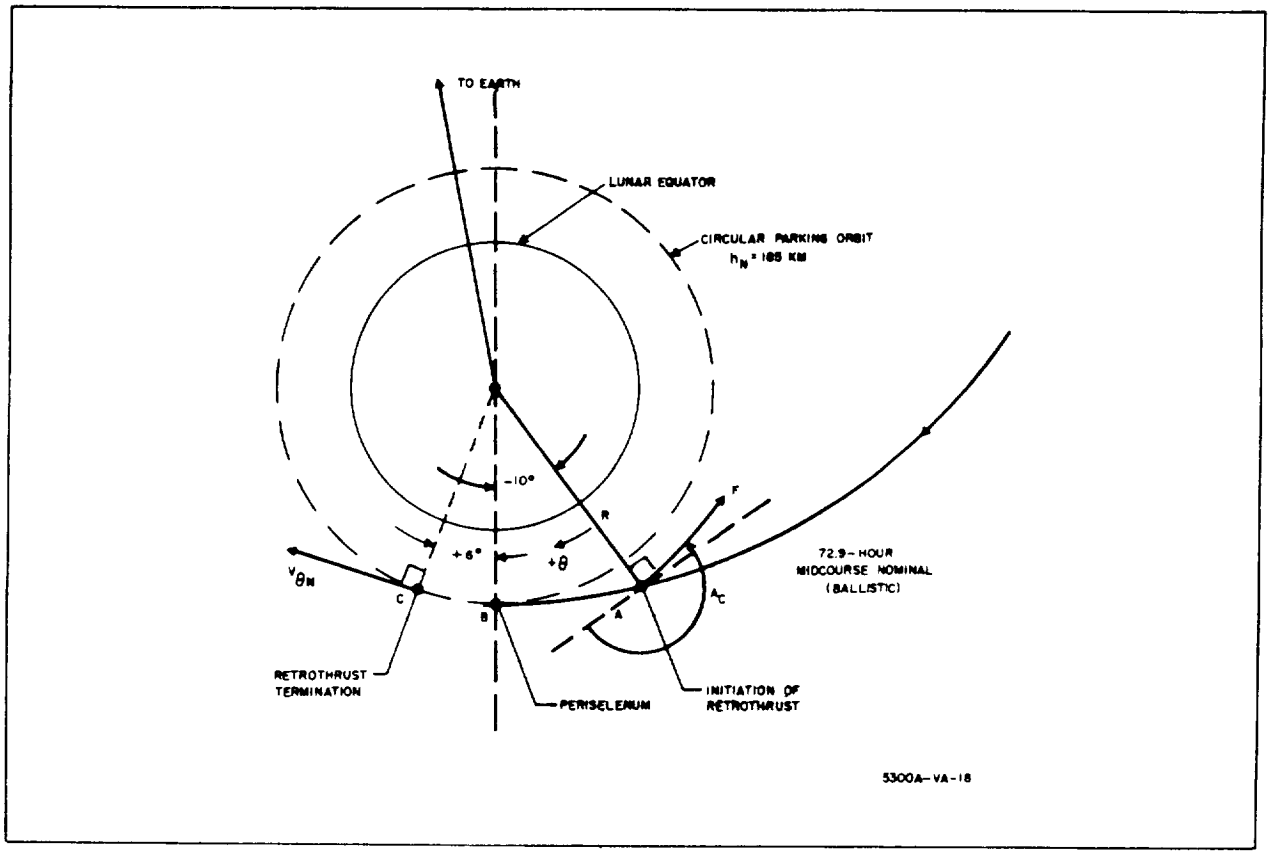

Figure 2-9. Retrothrust Maneuver Profile

2.1.2.2 Navigation, Guidance, and Control System Model

The optimum retrothrust maneuver (from the standpoint of fuel consumption) is an impulsive correction. An approximation to this is the utilization of the L-I engine at near maximum thrust with the employment of thrust direction for trajectory control. A constant thrust, variable thrust direction type of engine control is therefore assumed.

With regard to navigation, reasonably available information during the maneuver consists of initial condition information obtained from midcourse approach guidance, vehicle incremental attitude with respect to local vertical and orbital plane directions obtained from the inertial measurement unit, incremental velocity obtained from the inertial measurement unit, and possibly altitude above the lunar surface obtained by altimeter measurements. Direct measurement of crosstrack or horizontal displacement error perpendicular to the desired orbital plane is not easily measured and would entail

considerable system complexity. Preliminary analysis showed that out-of-plane errors as incurred during midcourse, together with those accrued during retrothrust, are of a magnitude which can be efficiently corrected during the subsequent main braking phase. The validity of this assumption is established in paragraph 2.1.4.1. No cross-track navigation or guidance, therefore, is assumed.

Information available for retrothrust guidance at initiation is estimated vehicle position and velocity, a reference triad in terms of measured local vertical and orbital plane directions and time.* Nominal maneuver duration is known and the desired terminal conditions are known. The approach taken, therefore, is essentially that of G. W. Cherry in reference 9 and assumes a radial acceleration program, which is a simple function of applied thrust acceleration, based on an assumed maneuver time (nominal) and an assumed set of initial and desired set of terminal conditions.

The result is a fairly simple guidance computation which, while non-optimized, is subject to optimization should this be desired and, as utilized in this report, is within 5 percent of optimum as determined by the equivalent impulsive maneuver time. A detailed description of the guidance logic is given in Section 6. A two-dimensional analysis is assumed.

A block diagram of the navigation, guidance, and control system, including the possible use of an altimeter, is shown in figure 2-10.

Navigation observables are the measured radial and horizontal components of vehicle thrust acceleration obtained from the inertial platform, which is assumed precessed at estimated orbital rate. (An equivalent system would

---

* The reference triad is established by placing the inertial platform in a gyrocompassing mode approximately 1 hour prior to retrothrust initiation (see section 12). Since horizon scanner information may be distorted by engine exhaust during retrothrust, the platform will be placed in a free-heading mode. To make gyrocompassing possible following retrothrust, however, the platform will be precessed at estimated orbital rate during the maneuver.

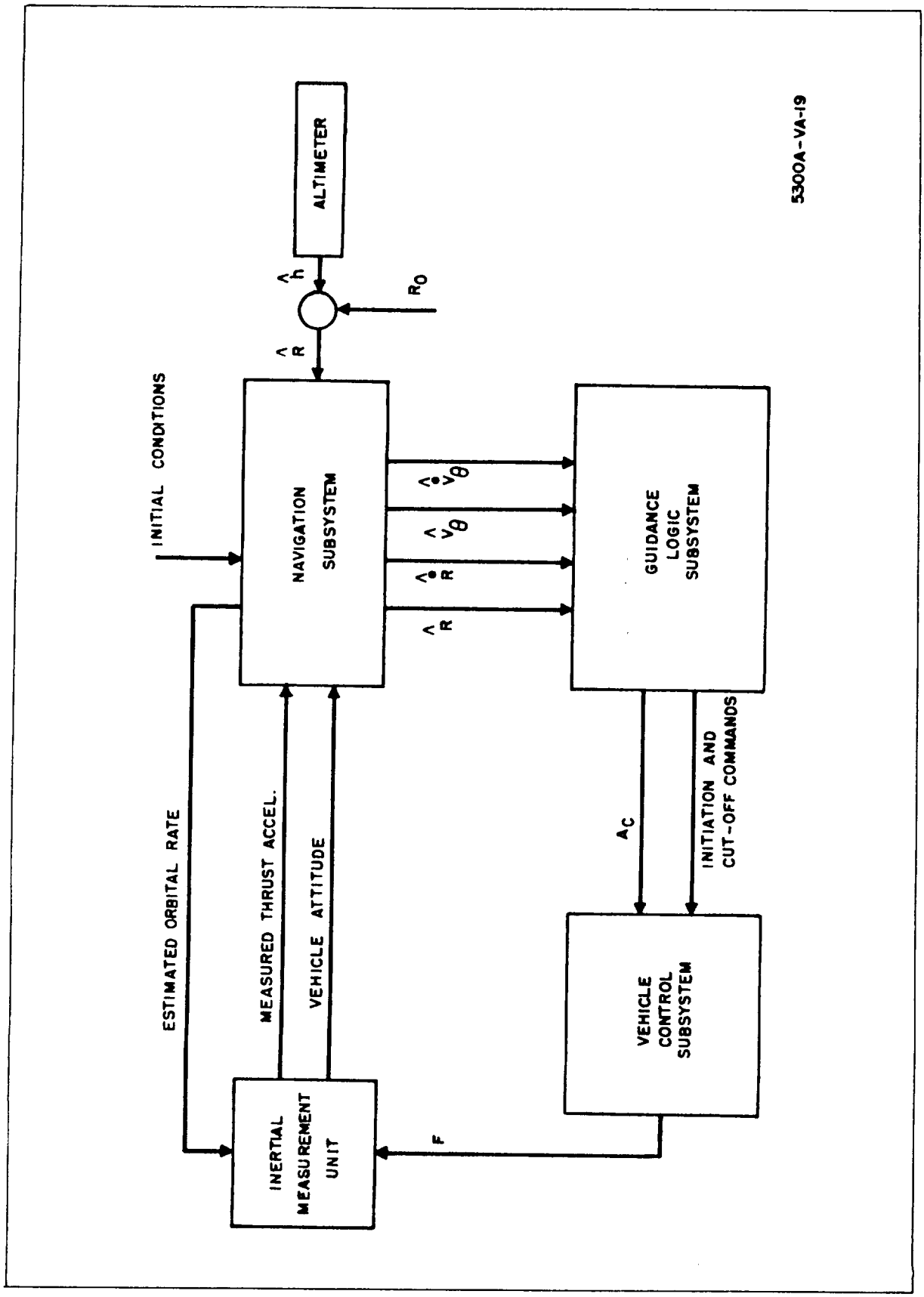

Figure 2-10. Navigation, Guidance, and Control System

involve measurement of acceleration in fixed coordinates and resolution through the estimated orbital angle). An alternate radial measurement assumes the use of an altimeter.

From these are obtained radial distance and its derivative and horizontal velocity and its derivative which form the inputs to the guidance calculation. Control outputs are thrust vector angle, initiation, and cutoff commands.

A two-dimensional digital simulation of the overall guidance and control system was performed to obtain a realistic evaluation of the effect of navigation and control sensor errors on the retrothrust maneuver, to compare two candidate navigation subsystems, and to determine the validity of an impulsive analysis. A block diagram representation of the simulation model is shown in figure 2-11. While trajectory optimization was not an objective of this study, the time of retrothrust initiation was varied to determine the most efficient value and sensitivity to its variation. The relation of maneuver time to the nominal value of Θ at retrothrust initiation is shown in figure 2-12. From this data the most efficient time of retrothrust initiation was determined to be 2 or 3 minutes prior to periselenum (Θ_{iN} = -10 degrees). -10 degrees).

2.1.2.3 Error Sources and Methods of Analysis

Three types of navigation and control sensor errors are treated in this analysis.

- Initial state estimation errors
- Actual initial state deviations from nominal
- Navigation and control sensor bias errors

The following paragraphs constitute a brief discussion of these error sources.

2.1.2.3.1 Initial State Estimation Errors. Initial state estimation errors are a result of navigation and control uncertainties in the midcourse phase prior to retrothrust into orbit. The estimated, initial state vector is:

$$\left[\hat{P}_i\right] = \left[P_i\right] + \left[\tilde{P}_i\right] \qquad (2\text{-}4)$$

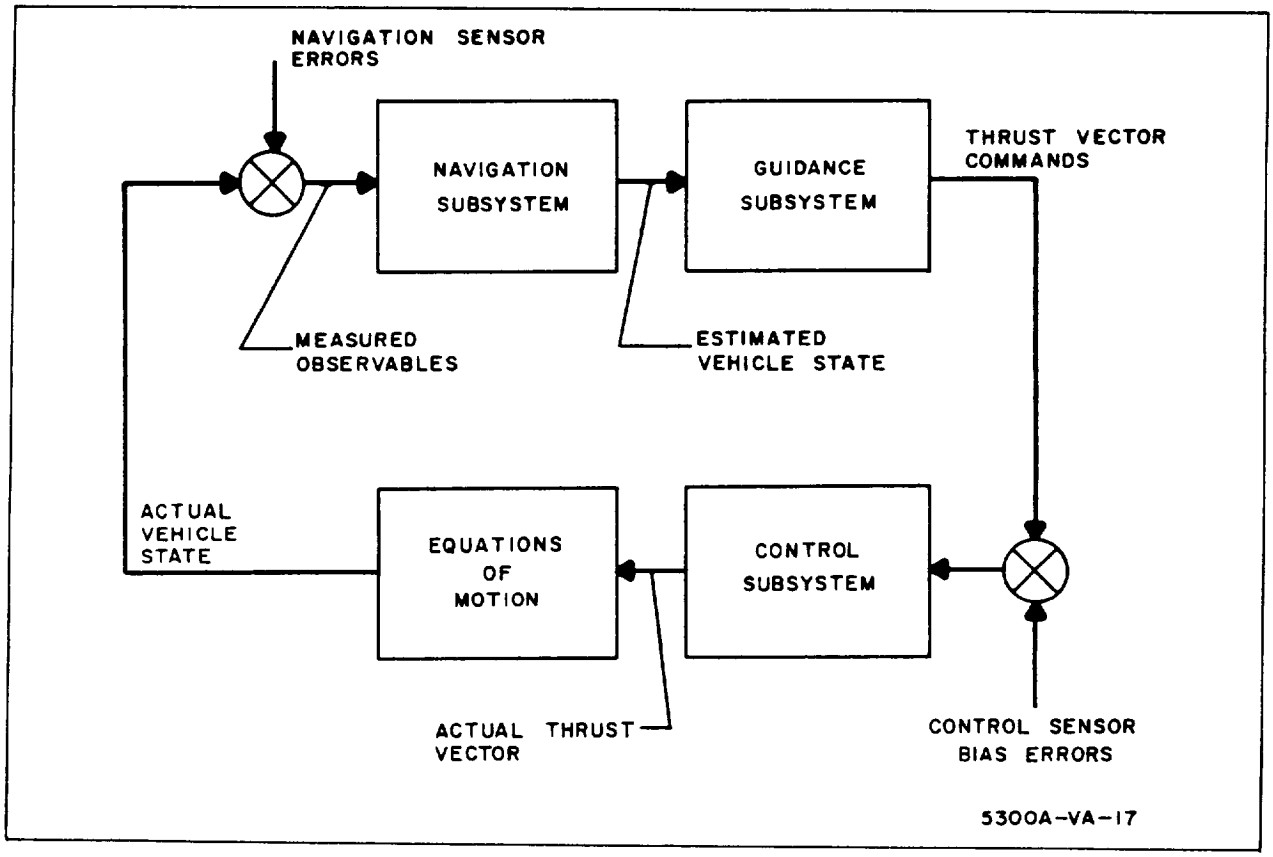

Figure 2-11. Block Diagram Representation of Simulation Model

The initial state estimation errors, $\left[\tilde{P}_i\right]$, are deterministic for a given mission but random over the ensemble of missions.* In this analysis their statistics are characterized by stationary, gaussian distributions having zero mean.

2.1.2.3.2 Actual Initial State Deviations - Actual initial state deviations from the reference trajectory result from navigation, guidance, and control errors prior to retrothrust into orbit. The actual initial state vector of the space vehicle is:

$$\left[P_i\right] = \left[P_{iN}\right] + \left[P_i\right] \qquad (2\text{-}5)$$

*It should be noted that their magnitudes are constant after initiation of retrothrust.

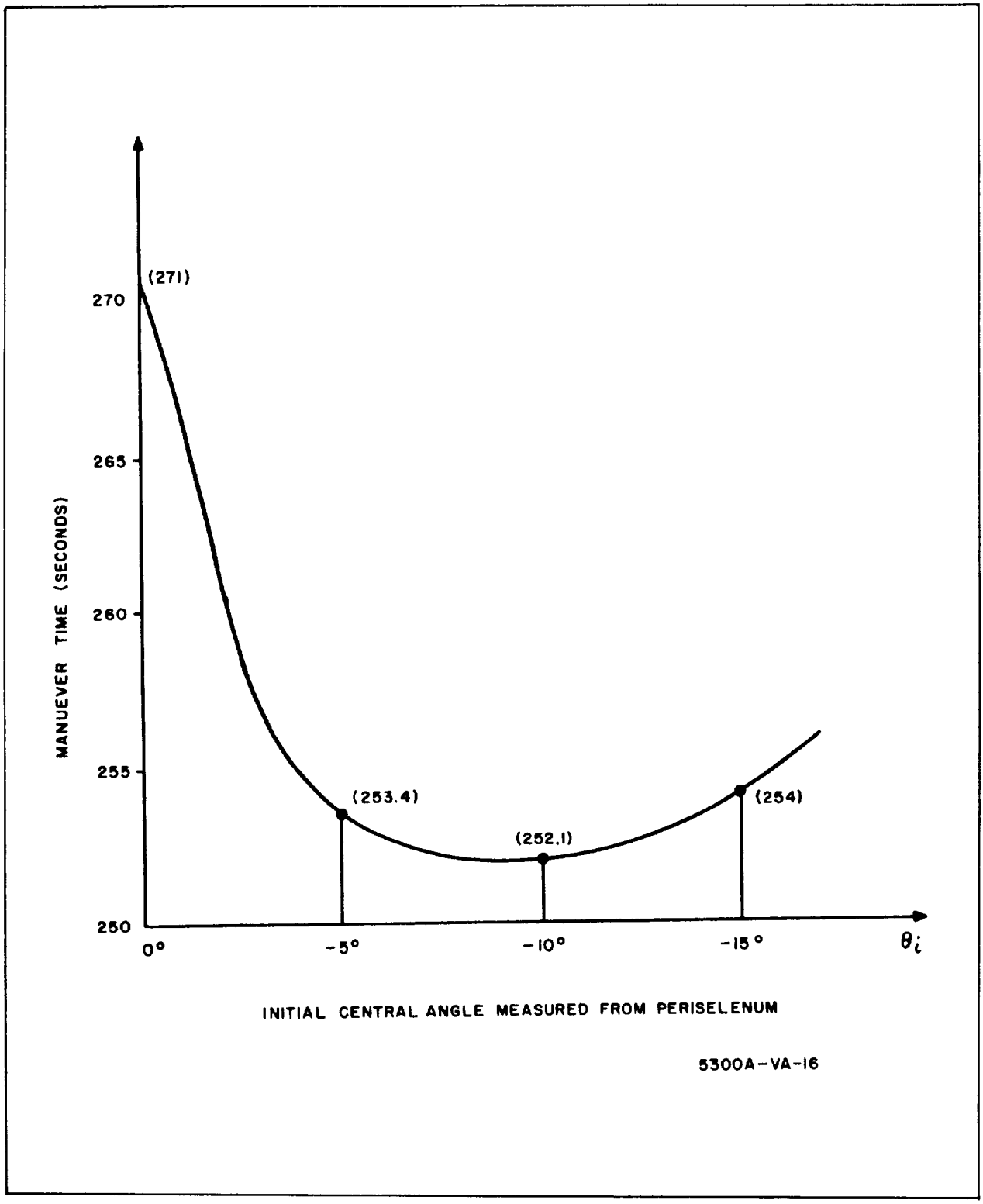

Figure 2-12. Relation of Manuever Time to the Central Angle at Initiation of Retrothrust

The initial state deviations, $[p_i]$, are deterministic for a given mission but random over the ensemble of missions. For the purpose of this analysis their statistics are characterized by stationary, gaussian distributions having zero mean.

2.1.2.3.3 Navigation and Control Sensor, Bias Errors - The observed value of any navigation or control quantity is representable as:

$$\left[\hat{Q}\right] = [Q] + [\tilde{q}] \tag{2-6}$$

The bias errors, $[\tilde{q}]$, are constant for a given mission but random over the ensemble of missions. Their statistics are also assumed to be stationary and gaussian, with zero mean.

2.1.2.3.4 Method of Analysis - As stated earlier, the purpose of this analysis is to relate expected excursions of the space vehicle from nominal to the error sources described above. This paragraph presents a brief mathematical formulation of the problem.

If the variational equations applicable during retrothrust are linear, then the following solution to the problem is valid:

$$[P] = \left[K_B(t)\right]\ [p_i] + \left[K_{\tilde{P}}(t)\right]\ [\tilde{p}_i] + \left[K_{\tilde{q}}(t)\right]\ [\tilde{q}] \tag{2-7}$$

Since the navigation and control sensor errors are random over the ensemble of missions, the quantity of interest is the covariance of $[P]$ at the end of retrothrust. Defining final time as T_B, then the problem is to evaluate:

$$\text{cov}\left[[p], [p]\right]_{T_B} \triangleq E\left[[p]\ [p]^T\right]_{T_B} \tag{2-8}$$

Substituting equation 2-7 into 2-8:

$$E\left[[p][p]^T\right]_{T_B} = E\left[\left(\left[K_{B_T}\right][p_i]\right)\left(\left[K_{B_T}\right][p_i]\right)^T\right] +$$

$$E\left[\left(\left[K_{\tilde{P}_T}\right][\tilde{p}_i]\right)\left(\left[K_{\tilde{P}_T}\right][\tilde{p}_i]\right)^T\right] + E\left[\left(\left[K_{\tilde{q}_T}\right][\tilde{q}]\right)\left(\left[K_{\tilde{q}_T}\right][\tilde{q}]\right)^T\right] \tag{2-9}$$

Noting that the matrices of sensitivity coefficients are deterministic over the ensemble of missions, they can be removed from the averaging process.

$$E\ [p][p]^T = [K_{B_T}]\ E\left[[p_i][p_i]^T\right][K_{B_T}]^T + [K_{\tilde{P}_T}]\ E\left[[\tilde{p}_i][\tilde{p}_i]^T\right][K_{\tilde{P}_T}]^T + [K_{\tilde{q}_T}]\ E\left[[\tilde{q}][\tilde{q}]^T\right][K_{\tilde{q}_T}]^T \tag{2-10}$$

Rewriting equation 2-10:

$$\mathrm{cov}\left[[p_T],[p_T]\right] = [K_{B_T}]\ \mathrm{cov}\left[[p_i],[p_i]\right][K_{B_T}]^T + [K_{\tilde{P}_T}]\ \mathrm{cov}\left[[\tilde{p}_T],[\tilde{p}_T]\right][K_{\tilde{P}_T}]^T + [K_{\tilde{q}_T}]\ \mathrm{cov}\left[[\tilde{q}_T],[\tilde{q}_T]\right][K_{\tilde{q}_T}]^T \tag{2-11}$$

Equation 2-11 thus allows the covariance of $[p_T]$ to be determined once the matrices of sensitivity coefficients and the covariance of the sensor errors, over the ensemble of missions, are known. If the covariance matrices of $[p_T]$, $[p_i]$, $[\tilde{p}_i]$, and $[\tilde{q}]$ are essentially diagonal (negligible cross-correlations) then equation 2-11 can be simplified considerably. Representing the trace of each covariance matrix as a column matrix of mean squared terms $[\sigma^2]$, the following relation can be shown to be valid.

$$\left[\sigma_{P_T}^2\right] = \left[K_{B_T}^2\right]\left[\sigma_{P_i}^2\right] + \left[K_{\tilde{P}_T}^2\right]\left[\sigma_{\tilde{P}_T}^2\right] + \left[K_{\tilde{q}_T}^2\right]\left[\sigma_{\tilde{q}}^2\right] \tag{2-12}$$

where

$[K_T^2]$ is the original matrix of sensitivity coefficients squared term by term.

In the nonimpulsive treatment of retrothrust, the sensitivity matrices were determined by digital simulation. Direct evaluation was made possible by assuming that the various components of sensor errors are linearly independent. The validity of this assumption was then established by comparing the results predicted by equation 2-12 to those obtained when the error

sources acted simultaneously. As indicated earlier, the sensitivity coefficients were determined by hand in the impulsive treatment of retrothrust.

2.1.2.4 Results

In this paragraph the sensitivity coefficients defined in paragraph 2.1.2.3 are presented for both a nonimpulsive and impulsive retrothrust maneuver. As explained in Section 6, these coefficients are based on the velocity cutoff criterion in equation 2-13 rather than nominal time.

$$\hat{V}_{\theta} = \sqrt{\frac{\mu}{R_{NF}}} \tag{2-13}$$

Because of the excellent linearity of the variational equations over the range of navigation and control errors treated in this study, only one set of matrices is documented in each case.

2.1.2.4.1 Nonimpulsive Maneuver* - For the pure inertial navigation subsystem, the sensitivity coefficients are:

$$\begin{bmatrix} r_T \\ \theta_T \\ \dot{r}_T \\ \dot{\theta}_T \end{bmatrix} = \begin{bmatrix} 0.184\,(10^{-2}) & 0 & 0.205 & 0 \\ 0.35\,(10^{-6}) & 1.0 & -0.605\,(10^{-4}) & .659\,(10^{3}) \\ 0 & 0 & 0 & 0 \\ 0 & 0 & 0 & 0 \end{bmatrix} \begin{bmatrix} r_i \\ \theta_i \\ \dot{r}_i \\ \dot{\theta}_i \end{bmatrix} +$$

$$\begin{bmatrix} -1.09 & -.107\,(10^{6}) & -.246\,(10^{3}) & -.14\,(10^{9}) \\ -0.35\,(10^{-6}) & -.003 & -.348\,(10^{-4}) & -.405\,(10^{3}) \\ -0.723\,(10^{-3}) & 0 & -.941 & -10^{6} \\ -0.14\,(10^{-9}) & 0 & -.243\,(10^{-6}) & -.885 \end{bmatrix} \begin{bmatrix} \tilde{r}_i \\ \tilde{\theta}_i \\ \tilde{\dot{r}}_i \\ \tilde{\dot{\theta}}_i \end{bmatrix} + \tag{2-14}$$

*When lunar central angle is used to initiate retrothrust rather than nominal time, equations 2-14 and 2-15 are valid except that $\frac{\theta_T}{\theta_i} = 0$ and $\frac{\theta_T}{\tilde{\theta}_i} = -1.0$.

$$\begin{bmatrix} 0 & .229(10^{4}) & .108(10^{6}) & -.307(10^{5}) & -.597(10^{4}) \\ -0.185(10^{-5}) & 0 & -.839(10^{-2}) & 0 & .05 \\ 0 & 0 & -.882(10^{3}) & -.246(10^{3}) & 0 \\ 0 & 0 & -.786(10^{-4}) & 0 & -.115(10^{-3}) \end{bmatrix} \begin{bmatrix} \tilde{f}_c \\ \tilde{\alpha}_c \\ \tilde{\gamma}_i \\ \tilde{a}_{FR} \\ \tilde{a}_{F_\theta} \end{bmatrix}$$

For the composite navigation subsystem, equation 2-14 becomes

$$\begin{bmatrix} r_T \\ \theta_T \\ \dot{r}_T \\ \dot{\theta}_T \end{bmatrix} = \begin{bmatrix} .184(10^{-2}) & 0 & .205 & 0 \\ .35(10^{-6}) & 1.0 & -.605(10^{-4}) & .659(10^{3}) \\ 0 & 0 & 0 & 0 \\ 0 & 0 & 0 & 0 \end{bmatrix} \begin{bmatrix} r_i \\ \theta_i \\ \dot{r}_i \\ \dot{\theta}_i \end{bmatrix} +$$

(2-15)

$$\begin{bmatrix} -.172(10^{-2}) & -.107(10^{6}) & -.389(10^{2}) & -.407(10^{8}) \\ -.851(10^{-7}) & -.033 & .265(10^{-4}) & .405(10^{3}) \\ 0 & 0 & -.859 & -10^{6} \\ -.711(10^{-9}) & 0 & .173(10^{-6}) & -.913 \end{bmatrix} \begin{bmatrix} \tilde{r}_i \\ \tilde{\theta}_i \\ \tilde{\dot{r}}_i \\ \tilde{\dot{\theta}}_i \end{bmatrix} +$$

$$\begin{bmatrix} 0 & .229(10^{4}) & .33(10^{5}) & -.889(10^{4}) & -.243(10^{4}) & 1.03 \\ -.185(10^{-5}) & 0 & -.215(10^{-2}) & -.367(10^{-2}) & .05 & .32(10^{-6}) \\ 0 & 0 & .859(10^{3}) & -.24(10^{3}) & 0 & -.703(10^{-3} \\ 0 & 0 & -.61(10^{-4}) & 0 & -.116(10^{-3}) & 0 \end{bmatrix} \begin{bmatrix} \tilde{f}_c \\ \tilde{a}_c \\ \tilde{\gamma}_i \\ \tilde{a}_{FR} \\ \tilde{a}_{F\theta} \\ \tilde{r}_h \end{bmatrix}$$

Equations 2-14 and 2-15 indicate that the effect of actual initial deviations from nominal is independent of the choice of navigation subsystem. This is a direct result of assuming the various error sources to be linearly independent.* Thus, the matrix $[K_{B_T}]$ measures the ability of the guidance logic to satisfy boundary conditions with non-nominal initial conditions.

An examination of the matrices, $[K_{\tilde{P}_T}]$, indicates that the altimeter significantly reduces the error in range and range rate caused by $\tilde{r}_i$. Also, the propagation of the radial velocity estimation error into a range error is reduced by an order of magnitude.

Equations 2-14 and 2-15 further indicate that the effect of the bias errors, $\tilde{f}_c$ and $\tilde{a}_c$, is independent of the choice of navigation subsystem. These errors are detected by the platform accelerometers (see Section 6). The degradation of system performance by the errors $\tilde{\gamma}_i$, $\tilde{a}_{FR}$, and $\tilde{a}_{F\Theta}$, however, is significantly reduced by the use of an altimeter.

The advantages of the composite navigation subsystem listed above are offset if the errors contributed by $\tilde{r}_h$ are large. A composite picture of the relative performance of the candidate navigation subsystems can be obtained by propagating a simplified set of error inputs through the retrothrust maneuver.** Assuming that the covariance matrices of navigation and control sensor errors are diagonal (no crosscorrelations), equation 2-12 can be used to propagate the errors in table 2-8 through the retrothrust maneuver.

---

* When all error sources were applied simultaneously, the results predicted by the sensitivity coefficients were in agreement with simulation results.

** The numerical results presented here are intended to give the reader more insight into the problem and do not reflect the approach taken in paragraph 2.1.6.

TABLE 2-8

ASSUMED VALUES OF NAVIGATION AND CONTROL SENSOR ERRORS (RMS)

$r_i = 5(10^3)$ meters	$\tilde{r}_i = 10^3$ meters	$\tilde{f}_c = 10^3$ newtons
$\theta_i = 5(10^{-3})$ radians	$\tilde{\theta}_i = 10^{-3}$ radians	$\tilde{a}_c = 10^{-2}$ radians
$\dot{r}_i = 5$ meters/second	$\tilde{\dot{r}}_i = 1.0$ meters/second	$\tilde{\gamma}_i = 10^{-3}$ radians
$\dot{\theta}_i = 5(10^{-6})$ radians/second	$\tilde{\dot{\theta}}_i = 10^{-6}$ radians/second	$\tilde{a}_{FR} = 2(10^{-3})$ meters/second^2
		$\tilde{a}_{F\theta} = 2(10^{-3})$ meters/second^2
		$\tilde{r}_h = .7(10^3)$ meters

The root-sum-square (RSS) final state errors which result are listed in table 2-9.

TABLE 2-9

ROOT-SUM-SQUARE FINAL STATE ERRORS RESULTING FROM SENSOR ERRORS IN TABLE 2-8

Pure Inertial Navigation	Composite Navigation
$\sigma_{r_T} = 1.12(10^3)$ meters	$\sigma_{r_T} = .72(10^3)$ meters
$\sigma_{\theta_T} = 4.31(10^{-3})$ radians	$\sigma_{\theta_T} = 4.29(10^{-3})$ radians
$\sigma_{\dot{r}_T} = 1.56$ meters/second	$\sigma_{\dot{r}_T} = 1.73$ meters/second
$\sigma_{\dot{\theta}_T} = 10^{-6}$ radians/second	$\sigma_{\dot{\theta}_T} = 1.17(10^{-6})$ radians/second

An examination of these results indicates that except for a reduction of the error in range, the altimeter affords no improvement in the overall

guidance system performance. If $\tilde{r}_h$ is increased beyond 1 kilometer, the use of an altimeter actually degrades the performance of the inertial navigation subsystem.* Thus, two prime conclusions are drawn.

a. An altimeter is useful during the retrothrust maneuver only if the error in measuring range to the center of the moon is less than one-half the value of $\tilde{r}_i$ (except as a safety measure).

b. The improvement in the guidance system performance during retrothrust due to range information is not sufficient to warrant the addition of an altimeter. If the sensor is onboard and meets the above accuracy requirement, however, then the composite navigation subsystem would be preferred to a pure inertial subsystem.

It should be noted that the merits of the composite navigation subsystem become increasingly significant as initial estimation errors are increased.

2.1.2.4.2 Impulsive Maneuver - The sensitivity coefficients applicable during the impulsive maneuver are: **

$$\begin{bmatrix} r_T \\ \theta_T \\ \dot{r}_T \\ \dot{\theta}_T \end{bmatrix} = \begin{bmatrix} 1 & 0 & 0 & 0 \\ 0 & 1 & 0 & 0 \\ 0 & 0 & 0 & 0 \\ 0 & 0 & 0 & 0 \end{bmatrix} \begin{bmatrix} r_i \\ \theta_i \\ \dot{r}_i \\ \dot{\theta}_i \end{bmatrix} + \begin{bmatrix} 0 & 0 & 0 & 0 \\ 0 & 0 & 0 & 0 \\ 0 & 0 & -1 & 0 \\ -V_{\theta_i}/R_i^2 & 0 & 0 & -1 \end{bmatrix} \begin{bmatrix} \tilde{r}_i \\ \tilde{\theta}_i \\ \tilde{\dot{r}}_i \\ \tilde{\dot{\theta}}_i \end{bmatrix} \qquad (2\text{-}16)$$

$$+ \begin{bmatrix} 0 & 0 \\ 0 & 0 \\ \sin A_c & |\Delta\underline{V}| \cos A_c \\ \cos(A_c)/R_i & -|\Delta\underline{V}| \sin(A_c)/R_i \end{bmatrix} \begin{bmatrix} \delta\ \Delta\underline{V} \\ \tilde{\alpha}_c \end{bmatrix}$$

*At present the uncertainty in mean lunar radius is approximately 1 kilometer. This number is a lower limit for the value of $\tilde{r}_h$.

**When central angle is used to initiate retrothrust, equation 2-16 is valid except that $\theta_T/\theta_i = 0$ and $\theta_T/\tilde{\theta}_i = -1.0$.

As in paragraph 2.1.2.4.1, the RSS final state errors can be determined for the assumed sensor errors in table 2-8. In this study the value of $\delta|\Delta\underline{V}|$ is assumed to be 0.1 meters/second. The resulting errors are listed in table 2-10.

TABLE 2-10

ROOT-SUM-ERRORS RESULTING FROM SENSOR ERRORS IN TABLE 2-8

Impulsive Correction Logic		
σ_{r_T}	=	$5(10^3)$ meters
σ_{θ_T}	=	10^{-3} radians
$\sigma_{\dot{r}_T}$	=	8.85 meters/second
$\sigma_{\dot{\theta}_T}$	=	$1.17(10^{-6})$ radians/second

The validity of the impulsive treatment can now be determined by comparing these results to those in table 2-9.

A cursory examination indicates that an impulsive maneuver is not representative of the physical situation. In general, the prediction of both final position and velocity errors is unrealistic. Three prime reasons for the inadequacy of the impulsive model are:

- No control over final position error is possible once the maneuver is initiated.
- Since the maneuver is considered to be instantaneous, the propagation of velocity errors into position errors does not occur.
- The overall control system operates in an open-loop mode. As a result, the effect of implementing guidance commands is greatly magnified.

Thus, the impulsive analysis yields very pessimistic predictions of the final state errors.

2.1.3 Parking Orbit and Descent Coast

This paragraph discusses that portion of the lunar landing vehicle mission from immediately after retrothrust termination to immediately before main braking. The retrothrust maneuver places the vehicle nominally in a 185-km altitude circular parking orbit, which persists for 130 degrees and is terminated by a tangentially applied 67-m/sec descent kick. The resulting elliptical descent-coast orbit, in turn, is terminated by main braking initiation, nominally after an additional central angle of 60 degrees. A list of definitions of terms used in this paragraph is as follows:

Glossary

Symbols

$\underline{u}$	vector of descent kick application errors
X_1, Y_1, Z_1	Cartesian coordinate system centered at nominal point of retrothrust termination
X_2, Y_2, Z_2	Cartesian coordinate system centered at nominal point of descent kick application
X_3, Y_3, Z_3	Cartesian coordinate system centered at the nominal point of main braking initiation
α, γ	descent kick application angles
ΔV_2	descent kick magnitude
$[\Phi]$	state transition matrix

Subscripts

1	refers to quantity evaluated in coordinate frame X_1, Y_1, Z_1.
2	refers to quantity evaluated in coordinate frame X_2, Y_2, Z_2.
3	refers to quantity evaluated in coordinate frame X_3, Y_3, Z_3.

2.1.3.1 Navigation, Guidance, and Control System Model

Possible navigation observables available for consideration during the parking orbit and descent-coast phases are local vertical, altitude to the lunar surface, and angles to stars or local landmarks. Knowledge of local vertical and orbital plane directions with respect to the vehicle is required

for the descent kick, and orbital plane direction with respect to the vehicle for main braking. These are reasonably obtained with the required accuracy by gyrocompassing the inertial platform through employment of a horizon scanner to measure local vertical (see Section 12). An altimeter would give orbital information in the orbital plane, but angle measurements to stars and/or local landmarks would be required for estimation of orbital plane celestial orientation. Preliminary analysis indicated that expected initial and terminal errors were such that altitude and orbit plane celestial orientation determination could be dispensed with for the parking and descent-coast orbits. In line with selecting the simplest possible navigation and guidance concept, gyrocompassing alone is assumed during orbital phases and is shown in later paragraphs of this report to be adequate for the mission.

The navigation and guidance concept, assumed and validated in this report, assumes a nominal coasting period of 45.5 minutes measured from termination of retrothrust to initiation of descent kick, which is commanded to be the nominal value of 67 m/sec, applied horizontally in the orbit plane and is initiated at the nominal time. Gyrocompassing only is assumed, which provides a coordinate reference for the descent kick. Gyrocompassing, only, is again assumed for the descent coast, until onboard acquisition of the line of sight to the beacon, after which vehicle-beacon range is measured. Main braking is initiated at the nominal estimated central angle separation from the beacon of 10.6 degrees. The assumption of gyrocompassing during descent coast provides out-of-plane beacon displacement information for correction of out-of-plane errors during main braking and a reference coordinate frame to aid in beacon acquisition.

2.1.3.2 Error Propagation

The desired result of the error analysis of the orbital operations is the estimation of deviations from the nominal point of main braking initiation at the nominal time of main braking initiation caused by deviations from the nominal state at the beginning of the circular parking orbit and by errors

in applying the nominal descent kick. In performing this analysis, the descent kick is treated as an impulsive maneuver.

The following definitions are made:

$\underline{p}_1$ - the vector of deviations from the nominal state at the time of parking orbit initiation (retrothrust termination), expressed in coordinate system X_1, Y_1, Z_1.

$\underline{p}_2^-$ - the vector of deviations from the nominal state after the nominal time in parking orbit prior to application of the descent kick, expressed in coordinate system X_2, Y_2, Z_2.

$\underline{p}_2^+$ - the vector of deviations from the nominal state immediately after descent kick application expressed in coordinate system X_2, Y_2, Z_2.

$\underline{p}_3$ - the vector of deviations from the nominal state after waiting the nominal time in the descent coast orbit (hence at the nominal time of main braking initiation) expressed in coordinate system X_3, Y_3, Z_3.

The coordinate systems mentioned are illustrated in figure 2-13 and defined below.

X_1, Y_1, Z_1 - a Cartesian coordinate frame centered at the nominal point of parking orbit initiation.

X_2, Y_2, Z_2 - a Cartesian coordinate frame centered at the nominal point of descent kick application.

X_3, Y_3, Z_3 - a Cartesian coordinate frame centered at the nominal point of main braking initiation.

In all three frames, the Z-coordinate is along local vertical at the point of interest, and the X-axis is in the nominal plane of motion, but opposite to the general direction of motion.

2.1.3.2.1 Error Propagation Through Coasting Phases - The propagation of initial deviations from the nominal path is estimated by linearizing about the nominal trajectory and using the concept of a state transition matrix. This approach is used to treat both orbital phases: circular parking orbit and descent coast. The elements of the transition matrices are evaluated

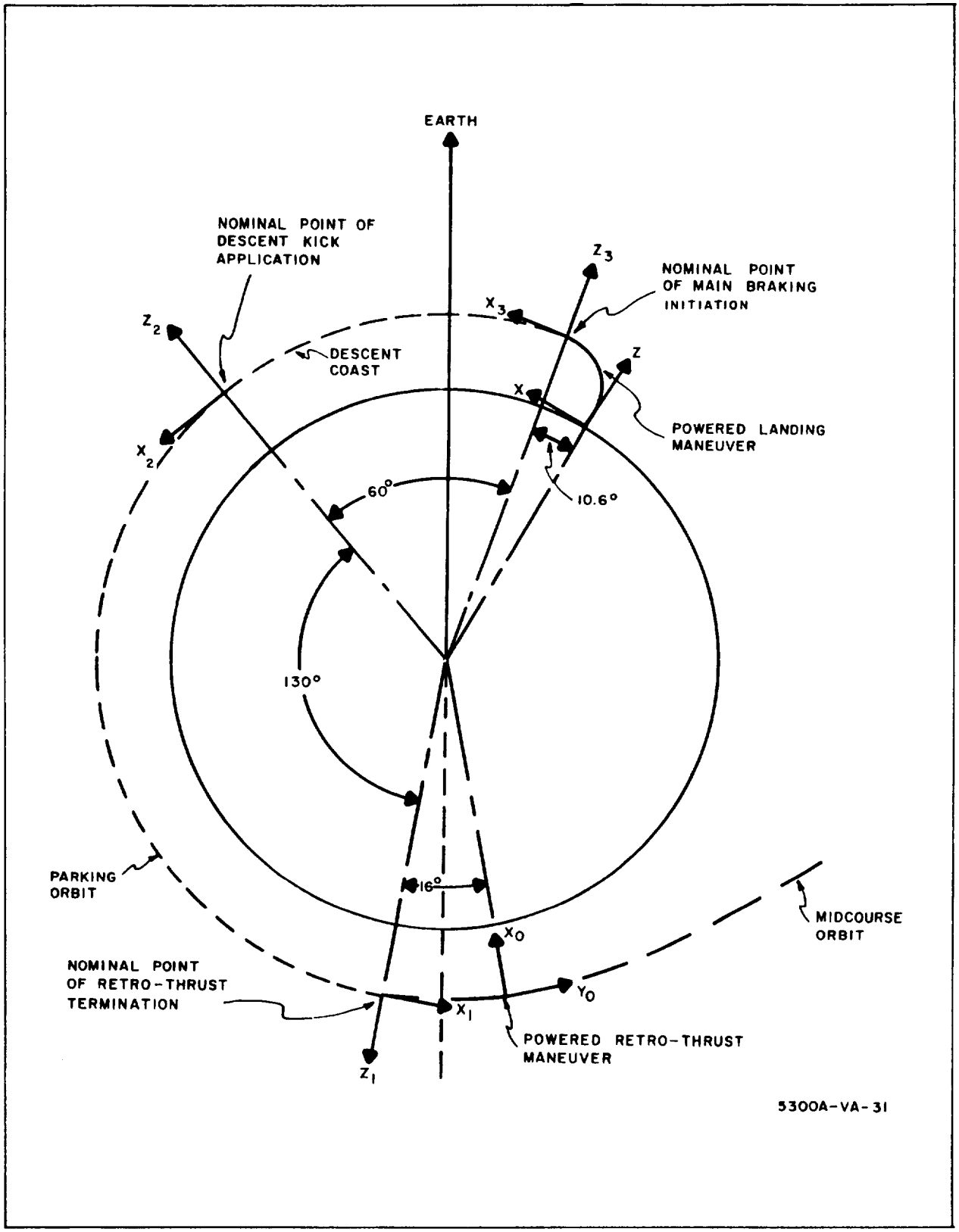

Figure 2-13. Orbit Phase Geometry

from analytical expressions* which have been programmed on the IBM 7094 computer.

Using results obtained, we can express deviations from nominal at the nominal time of descent kick application (but prior to it) as a linear function of the deviations from nominal at the end of retrothrust.

$$\underline{p}_2^- = \left[\Phi_{21}\right] \underline{p}_1 \tag{2-17}$$

Similarly the vector of deviations from nominal at the nominal time of main braking initiation is expressible in terms of the vector of deviations from nominal at the nominal time of descent kick application (but after application of the descent kick).

$$\underline{p}_3 = \left[\Phi_{32}\right] \underline{p}_2^+ \tag{2-18}$$

As a check on the accuracy of the transition matrices, deviations resulting from actual simulation runs were compared with deviations predicted using transition matrices. Excellent agreement was obtained.

2.1.3.2.2 Descent Kick Analysis - To complete the analysis, the vector $\underline{p}_2^+$ must be related to $\underline{p}_2^-$. The analysis performed to describe the injection is given in paragraph 7.1. Briefly, the maneuver is assumed to be impulsive so that only the velocity components are affected. Nominally, the injection velocity change is directed along the X_2-axis and is equal (in magnitude) to ΔV_2. Control errors result in an error in the velocity correction magnitude, δV_2, as well as deviations from the nominal direction, $\delta\alpha$, (about the Y_2-axis) and $\delta\gamma$ (about the Z_2-axis).

As a result of these control, or application errors, the deviation vector $\underline{p}_2^+$ is not equal to vector $\underline{p}_2^-$. It is shown in paragraph 7.1 that $\underline{p}_2^+$ can be described as a function of $\underline{p}_2^-$ and the application errors as follows:

*The origin of these expressions is a vector solution of the two-body problem appearing in reference 12.

$$\underline{p}_2^+ = \underline{p}_2^- + \begin{bmatrix} 0 & 0 & 0 \\ 0 & 0 & 0 \\ 0 & 0 & 0 \\ 1 & 0 & 0 \\ 0 & \Delta V_{2n} & 0 \\ 0 & 0 & -\Delta V_{2n} \end{bmatrix} \begin{bmatrix} \delta V_2 \\ \delta \gamma \\ \delta \alpha \end{bmatrix} \tag{2-19}$$

or

$$\underline{p}_2^+ = \underline{p}_2^- + [C]\ \underline{u} \tag{2-20}$$

where the matrix $[C]$ and the vector of application errors $\underline{u}$ are defined by comparison with equation 2-19. For numerical evaluation of $[C]$, ΔV_{2n} is set equal to 67 m/sec.

2.1.3.2.3 Combination - It is now possible to write a total expression giving the deviations from nominal at the nominal time of main braking initiation ($\underline{p}_3$) in terms of deviations at the end of retrothrust ($\underline{p}_1$) and the descent kick application errors ($\underline{u}$). By combining equations 2-17, 2-18, and 2-19, this expression is:

$$\underline{p}_3 = [\Phi_{32}]\ [\Phi_{21}]\ \underline{p}_1 + [\Phi_{32}]\ [C]\ \underline{u} \tag{2-21}$$

Which we write as

$$\underline{p}_3 = [S_{p_3 p_1}\ \underline{p}_1] + [S_{p_3 u}]\ \underline{u} \tag{2-22}$$

Defining sensitivity coefficient matrices $[S_{p_3 p_1}]$ and $[S_{p_3 u}]$ to be

$$[S_{p_3 p_1}] \equiv [\Phi_{32}]\ [\Phi_{21}] \tag{2-23}$$

$$[S_{p_3 u}] \equiv [\Phi_{32}]\ [C] \tag{2-24}$$

2.1.3.3 Results

The results presented here consist of the numerical evaluation of matrices $[\Phi_{21}]$, $[\Phi_{32}]$, $[S_{p_3p_1}]$, and $[S_{p_3u}]$. These results are used further in paragraph 2.1.6 where the various mission phase analyses are integrated.

$$[\Phi_{21}] = \begin{bmatrix} -2.28\times10^{0} & 0 & 5.27\times10^{0} & -4.50\times10^{3} & 0 & 3.95\times10^{3} \\ 0 & -6.41\times10^{-1} & 0 & 0 & 9.25\times10^{2} & 0 \\ -7.60\times10^{-1} & 0 & 2.62\times10^{0} & -3.94\times10^{3} & 0 & 9.13\times10^{2} \\ -6.39\times10^{-4} & 0 & 1.38\times10^{-3} & -2.30\times10^{0} & 0 & 7.77\times10^{-1} \\ 0 & -6.37\times10^{-4} & 0 & 0 & -6.41\times10^{-1} & 0 \\ -1.36\times10^{-3} & 0 & 5.00\times10^{-3} & -5.26\times10^{0} & 0 & 2.64\times10^{0} \end{bmatrix} \quad (2\text{-}25)$$

$$[\Phi_{32}] = \begin{bmatrix} -2.19\times10^{-2} & 0 & 1.44\times10^{0} & 3.76\times10^{2} & 0 & 1.23\times10^{3} \\ 0 & 4.78\times10^{-1} & 0 & 0 & 1.04\times10^{3} & 0 \\ -8.66\times10^{-1} & 0 & 1.56\times10^{0} & -1.23\times10^{3} & 0 & 1.09\times10^{3} \\ -7.50\times10^{-4} & 0 & 4.32\times10^{-4} & -4.53\times10^{-2} & 0 & 8.68\times10^{-1} \\ 0 & -7.5\times10^{-4} & 0 & 0 & 4.55\times10^{-1} & 0 \\ -4.53\times10^{-4} & 0 & 2.05\times10^{-3} & -1.47\times10^{0} & 0 & 1.62\times10^{0} \end{bmatrix} \quad (2\text{-}26)$$

$$[S_{p_3p_1}] = \begin{bmatrix} -2.96\times10^{0} & 0 & 1.03\times10^{1} & -1.25\times10^{4} & 0 & 4.77\times10^{3} \\ 0 & -9.69\times10^{-1} & 0 & 0 & -2.24\times10^{2} & 0 \\ 9.24\times10^{-2} & 0 & 3.27\times10^{0} & -5.15\times10^{3} & 0 & -7.45\times10^{1} \\ 2.33\times10^{-4} & 0 & 1.45\times10^{-3} & -2.78\times10^{0} & 0 & -3.15\times10^{-1} \\ 0 & 1.91\times10^{-4} & 0 & 0 & -9.86\times10^{-1} & 0 \\ -1.79\times10^{-3} & 0 & 9.05\times10^{-3} & -1.12\times10^{1} & 0 & 3.21\times10^{0} \end{bmatrix} \quad (2\text{-}27)$$

$$\left[S_{p_3 u}\right] = \begin{bmatrix} 3.76\times10^{2} & 0 & -8.24\times10^{4} \\ 0 & 6.95\times10^{4} & 0 \\ -1.23\times10^{3} & 0 & -7.30\times10^{4} \\ -4.53\times10^{-2} & 0 & -5.82\times10^{1} \\ 0 & 2.98\times10^{1} & 0 \\ -1.47\times10^{0} & 0 & -1.09\times10^{2} \end{bmatrix} \tag{2-28}$$

2.1.4 Main Braking Phase

This paragraph covers the description of trajectory and guidance system models, analytical techniques used, and results obtained in investigating the main braking phase of the orbital mission profile.

The geometry for this phase is shown in figure 2-14. A glossary of terms and symbols as used in this paragraph follows:

Symbols

M	Vehicle mass
R	Range from beacon to vehicle
X, Y, Z	Beacon-centered Cartesian coordinates
α	Angle between velocity vector and thrust vector
Γ_{los}	Angle between line-of-sight to beacon and velocity vector
Θ	Lunar central angle from beacon to vehicle
Θ_a	Vehicle attitude angle
Θ_{los}	Angle between line of sight to beacon and thrust axis
Ψ	Angle between beacon local vertical and range vector from beacon to vehicle

Subscripts

f	Final value (at the end of main braking phase)
i	Initial value (at the start of main braking)
j, k	Matrix and vector indices
n	Nominal value
ref.	Reference value

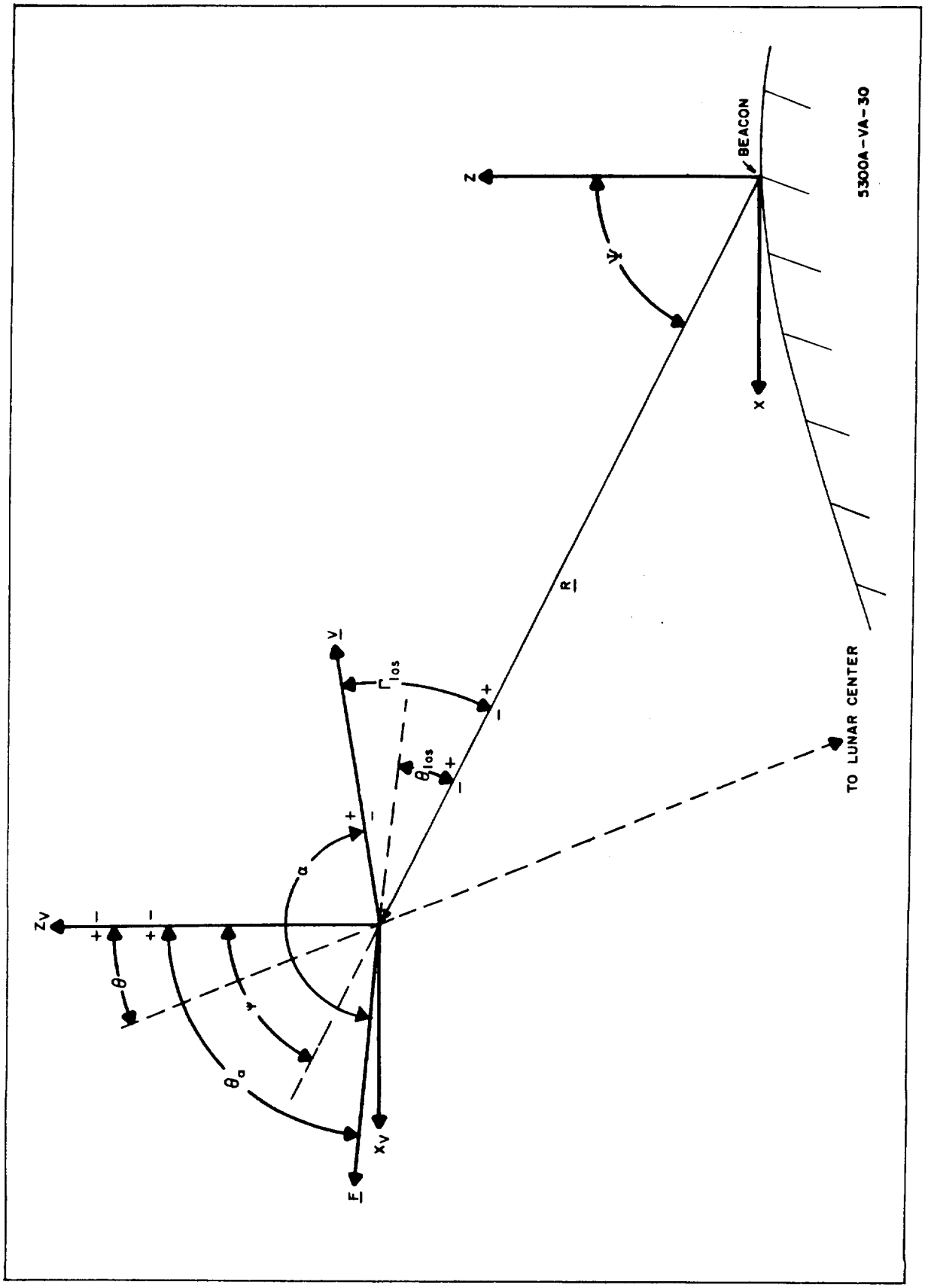

Figure 2-14. Main Breaking Phase Geometry

2.1.4.1 Requirements, Trajectory Model, and Geometry

Nominally, L-II stage engine ignition for the main braking phase occurs at the end of the 60-degree descent coast when the vehicle is at a central angle of 10.6 degrees from the beacon. The main braking maneuver is terminated at 300-meter altitude over the target and is followed by the touchdown phase, requirements for which differ sufficiently from main braking to warrant a separate analysis (paragraph 2.1.4).

The geometry for the two-dimensional orbital plane analysis constituting the principal study effort for main braking is shown in figure 2-14. Expected out-of-plane initial condition errors were small enough (see paragraph 2.1.1.4) to be considered independently. *

The nominal trajectory for this study is generated by an iterative technique implemented on the IBM 7094 as discussed in paragraph 8.1 and is specified by the simple pitch program given in reference 4. It is shown there that the trajectory generated yields fuel consumption only about 1 percent greater than that of the theoretically optimum trajectory.

The thrust angle program is:

α = 195 degrees for R > 12.8 km

α = 180 degrees for R $\leq$ 12.8 km

where α is the angle between the thrust and velocity vectors (see figure 2-14). Thus, the α = 180 degree portion generates a gravity turn.

A constant thrust level of 106,750 newtons (24,000 lb) is taken to be the nominal thrust magnitude profile. This is 80 percent of the maximum thrust available from the 2 RL-10-type engines postulated to be on the spacecraft, allowing a 20-percent margin for correction of errors.

* A brief investigation to estimate fuel requirements to correct out-of-plane errors during main braking was done assuming an extremely simple system model. Results show that to correct out-of-plane errors of the magnitude indicated in paragraph 2.1.1.4 requires an amount of fuel that is less than 5 percent of the nominal landing fuel consumption (see paragraph 8.5).

The resulting nominal initial and final conditions of the vehicle are summarized below, with geometrical quantities expressed in the target local vertical coordinate system (figure 2-14).

- Initial Conditions

X_{in} = 340.56 km

Z_{in} = 70.11 km

$\dot{X}_{in}$ = -1593.4 m/s

$\dot{Z}_{in}$ = 195.85 m/s

t_i = 0

M_{in} = 30,040 kg

- Final Conditions

X_{fn} = -250 m

Z_{fn} = 300 m

$\dot{X}_{fn}$ = -9.30 m/s

$\dot{Z}_{fn}$ = -37.0 m/s

t_{fn} = 435.3 sec

M_{fn} = 19,271 kg

It will be noted that:

- The nominal end point is horizontally offset from the target by 250 meters, ensuring that the vehicle does not land directly on the target site beacon; and the offset is in a direction to require the spacecraft to fly over the target site, which is preferred because of practical beacon tracking requirements.
- The nominal horizontal velocity at the end of main braking is not zero, a factor to be considered when specifying allowable deviations from the nominal horizontal velocity at the end of main braking.
- The nominal vertical velocity at the end of main braking is a specified input to the nominal trajectory determination digital program. The particular value given (-37 m/sec) results in a required thrust in the middle of the available thrust range to reduce vertical velocity to zero while the vehicle descends the remaining 300 meters to the surface. It is felt that such a specification allows a reasonably efficient final touchdown maneuver with adequate capability for correcting deviations from nominal at the end of main braking.

- Nominal motion is entirely contained in the X-Z plane. Therefore Y and $\dot{Y}$ are zero.

2.1.4.2 Navigation, Guidance, and Control System Model

The analytical system model used in this study is shown in figure 2-15. Dashed lines are used to indicate the divisions between navigation, guidance, and control functions. The blocks labeled "dynamics" and "geometry" represent the vehicle equations of motion and the transformation between the Cartesian X-Z coordinates and beacon tracker observables. These blocks would not be mechanized on board the vehicle and are not detailed here.

2.1.4.2.1 Navigation - The most readily available set of navigation observables are those available from measurements to the specified landing site beacon. As shown in figure 2-14, these observables, in the vertical plane, are:

R	Range to the beacon
$\dot{R}$	Range rate to the beacon
Θ_{los}	Angle between beacon sightline and vehicle roll axis
Ψ	Inertial rate of beacon sightline

The attitude angle Θ_a is also observable on board the vehicle so that the angle Ψ could be computed, if desired, although this is not used in the system shown in figure 2-15.

To represent the sensing process in the analytical model, a dynamic response of the form following is assigned:

$$\frac{1}{1 + T_{Q_j} s}$$

to represent the relationship between the actual value of the observable and the value observed on board the vehicle (where s is the Laplace variable). This provides the shaping function to define the characteristics of wideband noise entering the system, and is felt to be an adequate approximation to actual sensor dynamic performance.

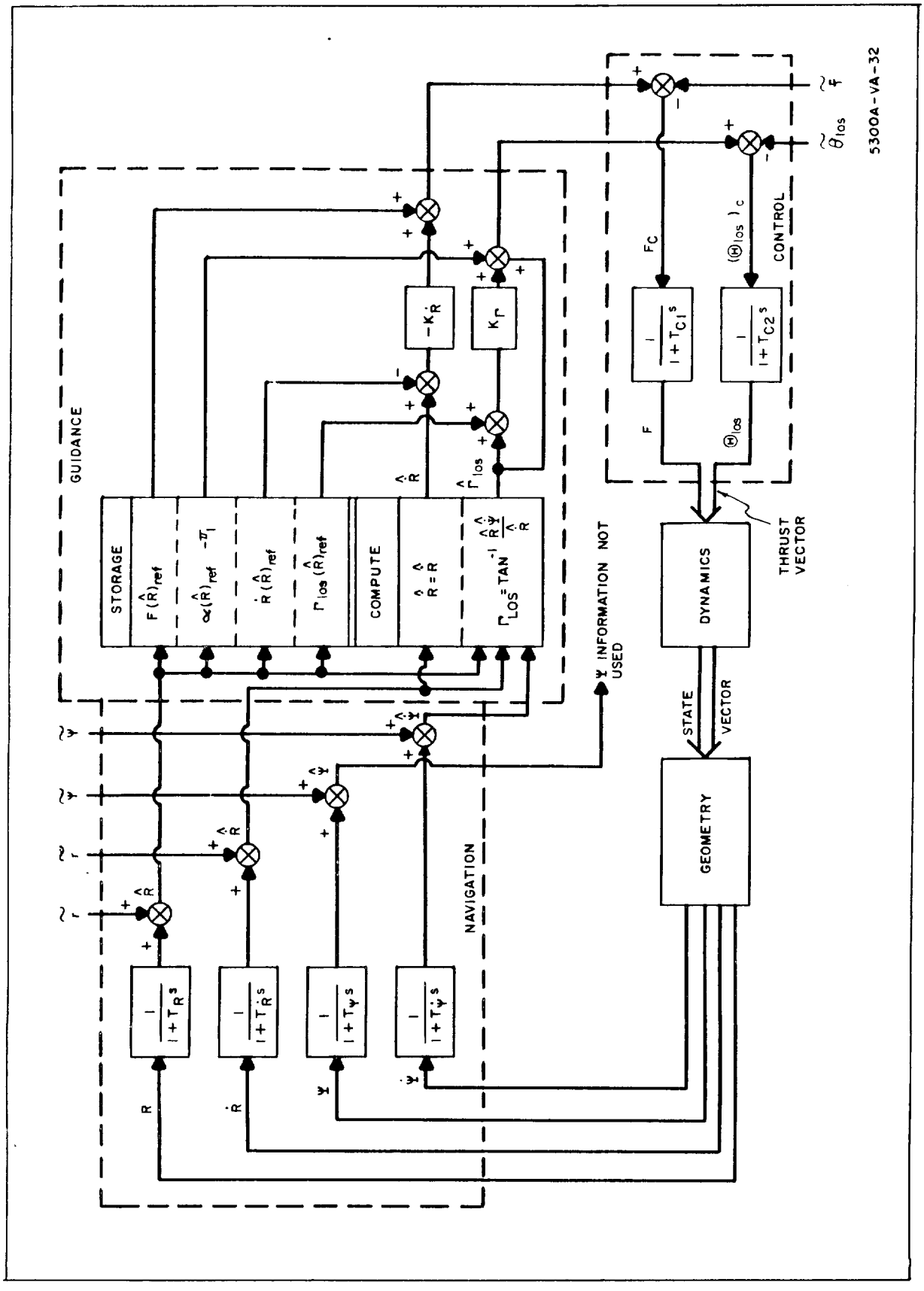

Figure 2-15. Navigation, Guidance, and Control System Model

For this study, the time constants T_{Q_j} of all the sensor response characteristics are set equal to 0.25 second. The equivalent 1-cps noise bandwidth is typical of sensors considered.

The sensor output is degraded by the addition random noise and bias errors. For example, the total error in observing R is denoted $\tilde{r}$. Then the estimated value of R is denoted $\hat{R}$ and is equal to $R + \tilde{r}$. The detailed characterization of the sensor error model is presented in paragraph 2.1.4.3.

2.1.4.2.2 Guidance - The basic guidance equations used for this study, given in references 4 and 5, represent an implicit scheme wherein the guidance parameters are computed from navigation information and are then compared to precomputed reference values, which are stored in the guidance computer as functions of range to the beacon. The differences between estimated and reference values are used to generate deviations from the nominal thrust program to force the vehicle back to the nominal flightpath.

The two-dimensional guidance law, referred to as line-of-sight rate guidance, is represented by the following equations.

$$F_c = F_{ref}(\hat{R}) - K_{\dot{R}} \left| \dot{\hat{R}} - \dot{\hat{R}}_{ref}(\hat{R}) \right| \tag{2-29}$$

$$\alpha_c = \alpha_{ref}(\hat{R}) + K_{\Gamma} \left| \hat{\Gamma}_{los} - \left(\Gamma_{los}(\hat{R})\right)_{ref} \right| \tag{2-30}$$

Thus, the commanded thrust magnitude F_c is equal to the reference level minus a positive constant $K_{\dot{R}}$ times the difference between the observed range rate and the reference range rate. Similarly, the commanded thrust angle α_c is equal to the reference value plus a positive constant times the difference between the estimated value of Γ_{los} and the stored reference value. The reference values are stored as functions of the estimated beacon-to-spacecraft range.

To implement F_c, it is assumed that the thrust level is monitored, perhaps by monitoring throttle position. However, the angle α is not observable so the

corresponding guidance equation is modified as follows. The angle Θ_{los} is directly observable from beacon tracking information. Then, from the geometry shown in figure 2-14 it is seen that

$$\Theta_{los} + \pi = \alpha + \Gamma_{los} \tag{2-31}$$

Then, the commanded value of Θ_{los} is:

$$\left(\Theta_{los}\right)_c = \alpha_c + \Gamma_{los} - \pi \tag{2-32}$$

which expanded is:

$$\left(\Theta_{los}\right)_c = \alpha_{ref}(\hat{R}) - \pi + \hat{\Gamma}_{los} + K_\Gamma \left[\Gamma_{los} - \left(\Gamma_{los}(\hat{R})\right)_{ref}\right] \tag{2-33}$$

Equations 2-29 and 2-33 constitute the guidance equations for the analytical model.

The guidance parameters are readily expressible in terms of beacon tracker observables:

$$\dot{\hat{R}} = \dot{\hat{R}} \tag{2-34}$$

$$\hat{\Gamma}_{los} = \tan^{-1}\left[\frac{\hat{R}\dot{\hat{\Psi}}}{\dot{\hat{R}}}\right] \tag{2-35}$$

Based on previous investigations outside the scope of the present study, references 4 and 5, the reference thrust vector and gain constants are

$$F_{ref}(\hat{R}) = 106,750 \text{ N for all } \hat{R}$$

$$\alpha_{ref}(\hat{R}) = \begin{cases} 195^\circ; & \hat{R} > 12.8 \text{ km} \\ 180^\circ; & \hat{R} \leq 12.8 \text{ km} \end{cases}$$

$$K_{\dot{R}} = 5115 \text{ newtons/m/sec}$$

$$K_\Gamma = 4.00 \text{ rad./rad.}$$

The reference curves $\dot{R}_{ref}(\hat{R})$ and $\left(\Gamma_{los}(\hat{R})\right)_{ref}$ used in this study are polynominal approximations based on nominal trajectory data, and are given in paragraph 8.1.

2.1.4.2.3 Control - Reference 4 goes into a great deal of detail in discussing the thrust magnitude and the attitude control loops, particularly

stability considerations of the attitude loop. One of the useful findings is that proper design of these loops to ensure stability (particularly the attitude loop where compensation is used) leads to a system whose dynamic characteristics can be described adequately by simple transfer functions of the form

$$\frac{1}{1 + Ts}$$

Since this study is concerned primarily with determining the effects of navigation errors, it is felt that the control function can be represented by these simple functions. Hence, in the system model, the actual thrust vector parameters F and Θ_{los} are related to the commanded values by the following transfer functions.

$$\frac{F}{F_c}(s) = \frac{1}{1 + T_{C1}s} \tag{2-36}$$

$$\frac{\Theta_{los}}{(\Theta_{los})_c}(s) = \frac{1}{1 + T_{C2}s} \tag{2-37}$$

where s is the Laplace variable based on information in reference 4 the time constants T_{C1} and T_{C2} are set equal to 2 seconds.

Note that the commanded values of F and Θ_{los} derived from the guidance law are degraded by errors denoted $\tilde{f}$ and $\tilde{\theta}_{los}$. These represent errors introduced by the sensors used to close the control loops. The detailed characteristics of the error model used is discussed in paragraph 2.1.4.3 and also in paragraphs 8.2 and 8.3.

2.1.4.3 Error Model

This paragraph discusses main braking system error sources and their characterization. Error sources considered are: (1) initial deviations from the nominal flightpath, and (2) random and bias navigation and control sensor errors existing throughout the main braking maneuver. Because, in the vertical plane, thrust angle is commanded with respect to the vehicle--beacon line of sight in the guidance law used, inertial platform misalignment

is not a consideration and is significant only with regard to measurement of out-of-plane errors.

In the following paragraphs, nomenclature and characteristics of the error models used are defined.

2.1.4.3.1 Initial Deviations from Nominal - The state of the vehicle during main braking is defined in terms of an X-Z coordinate system fixed to the beacon site with Z along beacon local vertical and X along beacon horizontal, positive in the direction of the initial spacecraft position (see figure 2-14). If the actual vehicle initial state vector is denoted by $\underline{P}_i$, and $\underline{P}_{in}$ is the nominal initial state, then the vector of initial deviations from nominal, $\underline{p}_i$ is defined as the difference:

$$\underline{p}_i = \underline{P}_i - \underline{P}_{in} \tag{2-38}$$

or

$$\underline{p}_i = \begin{bmatrix} x_i \\ z_i \\ \dot{x}_i \\ \dot{z}_i \end{bmatrix} = \begin{bmatrix} X_i \\ Z_i \\ \dot{X}_i \\ \dot{Z}_i \end{bmatrix} - \begin{bmatrix} X_{in} \\ Z_{in} \\ \dot{X}_{in} \\ \dot{Z}_{in} \end{bmatrix} \tag{2-39}$$

These deviations are, of course, fixed for any particular flight by that part of the flight preceding main braking. However, over the ensemble of possible repetitions of the mission flight, they become random and can be discussed only in terms of statistical averages. For this study, the ensemble statistical distributions of the elements of $\underline{p}_i$ are assumed to be gaussian with zero mean. The elements of $\underline{p}_i$ are not assumed to be statistically independent of one another. The correlations involved are determined by the characteristics of previous mission phases.

2.1.4.3.2 Sensor Errors - The quantities observed by the navigation and control system sensors are:

R Range to the beacon

$\dot{R}$ Range rate to the beacon

Ψ Line of sight angle from beacon local vertical

$\dot{\Psi}$ Line of sight angle rate

F Thrust magnitude

Θ_{los} Angle between line of sight to beacon and vehicle roll axis.

These quantities are defined geometrically in figure 2-15. The vector of observables, $\underline{Q}$, has as its elements these observable quantities in the following form:

$$\underline{Q} \equiv \begin{bmatrix} R \\ \dot{R} \\ \Psi \\ \dot{\Psi} \\ F \\ \Theta_{los} \end{bmatrix} \tag{2-40}$$

The estimated observables, $\hat{\underline{Q}}$, are defined to be the actual values plus the estimation errors, $\tilde{\underline{q}}$

$$\hat{\underline{Q}} = \underline{Q} + \tilde{\underline{q}} \tag{2-41}$$

which expanded is

$$\hat{\underline{Q}} \equiv \begin{bmatrix} \hat{R} \\ \hat{\dot{R}} \\ \hat{\Psi} \\ \hat{\dot{\Psi}} \\ \hat{F} \\ \Theta_{los} \end{bmatrix} = \begin{bmatrix} R \\ \dot{R} \\ \Psi \\ \dot{\Psi} \\ F \\ \Theta_{los} \end{bmatrix} + \begin{bmatrix} \tilde{r} \\ \tilde{\dot{r}} \\ \tilde{\psi} \\ \tilde{\dot{\psi}} \\ \tilde{f} \\ \tilde{\theta}_{los} \end{bmatrix} \tag{2-42}$$

The general estimation error model is now described in terms of $\tilde{q}_j$, the general element of vector $\underline{\tilde{q}}$ where j can take on the values 1, 2, ... 6. For example,

$$\tilde{q}_2 = \tilde{r} \tag{2-43}$$

The total estimation error $\tilde{q}_j$ is the sum of four components

$$\tilde{q}_j(t) \equiv \tilde{q}_{jbc} + \tilde{q}_{jbs} \frac{Q_j(t)}{100} + \tilde{q}_{jnc}(t) + \tilde{q}_{jns}(t) \frac{Q_j(t)}{100} \tag{2-44}$$

where the four components have the following characteristics.

- $\tilde{q}_{jbc}$ A bias error in the j^{th} observable. $\tilde{q}_{jbc}$ is constant over any particular mission, but a zero mean, gaussian distributed random variable over the ensemble of missions. The ensemble mean squared value is denoted $\sigma^2_{\tilde{q}_{jbc}}$. The dimension of $\tilde{q}_{jbc}$ is the same as that of Q_j.
- $\tilde{q}_{jbs}$ A bias scale factor error coefficient. $\tilde{q}_{jbs}$ is constant over any particular mission, but a zero mean, gaussian distributed random variable over the ensemble of missions. The ensemble mean squared value is denoted $\sigma^2_{\tilde{q}_{jbs}}$ and the dimension of $\tilde{q}_{jbs}$ is percent.
- $\tilde{q}_{jnc}(t)$ A random fluctuation error (hence the argument t). The value of $\tilde{q}_{jnc}(t)$ fluctuates randomly during each mission, but the mean squared value is constant. Specifically, $\tilde{q}_{jnc}(t)$ is defined to be a sample of gaussian distributed, ergodic, zero mean noise. The dimension $\tilde{q}_{jnc}(t)$ is the same as that of Q_j and the mean squared value is denoted $\sigma^2_{\tilde{q}_{jnc}}$.
- $\tilde{q}_{jns}(t)$ A random scale factor fluctuation error. Definitively, $\tilde{q}_{jns}(t)$ is a sample of gaussian distributed, zero mean, ergodic noise. The dimension of $\tilde{q}_{jns}(t)$ is percent and the mean squared value denoted $\sigma^2_{\tilde{q}_{jns}}$ is a constant.

The constancy of the mean squared values of $\tilde{q}_{jnc}(t)$ and $\tilde{q}_{jns}(t)$ is implied by the assumption that these respective noise samples are ergodic. For ease

in writing, the time arguments are omitted in later expressions. However, they are to be understood as in equation 2-44 and the subsequent definitions.

Two other vectors which will be useful in later work are also defined:

$$\underset{\sim}{\sigma}^2_{q_{nc}} \equiv \begin{bmatrix} \underset{\sim}{\sigma}^2_{r_{nc}} \\ \underset{\sim}{\sigma}^2_{\dot{r}_{nc}} \\ \underset{\sim}{\sigma}^2_{\psi_{nc}} \\ \underset{\sim}{\sigma}^2_{\dot{\psi}_{nc}} \\ \underset{\sim}{\sigma}^2_{f_{nc}} \\ \sigma^2_{\left(\underset{\sim}{\theta}_{los}\right)_{nc}} \end{bmatrix} \tag{2-45}$$

and

$$\underset{\sim}{\sigma}^2_{q_{ns}} \equiv \begin{bmatrix} \underset{\sim}{\sigma}^2_{r_{ns}} \\ \underset{\sim}{\sigma}^2_{\dot{r}_{ns}} \\ \underset{\sim}{\sigma}^2_{\psi_{ns}} \\ \underset{\sim}{\sigma}^2_{\dot{\psi}_{ns}} \\ \underset{\sim}{\sigma}^2_{f_{ns}} \\ \sigma^2_{\left(\underset{\sim}{\theta}_{los}\right)_{ns}} \end{bmatrix} \tag{2-46}$$

2.1.4.4 Error Analysis

A linearized error analysis is performed, utilizing the principle of superposition to calculate separately the effect of the various error sources acting simultaneously. Matrices of sensitivity coefficients are obtained which are used to estimate deviations from the nominal point of main braking terminator

resulting from: (1) random navigation and control sensor errors, represented symbolically by the vectors $\underset{\sim}{\tilde{q}}_{nc}$ and $\underset{\sim}{\tilde{q}}_{ns}$ as defined in paragraph 2.1.4.3; (2) bias components, similarly represented by $\underset{\sim}{\tilde{q}}_{bc}$ and $\underset{\sim}{\tilde{q}}_{bs}$; and (3) state vector initial condition deviations, $\underset{\sim}{p}_i$. Methods and results are discussed in the following paragraphs.

2.1.4.4.1 Random Sensor Errors - A technique often used for determining random error propagation in nonlinear systems is to linearize the system around the nominal operating point (in this case, the nominal trajectory). This step leads to straightforward solution if the resulting linearized system is characterized by constant gain coefficients. However, in generating the linearized system model for use in this study (figure 8-2 in paragraph 8.3), many of the partial derivations obtained (which can be thought of system gains) are time varying in nature. While this in itself does not negate the applicability of the usual methods of linear system analysis (impulse response, power spectrum relationships, autocorrelation), it does mean that their use will be extremely inefficient in terms of computer time required.* This is especially true since another linear analysis technique, the method of adjoint systems, is available for use. This latter is the technique which has been used to investigate the effects of navigation and control system random error inputs.

The starting point is the linearized system model. From this model, the system model adjoint to the linearized system is easily generated (figure 8-3, paragraph 8.3). To the outputs of the adjoint system model are added some data processing computations and the resulting model is simulated on the Univac 1107 digital computer. The data processing is required so that program outputs are in immediately useful form.

---

* For detailed discussion of the reason behind this statement and for theoretical description of the method of adjoint system error analysis see references 10 and 11.

The outputs of the adjoint system simulation are sensitivity coefficients which relate mean squared deviations from the nominal end point after the nominal time of flight to the mean squared values of each of the input random errors. It is important to note the phrase "after the nominal time of flight." Since in the mission profile it is stated that main braking is terminated when the estimated altitude is equal to the desired final altitude (300 meters), it is clear that the sensitivity coefficients generated by the adjoint program are not, in general, evaluated at the proper time. To take this into account, the adjoint simulation results have been modified according to the method described in paragraph 8.4. The numerical results presented in this section are the adjoint simulation results after modification to compensate for the change in main braking termination criterion.

The results obtained from the adjoint simulation are the elements of two sensitivity coefficient matrices, $\left[S_{p_f \tilde{q}_{nc}}\right]$ and $\left[S_{p_f \tilde{q}_{ns}}\right]$. These matrices are then used to estimate the mean squared deviations from nominal at main braking termination caused by random sensor errors according to the expression

$$\underline{\sigma}^2_{p_f \tilde{q}_n} = \left| S_{p_f \tilde{q}_{nc}} \right| \underline{\sigma}^2_{\tilde{q}_{nc}} + \left| S_{p_f \tilde{q}_{ns}} \right| \underline{\sigma}^2_{\tilde{q}_{ns}} \tag{2-47}$$

$$= \underline{\sigma}^2_{p_f \tilde{q}_{nc}} + \underline{\sigma}^2_{p_f \tilde{q}_{ns}} \tag{2-48}$$

where

$$\underline{\sigma}^2_{p_f \tilde{q}_n} \equiv \begin{bmatrix} \sigma^2_{x_f \tilde{q}_n} \\ \sigma^2_{z_f \tilde{q}_n} \\ \sigma^2_{\dot{x}_f \tilde{q}_n} \\ \sigma^2_{\dot{z}_f \tilde{q}_n} \end{bmatrix} \tag{2-49}$$

and $\underline{\sigma}^2_{\tilde{q}_{nc}}$ and $\underline{\sigma}^2_{\tilde{q}_{ns}}$ are as defined in paragraphs 2.1.4.3. Qualitatively, $\sigma^2_{x_f \tilde{q}_n}$ is the total mean squared position deviation from nominal in the X direction at the end of main braking caused by random navigation and control sensor errors occurring during the main braking maneuver. The remaining elements of $\underline{\sigma}^2_{p_f \tilde{q}_n}$ are defined similarly.

As a result of this investigation, the sensitivity coefficient matrices have been found to have the following values.

$$\left[S_{p_f \tilde{q}_{nc}}\right] = \begin{bmatrix} 5.21\times10^{-3} & 1.60\times10^{-1} & 0 & 4.60\times10^{8} & 3.32\times10^{-8} & 1.24\times10^{3} \\ 5.90\times10^{-1} & 0 & 6.26\times10^{4} & 0 & 0 & 0 \\ 4.83\times10^{-4} & 2.14\times10^{-2} & 0 & 2.25\times10^{6} & 2.90\times10^{-10} & 1.18\times10^{1} \\ 7.02\times10^{-4} & 7.85\times10^{-2} & 0 & 6.64\times10^{7} & 2.86\times10^{-9} & 1.01\times10^{2} \end{bmatrix} \quad (2\text{-}50)$$

$$\left[S_{p_f \tilde{q}_{ns}}\right] = \begin{bmatrix} 2.87\times10^{0} & 9.79\times10^{0} & 0 & 2.60\times10^{-1} & 3.72\times10^{-2} & 2.82\times10^{-2} \\ 9.03\times10^{0} & 0 & 3.02\times10^{0} & 0 & 0 & 0 \\ 2.33\times10^{-2} & 3.66\times10^{-2} & 0 & 3.97\times10^{-3} & 3.31\times10^{-4} & 3.90\times10^{-4} \\ 3.00\times10^{-1} & 9.21\times10^{-1} & 0 & 2.38\times10^{-2} & 3.25\times10^{-3} & 3.26\times10^{-3} \end{bmatrix} \quad (2\text{-}51)$$

2.1.4.4.2 Bias and Initial Condition Errors - This discussion describes the technique used to investigate bias and initial condition errors which are characterized as being constant over any particular mission, but random over the ensemble of missions. Thus, the errors are in a sense random, and in another sense deterministic.

The deterministic nature is taken advantage of by using a direct simulation of the nonlinear system model as a tool in the investigation. The approach is to first generate the digital simulation program and with

provision for sensor bias error inputs and initial condition inputs. The resulting model is described and illustrated in paragraph 8.2. Then, a simulation run is made with all sensor error levels set to zero (no sensor error) and the initial conditions set to their nominal values. This is referred to as the standard run. Finally, a series of runs are made with one nonzero sensor error input or one nonstandard initial condition. * The resulting terminal state is compared to the standard run terminal state to determine the effect of the input error. By this technique (which is the same technique used for retrothrust phase analysis), sensitivity coefficients are generated which relate the vector of deviations from nominal at the end of main braking, $\underline{p}_f$ to the two vectors of sensor bias errors, $\underline{\tilde{q}}_{bc}$ and $\underline{\tilde{q}}_{bs}$ (constant and scale factor errors, respectively); and to the vector of deviations from nominal at the initiation of main braking, $\underline{p}_i$. The form of this relationship is illustrated by equation 2-52:

$$\underline{p}_f = \left[S_{p_f p_i}\right] \underline{p}_i + \left[S_{p_f \tilde{q}_{bc}}\right] \underline{\tilde{q}}_{bc} + \left[S_{p_f \tilde{q}_{bs}}\right] \underline{\tilde{q}}_{bs} \qquad (2\text{-}52)^{**}$$

Expressing the terminal deviation vector in this form assumes linearity in the region about the nominal trajectory. To support this assumption, further simulation runs are made with assumed input error levels several times larger than those used in the first group. (These runs also consider only one input at a time.) The results of these runs are compared to the standard case, generating new estimates of the sensitivity coefficient

---

* The error levels assumed in making these runs are typical of the error values expected to occur in practice; e.g., initial deviation on the order of kilometers and meters per second, and realistic estimates of sensor error levels.

** Note that this expression does not include random error effects, so that the vector given by evaluating equation 2-52 is actually only the contribution to the total terminal deviation vector resulting from the indicated error sources.

matrices. In all cases, excellent agreement with the initial estimates was obtained.

A second check on the linearity assumption is to make composite runs; i.e., runs with several error inputs acting simultaneously. The simulation results are compared with deviations predicted by application of sensitivity coefficients. In general, comparisons were good. The maximum deviation of an estimated final deviation from the value determined by simulation was only 10 percent, with differences on the order of 5 percent being more common.

On the basis of these checks of linearization assumptions, it is judged that the sensitivity coefficient matrices derived can be used to provide ensemble statistical information concerning the performance of the main braking guidance scheme in the presence of bias errors and initial condition errors. The ensemble referred to is the ensemble of missions. In particular, the statistical information which is sought is the covariance matrix of the terminal deviation vector $\underline{p}_f$. The detailed derivation of this quantity is postponed until paragraph 2.1.6 which deals with mission integration.

The numerical evaluation of the sensitivity coefficient matrices obtained by application of the technique described are given below:

$$\left[S_{p_f p_i}\right] = \begin{bmatrix} 4.0\times10^{-6} & -2.25\times10^{-3} & -1.01\times10^{-1} & -2.32\times10^{-1} \\ 0 & 0 & 0 & 0 \\ -6.2\times10^{-7} & 2.67\times10^{-4} & 9.62\times10^{-3} & 2.82\times10^{-2} \\ 6.07\times10^{-7} & -1.94\times10^{-2} & -1.94\times10^{-2} & -2.66\times10^{-2} \end{bmatrix} \quad (2\text{-}53)$$

$$\left[S_{p_f \tilde{q}_{bc}}\right] = \begin{bmatrix} 7.52\times10^{-1} & 5.16\times10^{0} & 0 & -3.39\times10^{5} & -4.34\times10^{-4} & -9.26\times10^{2} \\ -7.69\times10^{-1} & 0 & -2.50\times10^{2} & 0 & 0 & 0 \\ 4.11\times10^{-2} & -2.94\times10^{-2} & 0 & 4.10\times10^{4} & -5.39\times10^{-5} & 9.01\times10^{1} \\ -4.92\times10^{-2} & -9.33\times10^{-1} & 0 & -4.02\times10^{4} & -3.87\times10^{-4} & -1.28\times10^{2} \end{bmatrix}$$

(2-54)

$$\left[S_{p_f \tilde{q}_{bs}}\right] = \begin{bmatrix} 1.15\times10^{1} & -6.16\times10^{0} & 0 & 1.20\times10^{1} & \text{n. c.}* & \text{n. c.}** \\ -3.00\times10^{0} & 0 & 1.74\times10^{0} & 0 & 0 & 0 \\ -6.56\times10^{-1} & 5.28\times10^{-1} & 0 & -9.02\times10^{-1} & \text{n. c.}* & \text{n. c.}** \\ 7.86\times10^{-1} & -8.2\times10^{-2} & 0 & 1.75\times10^{0} & \text{n. c.}* & \text{n. c.}** \end{bmatrix}$$

(2-55)

It will be noted that there is a preponderance of zeroes in the second row of each of these matrices. The reason is that vertical position is used as the criterion for terminating the main braking maneuver. Therefore, only errors in estimating the value of Z contribute to terminal vertical (Z-direction) position errors. These contributions are represented by the nonzero elements in the second row of the sensor error matrices $\left[S_{p_f \tilde{q}_{bc}}\right]$ and $\left[S_{p_f \tilde{q}_{bs}}\right]$.

---

*The coefficients of the fifth column of $\left[S_{p_f \tilde{q}_{bs}}\right]$ are not computed because the nature of the corresponding error source, a scale factor error in measuring applied thrust. Since the thrust level is nearly constant throughout main braking a bias scale factor error is essentially the same as a constant bias error. This type of error is taken into account by the matrix, $\left[S_{p_f \tilde{q}_{bc}}\right]$.

** The coefficients of the sixth column of $\left[S_{p_f \tilde{q}_{bs}}\right]$ are not computed because the corresponding error source is an angle measurement (Θ_{los}) and scale factor errors are not customarily considered as components of angle measurement errors.

The large number of zeroes in the third column of matrices $\left[S_{p_f \tilde{q}_{bc}}\right]$ and $\left[S_{p_f \tilde{q}_{bs}}\right]$ results from the fact that line-of-sight angle measurement information (the corresponding error source) is not used in the two-dimensional guidance law used as the guidance model in this study. Given this, one might expect all the third column elements to be zero. The reason they are not is that observations of the angle Ψ are required to estimate vertical position. This information is used in turn to terminate the main braking maneuver. Hence, errors in observing Ψ contributes to vertical (Z-direction) position deviations at the end of main braking.

The results derived in this section are useful in themselves; for if the characteristics of initial deviations from the nominal flight profile are known, main braking system performance can be evaluated. However, in this report, further use of these results is postponed until discussion of the integration of the independent analyses of the orbital mission phases.

2.1.5 Final Touchdown Maneuver

A glossary of terms and symbols in this paragraph follows:

Symbols:

a_F	Magnitude of thrust acceleration vector
t_l	Time of inertial navigation initiation
t_I	Time of impact
X, Y, Z	Beacon local vertical coordinate frame
X_v, Y_v, Z_v	Vehicle coordinate frame
$\tilde{\dot{x}}_l, \tilde{\dot{y}}_l, \tilde{\dot{z}}_l$	Velocity errors in initiating inertial navigator
$\tilde{\ddot{x}}_b, \tilde{\ddot{y}}_b, \tilde{\ddot{z}}_b$	Acceleration sensor bias errors
Z_s	Standoff altitude
ζ, ξ	Euler angles describing misalignment between X, Y, Z, and X_v, Y_v, Z_v coordinate frames

Θ, Φ Euler angles describing thrust vector orientations with respect to X_v, Y_v, Z_v coordinate frame

Subscripts:

I Indicates quantity evaluated at t_1

D Indicates a desired value

F Indicates component of acceleration caused by vehicle thrust

I Indicates quantity evaluated at t_I

There are many navigation and guidance concepts which could be used to define the final touchdown maneuver. Since no particular approach was designated as an input to this study, one has been selected for investigation which is felt to be typical of the possibilities. This approach is outlined below.

- At 300-meter altitude (final touchdown phase initiation altitude), an acceleration vector is computed which will reduce vehicle velocity to the desired touchdown velocity at some selected altitude above the surface.
- At 100-meter altitude, the vehicle switches to an all inertial navigation and guidance system. Initial conditions for the inertial navigator are obtained from the main braking phase navigation system which continues to function to an altitude of 100 meters.
- During the period of inertial navigation and guidance, motion in the three coordinate directions are considered to be essentially independent, with guidance based on nulling the horizontal velocity components ($\dot{X}$ and $\dot{Y}$) and making the vertical velocity equal to the desired touchdown velocity Z_D.

The principal analysis discussed in this paragraph deals only with the all inertial phase of the final touchdown maneuver. This is the portion which determines the impact errors.

It is noted from the preceding broad description of the final touchdown maneuver concept that:

- No explicit control is maintained over the horizontal components of vehicle position. It is felt that the allowed touchdown area specified as a study input is large enough, and the deviations from nominal at

the end of main braking small enough such that no horizontal position control is required to achieve satisfactory performance.

- The desired vertical velocity at impact is not zero. For this study, Z_D is taken to be -2.5 m/sec which is in the middle of the specified range of allowable touchdown velocities (0 to -5 m/sec, 3σ).

In the analysis to follow, two coordinate systems are used. These are illustrated in figure 2-16 and defined below:

- X, Y, Z: Beacon coordinates. A beacon-centered coordinate frame with Z along local vertical. X is in the nominal plane of the main braking maneuver and positive toward the position of the vehicle at main braking initiation.
- X_v, Y_v, Z_v: Vehicle coordinates. The vehicle inertial reference coordinate system. Nominally X_v, Y_v, Z_v are identical to X, Y, Z, however, misalignment will occur and is represented by the alignment error angles ζ and ξ (see figure 2-16).

The onboard navigation and guidance system makes observations and commands accelerations with respect to the coordinate frame X_v, Y_v, Z_v.

In establishing the system model and performing the subsequent analysis, it is assumed that the vehicle is operating in a uniform constant gravitational field. The region occupied by the maneuver is so small that this assumption is very good. The gravitational acceleration is

$$g_m = 1.63 \text{ m/sec}^2$$

In addition, the following constants are assumed.

- Maximum thrust level: 133,400 N
- The maximum allowed attitude deviation from estimated local vertical is 10 degrees at impact. This restriction limits the available horizontal acceleration levels.

Finally, the touchdown requirements which are used to determine requirements for performing the final touchdown maneuver using inertial navigation are:

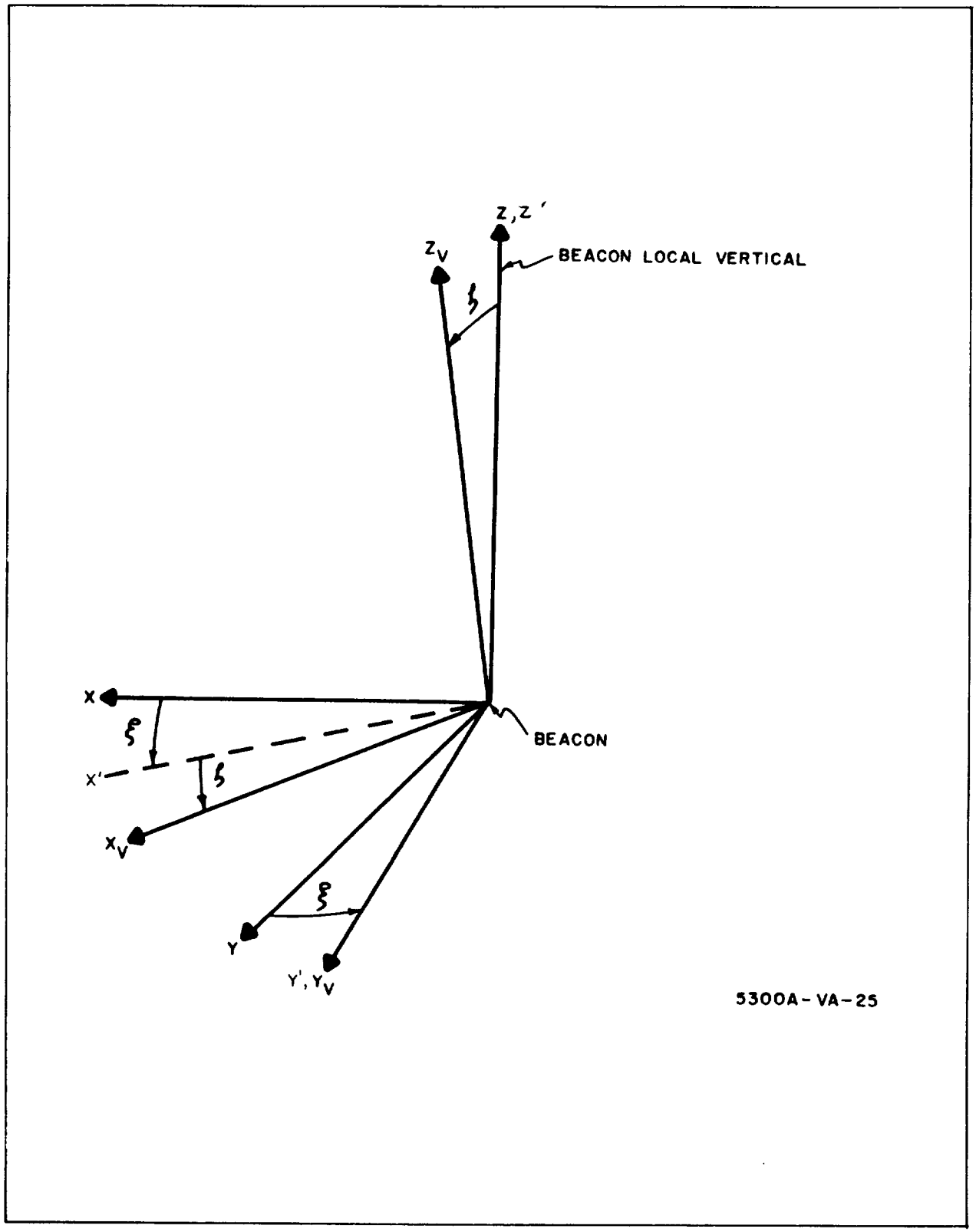

Figure 2-16. Coordinate Systems for Final Touchdown Maneuver

- Impact velocity constraints:

$|\dot{X}_I| < 0.707$ m/sec (3σ)

$|\dot{Y}_I| < 0.707$ m/sec (3σ)

$|\dot{Z}_I| < 5.0$ m/sec (3σ)*

- Position constraint: The touchdown point can be anywhere within a circle of radius 250 m (3σ), the center of which lies anywhere on a circle of radius 250 m centered at the beacon. Thus, the target area is offset from the beacon.

2.1.5.1 Navigation, Guidance, and Control System Model

2.1.5.1.1 Independence - In generating the system model used for analysis, it has been assumed that navigation guidance and control in the three coordinate directions (X_v, Y_v, Z_v) are essentially independent operations. To justify this, consider that the total applied thrust vector $\underline{a}_F$ is defined with respect to the vehicle coordinate frame by its magnitude, a_F, and two Euler angles Θ and Φ (as shown in figure 2-17. It has been specified that the angles Θ and Φ (which are essentially vehicle attitude angles) are to be less than 10 degrees at impact so it is reasonable to expect that these angles will be restricted to something on the order of 15 to 20 degrees over most of the final maneuver and to 10 degrees or less just before impact. Using small angle approximations, it can be seen that

$$\ddot{X}_{vF} \doteq a_F \Theta$$

$$\ddot{Y}_{vF} \doteq a_F \Phi$$

$$\ddot{Z}_{vF} \doteq a_F$$

Letting the commanded value of a_F be determined by the Z channel guidance law, then the horizontal acceleration requirements are satisfied by varying

*It is to be understood that the vertical component of impact velocity can never be positive.

the angle Θ and Φ. The allowed values of a_F are determined by the engine thrust limits while the allowed horizontal acceleration levels are determined by the limits on Θ and Φ as well as by the allowable thrust levels. Thus, the X_v and Y_v direction accelerations can be controlled independently of each other and also of the Z_v acceleration (within limits) by controlling the variables Θ and Φ. Although the assumption of independence is not really very good, it is felt to be adequate for the investigation of navigation error effects to be undertaken here.

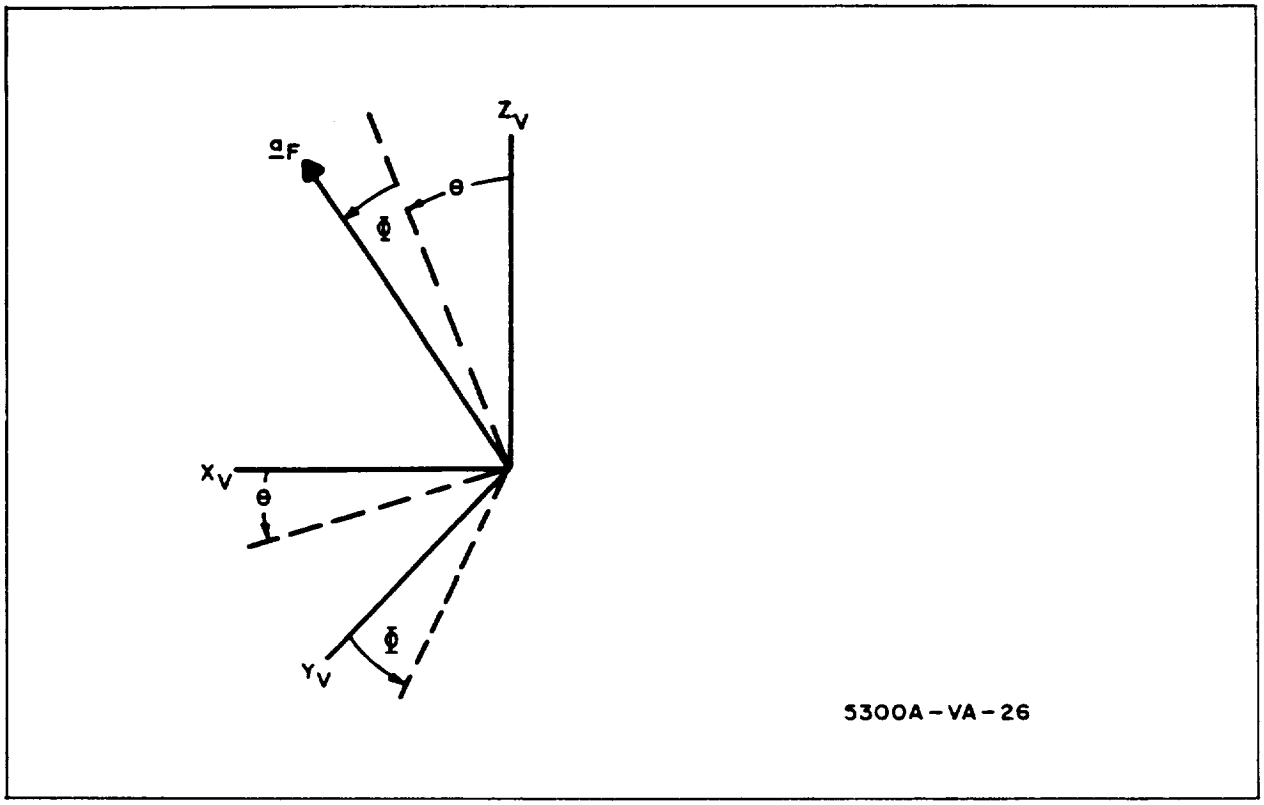

Figure 2-17. Thrust Acceleration Vector in Vehicle Coordinates

2.1.5.1.2 Guidance Logic - The basic aim of the guidance logic during the period of inertial navigation is to null the horizontal components of velocity while making the vertical velocity equal to the desired touchdown velocity Z_D which is -2.5 m/sec. The simplest guidance equations which perform this task are:

$$\ddot{X}_{vFc} = K_{\dot{X}} (\dot{X}_D - \hat{\dot{X}}_v) \tag{2-56}$$

$$\ddot{Y}_{vFc} = K_{\dot{Y}} (\dot{Y}_D - \hat{\dot{Y}}_v) \tag{2-57}$$

$$\ddot{Z}_{vFc} = K_{\dot{Z}} (\dot{Z}_D - \hat{\dot{Z}}_v) + g_m \tag{2-58}$$

where $\ddot{X}_{vFc}$, $\ddot{Y}_{vFc}$, $\ddot{Z}_{vFc}$ are the commanded thrust accelerations in vehicle coordinates; $\dot{X}_D$, $\dot{Y}_D$, $\dot{Z}_D$ are the desired impact velocities; $\hat{\dot{X}}_v$, $\hat{\dot{Y}}_v$, $\hat{\dot{Z}}_v$ are the estimated velocity vector components (obtained by inertial navigation) and g_m is lunar surface gravity. When $\hat{\dot{Z}}_v$ equals $\dot{Z}_D$, it is seen that the commanded thrust acceleration in the Z_v direction is such as to negate gravity. In the work that follows, $\dot{X}_D$ and $\dot{Y}_D$ are zero and $\dot{Z}_D$ is -2.5 m/sec.

2.1.5.1.3 Control - The formulation of the control characteristic is based on assumed first order transfer functions of the form:

$$\frac{\ddot{X}_{vF}}{\ddot{X}_{vFc}}(s) = \frac{1}{1 + T_X s} \tag{2-59}$$

$$\frac{\ddot{Y}_{vF}}{\ddot{Y}_{vFc}}(s) = \frac{1}{1 + T_Y s} \tag{2-60}$$

$$\frac{\ddot{Z}_{vF}}{\ddot{Z}_{vFc}}(s) = \frac{1}{1 + T_Z s} \tag{2-61}$$

A transfer function of this form can be represented in block diagram form as shown in figure 2-18 (using the X_v channel as an example). For this study, the block diagram shown in figure 2-18 is modified by the insertion of an additional time lag transfer function to represent the dynamics of the acceleration sensor used to close the control loop. In addition, an error input is

added to represent an accelerometer bias error. The resulting control system block diagrams for the X_v, Y_v, and Z_v channels are shown in figure 2-19 a, b, and c, respectively. In these figures, $\ddot{X}_{vFI}$, $\ddot{Y}_{vFI}$, and $\ddot{Z}_{vFI}$ are constants added to represent the initial condition ($t = t_1$) at the output of the integrator. Also, $\tilde{\ddot{x}}_b$, $\tilde{\ddot{y}}_b$, $\tilde{\ddot{z}}_b$ are the accelerometer bias errors; $\tilde{\ddot{X}}_{fF}$, $\tilde{\ddot{Y}}_{vF}$, $\tilde{\ddot{Z}}_{vF}$ are the estimated values of the three components of thrust acceleration; and $T_{\ddot{X}}$, $T_{\ddot{Y}}$, $T_{\ddot{Z}}$ are the time constants of the three acceleration sensors.

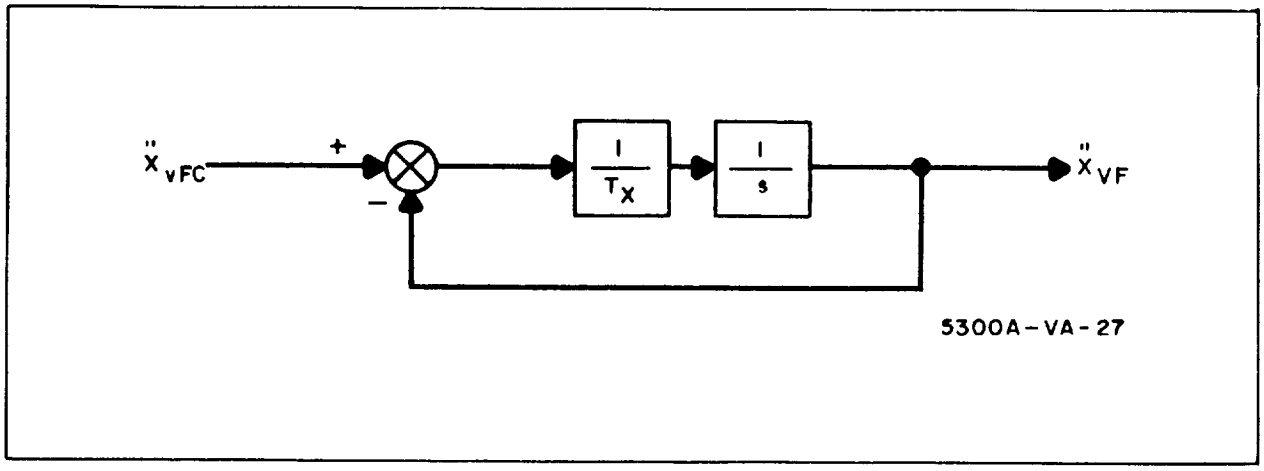

Figure 2-18. Basic Control Model

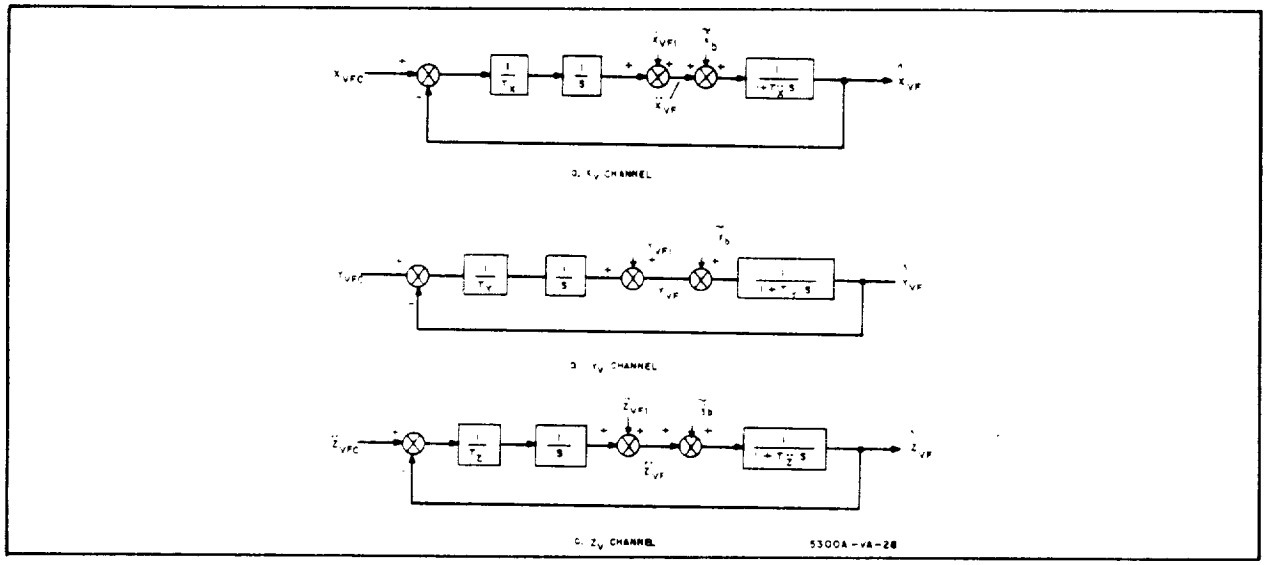

Figure 2-19. Modified Control Model

In the discussion to follow, it is desirable at times to assign numerical values to the system time constants. The values that are used are : $T_{\ddot{X}}$, $T_{\ddot{Y}}$, $T_{\ddot{Z}}$ equal 0.0025 second corresponding to an acceleration sensor noise bandwidth of 100 cps (3-db bandwidth 64 cps); and T_X, T_Y, T_Z equal 1 second corresponding to an overall 3-db control bandwidth of 0.16 cps.

2.1.5.1.4 Navigation - Subsequent to time t_1, onboard navigation is performed by updating the estimated state at time t_1 according to the equations:

$$\hat{X}_v = \hat{\dot{X}}_{v1} + \int_{t_1}^{t} \hat{\ddot{X}}_v \, dt \tag{2-62}$$

$$\hat{Y}_v = \hat{\dot{Y}}_{v1} + \int_{t_1}^{t} \hat{\ddot{Y}}_v \, dt \tag{2-63}$$

$$\hat{Z}_v = \hat{\dot{Z}}_{v1} + \int_{t_1}^{t} \hat{\ddot{Z}}_v \, dt \tag{2-64}$$

In addition to these expressions

$$\hat{\dot{X}}_{v1} = \dot{X}_{v1} + \tilde{\dot{x}}_1 \tag{2-65}$$

$$\hat{\dot{Y}}_{v1} = \dot{Y}_{v1} + \tilde{\dot{y}}_1 \tag{2-66}$$

$$\hat{\dot{Z}}_{v1} = \dot{Z}_{v1} + \tilde{\dot{z}}_1 \tag{2-67}$$

$$\hat{\ddot{X}}_v = \hat{\ddot{X}}_{vF} \tag{2-68}$$

$$\hat{\ddot{Y}}_v = \hat{\ddot{Y}}_{vF} \tag{2-69}$$

$$\hat{\ddot{Z}}_v = \hat{\ddot{Z}}_{vF} - g_m \tag{2-70}$$

where $\tilde{\dot{x}}_l$, $\tilde{\dot{y}}_l$, $\tilde{\dot{z}}_l$ are initial condition estimation errors; and $\hat{\ddot{X}}_{vF}$, $\hat{\ddot{Y}}_{vF}$, $\hat{\ddot{Z}}_{vF}$ are the outputs of the acceleration sensors. The term $(-g_m)$ is included in the equation for $\hat{\ddot{Z}}_v$ to take into account lunar gravitation which is not sensed directly.

2.1.5.1.5 Actual State - In addition to knowing the estimated vehicle velocity components, the system models used must also yield the actual vehicle velocity. The equations implemented in the model to perform this task are:

$$\dot{X}_v = \dot{X}_{vl} + \int_{t_l}^{t} \ddot{X}_v \, dt \tag{2-71}$$

$$\dot{Y}_v = \dot{Y}_{vl} + \int_{t_l}^{t} \ddot{Y}_v \, dt \tag{2-72}$$

$$\dot{Z}_v = \dot{Z}_{vl} + \int_{t_l}^{t} \ddot{Z}_v \, dt \tag{2-73}$$

where $\dot{X}_v$, $\dot{Y}_v$, $\dot{Z}_v$ are the actual velocity vector components in vehicle coordinates; $\dot{X}_{vl}$, $\dot{Y}_{vl}$, $\dot{Z}_{vl}$ are the actual initial values ($t = t_l$); and $\ddot{X}_v$, $\ddot{Y}_v$, $\ddot{Z}_v$ are the total vehicle accelerations in vehicle coordinates. The total accelerations are expressible in terms of the actual applied thrust accelerations and gravitational acceleration as follows:

$$\ddot{X}_v = \ddot{X}_{vF} + g_m \sin \zeta \tag{2-74}$$

$$\ddot{Y}_v = \ddot{Y}_{vF} \tag{2-75}$$

$$\ddot{Z}_v = \ddot{Z}_{vF} - g_m \cos \zeta \tag{2-76}$$

Using small angle approximations for $\sin \zeta$ and $\cos \zeta$, equations 2-71, 2-72, and 2-73 become:

$$\dot{X}_v = \dot{X}_{vl} + \int_{t_l}^{t} \left[\ddot{X}_{vF} + g_m \zeta \right] dt \tag{2-77}$$

$$\dot{Y}_v = \dot{Y}_{vl} + \int_{t_l}^{t} \left[\ddot{Y}_{vF} \right] dt \tag{2-78}$$

$$\dot{Z}_v = \dot{Z}_{v1} + \int_{t_1}^{t} \left[\ddot{Z}_{vF} - g_m \right] dt \qquad (2\text{-}79)$$

2.1.5.1.6 Limiting - The nature of the guidance law equations (2-56, 2-57, 2-58) is such that for reasonable values of gains K_X, K_Y, and K_Z, it could easily happen that the initial commanded accelerations would exceed the engine capabilities. This is especially likely in the X_v and Z_v channels where the nominal velocity components at the end of main braking differ significantly from zero. When this happens, the maximum available thrust is applied until the difference between the estimated velocity and the desired velocity becomes small enough so that something less than maximum thrust is required. The time when this occurs is designated t_2 where $t_2 \geq t_1$. The transition from the nonlinear mode to the linear mode does not occur at the same time in all three channels so t_{2X}, t_{2Y}, and t_{2Z} are defined.

In this study, it is assumed that once each channel enters the linear region of operation, there is sufficient damping such that the operation remains linear for the remainder of the maneuver which terminates at the time of impact t_I.

2.1.5.1.7 System Models - To take into account the nonlinear mode which may occur, two system models for each channel are used. For $t > t_2$ (the linear region) we use the complete system as generated by putting together the navigation guidance and control models discussed previously in this section. The three system models resulting are shown in figure 2-20.

For $t_1 < t < t_2$ the system is in the nonlinear region. In this region the commanded thrust is assumed to be constant at the maximum value and the sensed information that is used as feedback has essentially no effect except to keep the system in the nonlinear region. For this part of the maneuver (which actually precedes the interval of linear operation) the open loop system models shown in figure 2-21 are used for analysis. In figure 2-20, the subscript (2) refers to the value of the quantity at time t_2. Such quantities are initial conditions for the interval $t_2 < t < t_I$.

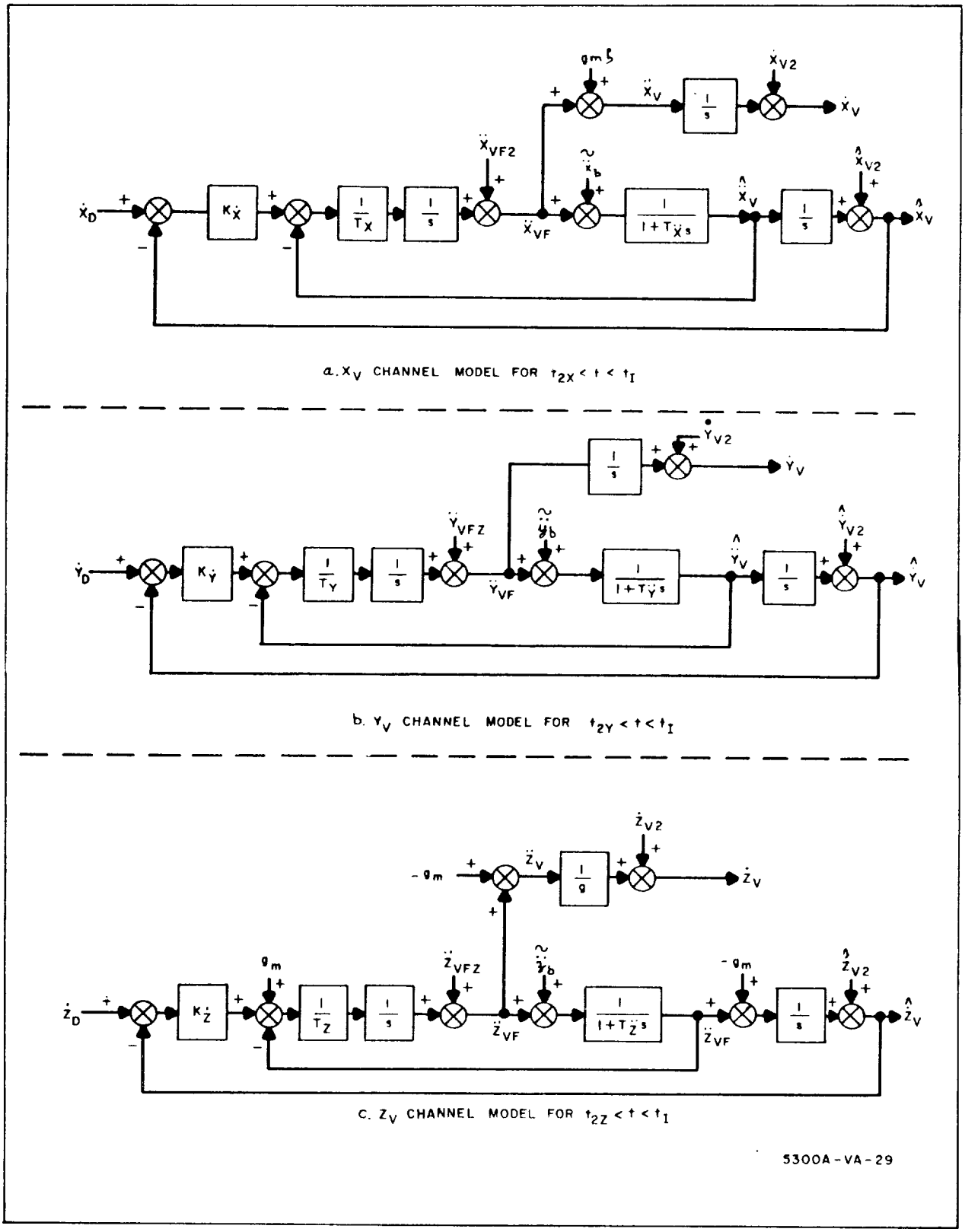

Figure 2-20. X_V, Y_V, and Z_V Channel Models

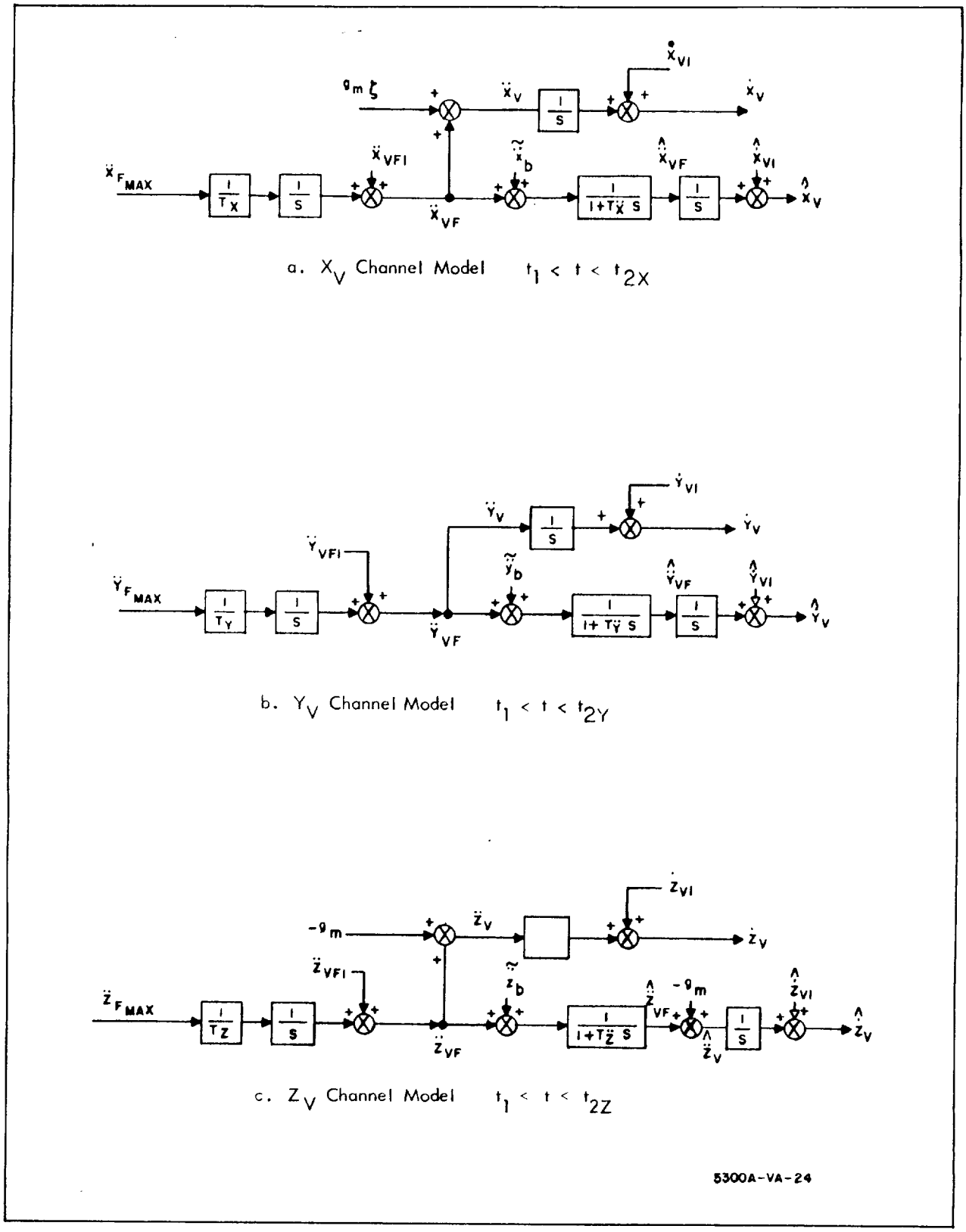

Figure 2-21. X_v, Y_v, and Z_v Channel Models

2.1.5.1.8 Error Source Characteristics - The error sources investigated are velocity estimation errors at time t_1 denoted $\tilde{\dot{x}}_1$, $\tilde{\dot{y}}_1$, $\tilde{\dot{z}}_1$; acceleration sensor bias errors $\tilde{\ddot{x}}_b$, $\tilde{\ddot{y}}_b$, $\tilde{\ddot{z}}_b$; and the vehicle coordinate misalignment angle ζ. All of these error sources are considered to be constant over any particular mission, but random over the ensemble of missions. The mean squared values (averaged over the ensemble of missions) are $\sigma^2_{\tilde{\dot{x}}_1}$, $\sigma^2_{\tilde{\dot{y}}_1}$, $\sigma^2_{\tilde{\dot{z}}_1}$, $\sigma^2_{\tilde{\ddot{x}}_b}$, $\sigma^2_{\tilde{\ddot{y}}_b}$, $\sigma^2_{\tilde{\ddot{z}}_b}$, and σ^2_{ζ}; while the mean values are all zero.

2.1.5.2 Analytical Approach

The analysis required to estimate the derivations from the nominal impact velocity components (x_{vI}, y_{vI}) as functions of the initial condition estimation errors ($\tilde{\dot{x}}_1$, $\tilde{\dot{y}}_1$, $\tilde{\dot{z}}_1$); the accelerometer bias errors ($\tilde{\ddot{x}}_b$, $\tilde{\ddot{y}}_b$, $\tilde{\ddot{z}}_b$); and the coordinate system misalignment angle (ζ) is described in paragraph 9.1. Each channel is treated by dividing the time of the total landing maneuver into two intervals: t_1 to t_2, and t_2 to t_I. Standard Laplace transform techniques are used in the analysis.

In performing the analysis described in paragraph 9.1 is tacitly assumed that the initial deviations from nominal are within the correction capability of the guidance system. To get some idea of what this capability is, the analysis described in paragraph 9.2 is performed. Engine and vehicle limitations are used to estimate the maximum allowed deviations from nominal at the end of main braking (final touchdown initiation).

2.1.5.3 Results

2.1.5.3.1 Determination of Allowable Initial Deviations - The investigation described in paragraph 9.2 is performed to estimate the allowable initial errors with the following results:

- Maximum allowable horizontal position deviations from nominal

$$3(\sigma_{x_f})_{max} = 3(\sigma_{y_f})_{max} = 120 \text{ m}$$

- Maximum allowable velocity deviations from nominal.

$3(\sigma_{\dot{x}_f})_{max} = 10.2$ m/sec

$3(\sigma_{\dot{y}_f})_{max} = 19.2$ m/sec

$3(\sigma_{\dot{z}_f})_{max} = 15$ m/sec

The subscript (f) indicates that these are deviations from nominal at time t_f which is defined in paragraph 2.1.4 to be the actual time of main braking termination.

These results are used in paragraph 2.1.6 for determining navigation requirements for the integrated mission.

2.1.5.3.2 Determination of Navigation Accuracy Requirements - The results obtained from analysis described in paragraph 9.1 are expressions for the impact velocity components in vehicle coordinates. Since vehicle coordinates differ from beacon coordinates only by the alignment error angles ξ, and ζ it can be shown that $\dot{X}_I = \dot{X}_{vI}$, $\dot{Y}_I = \dot{Y}_{vI}$, $\dot{Z}_I = \dot{Z}_{vI}$ by writing the equations relating velocity in vehicle coordinates to velocity in beacon coordinates and retaining only first order error terms. Thus, the impact velocity deviations from desired conditions are:

$$\dot{x}_I \equiv \dot{X}_I - \dot{X}_D \doteq (g_m \zeta - \tilde{\ddot{x}}_b)(t_I - t_1) - \tilde{\dot{x}}_1 - \frac{T_{\ddot{X}}^2 \ddot{X}_{F\,max}}{T_X} \qquad (2\text{-}80)$$

$$+ \frac{T_{\ddot{X}} \ddot{X}_{F\,max}(t_{2X} - t_1)}{T_X} + T_{\ddot{X}}(\ddot{X}_{vF1} + \tilde{\ddot{x}}_b)$$

$$\dot{y}_I \equiv \dot{Y}_I - \dot{Y}_D \doteq -\tilde{\ddot{y}}_b (t_I - t_1) - \tilde{\dot{y}}_1 + \frac{T_{\ddot{Y}} \ddot{Y}_{F\,max} (t_{2Y} - t_1)}{T_Y} \tag{2-81}$$

$$- \frac{T_{\ddot{Y}}^2}{T_Y} \ddot{Y}_{F\,max} + T_{\ddot{Y}} (\ddot{Y}_{vF1} + \tilde{\ddot{y}}_b)$$

$$\dot{z}_I \equiv \dot{Z}_I - \dot{Z}_D \doteq -\tilde{\ddot{z}}_b (t_I - t_1) - \tilde{\dot{z}}_1 + \frac{T_{\ddot{Z}} \ddot{Z}_{Fmax} (t_{Z2} - t_1)}{T_Z} \tag{2-82}$$

$$- \frac{T_{\ddot{Z}}^2 \ddot{Z}_{F\,max}}{T_Z} + T_{\ddot{Z}} (\ddot{Z}_{vF1} + g_m + \tilde{\ddot{z}}_b)$$

By making use of the time constant values specified in paragraph 2.1.5.1.3 and also the acceleration limits imposed by engine limitations it is possible to simplify the impact error expressions prior to applying them to the problem of determining navigation accuracy requirements. This is done by showing that terms in the expressions for $\dot{x}_I$, $\dot{y}_I$, $\dot{z}_I$ which do not include navigation error sources make contributions to the total impact error which are small compared to the maximum allowed impact errors which have been specified as study inputs:

$$|(\dot{x}_I)_{max}| = 3(\sigma_{\dot{x}_I})_{max} = 0.707 \text{ m/sec} \tag{2-83}$$

$$|(\dot{y}_I)_{max}| = 3(\sigma_{\dot{y}_I})_{max} = 0.707 \text{ m/sec} \tag{2-84}$$

$$|(\dot{z}_I)_{max}| = 3(\sigma_{\dot{z}_I})_{max} = 2.5 \text{ m/sec} \tag{2-85}$$

When this is true these terms can be ignored, and navigation requirements determined by making sure that the following inequalities are satisfied.

$$|(\dot{x}_I)_{max}| > |g_m (t_I - t_1)\,\zeta - \tilde{\ddot{x}}_b (t_I - t_1 - T_{\ddot{X}}) - \tilde{\dot{x}}_1| \tag{2-86}$$

$$|\dot{y}_I)_{max}| > |-\tilde{\ddot{y}}_b (t_I - t_1 - T_{\ddot{Y}}) - \tilde{\dot{y}}_1| \tag{2-87}$$

$$|(\dot{z}_I)_{max}| > |-\tilde{\ddot{z}}_b (t_I - t_1) - \tilde{\dot{z}}_1| \tag{2-88}$$

Which is equivalent to writing

$$(\sigma^2_{\dot{x}_I})_{max} = 0.0555 > g_m{}^2 (t_I - t_1)^2 \sigma^2_{\zeta} + \sigma^2_{\tilde{\dot{x}}_1} + (t_I - t_1 - T_{\ddot{X}})^2 \sigma^2_{\tilde{\ddot{x}}_b} \quad (m/sec)^2 \tag{2-89}$$

$$(\sigma^2_{\dot{y}_I})_{max} = 0.0555 > \sigma^2_{\tilde{\dot{y}}_1} + (t_I - t_1 - T_{\ddot{Y}})^2 \sigma^2_{\tilde{\ddot{y}}_b} \quad (m/sec)^2 \tag{2-90}$$

$$(\sigma^2_{\dot{z}_I})_{max} = 0.695 > \sigma^2_{\tilde{\dot{z}}_1} + (t_I - t_1 - T_{\ddot{Y}})^2 \sigma^2_{\tilde{\ddot{z}}_b} \quad (m/sec)^2 \tag{2-91}$$

From the in-plane navigation equations, the expressions for $\dot{X}$ and $\dot{Z}$ in terms of the beacon tracker observables are

$$\dot{X} = R\,\dot{\Psi} \cos \Psi + \dot{R} \sin \Psi \tag{2-92}$$

$$\dot{Z} = \dot{R} \cos \Psi - R\,\Psi \sin \Psi \tag{2-93}$$

Linearizing about the nominal state at time t_1 (inertial navigation initiation time) yields the following expressions

$$\begin{aligned}\sigma^2_{\tilde{\dot{x}}_1} = {} & (\dot{\Psi}_{1n} \cos \Psi_{1n})^2 \sigma^2_{\tilde{r}_1} + (\sin \Psi_{1n})^2 \sigma^2_{\tilde{\dot{r}}_1} \\ & + (\dot{R}_{1n} \cos \Psi_{1n} - R_{1n} \Psi_{1n} \sin \Psi_{1n})^2 \sigma^2_{\tilde{\psi}_1} \\ & + (R_{1n} \cos \Psi_{1n})^2 \sigma^2_{\tilde{\dot{\psi}}_1}\end{aligned} \tag{2-94}$$

$$\sigma^2_{\tilde{\dot{z}}_1} = (\dot{\Psi}_{1n} \sin \Psi_{1n})^2 \sigma^2_{\tilde{r}_1} \quad (\cos \Psi_{1n})^2 \sigma^2_{\tilde{\dot{r}}_1}$$

$$+ (R_{1n} \dot{\Psi}_{1n} \cos \Psi_{1n} + \dot{R}_{1n} \sin \Psi_{1n})^2 \sigma^2_{\tilde{\psi}_1} \qquad (2\text{-}95)$$

$$+ (R_{1n} \sin \Psi_{1n})^2 \sigma^2_{\tilde{\dot{\psi}}_1}$$

These expressions are substituted into equations 2-89 and 2-90 and the sensitivity coefficients are evaluated using the values

$R_{1n} = 270$ m

$\dot{R}_{1n} = -7.5$ m/sec

$\Psi_{1n} = -68$ deg

$\dot{\Psi}_{1n} = -0.0693$ rad/sec

In addition the quantity $(t_I - t_1)$ is assigned the maximum possible value which is 40 seconds. (This is the value that occurs if $\dot{Z}$ is already equal to $\dot{Z}_D$ at time t_1.) Out of plane navigation equations are not derived so that the expression for $(\sigma^2_{\dot{y}_I})_{max}$ is temporarily dropped from consideration. The resulting inequalities are:

$$(\sigma^2_{\dot{x}_I})_{max} = 0.0555 > (4.25 \times 10^3)\, \sigma^2_{\zeta} + (1.6 \times 10^3)\, \sigma^2_{\tilde{\dot{x}}_b}$$

$$+ (6.7 \times 10^{-4})\, \sigma^2_{\tilde{r}_1} + (8.6 \times 10^{-1})\, \sigma^2_{\tilde{\dot{r}}_1} \qquad (2\text{-}96)$$

$$+ (4.0 \times 10^2)\, \sigma^2_{\tilde{\psi}_1} + (1.0 \times 10^4)\, \sigma^2_{\tilde{\dot{\psi}}_1}$$

$$(\sigma^2_{\dot{z}_I})_{max} = 0.695 > (1.6 \times 10^3)\, \sigma^2_{\tilde{\dot{z}}_b} + (4.1 \times 10^{-3})\, \sigma^2_{\tilde{r}_1}$$

$$+ (1.4 \times 10^{-1})\, \sigma^2_{\tilde{\dot{r}}_1} \quad (2.5 \times 10^{-3})\, \sigma^2_{\tilde{\psi}_1}$$

$$+ (6.25 \times 10^4)\, \sigma^2_{\tilde{\dot{\psi}}_1}$$

As an aid to determining sensor requirements, a sample computation is performed using typical rms values for the error sources. Based on the results of this computation, the error input levels are adjusted until the estimated rms value of $\dot{x}_I$ is equal to the maximum allowed value.

As a result of this process, we arrive at the following set of specifications which defines a system capable of satisfying mission requirements.

$\sigma_{\zeta} < 0.002$ rad

$\sigma_{\tilde{r}_l} < 3.0$ m

$\sigma_{\tilde{\dot{r}}_l} < 0.14$ m/sec

$\sigma_{\tilde{\psi}_l} < 0.0035$ rad

$\sigma_{\tilde{\dot{\psi}}_l} < 0.0007$ rad/sec

$\sigma_{\tilde{\dot{x}}_b} < 0.002$ m/sec^2

$\sigma_{\tilde{\dot{z}}_b} < 0.002$ m/sec^2

This set of inequalities can be regarded as a set of sensor requirements for performing the final touchdown maneuver using inertial navigation. However, it must be remembered that trade-offs exist; i.e., if one sensor error level is below the specified level, another may exceed its specified level without causing the total error to exceed the allowed magnitude. The individual contributions of each source to the mean squared impact errors are given in table 2-11.

With regard to the feasibility of realizing the specified accuracies, the following comments are made:

- Radar errors: The radar accuracies specified can be satisfied with present state-of-the art capability, but just barely. The values specified also turn out to agree quite well with the requirements for satisfactory completion of the rest of the mission (paragraph 2.1.6)

TABLE 2-11

DISTRIBUTION OF TOTAL IMPACT ERROR USING SPECIFIED NAVIGATION ACCURACIES.

Error Source	rms Error level	Contribution to: $\dot{x}_I$ $(m/sec)^2$	Contribution to: $\dot{z}_I$ $(m/sec)^2$
Platform Misalignment	$\sigma_\zeta = 0.002$ rad	0.017	0.00
Range Observation	$\sigma_{\tilde{r}_1} = 3.0$ m	0.00605	0.0367
Range Rate Observation	$\sigma_{\dot{\tilde{r}}_1} = 0.14$ m/sec	0.0169	0.00275
Angle Observation	$\sigma_{\tilde{\psi}_1} = 0.0035$ rad	0.0049	0.00
Angle Rate Observation	$\sigma_{\dot{\tilde{\psi}}_1} = 0.0007$ rad/sec	0.0049	0.0306
X Axis Acceleration Sensor	$\sigma_{\ddot{\tilde{x}}_b} = 0.002$ m/sec^2	0.0064	0.00
Z Axis Acceleration Sensor	$\sigma_{\ddot{\tilde{z}}_b} = 0.002$ m/sec^2	0.000	0.0064
Total mean squared Errors		0.056	0.076
Total rms Error.		0.237 m/s	0.276 m/s

- Acceleration Sensors: The values specified are typical of state-of-the-art capability.
- Platform alignment to roughly 0. 1 degree is specified (1σ). This appears to be on the border line of state-of-the-art capability. The gyrocompassing analysis (Section 12) shows that alignment to local vertical at main braking initiation can be achieved with an error on the order of 0. 1 deg. (1σ). In addition, radar accuracies on the order of those required for the main braking phase are sufficient to allow computation of the central angle between initial local vertical and beacon local vertical to an accuracy of better than 0. 1 degree (1σ). These two errors are the primary causes of the misalignment angle ξ so that it appears that 1σ alignment accuracy on the order of 0. 1 deg to 0. 15 degree is attainable.

2. 1. 6 Integration of Orbital Mission Phases

This paragraph considers the problem of integrating the results of the studies of midcourse, retrothrust, orbital, and main braking phases to determine navigation and control error effects on the total mission performance, considering only the effects of inplane errors. (See paragraph 2. 1. 1. 4 for out-of-plane considerations).

The final touchdown Phase is not included in the overall mission integration. Instead, engine and vehicle limitations have been used to generate allowable errors at the end of the main braking phase (see paragraph 2. 1. 5).

The approach is to sequentially integrate the mission phases starting with midcourse. The end product is an expression relating deviations from nominal at the end of main braking to all the various error sources considered. This is then used to generate the covariance matrix of these terminal errors.

The nomenclature used is taken from the preceding sections wherever possible. New matrices of sensitivity coefficients are defined as they are introduced. *

2. 1. 6. 1 Sequential Integration of Mission Phases

At the end of midcourse, there are two error vectors of importance: the vector of actual deviations from nominal $\underline{p}_o$ and the vector of state estimation

*In this section, all state vectors are two dimensional, consisting only of coordinates in the plane of motion.

errors $\underset{\sim}{p}_o$.* Both of these error sources propagate through the retrothrust phase and contribute to the total deviation from the nominal retrothrust end point at the time of retrothrust termination. This deviation vector is $\underline{p}_1$.** In this study, a vector of navigation and control bias errors ($\underset{\sim}{q}$) during retrothrust is also considered to contribute to $\underline{p}_1$. As a result of the linearized analysis of paragraph 2.1.2 we have the expression.

$$\underline{p}_1 = \left[S_{p_1 p_o}\right] \underline{p}_o + \left[S_{p_1 \underset{\sim}{p}_o}\right] \underset{\sim}{p}_o + \left[S_{p_1 \underset{\sim}{q}}\right] \underline{q} \qquad (2\text{-}97)^{***}$$

where the elements of the sensitivity coefficient matrices have been evaluated.

From paragraph 2.1.3 (orbital phase) we have the following expression relating deviations from nominal at the nominal time of main braking initiation, $\underline{p}_3$ (time referenced to the actual time of parking orbit injection) to the deviation vector $\underline{p}_1$ and the vector of descent kick application errors $\underline{u}$.

$$\underline{p}_3 = \left[S_{p_3 p_1}\right] \underline{p}_1 + \left[S_{p_3 u}\right] \underline{u} \qquad (2\text{-}98)$$

where the coefficients of these matrices have been evaluated.

However, nominal time in orbit is not a good criterion for initiating the main braking phase when other information is available (from the beacon tracker which acquires prior to main braking initiation). Using the inertial reference maintained on board, and beacon tracking information, it is possible to estimate the lunar central angle separation between the landing site and the vehicle (angle Θ in figure 2-14). In an effort to reduce down range deviations from nominal at the start of main braking, it has been specified

---

*For definition of coordinate system X_o, Y_o, Z_o, in which vectors $\underline{p}_o$ and $\underset{\sim}{p}_o$ are defined, see paragraph 5.2 and/or 6.2.

**The coordinate systems in which vectors $\underline{p}_1$, $\underline{p}_2$, $\underline{p}_3$ are defined are described in paragraph 2.1.3.

***This expression appears in paragraph 6.2.

that main braking begins when the estimated value of Θ is equal to the nominal value. Then the initial deviations for main braking are not given by vector $\underline{p}_3$, but by $\underline{p}_3'$, a vector related to $\underline{p}_3$ by analysis presented in paragraph 10.1. $\underline{p}_3'$ is expressed in the same coordinate system as $\underline{p}_3$, and differs from $\underline{p}_3$ by the amount that the deviations change in the interval between nominal initiation time and actual initiation time. The relationship derived in paragraph 10.1 is:

$$\underline{p}_3' = [A]\,\underline{p}_3 - [B]\,\tilde{\underline{q}}_i \tag{2-99}$$

where $\tilde{\underline{q}}_i$ is a vector of errors contributing to the total error in estimating central angle Θ. Matrices $[A]$ and $[B]$ are evaluated in paragraph 10.1.

The result of the main braking phase analysis paragraph 2.1.4 is a matrix expression relating the errors at the end of main braking to a vector of initial deviations from the nominal $\underline{p}_i$; * to sensor bias errors represented by vectors $\tilde{\underline{q}}_{bc}$ and $\tilde{\underline{q}}_{bs}$; and to random sensor errors represented by $\tilde{\underline{q}}_{nc}$ and $\tilde{\underline{q}}_{ns}$. The integration would be complete if $\underline{p}_i$ were equal to $\underline{p}_3'$. They are not equal, but they can be related simply. Vectors $\underline{p}_i$ and $\underline{p}_3'$ are evaluated at the same time (actual time of main braking initiation), and with respect to coordinate systems fixed to the same point (nominal point of main braking initiation.) The only difference arises from the fact that the Z_i axis is aligned to beacon local vertical, while the Z_3 axis is aligned to local vertical at the nominal point of main braking initiation. The angle between these axis is therefore equal to the nominal lunar central angle subtended by the main braking maneuver (10.6 degrees). Thus the relationship between $\underline{p}_i$ and $\underline{p}_3'$ is simply a rotation matrix, denoted $[\Theta_{in}]$. Symbolically

$$\underline{p}_3' = [\Theta_{in}]\,\underline{p}_i \tag{2-100}$$

*Vector $\underline{p}_i$ is defined with respect to the beacon local vertical reference frame, X, Y, Z, described in paragraph 2.1.4.

Thus the results of the main braking analysis can be expressed as:

$$\underline{p}_f = \left[S_{p_f p_i}\right] \left[\Theta_{in}\right]^{-1} \underline{p}'_3 \left[S_{p_f \tilde{q}_{bc}}\right] \underline{\tilde{q}}_{bc} + \left[S_{p_f \tilde{q}_{bs}}\right] \underline{\tilde{q}}_{bs} + \underline{p}_f (\underline{\tilde{q}}_{nc}, \underline{\tilde{q}}_{ns}) \tag{2-101}$$

where the last term represents the contribution of the random errors which can only be given a meaningful form when the statistics of $\underline{p}_f$ are considered. Working with equations 2-97, 2-98, 2-99 and 2-101, an equation of the following form is obtained:

$$\underline{p}_f = \left[S_{p_f p_o}\right] \underline{p}_o + \left[S_{p_f \tilde{p}_o}\right] \underline{\tilde{p}}_o + \left[S_{p_f \tilde{q}}\right] \underline{\tilde{q}} + \left[S_{p_f u}\right] \underline{\mu} + \left[S_{p_f \tilde{q}_i}\right] \underline{\tilde{q}}_i + \left[S_{p_f \tilde{q}_{bc}}\right] \underline{\tilde{q}}_{bc} + \left[S_{p_f \tilde{q}_{bs}}\right] \underline{\tilde{q}}_{bs} + \underline{p}_f (\underline{\tilde{q}}_{nc}, \underline{\tilde{q}}_{ns}) \tag{2-102}$$

The next step is to determine the covariance matrix of $\underline{p}_f$ which is denoted $\left[P_f\right]$ where

$$\left[P_f\right] \equiv E\left[\underline{p}_f \underline{p}_f^T\right] \tag{2-103}$$

In determining the expression for $\left[P_f\right]$ the following assumptions are made.

- The elements of each error source vector are independent of the elements of any other error source vector, e.g.

$$E\ p_{oj} \tilde{p}_{ok} = 0; \text{ for all } j \text{ and } k \tag{2-104}$$

- The elements error vector $\underline{\tilde{q}}$ are independent of one another. Thus:

$$E\ \tilde{q}_j \tilde{q}_k = \begin{cases} \sigma_{q_j}^2; & k = j \\ 0; & k \neq j \end{cases} \tag{2-105}$$

Similar assumptions are made with respect to vectors $\underline{u}$, $\underline{\tilde{q}}_i$, $\underline{\tilde{q}}_{bc}$, $\underline{\tilde{q}}_{bs}$, $\underline{\tilde{q}}_{nc}$ and $\underline{\tilde{q}}_{ns}$.

Using the first assumption we can write the expression for $[P_f]$ in the form

$$[P_f] = [P_{fp_o}] + [P_{f\tilde{p}_o}] + [P_{f\tilde{q}}] + [P_{fu}] + [P_{f\tilde{q}_i}] + [P_{f\tilde{q}_{bc}}] + [P_{f\tilde{q}_{bs}}] + [P_{f\tilde{q}_{nc}}] + [P_{f\tilde{q}_{ns}}] \quad (2\text{-}106)$$

where $[P_{fp_o}]$ is considered to be the contribution to $[P_f]$ caused by the error source vector $\underline{p}_o$, defined as

$$[P_{fp_o}] \equiv [S_{p_f p_o}] \left\{ E [\underline{p}_o \underline{p}_o^T] \right\} [S_{p_f p_o}]^T \quad (2\text{-}107)$$

$$= [S_{p_f p_o}] [P_o] [S_{p_f p_o}]^T$$

Matrix $[P_o]$ is seen to be the covariance matrix of $\underline{p}_o$. Similarly:

$$[P_{f\tilde{p}_o}] \equiv [S_{p_f \tilde{p}_o}] [\tilde{P}_o] [S_{p_f \tilde{p}_o}]^T \quad (2\text{-}108)$$

$$[P_{f\tilde{q}}] \equiv [S_{p_f \tilde{q}}] [\tilde{Q}] [S_{p_f \tilde{q}}]^T \quad (2\text{-}109)$$

$$[P_{fu}] \equiv [S_{p_f u}] [U] [S_{p_f u}]^T \quad (2\text{-}110)$$

$$[P_{f\tilde{q}_i}] \equiv [S_{p_f \tilde{q}_i}] [\tilde{Q}_i] [S_{p_f \tilde{q}_i}]^T \quad (2\text{-}111)$$

$$[P_{f\tilde{q}_{bc}}] \equiv [S_{p_f \tilde{q}_{bc}}] [\tilde{Q}_{bc}] [S_{p_f \tilde{q}_{bc}}]^T \quad (2\text{-}112)$$

$$\left[P_{f\tilde{q}_{bs}}\right] \equiv \left[S_{p_f\tilde{q}_{bs}}\right] \left[\tilde{Q}_{bs}\right] \left[S_{p_f\tilde{q}_{bs}}\right]^T \tag{2-113}$$

The only information available concerning the final errors caused by random sensor errors are the contributions to the mean squared error given by vectors $\underline{\sigma}^2_{p_f\tilde{q}_{nc}}$, $\underline{\sigma}^2_{p_f\tilde{q}_{ns}}$ derived in paragraph 2.1.4.4. Therefore matrix $\left[P_{f\tilde{q}_{nc}}\right]$ is defined to be a diagonal matrix composed of the elements of $\underline{\sigma}^2_{p_f\tilde{q}_{nc}}$ and $\left[P_{f\tilde{q}_{ns}}\right]$ is a diagonal matrix composed of the elements of $\underline{\sigma}^2_{p_f\tilde{q}_{ns}}$.*

By virtue of the second assumption previously made, the input covariance matrices $[\tilde{Q}]$, $[U]$, $[\tilde{Q}_i]$, $[\tilde{Q}_{bc}]$ and $[\tilde{Q}_{bs}]$ are seen to be diagonal, while the covariance matrices $[P_o]$ and $[\tilde{P}_o]$, of deviations and estimation errors at the end of midcourse are not restricted to a diagonal form.

The results derived in the main body of this report are based on the assumption that vectors $\underline{p}_o$ and $\underline{\tilde{p}}_o$ are uncorrelated (thus $E\left[\underline{p}_o \underline{\tilde{p}}_o^T\right] = 0$). For a discussion of effect of correlation between $\underline{p}_o$ and $\underline{\tilde{p}}_o$ see paragraph 10.2. The general conclusion of the investigation is that correlations of the expected type lead to reduced final errors. Hence, the analysis as presented here, assuming independence, is pessimistic in some cases where no onboard navigation is performed after the second midcourse correction. For cases using navigation after the second correction, the correlation between $\underline{p}_o$ and $\underline{\tilde{p}}_o$ is expected to be low so that the assumption of independence is valid.

In using the expressions derived in this section it must be remembered that all the state vectors employed are two dimensional, retaining only the components in the plane of motion. Thus

*Diagonal, because the mean squared error terms are the diagonal elements of the covariance matrix.

$$\underline{p}_o^T = \left[x_o,\ y_o,\ \dot{x}_o,\ \dot{y}_o\right] \tag{2-114}*$$

$$\tilde{\underline{p}}_o^T = \left[\tilde{x}_o,\ \tilde{y}_o,\ \dot{\tilde{x}}_o,\ \dot{\tilde{y}}_o\right] \tag{2-115}$$

$$\underline{p}_f^T = \left[x_f,\ z_f,\ \dot{x}_f,\ \dot{z}_f\right] \tag{2-116}$$

The numerical evaluations of matrices $\left[S_{p_f p_o}\right]$, $\left[S_{p_f \tilde{p}_o}\right]$, $\left[S_{p_f \tilde{q}}\right]$, $\left[S_{p_f u}\right]$ and $\left[S_{p_f \tilde{q}_i}\right]$ are given below. Matrices $\left[S_{p_f \tilde{q}_{bc}}\right]$ and $\left[S_{p_f \tilde{q}_{bs}}\right]$ are given in paragraph 2.1.4.4.

$$\left[S_{p_f p_o}\right] = \begin{bmatrix} -5.88\times10^{-4} & -8.44\times10^{-4} & 9.99\times10^{-2} & -5.57\times10^{-1} \\ 0 & 0 & 0 & 0 \\ 6.60\times10^{-5} & 9.98\times10^{-5} & -1.18\times10^{-2} & 6.59\times10^{-2} \\ -6.88\times10^{-5} & -1.04\times10^{-4} & 1.23\times10^{-2} & -6.86\times10^{-2} \end{bmatrix} \tag{2-117}$$

$$\left[S_{p_f \tilde{p}_o}\right] = \begin{bmatrix} -7.63\times10^{-3} & -3.25\times10^{-6} & 4.16\times10^{0} & -8.82\times10^{0} \\ 0 & 0 & 0 & 0 \\ 9.01\times10^{-4} & 3.83\times10^{-7} & -4.92\times10^{-1} & 1.04\times10^{0} \\ -9.39\times10^{-4} & -4.00\times10^{-7} & 5.14\times10^{-1} & -1.09\times10^{0} \end{bmatrix} \tag{2-118}$$

$$\left[S_{p_f \tilde{q}}\right] = \begin{bmatrix} -3.00\times10^{-3} & -1.34\times10^{1} & 1.83\times10^{3} & -9.87\times10^{1} & 2.28\times10^{3} \\ 0 & 0 & 0 & 0 & 0 \\ 3.55\times10^{-4} & 1.58\times10^{0} & -2.16\times10^{2} & 1.16\times10^{1} & -2.70\times10^{2} \\ -3.70\times10^{-4} & -1.65\times10^{0} & 2.27\times10^{2} & -1.24\times10^{1} & 2.82\times10^{2} \end{bmatrix} \tag{2-119}$$

*The X_o, Y_o, Z_o coordinate frame referred to is that defined in paragraph 6.2.

$$\left[S_{p_f u}\right] = \begin{bmatrix} 3.22\times10^{0} & 0 & 1.38\times10^{2} \\ 0 & 0 & 0 \\ -3.82\times10^{-1} & 0 & -1.90\times10^{1} \\ 3.90\times10^{-1} & 0 & 2.00\times10^{1} \end{bmatrix} \tag{2-120}$$

$$\left[S_{p_f \tilde{q}_i}\right] = \begin{bmatrix} -4.16\times10^{-4} & 5.88\times10^{1} \\ 0 & 0 \\ 4.95\times10^{-5} & -7.00\times10^{0} \\ -5.06\times10^{-5} & 7.15\times10^{0} \end{bmatrix} \tag{2-121}$$

Note that the second row of each of these matrices is made up of zeroes. Thus none of these will contribute to the terminal vertical position error z_f. The reason is that estimated altitude is used as the main braking cutoff criterion. Hence the only error sources leading to a terminal altitude error are the main braking phase sensor errors.

2.1.6.2 Determination of Navigation Requirements

The approach is as follows:

- Use selected midcourse phase results to compute a set of covariance matrices $\left[P_{fp_o}\right]$ and $\left[P_{\tilde{fp}_o}\right]$ (defined previously). These represent the effects of midcourse correction time, correction accuracy, and navigation accuracy on the error distribution at the end of main braking.

- Use assumed sample rms error levels (selected with an eye toward the state of the art) for the components of $\underline{\tilde{q}}$, $\underline{u}$, $\underline{\tilde{q}}_i$, $\underline{\tilde{q}}_{bc}$, $\underline{\tilde{q}}_{bs}$, $\underline{\tilde{q}}_{nc}$, and $\underline{\tilde{q}}_{ns}$ (all defined previously) and determine the resulting mean-squared error components at the end of main braking.

- Use the allowed errors at main braking termination (paragraph 2.1.5.3.1), the sample computation results, and judgment to determine a rough distribution of the allowed terminal error among the error sources. For example, the portion of the total error to be alloted to main braking sensor errors or midcourse terminal deviations.

- On the basis of this rough distribution determine: which midcourse system concepts offer adequate performance and a set of accuracy specifications on the navigation and control accuracies for the other mission phases which yield satisfactory terminal errors.

The results of the computations indicated in steps one and two above are presented in paragraph 10.3 along with input errors used to get the results.

Based on these results, it appears that the allowed rms error in $\dot{X}_f$ (terminal horizontal velocity) is the most severe limitation. The maximum allowed value of $\sigma_{\dot{x}_f}$ is 11.6 $(m/sec)^2$. (Based on $3(\sigma_{\dot{x}_f})_{max} = 10.2$ $(m/sec.)^2$ It is also seen that the most significant error sources are: deviations from nominal and estimation errors at the end of midcourse, and a constant bias error in measuring the LOS rate, $\dot{\Psi}$, during the main braking phase. On the basis of this, we choose the following conditions as a goal to work toward:

a) Total contribution to $\sigma^2_{\dot{x}_f}$ caused by deviations and estimation errors at midcourse termination is to be less than 4.0 $(m/sec)^2$.

b) The contributions to $\sigma^2_{\dot{x}_f}$ caused by the bias error in measuring $\dot{\Psi}$ is to be 4.0$(m/sec)^2$ or less.

c) The total contribution of all other error sources to $\sigma^2_{\dot{x}_f}$ is to be less than 3.6$(m/sec)^2$.

The following midcourse system concepts yield accuracies which are sufficient to satisfy condition one.

- Second midcourse, correction at 66 hours, correction applied to an accuracy of 0.1 m/sec (1σ); correction monitored to an accuracy of 0.1 m/sec (1σ); nominal DSIF navigation prior to second midcourse correction; no navigation in the interval between second correction and retrothrust initiation; retrothrust initiation based on nominal time. Then, from tables 10-2 and 10-3 of paragraph 10.3

$$\sigma^2_{\dot{x}_f P_o} + \sigma^2_{\dot{x}_f \tilde{P}_o} = 0.217 + 1.23 = 1.45 \ (m/sec)^2$$

- Second midcourse correction at 50 hours with correction accuracies given above; nominal DSIF navigation prior to second midcourse correction; navigation based on horizon scanner observation of

local-vertical direction after the second correction; measurement accuracy: 0.002 rad (1σ); retrothrust initiation based on nominal time.

$$\sigma^2_{\dot{x}_f P_o} + \sigma^2_{\dot{x}_f \tilde{P}_o} = 1.16 + 1.18 = 2.34 \text{ (m/sec)}^2$$

- Second midcourse correction at 50 hours with correction accuracies given above; nominal DSIF navigation prior to second correction; onboard navigation after second correction using 3 altitude measurements, all made at attitude of less than 1000 km, measurement accuracy 2 km (1σ); retrothrust initiation based on nominal time.

$$\sigma^2_{\dot{x}_f P_o} + \sigma^2_{\dot{x}_f \tilde{P}_o} = 1.16 + 3.20 = 4.36 \text{ (m/s)}^{2\,*}$$

The two concepts described above, using onboard navigation are also adequate (in fact better) if the second correction time is moved to 66 hours.

None of the concepts described are adequate if degraded DSIF navigation is assumed. One reason for this is that retrothrust initiation is based on nominal time, so that the information gained by onboard navigation is not used to full advantage. It seems likely that if retrothrust were initiated on the basis of information obtained from onboard navigation concepts of the type considered in this study, then the mission could be performed satisfactorily, even with degraded DSIF navigation. However, this conclusion is based on judgment and is not supported by numerical results at this time.

To satisfy condition b, the maximum allowable magnitude of $\sigma_{\tilde{\dot{\psi}}_{bc}}$, the rms bias error in measuring $\dot{\Psi}$ is 0.00005 rad/sec. This is based on information in table 10-7 which shows that the contribution to $\sigma^2_{\dot{x}_f}$ caused by this source is 16.8 (m/sec)^2 when $\sigma_{\tilde{\dot{\psi}}_{bc}}$ is 0.0001 rad/sec.

Finally, based on data in tables 10-4, 10-5, 10-6, 10-7, 10-8, and 10-9; the input error levels of the remaining error sources are adjusted such that condition c is satisfied (but just barely). Here again judgment

*It can be seen that this is a marginal case, since the total mean-squared error exceeds the allowed value by a slight amount.

plays an important part in the adjustment procedure so that the specifications resulting are extremely flexible. Two statements can be made concerning these specifications however.

- Satisfaction of the specifications is sufficient to satisfy condition c.
- None of the specified tolerances can be exceeded by an order of magnitude without imposing severe limitations on the remaining error sources if condition c is to remain satisfied.

Since the sum of all contributions to $\sigma^2_{\dot{x}_f}$ contained in tables 10-4, 10-5, 10-6, 10-7, 10-8, and 10-9 (not including the contribution caused by $\tilde{\dot{\psi}}_{bc}$ which is considered separately) is just about 3 $(m/sec)^2$, which is nearly the allowed value, the procedure for adjusting the sample values to obtain specifications is as follows:

- Where the sample error levels yield significant contributions, use the sample values as specifications.
- Where the sample error levels yield insignificant contributions, the specified tolerance is made enough larger than the sample error level so that the resulting contribution to $\sigma^2_{\dot{x}_f}$ becomes marginally significant.

With the above discussion in mind, the specified error tolerances are: (note that all are quoted as (1σ) values).

a. Injection phase error tolerances

Thrust magnitude measurement:	$\sigma_{\tilde{f}_c} < 1000$ newtons
Thrust direction measurement:	$\sigma_{\tilde{\alpha}_c} < 0.05$ rad
Initial IMU alignment:	$\sigma_{\tilde{\gamma}_i} < 0.002$ rad
Radial acceleration sensor:	$\sigma_{\tilde{a}_{FR}} < 0.01$ m/sec^2
Transverse acceleration sensor:	$\sigma_{\tilde{a}_{F\Theta}} < 0.002$ m/sec^2

b. Descent kick application error tolerances

Descent kick magnitude:	$\sigma_{\delta V_2} < 1$ m/sec
Descent kick application: angle (in-plane)	$\sigma_{\delta \alpha} < 0.02$ rad

Descent kick application: angle (out-of-plane)		tolerance not determined*

c. Main braking initiation error tolerances

Initial range estimation	$\sigma_{\tilde{r}_i}$	< 3.5 km
Initial angle estimation	$\sigma_{(\tilde{\theta}_a)_i}$	< 0.025 rad

d. Main braking phase error tolerances

- Constant bias error levels

Range measurement:	$\sigma_{\tilde{r}_{bc}}$	< 3 m
Range rate measurement:	$\sigma_{\dot{\tilde{r}}_{bc}}$	< 0.2 m/sec
Angle measurement: **		Not considered
Angle rate measurement:	$\sigma_{\dot{\tilde{\psi}}_{bc}}$	< 0.00005 rad/sec
Thrust magnitude measurement:	$\sigma_{\tilde{f}_{bc}}$	< 3000 newton
Thrust angle measurement:	$\sigma_{(\tilde{\theta}_{los})_{bc}}$	< 0.01 rad

- Scale factor bias errors

Range measurement:	$\sigma_{\tilde{r}_{bs}}$	< 1.0 %
Range rate measurement:	$\sigma_{\dot{\tilde{r}}_{bs}}$	< 0.3 %
Angle measurement:		not considered
Angle rate measurement:	$\sigma_{\dot{\tilde{\psi}}_{bs}}$	< 1.0 %
Thrust magnitude measurement:		not considered***
Thrust angle measurement:		not considered***

---

*The integration analysis considers only in-plane errors so that no information is available concerning the tolerance on $\sigma_{\delta\gamma}$. It seems likely $\sigma_{\delta\gamma} = \sigma_{\delta\alpha}$ would give sufficient accuracy.

**This measurement is not used by the in-plane guidance system used for main braking analysis.

***Scale factor errors are not considered as components of these error sources.

- Random error, constant rms value

Range measurement:	$\sigma_{\tilde{r}_{nc}}$	< 3.0 m
Range rate measurement:	$\sigma_{\tilde{\dot{r}}_{nc}}$	< 0.25 m/sec
Angle measurement:		not considered
Angle rate measurement:	$\sigma_{\tilde{\dot{\psi}}_{nc}}$	< 0.0001 rad/sec
Thrust magnitude measurement:	$\sigma_{\tilde{f}_{nc}}$	< 1500 newton
Thrust angle measurement:	$\sigma_{(\tilde{\theta}_{los})_{nc}}$	< 0.01 rad

- Random error

Range measurement:	$\sigma_{\tilde{r}_{ns}}$	< 0.5 %
Range rate measurement:	$\sigma_{\tilde{\dot{r}}_{ns}}$	< 0.2 %
Angle measurement:		not considered
Angle rate measurement:	$\sigma_{\tilde{\dot{\psi}}_{ns}}$	< 1.0 %
Thrust magnitude measurement:		not considered
Thrust angle measurement:		not considered

Using these numbers, it can be shown that the total contributions to $\sigma^2_{x_f}$, $\sigma^2_{\dot{x}_f}$, and $\sigma^2_{\dot{z}_f}$ caused by navigation and control errors in all phases from retrothrust to main braking termination are:

$$\sigma^2_{x_f} - (\sigma^2_{x_f p_o} + \sigma^2_{x_f \tilde{p}_o}) = 763\ (\text{m})^2$$

$$\sigma^2_{\dot{x}_f} - (\sigma^2_{\dot{x}_f p_o} + \sigma^2_{\dot{x}_f \tilde{p}_o}) = 7.47\ (\text{m/sec})^2$$

$$\sigma^2_{\dot{z}_f} - (\sigma^2_{\dot{z}_f p_o} + \sigma^2_{\dot{z}_f \tilde{p}_o}) = 14.5\ (\text{m/sec})^2$$

For the poorest of the midcourse concepts which satisfy condition (a) stated previously in this section (second correction at 50 hours with on-board navigation using 3 altitude measurements accurate to 2 km (1σ)) the following mean-squared errors result. (From tables 10-2 and 10-3)

$$\sigma^2_{x_f p_o} + \sigma^2_{x_f \tilde{p}_o} = 82.4 + 229 = 311\ (m)^2$$

$$\sigma^2_{\dot{x}_f p_o} + \sigma^2_{\dot{x}_f \tilde{p}_o} = 1.16 + 3.20 = 4.36\ (m/sec)^2$$

$$\sigma^2_{\dot{z}_f p_o} + \sigma^2_{\dot{z}_f \tilde{p}_o} = 1.26 + 3.47 = 4.73\ (m/sec)^2$$

Thus, in this case, the total rms errors at the end of main braking are:

$$\sigma_{x_f} = (1074)^{1/2} = 33\ m < (\sigma_{x_f})_{max} = 40\ m$$

$$\sigma_{\dot{x}_f} = (11.8)^{1/2} = 3.4\ m/sec = (\sigma_{\dot{x}_f})_{max} = 3.4\ m/sec$$

$$\sigma_{\dot{z}_f} = (19.2)^{1/2} = 4.4\ m/sec < (\sigma_{\dot{z}_f})_{max} = 5.0\ m/sec$$

These values are seen to be less than the maximum allowed values derived in paragraph 2.1.5 with the exception of $\sigma_{\dot{x}_f}$ which (as intended) is equal to the allowed value.

2.2 DIRECT DESCENT MISSION

An alternate profile for the unmanned lunar landing mission is a flight direct to the target site on the visible face of the moon, rather than the parking orbit descent previously discussed. A possible advantage of such a direct-descent mission profile is that simpler guidance requirements should result from the elimination of the retrothrust and descent kick orbital maneuvers; and advantage may be taken of the unrestricted visibility of the landing site beacon. Disadvantages include restrictions on the choice of

target sites and the problem of separating the L-I stage from the L-II while in nearly vertical descent.

In this study, since the direct descent mode is considered secondary to the parking orbit mode, an extensive analysis has not been made. Instead, emphasis has been placed on a comparison between the direct-descent and parking orbit modes, especially with regard to the payload capabilities and main braking guidance requirements of each. In addition, a brief analysis of the effect of target location on the direct descent was made.

The direct-descent mission profile consists of four distinct mission phases: midcourse, preliminary braking, main braking, and final touchdown. Of these, the first and last are self-explanatory. Preliminary braking and main braking require some elaboration.

As a ground rule for the direct-descent mission it is assumed that the same two-stage vehicle is used for each mission profile. Stage sizing is then determined by the orbital mission profile: L-I stage for retrothrust maneuver (then jettisoned in orbit); L-II stage for descent kick, main braking, and final touchdown. Thus at the end of midcourse in the direct descent mission profile we have a two-stage vehicle. The firing of the L-I stage is called preliminary braking. After the L-I stage firing is completed, the stage is jettisoned* and the L-II stage is ignited to initiate the main braking phase.

2.2.1 Effect of Target Location

For direct-descent, mission flight time, target longitude (assuming a flight path approximately in the lunar equatorial plane), and impact angle (for hard impact) are interrelated parameters and choosing two of them

*The L-I stage will impact the lunar surface so that care must be taken to insure that this impact occurs without endangering the personnel or equipment on the surface. Since the midcourse approach is several degrees away from local vertical it is expected that the momentum of the L-I stage will be sufficient to insure impact at a safe distance from the target area.

fixes the third. In addition, use of direct descent limits the feasible target regions on the moon. Thus, it is desired to investigate the relationships between the three parameters to determine if direct descent imposes fundamental limitations on the guidance systems considered.

In order to determine the relations between flight time, impact longitude, and angle-off-vertical at impact, a patched conic method of analysis is used, with several checks by integrated trajectories. The results are shown in figures 2-22, 2-23, and 2-24. In figure 2-22, the longitude of vertical impact (west of the earth-moon (EM) line) is plotted as a function of trip time from earth injection. It can be seen that with flight times on the order of 70 hours, it is not possible to achieve vertical descent in the target area. Thus, it is desirable to investigate the angle-off-vertical which results from flights to a target at 27.5° W longitude which is near the center of the target area. In figure 2-23, the angle-off-vertical as a function of flight time is plotted. It can be seen that by allowing the initial angle off vertical to vary by 25 degrees, a wide range of flight times can be used.

In figure 2-24, a plot of angle-off-vertical at impact vs central angle from vertical impact is given for flight times of approximately 72 hours. It can be seen that over the whole range of target latitudes (20° W to 40° W), the initial angle-off-vertical varies by only 14 degrees.

In summary, the results show that although the requirement for vertical descent would be a very stringent constraint on the mission flight time, the whole target area can easily be reached by allowing the initial angle-off-vertical to be as large as 25 degrees. In addition, a wide range of flight times can be handled by allowing the above variation in initial angle-off-vertical.

2.2.2 Direct vs Parking Orbit Fuel Comparison

Since payload weight is the ultimate criterion which must be applied to all space missions, a comparison of the mass landed by direct and parking orbit methods was made. The comparison assumed that the injection velocities

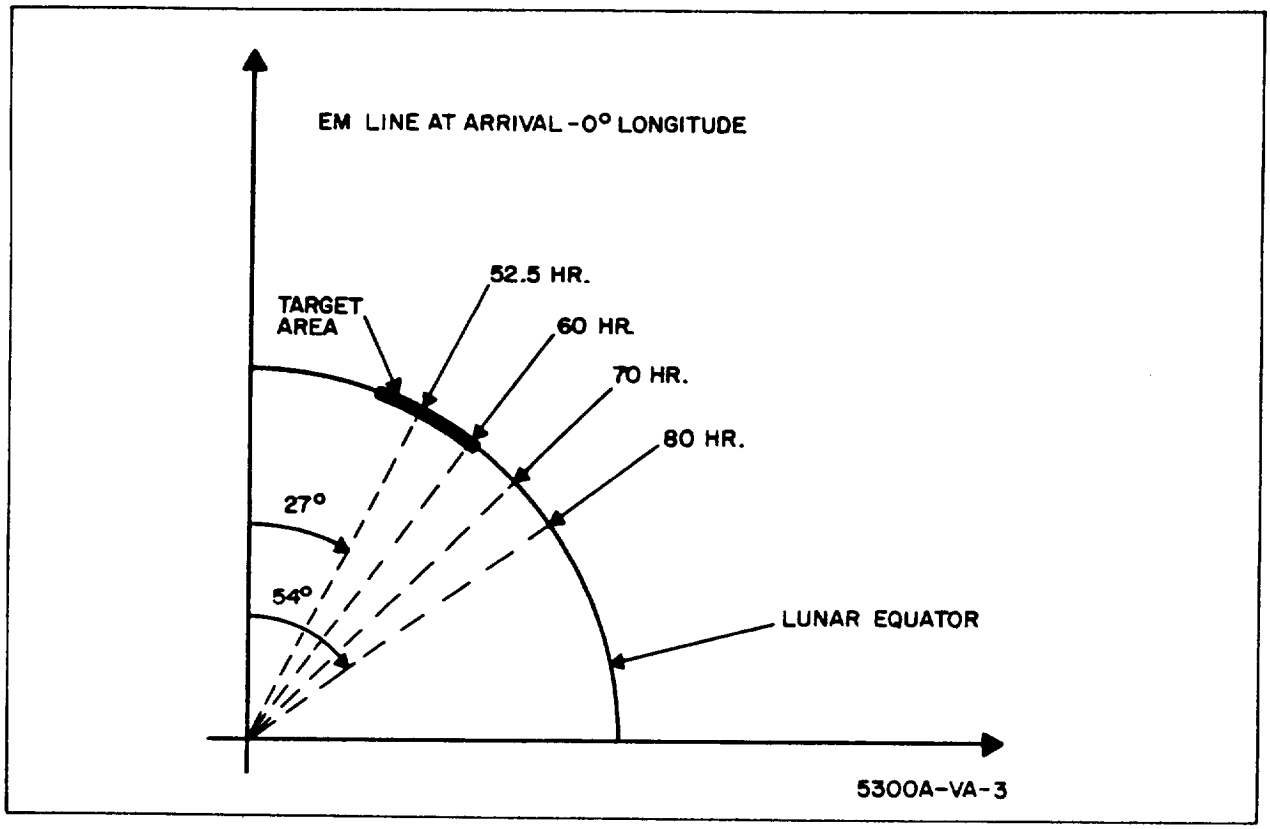

Figure 2-22. Locus of Vertical Impacts

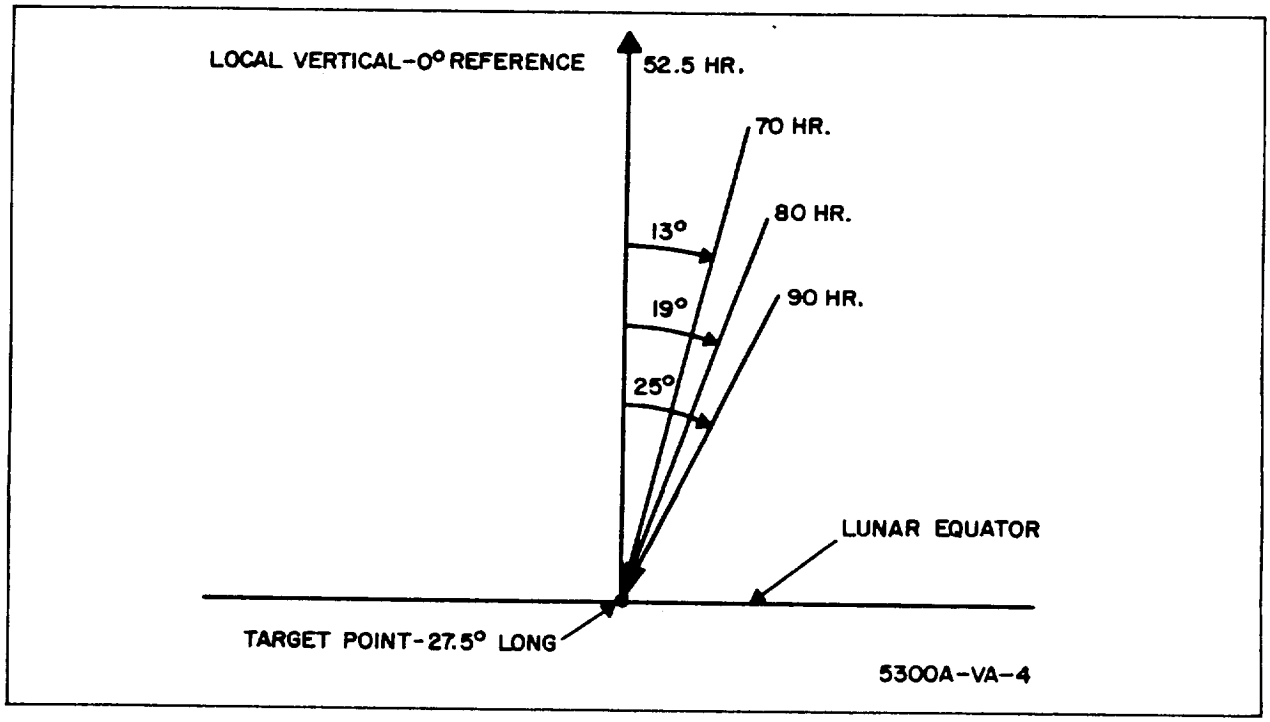

Figure 2-23. Impact Angle vs Transit Time (Constant Target)

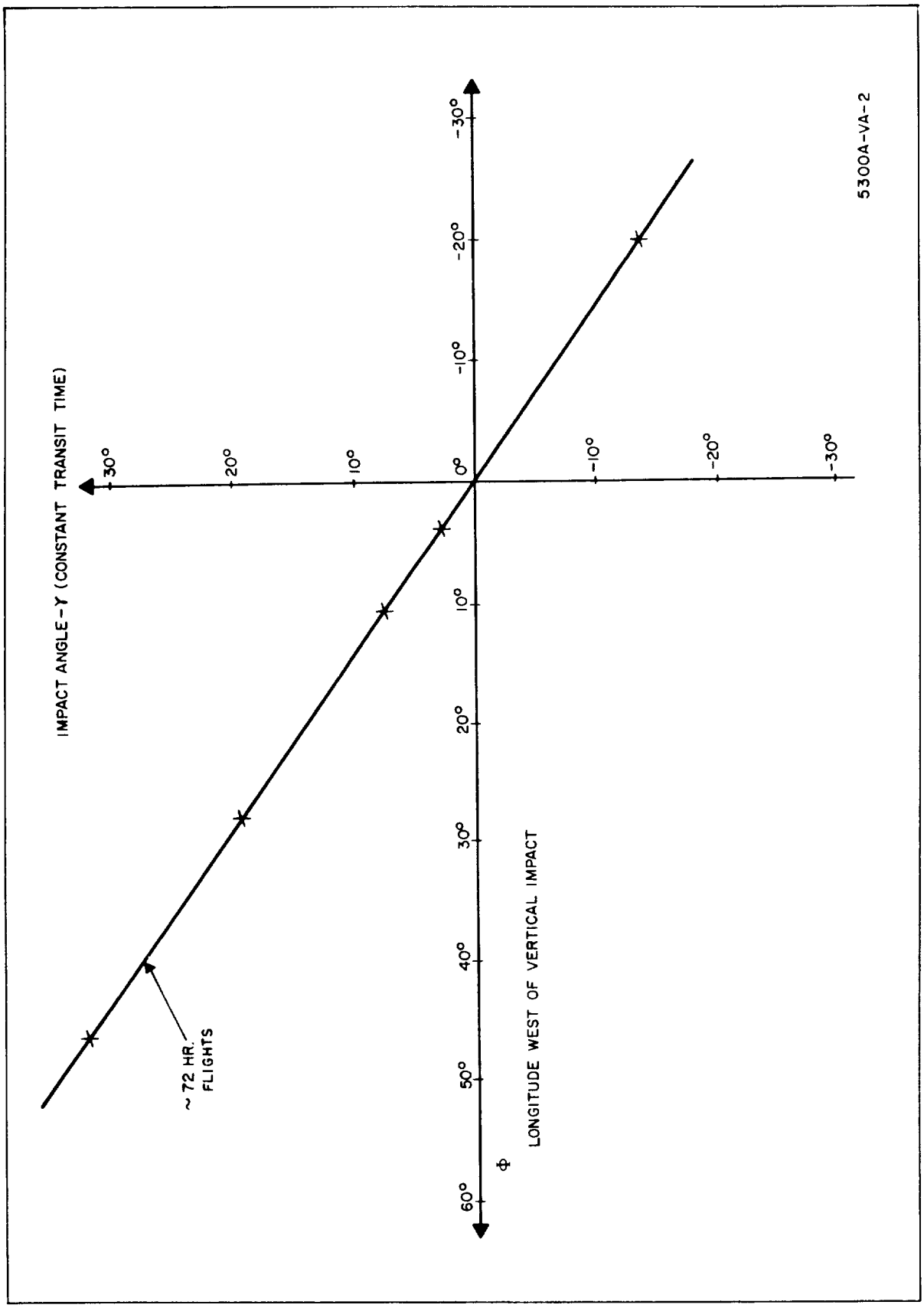

Figure 2-24. Relation of Impact to Target Location

(from earth orbit) are identical for each case and that the vehicles used in each case are identical. The results of a computer simulation of the mass landed by the direct and parking orbit mission profiles are shown in figure 2-25.

The mass landed using the parking orbit method is 19,397 kg. Using direct descent, the mass landed varies with target longitude (and with initial angle-off-vertical) but always is less than that landed by the parking orbit method. In general, the mass landed is at a minimum at the longitude of direct impact and increases with longitude to either side; i.e., the more grazing the trajectory, the more mass landed. The target area is in a region of near-minimum mass landed, and the mass landed by direct flight at 27° W is 18,580 kg, a reduction of 817 kg (or 4.2 percent) from that landed by the orbital approach.

2.2.3 Midcourse Nominal Trajectory

Since the midcourse trajectory used for direct descent is similar to that used for the parking orbit mode, a separate description of the nominal midcourse trajectory is not given here. However, the end point conditions, which are the initial conditions for the beginning of preliminary braking, are shown in figure 2-26. The nominal powered trajectory consists of two gravity turn trajectories separated by a stage separation (of 5 to 10 seconds) which culminate in a landing at 27.5° W longitude. The nominal powered trajectory is described more fully in paragraph 2.2.5.

2.2.4 Approach Guidance

For the system under consideration, beacon acquisition occurs prior to ignition of the L-I stage to start preliminary braking. The L-I ignition criterion is based on observed range to the beacon.

With this type of system, the most important parameters relative to midcourse are the initial cross-track errors at the beginning of preliminary braking. The results of a brief analysis of these cross-track deviations are presented here.

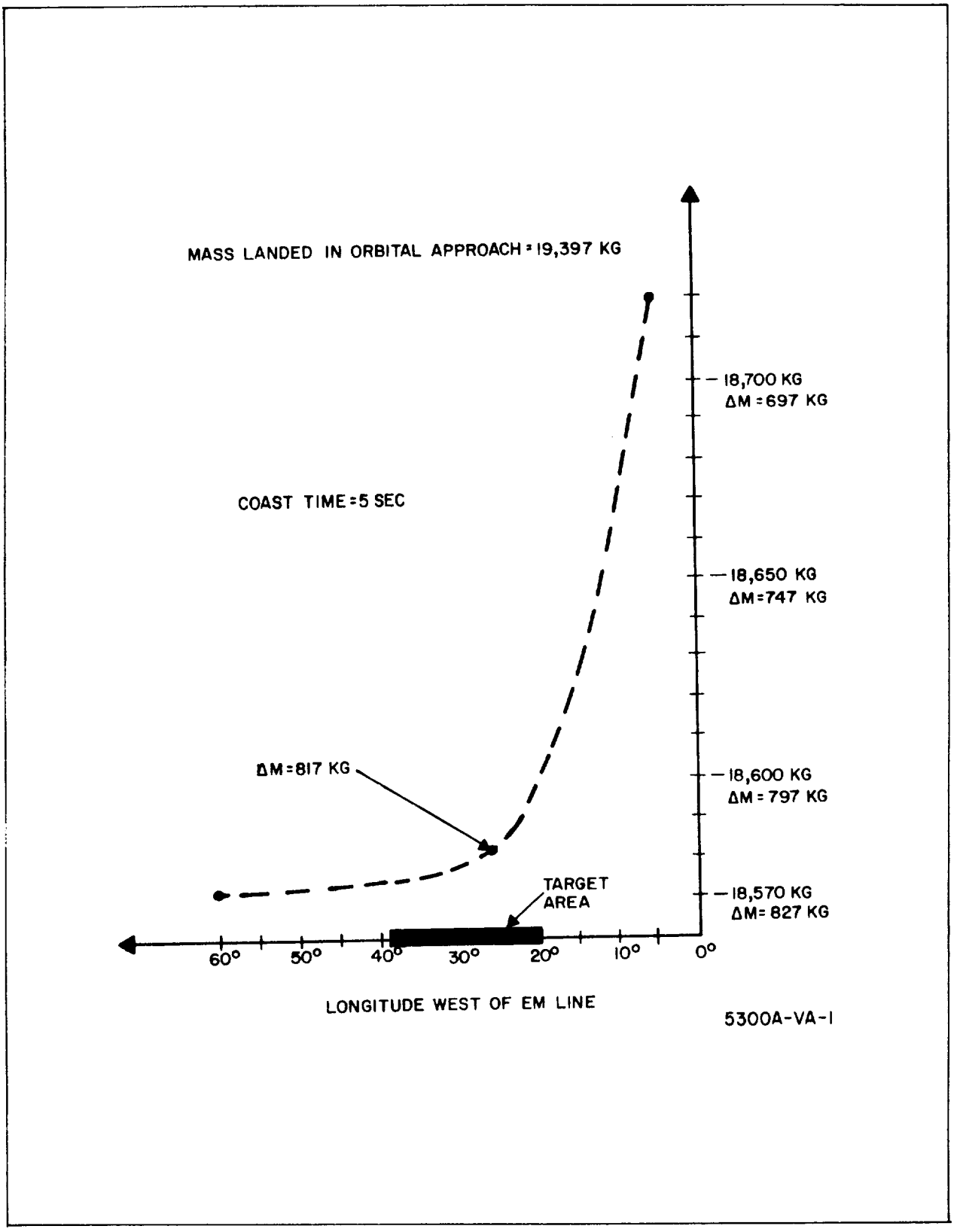

Figure 2-25. Mass Landed in Direct-Descent Mode

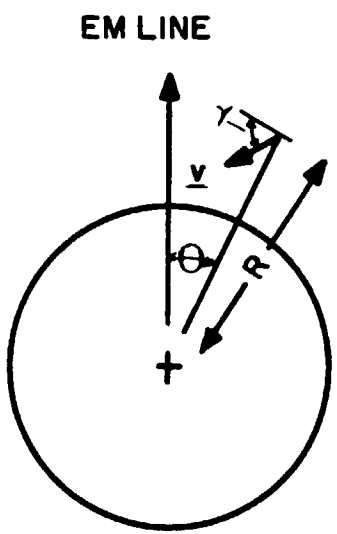

INITIAL CONDITIONS FOR POWERED DIRECT DESCENT

R = 2605 KM (RANGE TO CENTER OF MOON)

V = 2.1977 KM/SEC (VELOCITY)

τ = 77° (VELOCITY ANGLE FROM LOCAL HORIZONTAL)

θ = 31.274° (CENTRAL ANGLE MEASURED POSITIVE WEST FROM E-M LINE.)

5300-VA-41

Figure 2-26. Direct-Descent Parameters

The sensitivity coefficients relating deviations from the nominal trajectory to errors at the time of the second midcourse velocity correction at 50 hours were calculated to be:

$$\frac{\partial \xi}{\partial R} = 5.44\ (10^{-4})\ \text{km/km}$$

$$\frac{\partial \xi}{\partial R} = 90.9\ \text{km/mrad}$$

$$\frac{\partial \xi}{\partial V} = 0.0423\ \text{km/(m/sec)}$$

$$\frac{\partial \xi}{\partial \theta} = 1.63\ \text{km/mrad}$$

where ξ is the cross-track error at initiation of second stage firing caused by errors in R, θ, V, and γ at $T_o = 50$ hours. (R, V, θ and γ are defined in Fig. 2-26). Evidently the limiting factor is the velocity angle error, γ. At $t_o = 50$ hours, $V \cong 1$ km sec, so that a 1 m/sec cross-track velocity error causes a miss of approximately 91 km. From this it can be seen that to keep initial deviations to less than 10 km (rms), then the cross track velocity error after ΔV_2 must be less than 0.1 m/sec. Although a separate computer analysis of the direct descent midcourse was not done, examination of several parking orbit cases just after the second correction revealed cross-track velocity errors on the order of 0.07 m/sec, rms for the standard error cases. Thus, the assumption of no navigation during the midcourse is reasonable. In addition, since the miss distance due to cross track velocity is essentially proportional to $R\delta\gamma$ where $\delta\gamma$ is the angle deviation due to velocity errors and R is the range to the moon, then reducing this range will reduce the miss distance proportionally. Thus, postponement of ΔV_2 from $t_o = 50$ hours to $t_o = 66$ hours results in a reduction of cross-track miss by a factor of about 2.5. Thus, for the direct-descent case, a

significant improvement in system performance can be obtained by postponing ΔV_2 until t_o = 66 hours.

2.2.5 Preliminary Braking and Main Braking

2.2.5.1 Preliminary Braking

Very little detailed investigation of the preliminary braking phase has been performed other than determination of the nominal trajectory which is a constant thrust gravity turn.

It is presumed that the beacon tracker system to be used for navigation during main braking will acquire the beacon prior to the start of the preliminary braking phase, and thus at a range in excess of 850 km. In this way, preliminary braking can be initiated on the basis of information concerning the state of the vehicle relative to the beacon. By proper selection of the initiation criterion, it is possible to reduce the effective down-range error at the end of midcourse. In this case the down-range error at the end of midcourse is nearly all along the initial beacon-to-vehicle range vector so that observed range equal to nominal initial range appears to be a good ignition criterion.

Detailed navigation and guidance concepts have not been specified for the preliminary braking phase so that significant error analysis was not feasible.

2.2.5.2 Main Braking

The main braking phase* nominal trajectory is a constant thrust, gravity turn trajectory with the following initial and final conditions. The values are expressed in a coordinate system centered at the beacon with Z along beacon local vertical, and X along local horizontal in the nominal plane of vehicle motion with X positive toward the initial position of the vehicle.

---

*The main braking phase as defined here begins when the L-II stage is fired and does not include the preliminary braking phase.

- Initial Conditions

  X_{in} = 100.82 km

  Z_{in} = 403.18 km

  $\dot{X}_{in}$ = -437.35 m/sec

  $\dot{Z}_{in}$ = -1453.3 m/sec

  t_i = 0

  M_{in} = 31,068 kg

- Final Conditions

  X_{fn} = -250 m

  Z_{fn} = 300 m

  $\dot{X}_{fn}$ = 2.234 m/sec

  $\dot{Z}_{fn}$ = -37.41 m/sec

  t_{fn} = 494 sec

  M_{fn} = 18,846 kg

- Nominal Thrust Program

  F = 106,750 N = constant

  α = 180° = constant

The navigation, guidance, and control system model used in the direct descent analysis is identical in form to that described in paragraph 2.1.4.2. The only change made is the generation of new reference curves for $\dot{R}$ and Γ_{los} to reflect the new nominal trajectory. The direct descent reference curves used are given in paragraph 8.1.

The error model used for the direct-descent study is the same as that used for orbital descent (paragraph 2.1.4.3) as are the analytical techniques used (paragraph 2.1.4.4). In fact, the same digital programs are directly applicable modified only to the extent required to include the new reference curves and the new nominal trajectory.

The numerical results, obtained from analysis, that is the sensitivity coefficient matrices, $\left[S_{p_f p_i}\right]$, $\left[S_{p_f \tilde{q}_{bc}}\right]$, $\left[S_{p_f \tilde{q}_{bs}}\right]$, $\left[S_{p_f \tilde{q}_{nc}}\right]$, and $\left[S_{p_f \tilde{q}_{ns}}\right]$

are presented below. The nomenclature is identical to that used in paragraph 2.1.4. The random error sensitivity matrices obtained by adjoint system simulation have been transformed from the nominal time criterion to the cutoff criterion based on observed altitude by the same technique used to transform the orbital mission results. (See paragraph 2.1.4.4 and 8.4.)

$$\left[S_{p_f p_i}\right] = \begin{bmatrix} 1.90\times10^{-3} & -5.39\times10^{-4} & 1.76\times10^{-1} & -5.5\times10^{-2} \\ 0 & 0 & 0 & 0 \\ -2.13\times10^{-4} & 6.13\times10^{-5} & -2.00\times10^{-2} & 5.26\times10^{-3} \\ 2.15\times10^{-4} & -5.40\times10^{-5} & 1.75\times10^{-2} & -1.42\times10^{-2} \end{bmatrix}$$

$$\left[S_{p_f \tilde{q}_{bc}}\right] = \begin{bmatrix} 6.39\times10^{-1} & 4.09\times10^{0} & 0 & -4.00\times10^{5} & -9.8\times10^{-5} & -9.11\times10^{2} \\ -7.69\times10^{-1} & 0 & -2.50\times10^{2} & 0 & 0 & 0 \\ 4.93\times10^{-2} & 1.36\times10^{-1} & 0 & 4.68\times10^{4} & -3.00\times10^{-5} & 9.17\times10^{1} \\ -7.61\times10^{-2} & -1.18\times10^{0} & 0 & -4.09\times10^{4} & -3.54\times10^{-4} & -1.09\times10^{2} \end{bmatrix}$$

$$\left[S_{p_f \tilde{q}_{bs}}\right] = \begin{bmatrix} 6.26\times10^{0} & -3.15\times10^{0} & 0 & 4.31\times10^{0} & \text{NC*} & \text{NC*} \\ -3.00\times10^{0} & 0 & 1.74\times10^{0} & 0 & 0 & 0 \\ -1.73\times10^{-1} & 1.73\times10^{-1} & 0 & -1.83\times10^{-1} & \text{NC*} & \text{NC*} \\ -8.14\times10^{-2} & 4.81\times10^{-1} & 0 & 5.96\times10^{-1} & \text{NC*} & \text{NC*} \end{bmatrix}$$

*Not computed (NC) because bias scale factor errors are not considered as components of the corresponding error sources. (See paragraph 2.1.4.4.)

$$\left[S_{p_f \tilde{q}_{nc}}\right] = \begin{bmatrix} 1.29\times10^{-2} & 4.62\times10^{-1} & 0 & 1.98\times10^{8} & 1.35\times10^{-8} & 2.00\times10^{0} \\ 5.90\times10^{-1} & 0 & 6.26\times10^{4} & 0 & 0 & 0 \\ 1.52\times10^{-3} & 5.90\times10^{-2} & 0 & 1.51\times10^{6} & 2.74\times10^{-10} & 3.21\times10^{1} \\ 9.28\times10^{-4} & 1.84\times10^{-1} & 0 & 1.06\times10^{6} & 7.97\times10^{-9} & 2.13\times10^{1} \end{bmatrix}$$

$$\left[S_{p_f \tilde{q}_{ns}}\right] = \begin{bmatrix} 9.10\times10^{-1} & 2.36\times10^{0} & 0 & 2.08\times10^{-1} & 1.54\times10^{-2} & 1.06\times10^{-2} \\ 9.03\times10^{0} & 0 & 3.02\times10^{0} & 0 & 0 & 0 \\ 4.86\times10^{-2} & 2.86\times10^{-2} & 0 & 8.84\times10^{-3} & 2.96\times10^{-4} & 5.52\times10^{-4} \\ 2.38\times10^{-1} & 1.01\times10^{2} & 0 & 3.42\times10^{-3} & 9.07\times10^{-3} & 1.67\times10^{-4} \end{bmatrix}$$

Comparison with results obtained for the orbital main braking indicates that the deviations from nominal at the end of main braking caused by main braking sensor errors are roughly the same for either case (assuming equal sensing accuracy).

With regard to the sensitivity to bias errors in sensing line of sight rate $\dot{\psi}$, the direct descent appears to be more sensitive than the orbital descent. This particular fact is pointed out because it is shown in paragraph 2.1.6 and also in paragraph 3.1 that bias errors in measuring the angle rate are perhaps the single most important error source in the orbital mission system concept. One must also expect this error source to be significant in the direct-descent concept. A plausible explanation for this particular increase in sensitivity is easily found. In general, the nominal value of the magnitude of $\dot{\psi}$ is smaller than it is for the orbital descent profile. Therefore, the identical constant bias error level is equivalent to a greater percent of error during direct descent.

2.2.6 Final Touchdown

The discussion of the final touchdown phase presented in paragraph 2.1.5 is equally applicable to either the orbital or direct-descent mission profile,

with one minor change. In direct descent, the magnitude of the nominal horizontal (in-plane) component of velocity at main braking termination ($\dot{X}_{f_n}$) is on the order of 2 m/sec as opposed to 9 m/sec for the orbital descent profile. This results in an increase in the allowable initial deviation of $\dot{X}_f$ from $\dot{X}_{f_n}$ as evaluated in paragraph 2.1.5.3.1 from $3(\sigma_{\dot{x}_f})_{max}$ = 10 m/sec to $3(\sigma_{\dot{x}_f})_{max}$ = 17 m/sec.

Since this component of the allowable deviations at final touchdown initiation (main braking termination) was found to be the most stringent with regard to the orbital mission, the relaxation of this requirement indicated above serves to relax navigation accuracy requirements for direct descent somewhat. However, this should not be taken as a strong point in favor of a direct-descent profile for the following reasons:

- The entire increase in allowable horizontal velocity error cannot be converted to relaxed navigation requirements. After only a fraction of the total increase, the allowed vertical velocity deviation becomes the most stringent performance requirement.
- The nominal horizontal velocity at the end of main braking for the orbital profile can be reduced with only slight modification to the nominal trajectory. Such modification would not be expected to alter orbital mission requirements to any significant degree.

2.2.7 Summary of Direct-Descent Results

This paragraph consists of a summary of results of the analyses of the direct descent mission:

a. Direct descent to any point in the target area can be made to within 25 degrees of local vertical for all reasonable trip times.

b. The mass landed with the direct-descent mode is 4.2 per cent less than a similar vehicle using the parking orbit mode.

c. The standard DSIF errors (defined in paragraph 2.1.1.3) result in small enough deviations (at the beginning of powered flight) such that navigation need not be performed before L-I stage ignition.

d. The deviation at the beginning of powered flight can be reduced by a factor of about 2.5 by postponing the second velocity correction until 66 hours.

e. The sensitivity of errors at the end of main braking to initial condition errors and sensor errors is roughly equivalent to that determined for the descent main braking phase.

3. RESULTS

3.1 RECOMMENDED SYSTEM

The following paragraphs present a phase-by-phase summary of the recommended system for performing the unmanned lunar landing mission. The orbital mission is selected on the basis of fuel economy for the nominal profile, mission flexibility, and the fact that, for the initial and terminal conditions assumed, on-board system complexity for the orbital mission does not greatly exceed that for the direct descent, assuming a maximum utilization of on-board as opposed to earth-based guidance. Retrothrust guidance is the principal difference.

Symbols used in the following paragraphs are taken from the appropriate discussion in Section 2. All accuracies are given in terms of rms or 1σ values including bias levels. RMS bias levels should be multiplied by 3 to give what one ordinarily thinks of as a maximum bias level tolerance.

3.1.1 Midcourse Approach Phase

Earth-based navigation and guidance is assumed for the recommended mission until second midcourse correction which is assumed to take place at 66 hours, after injection into earth-lunar trajectory. Numerical values assumed for the complete estimation and deviation matrices at this point are as given in equations 5-25 and 5-26 of paragraph 5.4.

The second correction is assumed calculated on the basis of fixed-time-of-arrival at periselenum and the correction accuracies assumed are a 1σ magnitude error of 0.1 m/sec and a 1σ pointing accuracy of 1 degree.

Approximately 1 hour prior to retrothrust the inertial measurement unit is placed in a gyrocompassing mode utilizing a horizon scanner for the reasons summarized in paragraph 12.6. Allowable tolerance on gyro drift

bias for this purpose is approximately 0.1 deg/hr (1σ), assumed horizon scanner bias is 0.1 degree (rms).

Other than this no midcourse approach navigation is assumed.

3.1.2 Retrothrust

Retrothrust is assumed to begin at nominal time, measured from time of second midcourse correction, and the inertial measurement unit is used as the orbital plane reference, based on gyrocompassing during the preceding phase.

All inertial navigation is used based on updating the estimated state at retrothrust initiation according to measured thrust accelerations and computed gravitational accelerations. Thus, except for compensation of estimated in-plane residual velocity errors, the guidance system flies the nominal trajectory since the only available information concludes that position errors have been cancelled by the second midcourse correction.

The guidance scheme described in paragraph 2.1.2 is sufficient to perform the retrothrust maneuver nearly optimally (within 5 percent of equivalent impulsive thrust duration). This concept is basically a simplified version of a more sophisticated two-dimensional explicit guidance concept. The simplifications have reduced on-board computations required without seriously degrading performance. The nature of the guidance law is to control altitude and altitude rate explicitly. In addition, the horizontal (in-plane) velocity is controlled by using estimated horizontal velocity as the retrothrust termination criterion.

Gyrocompassing is discontinued during the maneuver because of the induced transient due to the velocity change and because of probable distortion of horizon scanner information due to vehicle engine exhaust, and the platform is assumed to be precessed at computed orbital rate or the equivalent.

The following 1σ bias tolerances will allow satisfactory performance of the mission:

- Thrust magnitude measurement: $\sigma_{\tilde{f}_c} < 1000$ N.
- Thrust direction measurement: $\sigma_{\tilde{\alpha}_c} < 0.05$ rad
- Initial inertial platform alignment to local vertical: $\sigma_{\tilde{\gamma}_i} < 0.002$ rad
- Radial direction acceleration measurement: $\sigma_{\tilde{a}_{FR}} < 0.01$ m/sec^2
- Transverse acceleration measurement: $\sigma_{\tilde{a}_{F\theta}} < 0.002$ m/sec^2

Gyro drift is not a problem in this phase because of the short time duration.

3.1.3 Parking Orbit, Descent Kick, and Descent Coast Orbit

The parking orbit following retrothrust is nominally circular at altitude 185 km, subtending 130 degrees of lunar central angle and lasting 45.5 minutes. During the time in parking orbit no navigation is assumed other than gyrocompassing to retain an attitude reference.

The nominal descent kick maneuver is performed at the nominal time with respect to the on-board reference frame. That is, a ΔV of 67 m/sec is applied horizontally in the orbit plane.

After descent kick application, the spacecraft is at apo-selene of the descent coast elliptical orbit. Again, no navigation other than keeping track of time, and gyrocompassing is assumed. Gyrocompassing is continued through the descent coast for the following reasons.

- To provide a reference coordinate frame to aid in locating the beacon prior to main braking
- So that an accurate estimate of the initial local vertical direction will be available at main braking initiation
- Orbital plane information from gyrocompassing, combined with radar measurements to the beacon, provides the first accurate information concerning the out-of-plane errors which must be corrected during the main braking maneuver.

The vehicle passes over the beacon horizon approximately 1.5 to 2 minutes prior to main braking initiation. During this interval, the following operations occur:

- Acquisition of landing site beacon
- Estimation of out-of-plane error
- Continuous estimation of central angle between beacon and spacecraft

The central angle estimate is used as the criterion for initiating the main braking maneuver. By initiating main braking when the estimated central angle (based on direct radar measurements and the onboard reference frame) is equal to the nominal initial central angle, practically all of the down range position error that would exist if time were the initiation criterion is eliminated. (This error can be large since no down range control is included in the retrothrust maneuver.) In addition, the central angle estimate, along with out-of-plane angle data, provides sufficient information such that the orientation of the onboard reference frame with respect to a beacon local vertical coordinate frame can be estimated. Thus, the onboard coordinate system can be aligned to beacon local vertical or maintained at a known orientation with respect to beacon local vertical if desired.

The only sources of error considered during the orbital phases are the errors in application of the descent kick and the errors in observing radar information required for estimation of beacon-to-vehicle central angle. The following error levels are recommended as being sufficient for mission success.

- Descent kick application errors (rms)
- Magnitude: $\sigma_{\delta V_2} < 1$ m/sec
- Pointing angle: $\sigma_{\delta\alpha} < 0.02$ radian
- Central angle estimation error sources (rms)
- Initial range measurement: $\sigma_{\tilde{r}_i} < 3.5$ km
- Initial angle measurement: $\sigma_{(\tilde{\theta}_a)_i} < 0.025$ radian

3.1.4 Main Braking Phase

As stated previously, the main braking phase is initiated on the basis of on-board estimation of the beacon-to-spacecraft central angle. The in-plane guidance concept used during main braking as well as the fact that a beacon is present at the desired landing site are specified inputs to the study so that recommendation of the main braking system reduces to specifying the navigation concept and the sensor accuracies required for mission success.

The main braking phase analysis discussed in paragraph 2.1.4 deals with the in-plane motion so that the following error specifications are given for those sensor errors which affect the in-plane guidance system.

Given the fact that a beacon is located at the desired landing site, the simplest navigation concept capable of providing complete (three-dimensional) navigation information is the use of a beacon tracking device observing range, range rate, LOS angle, and LOS angle rate to the beacon. Therefore, in line with study guidelines, this is the navigation concept studied.

Control during main braking is provided by two variable thrust, gimbaled engines. Engine commands are generated using an implicit guidance law as follows.

- Commanded thrust magnitude is equal to nominal thrust magnitude plus a deviation proportional to the difference between observed range rate and nominal range rate.
- Thrust direction (in-plane) is equal to the nominal direction plus a deviation proportional to the difference between the estimated angle between the velocity vector and the beacon sightline, and the nominal value of this same angle.

The main braking maneuver is terminated when the estimated vehicle altitude is 300 meters.

On the basis of study results, the navigation and control sensor error levels specified as being sufficient for mission success are as follows.

a. Constant bias error tolerances (rms)

- Range measurement: $\sigma_{\tilde{r}_{bc}} < 3.0$ m

- Range rate measurement: $\sigma_{\tilde{\dot{r}}_{bc}} < 0.2$ m/sec
- Angle measurement:* not specified
- Angle rate measurement: $\sigma_{\tilde{\dot{\psi}}_{bc}} < 0.00005$ rad/sec
- Thrust magnitude measurement: $\sigma_{\tilde{f}_{bc}} < 3000$ N
- Thrust angle measurement: $\sigma_{(\tilde{\theta}_{los})_{bc}} < 0.01$ rad

b. Scale factor bias error tolerances (rms)

- Range measurement: $\sigma_{\tilde{r}_{bs}} < 1.0\%$
- Range rate measurement: $\sigma_{\tilde{\dot{r}}_{bs}} < 0.3\%$
- Angle measurement:** not specified
- Angle rate measurement: $\sigma_{\tilde{\dot{\psi}}_{bs}} < 1.0\%$
- Thrust magnitude measurement:** not specified
- Thrust angle measurement:** not specified

c. Constant rms value Random Error Tolerances

- Range measurement: $\sigma_{\tilde{r}_{nc}} < 3.0$ m
- Range rate measurement: $\sigma_{\tilde{\dot{r}}_{nc}} < 0.25$ m/sec
- Angle measurement: not specified
- Angle rate measurement: $\sigma_{\tilde{\dot{\psi}}_{nc}} < 0.0001$ rad/sec
- Thrust magnitude measurement: $\sigma_{\tilde{f}_{nc}} < 1000$ N
- Thrust angle measurement: $\sigma_{(\tilde{\theta}_{los})_{nc}} < 0.01$ rad

d. Constant rms value Scale factor Random Error Tolerances

- Range measurement: $\sigma_{\tilde{r}_{ns}} < 0.5\%$

---

* Not determinable from in-plane error analysis

** Scale factor errors are not considered as part of the error model for angle measurements or for thrust measurement.

- Range rate measurement: $\sigma_{\dot{r}_{ns}} < 0.2\%$
- Angle measurement: not specified
- Angle rate measurement: $\sigma_{\dot{\psi}_{ns}} < 1.0\%$
- Thrust magnitude measurement: not specified
- Thrust angle measurement: not specified

Of all the requirements specified above, only one appears to present a feasibility problem. That is the requirement for a bias error in measuring line-of-sight rate ($\dot{\Psi}$) of something less than 0.05 milliradian/second (1σ). It has been ascertained from the literature that good inertial grade rate gyros (with all error sources taken into account) are capable of achieving maximum bias error levels on the order of 0.01 to 0.1 milliradian/second. The significance of the term "maximum" is to indicate that this is the range of 3σ error levels that can be expected. Since the specified error tolerance is 0.15 mr/sec (3σ), it appears the accuracy required is within the realm of feasibility.

3.1.5 Final Touchdown

A complete guidance system is not specified for final touchdown. The approach taken in this study is to assume that beacon tracker information and possibly altimeter information might not be available below an altitude of 100 meters (possibly because of dust kicked up by engine exhaust). Therefore the last 100 meters of descent is performed using inertial navigation, and guidance based on nulling horizontal velocity components and making the vertical velocity equal to the desired vertical impact velocity (selected to be 2.5 m/sec) is assumed.

The inertial navigator is initiated at an altitude of 100 meters using position and velocity estimates obtained from beacon tracker information. The resulting required accuracies are:

a. Beacon tracker accuracy* (rms)

- Range measurement: $\sigma_{\tilde{r}} < 3.0$ m
- Range rate measurement: $\sigma_{\dot{\tilde{r}}} < 0.14$ m/sec
- Angle measurement: $\sigma_{\tilde{\psi}} < 0.0035$ radian
- Angle rate measurement: $\sigma_{\dot{\tilde{\psi}}} < 0.0007$ rad/sec

b. Acceleration sensor bias error (rms)

X-direction: $\sigma_{\ddot{\tilde{x}}_b} < 0.002$ m/sec^2

Y-direction: $\sigma_{\ddot{\tilde{y}}_b} < 0.002$ m/sec^2

Z-direction: $\sigma_{\ddot{\tilde{z}}_b} < 0.002$ m/sec^2

c. IMU alignment to landing site local vertical (rms):

$\sigma_{\zeta} < 0.002$ rad

It is believed that the beacon tracker accuracies and the alignment accuracy (especially the latter) specifications can be satisfied marginally within the state of the art. The acceleration sensor specifications are known to be achievable.

3.1.6 Breakdown of Errors at Main Braking Termination for Recommended System

In previous paragraphs, the accuracy specifications given are quoted as being sufficient for mission success. Mission success as defined in this section is based on achieving deviations from the nominal at the end of main braking which are within the allowed limits established in paragraph 2.1.5. Using the specified error levels for each mission phase, computations similar to the sample computations in paragraph 10.3 have been performed. Computation results include not only the total errors at main braking termination but also the distributions of the total errors among the various error

---

* The numbers presented represent the total rms error (including biases and noise) in measuring the corresponding parameter, in the region of the nominal point of inertial navigation initiation.

sources. These distributions are illustrated in the form of bar graphs in figure 3-1. The individual rms contributions of each error source to the total rms errors in horizontal position (σ_{x_f}), horizontal velocity ($\sigma_{\dot{x}_f}$), and vertical velocity ($\sigma_{\dot{z}_f}$) at the end of main braking are illustrated. Vertical position errors are not shown because they are, by virtue of the specified main braking termination criterion, solely a function of how well altitude can be estimated in the region of the terminal point. The accuracy obtainable using beacon tracker accuracies specified is felt to be sufficient to guarantee terminal altitude accuracy within tolerable limits.

At the bottom of each graph, the total root sum square value of the terminal deviation obtained with the recommended system is presented along with maximum allowable rms value of the deviation as determined in paragraph 2.1.5.

It will be seen in figure 3-1 that for the specified error levels, main braking bias errors are significantly more important than main braking random errors, and that the single most significant error source is the constant bias error in measuring line of sight angular rate ($\dot{\Psi}$) during main braking. It appears that the most significant improvement to be made in overall performance is obtained through reduction of this error source, possibly by the use of alternate observables so that observation of $\dot{\Psi}$ is not required, at least during the initial portion of main braking, where the errors in observing $\dot{\Psi}$ have the most effect.

3.2 ALTERNATE CANDIDATE SYSTEMS

In this paragraph, methods of guidance and navigation are described which will reduce the large uncertainties caused by degraded DSIF. It should be kept in mind that with large estimation errors, large deviations are expected, since the estimation errors determine accuracy with the second correction can be made. Thus, the fixed-time system assumed for the primary recommended system would not be efficient due to the heavy fuel penalties required

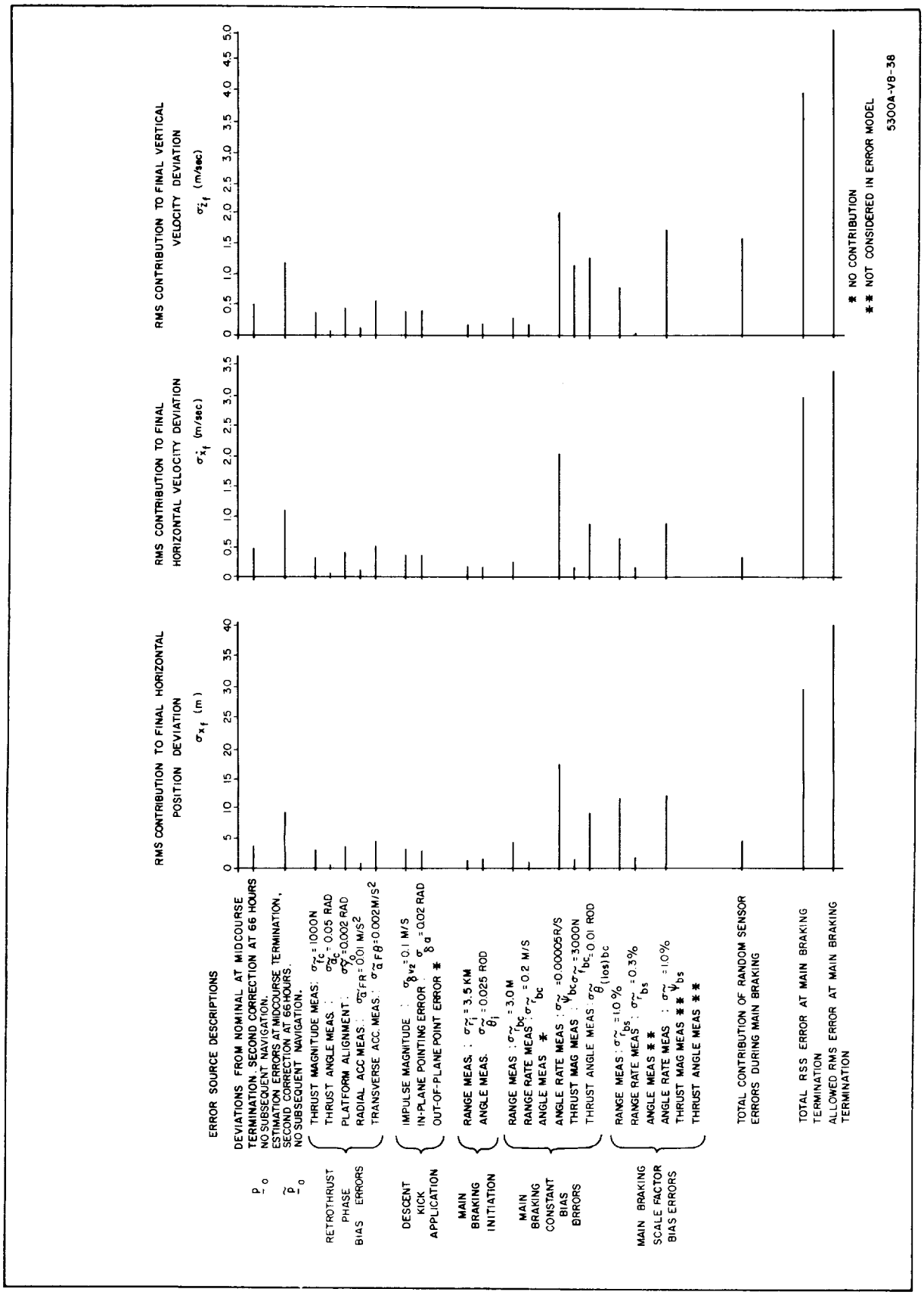

Figure 3-1. Breakdown of Terminal Errors Resulting Using Recommended System

to offset trajectory deviations in a given time. Hence, new independent variables to replace time are required for initiation of guidance for the successive phases. These would depend on the geometry of each phase, but reasonable assumptions would be as follows:

- Midcourse trajectory (ΔV_2) — Time.
- Retrothrust — Range.
- Descent kick — Central angle.
- Main braking — Range to beacon.

A discussion of alternate useful navigation, guidance, and control systems, within the ground rules of this study, applies primarily to midcourse approach, since for the orbital mission the reasonable choice of navigation sensors for the following phases and guidance for the landing are more or less fixed.

3.2.1 Midcourse Phase Alternate Systems

Two navigation systems which gave promising results in reducing large estimation errors were (1) an altimeter system and (2) an angle measurement system. The operation of each of these is described briefly here.

3.2.1.1 Altimeter Measurements

This mode of operation is similar to the primary recommended system described in paragraph 3.1, except that during the last 15 minutes before retrothrust initiation, measurements of the spacecraft altitude above the surface are used to update the trajectory estimate obtained from the DSIF. Altimeter accuracy of up to 500 meters is sufficient to give useful results, subject to the other measurement errors (terrain, lunar radius uncertainty, oblateness) being on the order of 2-km total. The range required is 1000 km. Data rate requirements are not high since it is not required to determine local terrain. Five to ten accurate range measurements during the 15-minute period are sufficient, and higher data rates would increase the computing load without necessarily yielding significantly better information.

The range data are processed, using the following equations:

$$\underline{p}\,(\text{updated}) = \underline{p} + K\left[R - R_p\right] \qquad (3\text{-}1)$$

where $\underline{p}$ (updated) is the state estimate including the last measurement, $\underline{p}$ is the previous estimate, K is a precomputed weighting vector and is the difference between the predicted and measured range.

The use of an altimeter during midcourse approach is not expected to interfere with the gyrocompassing mode of operation. In addition the horizon scanner tracking could be used to point the altimeter toward the moon.

3.2.1.2 Local Vertical - Angle Measurements

Measurements of the angle between local vertical and inertial reference can also be used to refine the midcourse trajectory estimate. It was found in paragraph 2.1.1.4 that angle measurements accurate to 2 mr were sufficient to give useful results. Two fundamental differences exist between this system and the altimeter system. For one, the altimeter can obtain only in-plane information while the angle measurements are not so restricted. Secondly, the angle measurements require an inertial reference. Thus, if only one stable platform is available, gyrocompassing can not be done, since the inertial (rather than local) reference system must be maintained. Also, this reference must be accurate to less than 1 mr to avoid degrading the angle measurements. The consequence, then, is that retrothrusting would have to be done with an inertial referenced platform rather than a local reference system.

3.2.2 Subsequent Phases

With regard to retrothrust, the retrothrust maneuver would be initiated based on nominal range, using range to the center of the moon as estimated by midcourse approach guidance as the criterion. The retrothrust in-plane guidance law used in this study is capable of handling much larger initial deviations than resulted from the standard error cases and would be utilized essentially as is. An out-of-plane correction capability would have to be

added however either to the retrothrust or the descent kick maneuver based upon out-of-plane error as computed at the end of midcourse guidance.

The descent kick would have to be initiated based on central angle as measured from initiation of retrothrust and based on initial conditions provided by midcourse approach guidance.

Main braking would be initiated as for the recommended system.

4. CONCLUSIONS AND RECOMMENDATIONS

4.1 OVERALL CONCLUSIONS

General conclusions are that: (1) mission requirements for the recommended system can be satisfied using state-of-the-art navigation capability and simple guidance concepts for the onboard system; (2) that out-of-plane errors at the end of midcourse approach are small enough so that they can be allowed to propagate to initiation of main braking before correction at an expense of something less than 5 percent of nominal main braking fuel consumption, thus obviating the need for out-of-plane navigation during prior orbital phases; and (3) that the complete covariance matrices of estimation errors and deviations should be used, as they were used in this analysis, in any similar multiphase mission error analyses, rather than simply the diagonal term approximations, since such approximations, repeated throughout the analysis, become unrealistically pessimistic.

Detailed overall conclusions are given in paragraph 3.1.

4.2 AREAS FOR FURTHER STUDY

Subject to the initial and terminal conditions assumed as a ground rule for this study, the navigation and control sensor accuracy requirements obtained for the recommended system are within the state of the art and in the main are not marginal. It is seen, however, in paragraph 3.1 that a large proportion of the total tolerance allotment resulting in the required terminal accuracy is taken up by the tolerance allowed for measurement of line-of-sight (LOS) rate during the main braking phase, and that even so, the tolerance is strict with regard to the navigation sensor involved. This occurs because of the small (LOS) rates to be measured at long ranges; i.e. 1.5 milliradians/sec. at 350 km. A major system improvement, and resulting relaxation on allowable tolerances for the remainder of the system sensors, would result from a modification of main braking navigation and guidance to reduce the sensitivity

to (LOS) rate error. The main braking guidance scheme for the recommended system utilizes the angle between vehicle velocity vector and vehicle-beacon LOS as an input, and this, in the present recommended system, is obtained by measurement of vehicle velocity components along and perpendicular to vehicle-beacon LOS through measurement of range rate, range, and LOS rate to the beacon. This angle could be obtained, possibly equally as well or better through: (1) measurement of range rate to the beacon and altitude rate to the lunar surface with knowledge of local vertical obtained from the inertial measurement unit, or (2) computation of vehicle velocity direction with respect to the inertial platform through use of inertial measurement and estimated main braking initial conditions and measurement of vehicle-beacon LOS with respect to the inertial platform by the radar, or (3) use of nominal LOS rate for computation for the first portion of the trajectory, or (4) some combination of the above. While the present navigation method is probably the best from all standpoints for the latter portion of the main braking trajectory, it is recommended,as an area for further study, that alternate navigation methods, as outlined above, be examined for the first portion of the main braking trajectory (i.e., greater than 20-km range), and resulting sensor requirements redetermined.

In the present study, the effect of out-of-plane errors was studied only to the extent necessary to determine that, subject to the assumed initial and terminal mission end conditions, out-of-plane navigation is not necessary for the recommended system for orbital phases prior to main braking. During main braking, out-of-plane navigation becomes feasible and simple using vehicle-beacon LOS direction with respect to the inertial platform, and it was shown, assuming an error-free system that less than a 5 percent increase in main braking fuel consumption was required, assuming a less than optimum guidance system. Nevertheless, a complete analysis of out-of-plane navigation, guidance, and control similar to the in-plane analysis

performed for this study should be conducted to properly delineate entire system performance. In part, this would involve the synthesis of a horizontal channel guidance system for the retrothrust and main braking phases.

The navigation requirements, if final touchdown is to be performed using inertial navigation and guidance, appear to be only marginally feasible within the state of the art. It is recommended that further study of this phase of the mission be undertaken with the following goals:

a. Refinement of the navigation accuracy requirements when inertial navigation and guidance is used for final touchdown

b. Determination of navigation requirements when radar or other techniques are assumed to provide navigation information all the way to impact

c. Evaluation of impact velocity requirements specified as inputs to this study (particularly horizontal components)

The study area dealt with in this report and in the discussion for further studies as above constitutes a determination of system parametric requirements without regard to hardware mechanization except to the extent necessary to determine feasibility. The next step in system development consists of a conversion of parametric requirements into an explicit definition of physical equipment. A first step in this direction might be termed preliminary mechanization.

With regard to preliminary mechanization studies, the following items warrant attention: (1) a preliminary mechanization study of the vehicle radar and lunar surface beacon transponder based on mission requirements for the main braking and subsequent mission phases; (2)a more complete study of retrothrust navigation and guidance as it would be mechanized for the onboard system; (3)a more complete study of main braking navigation and guidance as it would be mechanized for an onboard system; (4) the requirements for gimbaling the horizon sensor; the vehicle will undergo both limit-cycle oscillations and changes in attitude, the effects of which will appear in the

horizon sensor signals, if not gimbaled, and must be removed, whereas the horizon sensor functions most effectively as a null device.

5. MIDCOURSE APPROACH APPENDIX

5.1 ANALYSIS OF HORIZON SCANNER RANGING NAVIGATION AND DOPPLER NAVIGATION

Two methods of analysis which were considered briefly in this study include horizon scanner ranging and doppler navigation. Analyses of each follow.

5.1.1 Horizon Scanner (Subtense Angle) Ranging

Figure 5-1 illustrates the geometry involved, together with the pertinent error sources. The range R from the spacecraft to the center of the planet may be determined by measuring 2θ, the angle subtended by the visible disc of the planet, and using the relation

$$R = \frac{R_o}{\sin \theta} \tag{5-1}$$

where R_o is the assumed planet radius. The uncertainties inherent in this operation are δR_o, the error in estimating the planet radius and $\delta\theta$, the error in measuring the half-subtense angle. Thus, from equation 5-1, the following error equation may be written:

$$\delta R = \left(\frac{\delta R}{\delta R_o}\right) \delta R_o + \left(\frac{\delta R}{\delta \theta}\right) \delta\theta \tag{5-2}$$

Assuming random independent errors, which is reasonable since $\delta\theta$ is a measurement error and δR_o is an estimation error, then the variance of the range-determination error, σ_R^2, can be written:

$$\sigma_R^2 = \left(\frac{\delta R}{\delta R_o}\right)^2 \sigma_{R_o}^2 + \left(\frac{\delta R}{\delta \theta}\right)^2 \sigma_\theta^2 \tag{5-3}$$

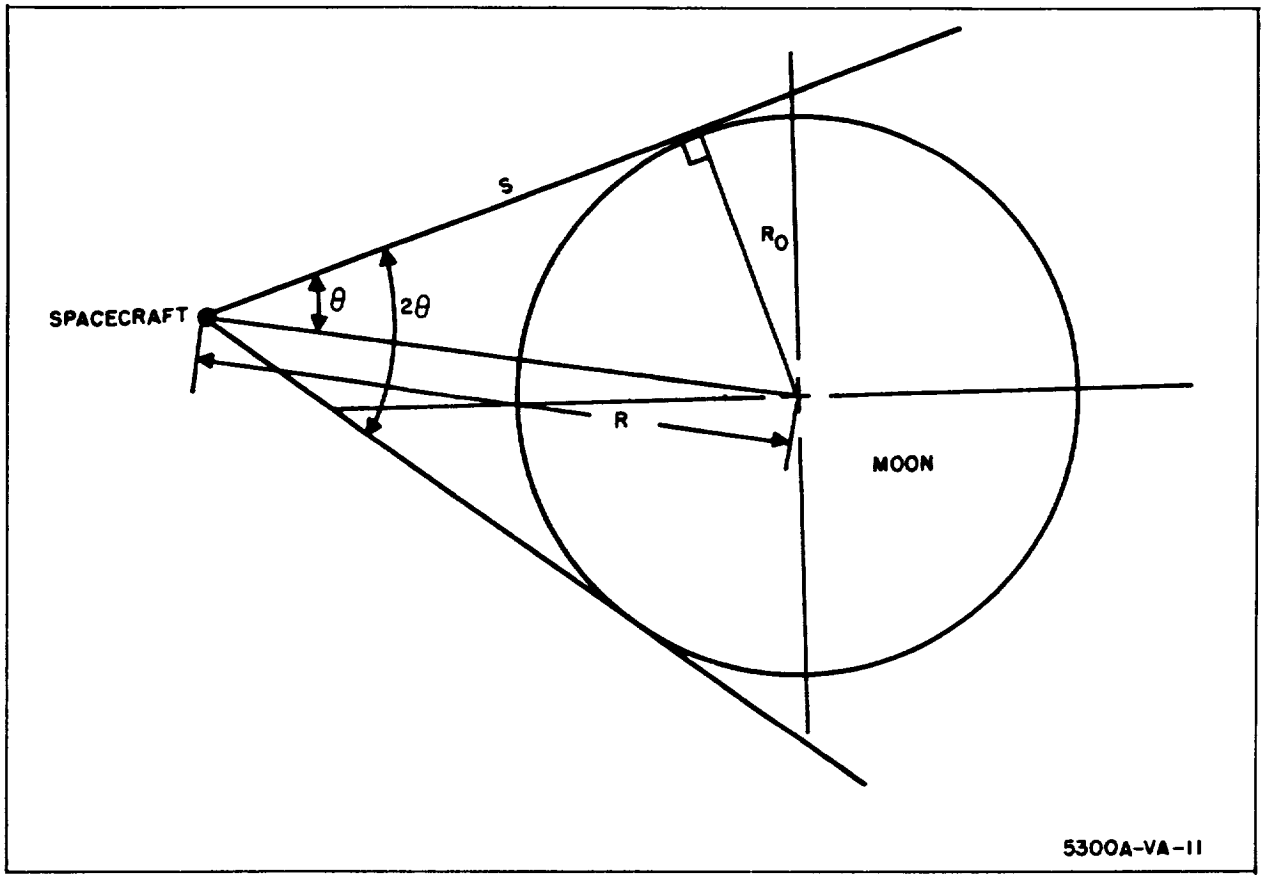

Figure 5-1. Geometry of Range Estimation by Subtense Angle Measurement

where σ_θ^2 is the variance of errors in measuring the half-subtense angle θ and $\sigma_{R_o}^2$ is the assumed variance in estimating the lunar radius (assuming an ensemble average). Equation 5-3 may be written

$$\sigma_R = \frac{1}{\sin\theta} \sqrt{\sigma_{R_o}^2 + R_o^2 \cot^2\theta \, \sigma_\theta^2} \tag{5-4}$$

Since σ_θ is the total measurement error and consists of angle errors due to both (a) instrument errors and (b) horizon irregularities, then σ_θ is given by:

$$\sigma_\theta = \sqrt{\sigma_I^2 + \sigma_H^2} \tag{5-5}$$

where σ_I^2 is the variance of instrument errors and σ_H^2 is the variance of horizon irregularities. Figure 5-2 shows that the angle error $\delta\theta_H$ caused by horizon irregularities is given approximately by

$$\delta\theta = \delta\epsilon / S \tag{5-6}$$

where $\delta\epsilon$ is the height (above the reference sphere) of the terrain which forms the effective horizon, and S is the distance between this point and the spacecraft.

S is given by:

$$S = \sqrt{R^2 - R_o^2} = R_o^2 \cot^2 \theta \tag{5-7}$$

so that the variance of the measurement errors is:

$$\sigma_\theta^2 \equiv \sigma_I^2 + \frac{\sigma_n^2}{R_o^2 \cot^2 \theta} \tag{5-8}$$

Substituting equation 5-8 in equation 5-5 there is:

$$\sigma_R = \frac{1}{\sin\theta} \sqrt{\sigma_{R_o}^2 + \sigma_H^2 + \sigma_I^2 R_o^2 \cot^2 \theta} \tag{5-9}$$

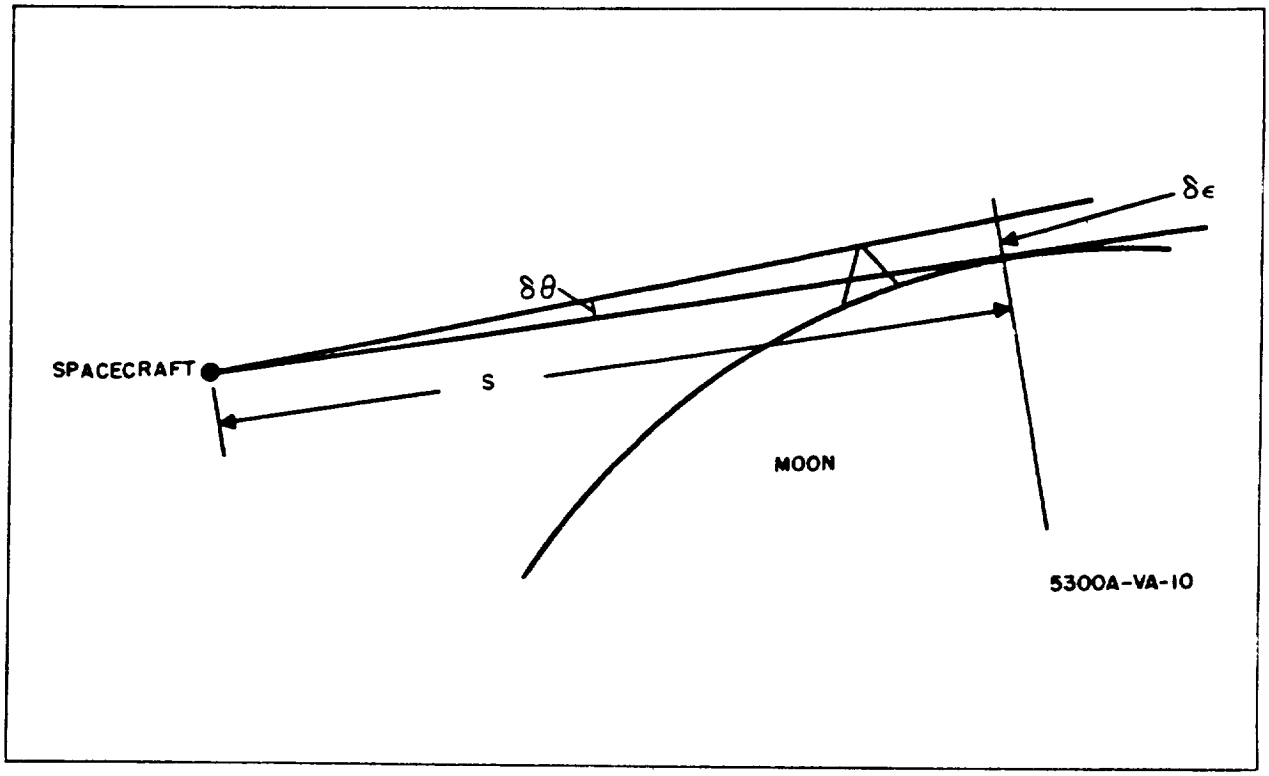

Figure 5-2. Effect of Lunar Peak on Angle Measurement

It can be seen in equation 5-9 that the effect of instrument errors (σ_I) on range estimation may vary from being the dominant error to being an insignificant error source, depending on the relative magnitude of the three error sources. Therefore, equation 5-9 was solved for several combinations of σ_{R_o}, σ_I, and σ_H. The results are shown and discussed in figure 2-7, paragraph 2.1.1.4.

5.1.2 Doppler Velocity Measurements

A problem connected with the use of single beam doppler measurements to the lunar surface is that a finite beamwidth and deviations of the radar boresight from the local vertical will tend to spread the returned frequencies over a considerable band, thus preventing the accurate estimation of radial rate. Figure 5-3 illustrates the pertinent geometry.

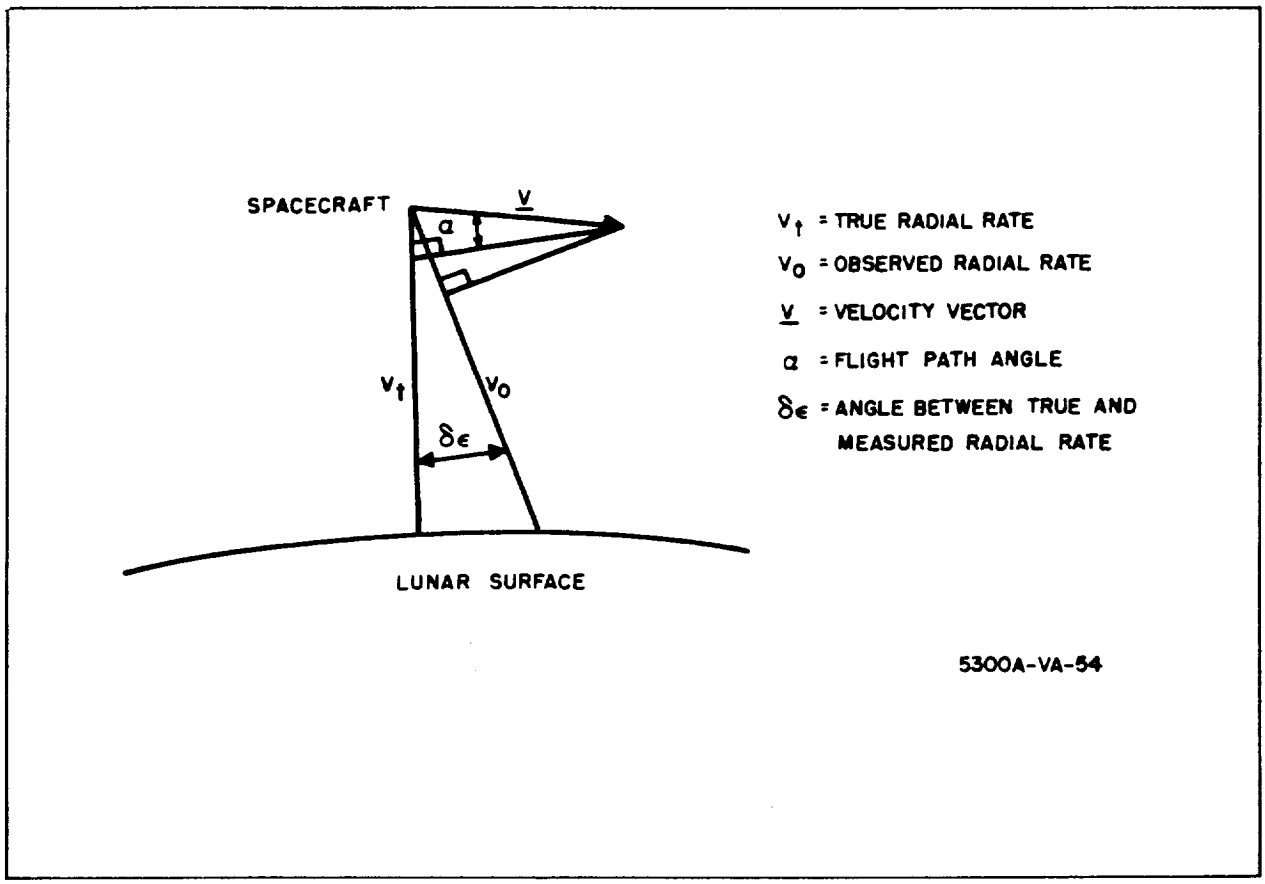

Figure 5-3. Geometry of Doppler Measurement Errors

If there is an error $\delta\epsilon$ in pointing the doppler beam with respect to the lunar local vertical then the measured velocity is V_o rather than V_t. (This type of error also may arise from a finite beamwidth of $\delta\epsilon$.) The resulting error in velocity estimation, δV, is calculated as follows:

$$\delta V = V_o - V_t = V \left[\cos(\alpha - \epsilon) - \cos\alpha\right] \tag{5-10}$$

where the symbols are defined in figure 5-3.

For small ϵ, equation (5-10) may be approximated:

$$\delta V = V\epsilon \sin\alpha \tag{5-11}$$

The results of evaluating equation (5-11) on the nominal approach trajectory, together with a discussion of the results are given in table 2-7, paragraph 2.1.1.4.

5.2 COVARIANCE MATRIX OUTPUTS OF MIDCOURSE COMPUTER RUNS

In this Appendix, some of the covariance matrices of estimation errors $[\tilde{P}_o]$ and trajectory deviations $[P_o]$ at nominal time of periselenum of the midcourse phase are listed. These matrices served as inputs to succeeding phases (after midcourse) of this study.

The coordinate system used is $X_o Y_o Z_o$ where X_o is toward the center of the moon (at periselenum, $-Y_o$ is downrange, and Z_o forms a right-handed set).

Run 108:

$$[\tilde{P}_o] = \begin{bmatrix} 5.64 & -4.37 & 0 & .379(10^{-2}) & -.299(10^{-2}) & 0 \\ -4.37 & 20.8 & 0 & -.121(10^{-1}) & .240(10^{-2}) & 0 \\ 0 & 0 & .345 & 0 & 0 & -.345(10^{-3}) \\ .379(10^{-2}) & -.121(10^{-1}) & 0 & .741(10^{-5}) & -.205(10^{-5}) & 0 \\ -.299(10^{-2}) & .240(10^{-2}) & 0 & -.205(10^{-5}) & .159(10^{-5}) & 0 \\ 0 & 0 & -.395(10^{-3}) & 0 & 0 & .459(10^{-6}) \end{bmatrix}$$

$$[P_o] = \begin{bmatrix} 5.64 & -4.37 & 0 & .379(10^{-2}) & -.299(10^{-2}) & 0 \\ & 20.8 & 0 & -.121(10^{-1}) & .240(10^{-2}) & 0 \\ & & .345 & 0 & 0 & -.395(10^{-3}) \\ & & & .293(10^{-4}) & .300(10^{-5}) & 0 \\ \text{symmetrical} & & & & .342(10^{-5}) & 0 \\ & & & & & .164(10^{-4}) \end{bmatrix}$$

Run 111:

$$[\tilde{P}_o] = \begin{bmatrix} 10.3 & -16.5 & 0 & .113(10^{-1}) & -.550(10^{-2}) & 0 \\ & 37.9 & 0 & -.242(10^{-1}) & .883(10^{-2}) & 0 \\ & & 43.9 & 0 & 0 & -.554(10^{-1}) \\ & & & .156(10^{-4}) & -.604(10^{-5}) & 0 \\ \text{symmetrical} & & & & .294(10^{-5}) & 0 \\ & & & & & .701(10^{-4}) \end{bmatrix}$$

Run 111 (Continued):

$$[P_o] = \begin{bmatrix} 255 & -500 & 0 & 0.326 & -.136 & 0 \\ & 3172. & 0 & -1.81 & .269 & 0 \\ & & 43.9 & 0 & 0 & -.554(10^{-1}) \\ \text{symmetrical} & & & .115(10^{-2}) & -.155(10^{-3}) & 0 \\ & & & & .844(10^{-4}) & 0 \\ & & & & & .462(10^{-3}) \end{bmatrix}$$

Run 121:

$$[\tilde{P}_o] = \begin{bmatrix} 11.5 & -17.8 & 0 & .126(10^{-1}) & -.608(10^{-2}) & 0 \\ & 39.2 & 0 & -.255(10^{-1}) & .946(10^{-2}) & 0 \\ & & 39.9 & 0 & 0 & -.494(10^{-1}) \\ \text{symmetrical} & & & .170(10^{-4}) & -.666(10^{-5}) & 0 \\ & & & & .323(10^{-5}) & 0 \\ & & & & & .618(10^{-4}) \end{bmatrix}$$

$$[P_o] = \begin{bmatrix} 230 & -438 & 0 & .287 & -.123 & 0 \\ & 2216 & 0 & -1.29 & .235 & 0 \\ & & 39.9 & 0 & 0 & -.494(10^{-1}) \\ \text{symmetrical} & & & .181(10^{-2}) & .120(10^{-3}) & 0 \\ & & & & .249(10^{-3}) & 0 \\ & & & & & .304(10^{-2}) \end{bmatrix}$$

Run 126:

$$[\tilde{P}_o] = \begin{bmatrix} 23.9 & -16.4 & 0 & .146(10^{-1}) & -.127(10^{-1}) & 0 \\ & 110. & 0 & -.626(10^{-1}) & .897(10^{-2}) & 0 \\ & & 1.38 & 0 & 0 & -.165(10^{-2}) \\ & & & .368(10^{-4}) & -.791(10^{-5}) & 0 \\ \text{symmetrical} & & & & .692(10^{-5}) & 0 \\ & & & & & .408(10^{-5}) \end{bmatrix}$$

$$[P_o] = \begin{bmatrix} 23.9 & -16.4 & 0 & .146(10^{-1}) & -.128(10^{-1}) & 0 \\ & 110. & 0 & -.626(10^{-1}) & .897(10^{-2}) & 0 \\ & & 1.38 & 0 & 0 & -.165(10^{-2}) \\ & & & .391(10^{-4}) & -.748(10^{-5}) & 0 \\ \text{symmetrical} & & & & .692(10^{-5}) & 0 \\ & & & & & .408(10^{-5}) \end{bmatrix}$$

Run 135:

$$[\tilde{P}_o] = \begin{bmatrix} 5.84 & 9.09 & 0 & -.351(10^{-2}) & -.311(10^{-2}) & 0 \\ & 25.1 & 0 & -.114(10^{-1}) & -.484(10^{-2}) & 0 \\ & & 43.9 & 0 & 0 & -.554(10^{-1}) \\ & & & .532(10^{-5}) & .187(10^{-5}) & 0 \\ \text{symmetrical} & & & & .166(10^{-5}) & 0 \\ & & & & & .701(10^{-4}) \end{bmatrix}$$

$[P_o]$ = Same as $[P]_o$ for Run 121.

Run 136:

$$[\tilde{P}_o] = \begin{bmatrix} 20.0 & 30.1 & 0 & -.115(10^{-1}) & -.107(10^{-1}) & 0 \\ & 88.4 & 0 & -.403(10^{-1}) & -.160(10^{-1}) & 0 \\ & & 43.9 & 0 & 0 & -.554(10^{-1}) \\ & & & .189(10^{-4}) & .611(10^{-5}) & 0 \\ & & & & .569(10^{-5}) & 0 \\ & & & & & .701(10^{-4}) \end{bmatrix}$$

$[P_o]$ same as $[P_o]$ for Run 121.

Run 146:

$$[\tilde{P}_o] = \begin{bmatrix} 230 & -438 & 0 & .287 & -.123 & 0 \\ & 2216 & 0 & -1.29 & .235 & 0 \\ & & 39.9 & 0 & 0 & -.494(10^{-1}) \\ & & & .755(10^{-3}) & -.154(10^{-3}) & 0 \\ \text{symmetrical} & & & & .659(10^{-4}) & 0 \\ & & & & & .618(10^{-4}) \end{bmatrix}$$

$[P_o]$ same as $[P]$ on Run 121

5.3 DETERMINATION OF CROSS-TRACK

It is desired to determine the cross-track error at the target which will result from plane errors during midcourse, assuming two-dimensional guidance throughout. Figure 5-4, illustrates the geometry.

In figure 5-4, $\underline{u}_n$ is the unit normal to the trajectory plane, $\underline{u}_t$ is a unit vector in the direction of the target and $\underline{u}_e$ is the unit vector along the projection of $\underline{u}_t$ in the trajectory plane. ϕ, the angle between the trajectory plane and $\underline{u}_t$ is the angular error between the target location and the trajectory plane. Then ϕ is given by:

$$\underline{u}_n \cdot \underline{u}_t = \cos (90 - \phi) = \sin \phi \qquad (5\text{-}12)$$

The cross track error $\delta\epsilon$ is then given by:

$$\delta\epsilon \cong R_o (\underline{u}_n \cdot \underline{u}_t) \qquad (5\text{-}13)$$

where R_o is the lunar radius.

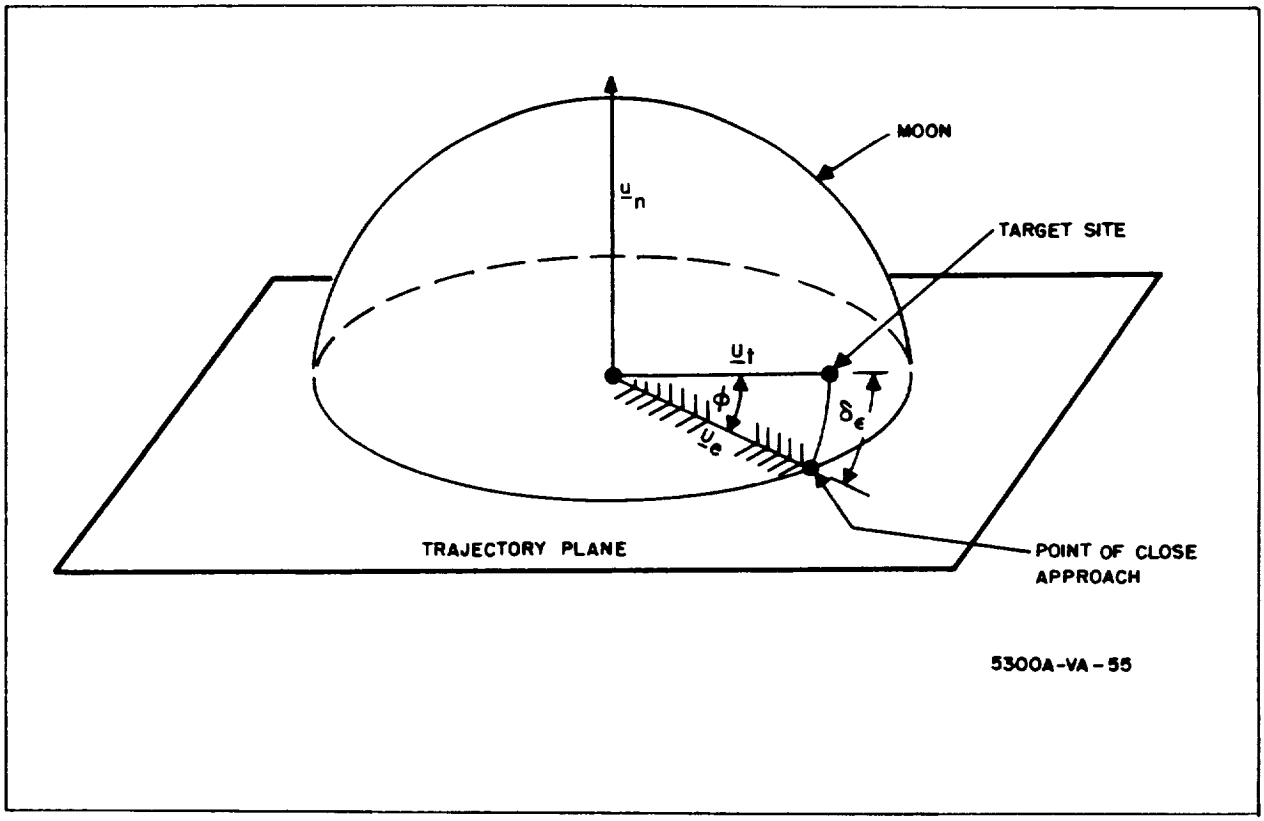

Figure 5-4. Geometry for Determination of Cross-Track Error

To determine the variance of the cross-track error $\delta\epsilon$, equation 5-13 must be evaluated in terms of the statistics of the trajectory deviations at retroburnout.

$$\underline{u}_n = \frac{\underline{V} \times \underline{R}}{VR} = \frac{(\dot{Y}Z - \dot{Z}Y)\underline{i} + (\dot{Z}X - \dot{X}Z)\underline{j} + (\dot{X}Y - \dot{Y}X)\underline{k}}{VR} \tag{5-14}$$

$$\underline{u}_t = \frac{T_x\underline{i} + T_y\underline{j} + T_z\underline{k}}{R_o} \tag{5-15}$$

$$\delta\epsilon = \frac{(\dot{Y}Z - \dot{Z}Y)T_x + (\dot{Z}X - \dot{X}Z)T_y + (\dot{X}Y - \dot{Y}X)T_z}{VR} \tag{5-16}$$

Writing equation 5-16 in terms of deviations from the nominal trajectory δx, δy, etc, there is:

$$\delta\epsilon = A\,\delta\underline{x}_i \tag{5-17}$$

where $$A = \frac{\left[(\dot{Z}T_y - \dot{Y}T_z)(\dot{X}T_z - \dot{Z}T_x)(\dot{Y}T_x - \dot{X}T_y)(YT_z - ZT_y)(ZT_x - XT_z)(XT_y - YT_x)\right]}{VR} \tag{5-18}$$

and $\delta\underline{x}_i$ is the column vector whose elements are δx, δy, δz, $\delta\dot{x}$, $\delta\dot{y}$, $\delta\dot{z}$. Now from equation 5-17

$$\delta\epsilon^2 = \left[A\delta\underline{x}_i\right]\left[A\delta\underline{x}_i\right]^T \tag{5-19}$$

Now the variance of the cross-track error is obtained by averaging equation 5-19

$$E(\delta\epsilon^2) = A\,[P]_o A^T \tag{5-20}$$

which gives the variance of the cross-track error in terms of the covariance matrix $[P]_o$ of trajectory deviations at retrothrust. Note that $(\delta\epsilon^2)$ is a scaler, as A is a row matrix.

The computation of equation 5-20 can be greatly simplified if the coordinates are properly chosen. Letting the nominal initial conditions be as follows:

$$
\begin{aligned}
X &= O \\
Y &= R \\
Z &= O \\
\dot{X} &= V \\
\dot{Y} &= O \\
\dot{Z} &= O
\end{aligned}
\tag{5-21}
$$

Then, equation 5-18 can be written:

$$
A' = \frac{-\left[O \quad O \quad VT_y \quad O \quad O \quad RT_x\right]}{VR} \tag{5-22}
$$

Equation 5-20 is given simply by

$$
E(\delta\epsilon^2) = \frac{T_y^2}{R^2} r_{33} + \frac{2T_x T_y}{VR} r_{36} + \frac{T_x^2}{V^2} r_{66} \tag{5-23}
$$

which gives the variance of the cross-track deviation as a function of the trajectory deviations at periselenum and the target coordinates. r_{ij} in equation 5-23 is the i^{th} row, j^{th} column component of the covariance matrix of deviations at periselenum.

5.4 GENERATION OF INITIAL ERRORS

In this study, it is assumed that DSIF tracking is utilized up until the second midcourse correction and terminated thereafter. Thus, initial conditions for the midcourse phase of the study include covariance matrices of both the estimation errors (as obtained from DSIF) and deviations from the nominal trajectory. Since these error matrices were not supplied as study inputs and since it is outside the scope of this contract to analyze DSIF performance, initial error matrices had to be approximated by consideration of other references.

The most appropriate and up-to-date study of DSIF tracking on lunar missions was found to be reference 8 by G. L. Smith of NASA Ames. In this study, a thorough statistical study of tracking is done including such effects

as station location uncertainties, speed of light, timing errors, radar bias errors, etc. Since no other report was found which treated the topic as well, reference 8 was used as a basis for generating the initial estimation errors used in this study.

From figures 5 and 6 in reference 8, it can be seen that the approximate rms position and velocity estimation errors at t_o = 50 hours (from earth injection) are:

$\tilde{r}$ = 2 km $\tilde{v}$ = 0.02 m/sec

These errors are used as a basis to define initial errors (just before the second midcourse correction at t_o = 50 hours) for this study.

It was assumed that the errors are oriented such that $\sigma_d = 2\sigma_c = 2\sigma_z$ where d is along the sightline from the earth and z is perpendicular to the trajectory plane. Then, assuming zero correlation between position and velocity errors, the following initial error matrix is generated.

$$[\tilde{P}]_{t_o}(e) = \begin{bmatrix} \overbrace{\begin{matrix} 2.447 & .618 & 0 \\ .618 & .899 & 0 \\ 0 & 0 & .667 \end{matrix}}^{km^2} & 0_{33} \\ 0_{33} & \underbrace{\begin{matrix} 2.447 & .618 & 0 \\ .618 & .899 & 0 \\ 0 & 0 & 0.667 \end{matrix}}_{(10^{-10})\ km^2/sec^2} \end{bmatrix} \quad (5\text{-}24)$$

which is expressed in the coordinate system defined for the hyperbolic trajectory (table 5-2, paragraph 5.7).

Equation 5-24 represents the uncertainty of the spacecraft in earth coordinates. Assuming an uncertainty in the position of the moon of 2 km in the radial (X) direction and 1 km in each of the cross-track directions, then equation 5-25 is incremented as follows:

$$[\tilde{P}]_{t_o} = \left[\begin{array}{ccc|ccc} \multicolumn{3}{c|}{\overbrace{\qquad\qquad}^{km^2}} & & & \\ 6.447 & .618 & 0 & & & \\ .618 & 1.899 & 0 & & 0_{33} & \\ 0 & 0 & 1.667 & & & \\ \hline & & & 2.447 & .618 & 0 \\ & 0_{33} & & .618 & .899 & 0 \\ & & & 0 & 0 & .667 \\ & & & \multicolumn{3}{c}{\underbrace{\qquad\qquad}_{(10^{-10})\ (km/sec)^2}} \end{array}\right] \tag{5-25}$$

which is the standard initial covariance matrix of estimation errors used in this study.

The covariance matrix of deviations from the nominal trajectory was assumed to be as follows:

$$[P]_{t_o} = (10^3)\ [\tilde{P}]_{t_o} \tag{5-26}$$

Thus, the deviations are assumed to be 31 times as large as the estimation errors. It is felt that this is a reasonable assumption, since the predicted deviations at periselenum should be considerably greater than the errors in estimation in order to make a correction desirable.

The magnitude of the velocity correction which results from the use of equation (5-26) for initial deviations is 1.34 m/sec for t_o = 50 hours and 3.88 m/sec for t_o = 66 hours. These figures are consistent with the results of other studies, though not reference 3 since that study assumes a different correction time and finer control accuracies than the accuracies specified for this study.

Although the initial covariance matrices used in reference 3 are not specified, an approximate comparison of the initial errors used in this study with those used in reference 3 is possible by considering the periselenum uncertainties which result from each. Table 5-1 lists the periselenum estimation errors (with no navigation) which result from the use of equation

5-2 as initial conditions from t_o = 66 hours together with similar results from reference 3 (figure 4-32).

TABLE 5-1

PERISELENUM ERRORS RESULTING FROM INITIAL COVARIANCE MATRICES AT t_o = 66 HOURS WITH NO NAVIGATION

Ref. 3	Westinghouse
σ_x = 0.8 km	σ_x = 2.37 km
σ_y = 2.1 km	σ_y = 4.56 km
σ_z = 0.3 km	σ_z = .59 km
$\sigma_{\dot{x}}$ = 1.3 m/sec	$\sigma_{\dot{x}}$ = 2.72 m/sec
$\sigma_{\dot{y}}$ = 0.4 m/sec	$\sigma_{\dot{y}}$ = 1.26 m/sec
$\sigma_{\dot{z}}$ = 0.4 m/sec	$\sigma_{\dot{z}}$ = 0.68 m/sec

It can be seen that the initial errors used in this study from t_o = 66 hours yield periselenum errors which are approximately twice as large as those used in reference 3. Data on what the initial errors are at earlier times in the flight (e.g., t = 50 hours) was not available in reference 3.

5.5 HORIZON SCANNER ERRORS IN MIDCOURSE APPROACH

This paragraph consists of a brief analysis of the errors involved in determining lunar local vertical with a horizon scanner, especially with regard to horizon irregularities. In figure 5-5, the geometry is illustrated.

Ideally, the angle θ is determined with respect to some inertial reference (-X in the illustrated case), by averaging of the angles θ_1, and θ_2. Thus,

$$\theta = \frac{\theta_1 + \theta_2}{2} \tag{5-27}$$

The measured value of local vertical angle θ_m is given by:

$$\theta_m = \frac{(\theta_1 - \delta\theta_1) + (\theta_2 + \delta\theta_2)}{2} \tag{5-28}$$

where $\delta\theta_1$ and $\delta\theta_2$ are errors due to horizon peaks h_1 and h_2.

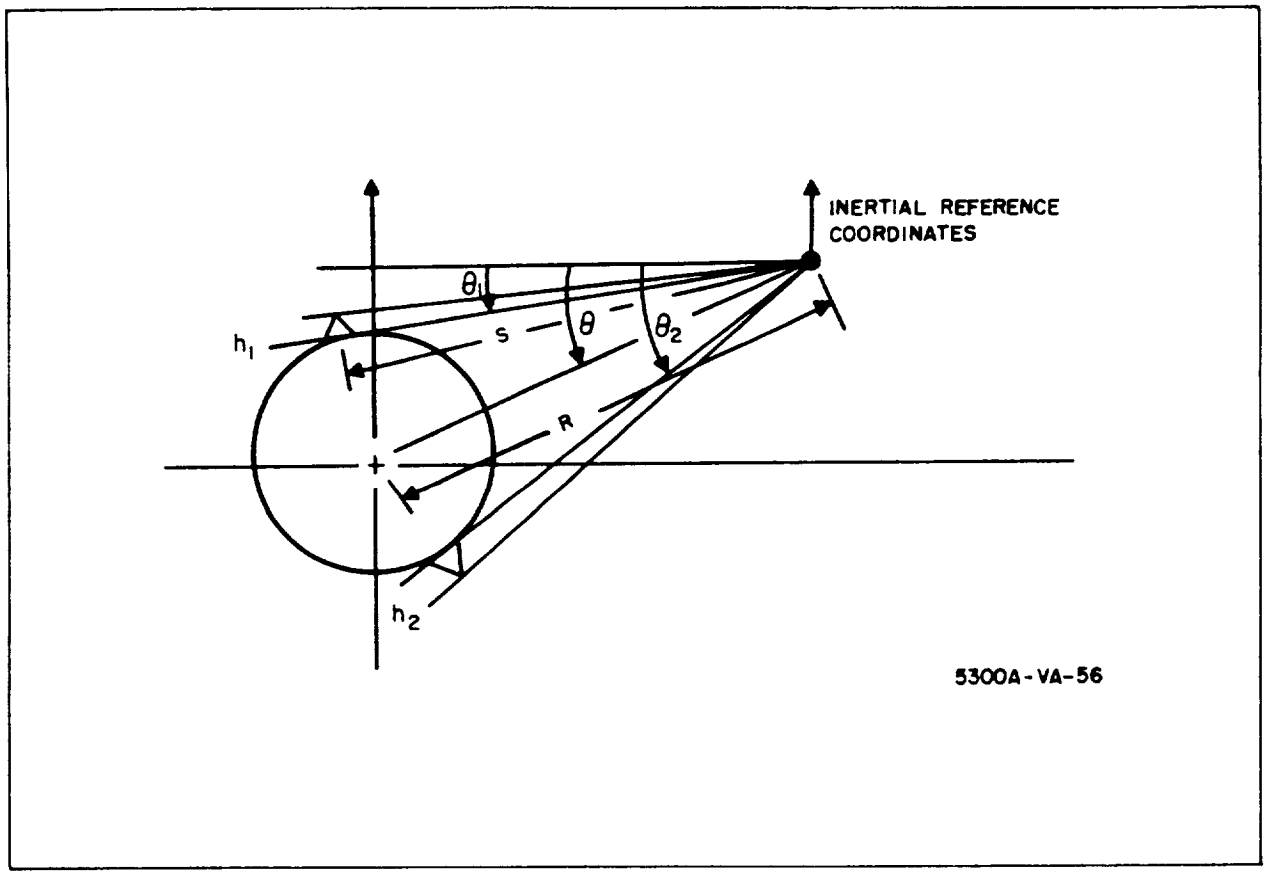

Figure 5-5. Geometry of Local Vertical Determination

Letting the local vertical error $\delta\theta = \theta_m - \theta$, and subtracting equation 5-27 from equation 5-28, there is:

$$\delta\theta = \frac{\delta\theta_2 - \delta\theta_1}{2} \tag{5-29}$$

Assuming that $\delta\theta_1$ and $\delta\theta_2$ have equal mean and are uncorrelated (a slightly pessimistic assumption), then the variance of $\delta\theta$ is given by:

$$E(\delta\theta^2) = \frac{E(\delta\theta_1^2)}{2} \tag{5-30}$$

Referring again to figure 5-5, it can be seen that

$$\delta\theta_1 = \frac{h_1}{S} \tag{5-31}$$

For R greater than 3 lunar radii, equation 5-31 may be approximated by

$$\delta\theta_1 = \frac{h}{R} \tag{5-32}$$

Substituting in equation 5-30 and taking the square root, there is

$$\sigma_{\delta\theta} = \frac{\sigma_h}{\sqrt{2}\,R} \tag{5-33}$$

where $\sigma_{\delta\theta}$ is the rms error in local vertical due to horizon and σ_h is the rms horizon deviation. Equation 5-33 does not consider horizon scanner or platform errors. Since these errors are expected to be independent of the horizon errors, the total error σ_θ in horizon determination is given by

$$\sigma_\theta = \sqrt{\sigma_{\delta\theta}^2 + \sigma_I^2} \tag{5-34}$$

where σ_I is the rms instrument error. Equation 5-34 was used to determine angle-measurement errors for the midcourse navigation in this study. Results for various values of σ_I are plotted in figure 2-3, paragraph 2.1.1.3.

5.6 RANGE MEASUREMENT ERRORS IN MIDCOURSE NAVIGATION

If an altimeter is used to measure range to the center of lunar gravity, then several error sources arise in addition to the radar altimeter error. In this paragraph a brief discussion of these errors and their expected magnitude is given.

Errors in the range measurement were broken down into four sources:

- Radar altimeter errors
- Irregularities in the local terrain
- Oblateness of the moon.
- Uncertainty in mean radius of the moon.

The first two errors are expected to be random while the second two are essentially bias-type errors. In order to define some standard range error for use in this study, an attempt was made to determine expected values for each of the above errors. However, it should be made clear that there is considerable uncertainty in the last three errors, due to lack of detailed knowledge of the moon.

Radar Noise (σ = 300 meters)

This figure is a factor of 10 greater than the accuracies known to be obtainable for a radar altimeter operating at orbital altitudes. The larger figure was chosen because of the greater ranges (1000 km) required for midcourse approach navigation and also because this source is still small compared to other range errors.

Local Terrain Fluctuation (σ = 1355 meters)

No official figures were available from NASA on what to use for this or the other two errors caused by the shape of the moon. Therefore, an estimate was made from USAF maps of the moon. In figure 5-6, an altitude profile plot of the region between Stadius and Hyginus is shown. The rms value of the altitude fluctuations about the mean reference level were found to be 1355 meters. This is considered to be a conservative choice as the region chosen seemed to exhibit the sharpest altitude variation of any of the maps examined.

Uncertainty in Main Lunar Radius (σ = 1000 meters)

This is a value commonly used in analyses, though not numerically justified. Also, JPL officials claim to have revised to estimate of lunar radius by 3 km due to range flight tracking. Thus, the figure of σ = 1 km is evidently not optimistic.

Uncertainty in Local Reference Level (σ = 1080 meters)

This figure was obtained by considering the estimated values for lunar radii in 3 axes given in reference 13. The values were a = 1738.57 km, b = 1738.21 km, c = 1737.49 km. Subtracting c from a yielded the indicated value.

Summary

In summary, the values used as standard for each of the error sources were as follows:

Radar	σ = 0.3 km	} random
Local terrain	σ = 1.355 km	} random

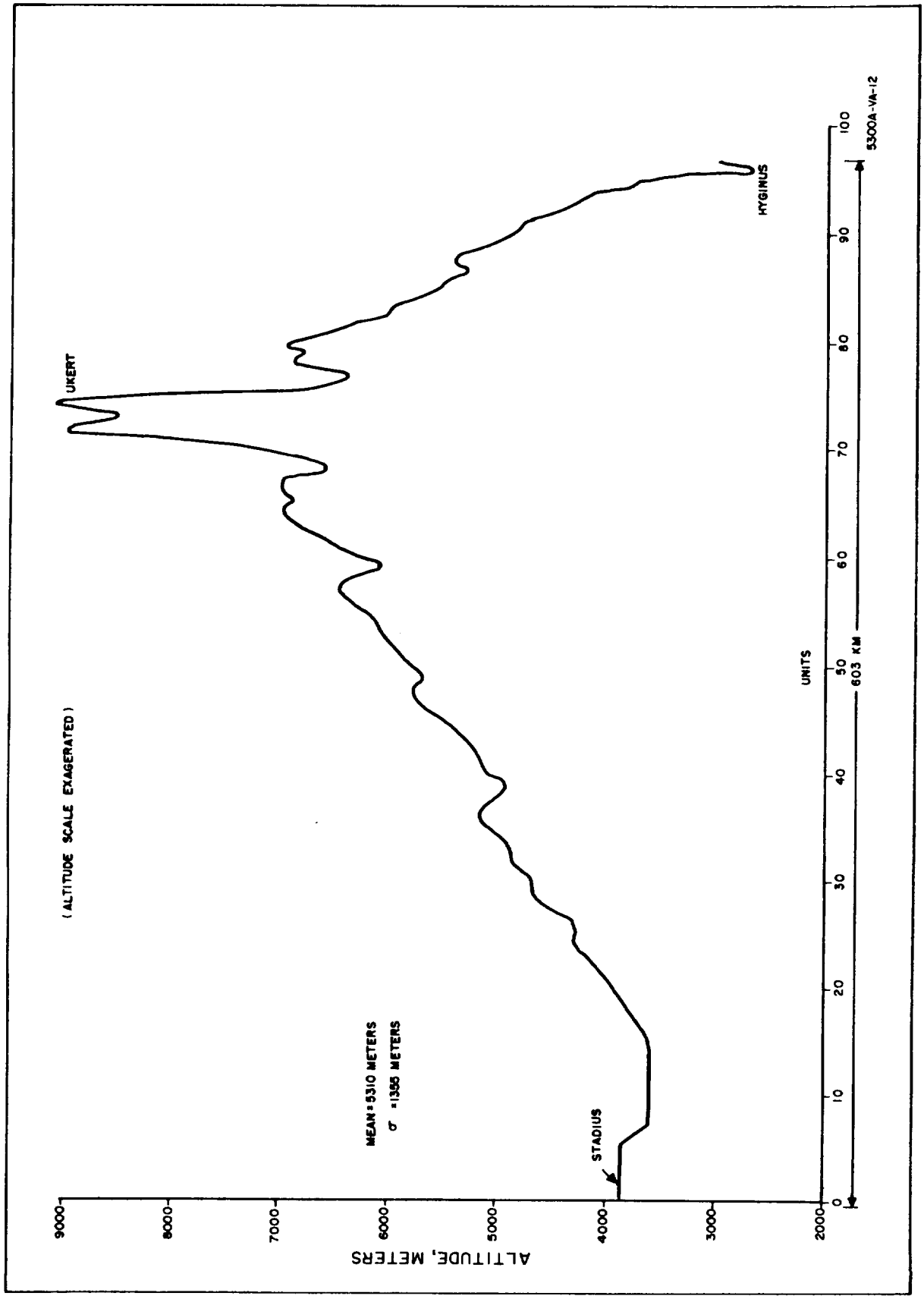

Figure 5-6. Altitude Profile Between Stadius and Hyginus

Lunar radius $\sigma = 1.0$ km
Oblateness $\sigma = 1.08$ km
} bias

The rms value of the above errors is $\sigma_R = 2$ km. This value was considered completely random and used as the standard value for altimeter navigation. However, results were also generated using other values of σ_R.

5.7 NOMINAL MIDCOURSE TRAJECTORY DATA

In this paragraph, the data which describe the initial and final points of the two nominal midcourse trajectories are listed in table 5-2. The data shown are for the earth-moon trajectory (72.88 hours) and the hyperbolic moon-approach trajectory (22.95 hours) which corresponds approximately to the last 23 hours of the earth-moon trajectory.

TABLE 5-2

NOMINAL TRAJECTORIES FOR MIDCOURSE GUIDANCE

Parameter	Earth-Moon Trajectory	Hyperbolic Approach Trajectory
Gravity field	Earth, moon, sun & oblateness	Moon
Coordinate system	Earth-centered, Z = North Pole, X = Ascending line of nodes of moon's orbit	Moon-centered inertial Z = perpendicular to orbit, -X = periselenum.
Initial position and velocity	$X_o = 1599.74$ km $Y_o = 5643.77$ km $Z_o = 2943.72$ km $\dot{X}_o = -10.8633$ km/sec $\dot{Y}_o = -1.2075$ km/sec $\dot{Z}_o = -0.6298$ km/sec $R_o = 6563.29$ km $V_o = 10.940$ km/sec	$X_o = 64,705.7$ km $Y_o = -70,199.1$ km $Z_o = 0$ $\dot{X}_o = -.75698$ km/sec $\dot{Y}_o = .74770$ km/sec $\dot{Z}_o = 0$ $R_o = 94,471.2$ km $V_o = 1.065$ km/sec

TABLE 5-2 (Continued)

Parameter	Earth-Moon Trajectory	Hyperbolic Approach Trajectory
Periselenum position and velocity (in lunar-centered coordinates parallel to earth coordinates)	X_p = -496.65 km Y_p = -1638.51 km Z_p = -876.49 km $\dot{X}_p$ = -2.3937 km/sec $\dot{Y}_p$ = .5508 km/sec $\dot{Z}_p$ = .3155 km/sec R_p = 1923.43 km V_p = 2.4764 km/sec	X_p = -1922.8 km Y_p = 0.8 km Z_p = 0 $\dot{X}_p$ = 0.0005 km/sec $\dot{Y}_p$ = 2.4751 km/sec $\dot{Z}_p$ = 0 R_p = 1922.8 km V_p = 2.4751 km/sec
Time of periselenum	72.88 hours	22.95 hours
Inclination of trajectory w/r lunar orbit	0°	N/A
Lunar longitude in orbit plane at t = 0	-138.662° from X-axis	N/A
Lunar Peroid	2.3587(10^6) secs	N/A
Inclination of Lunar Orbit w/r earth's equator	27.55°	N/A
Radial Distance of Moon	382,830 km	N/A

5.8 CROSS-TRACK ERRORS AS FUNCTION OF DESCENT KICK

This paragraph contains a brief analysis determining the necessity for out-of-plane guidance calculations at the descent kick maneuver. Thus, the relationship between the elliptical descent maneuver and the cross-track error at the target is derived here.

Two views of the nominal mission profile are shown in figure 5-7. View (a) is in the trajectory plane while view (b) is perpendicular to the trajectory plane. In (a) it can be seen that nominally a small velocity change ($\simeq$ 67 m/sec) will be made to send the LLV on an elliptical descent path from 185 km (at (a)) to 104 km over an arc of 65 degrees. At the 104-km altitude (b), main braking begins and continues over a central angle of 10 degrees at which point the vehicle lands.

In view (b) it can be seen that an error $\delta\psi$ in the plane of the velocity vector after the elliptical descent maneuver results in a crosstrack error, $\delta\epsilon$, at the target. The relationship between $\delta\psi$ and $\delta\epsilon$ is determined as follows:

Since the arc on which the LLV travels after the descent kick is an ellipse, then spherical trigonometry can not be applied directly. Thus, it is convenient to project the indicated miss $\delta\epsilon$ onto a sphere of radius $R_o + h$ as

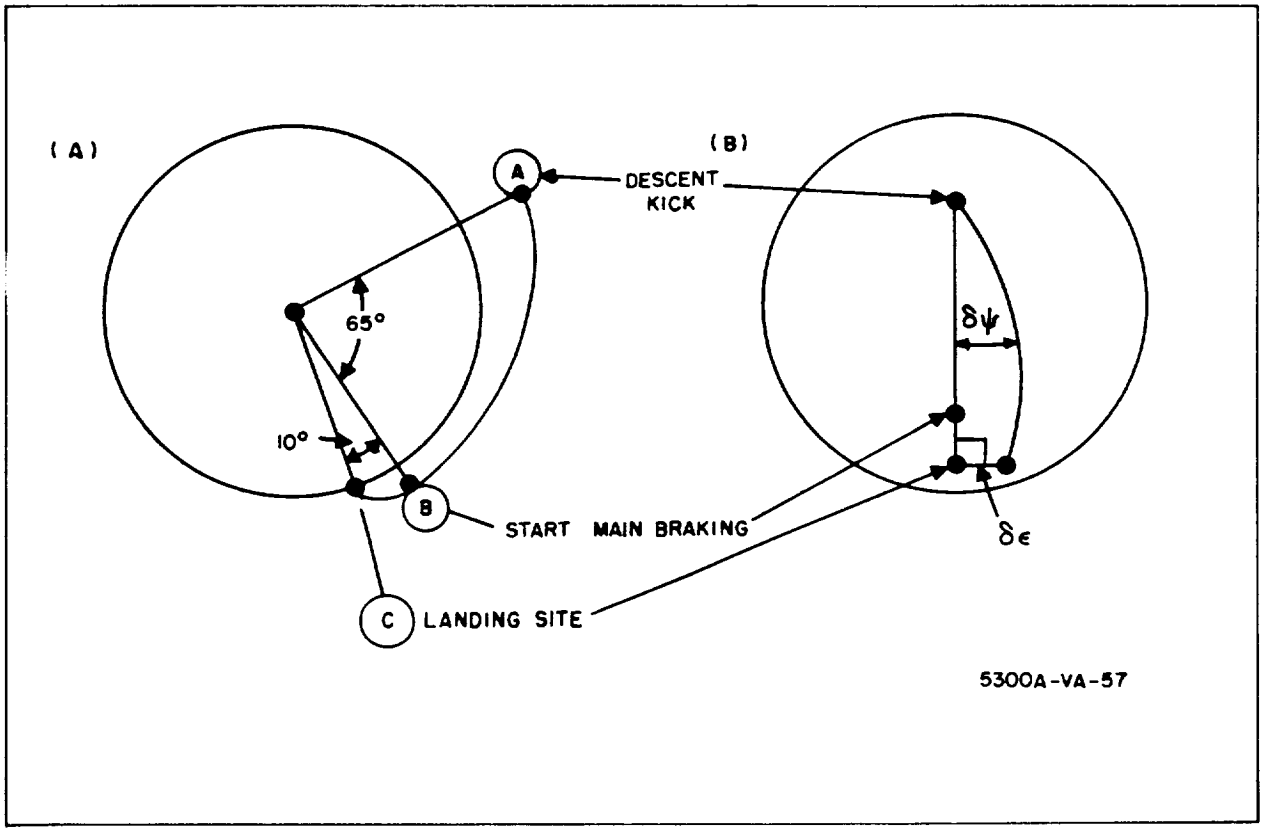

Figure 5-7. Nominal Mission Profile

shown in figure 5-8a, where R_o is the lunar radius and h is the parking orbit altitude. Figure 5-8b shows the relationship between $\delta\epsilon$ and $\delta\epsilon'$. For $\delta\epsilon$ and R_o in km, then

$$\delta\epsilon' \text{ (rads)} = \frac{\delta\epsilon}{R_o} \tag{5-35}$$

Now from the spherical right triangle in 5-8c, the velocity angle error is given by

$$\tan(\delta\psi) = \frac{\tan(\delta\epsilon')}{\sin\theta} \tag{5-36}$$

$$\delta\psi \cong \frac{\delta\epsilon}{R_o \sin\theta} \text{ (rads)} \tag{5-37}$$

The standard parameters used in this program are R_o = 1783 km, and θ = 75°. Then:

$$\delta\psi = 0.576\,(10^{-3})\,\delta\epsilon \quad \text{rads.} \tag{5-38}$$

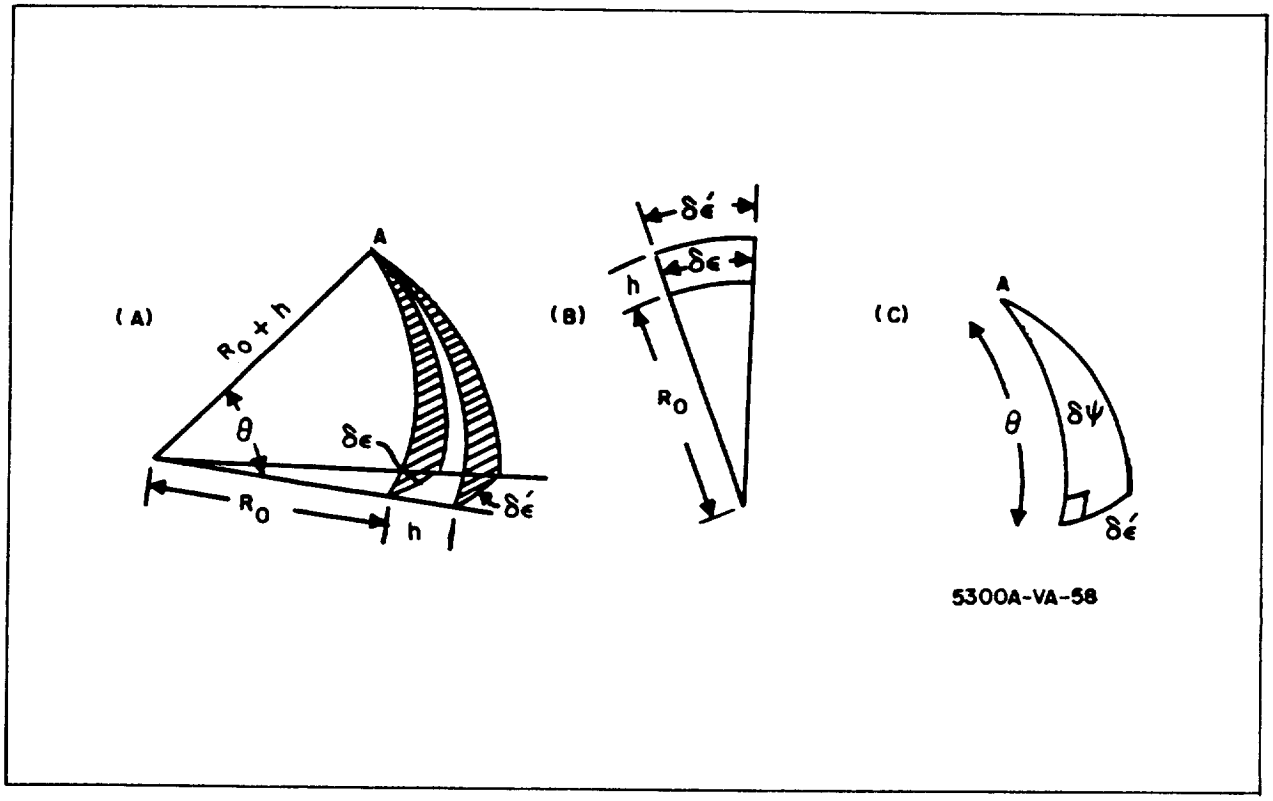

Figure 5-8. Projected Spherical Geometry of the Indicated Miss, $\delta\epsilon$

Now it is required to determine the effect of out-of-plane errors in applying the elliptical descent ΔV. The cause of these errors (i.e., control or estimation) is not considered here.

Figure 5-9 illustrates the situation. In the nominal case the resultant velocity V_r is given by $V_r = V_o - V_e$ where V_o is the initial (orbital) velocity, and V_e is the nominal 67 m/sec retro-velocity. The addition of a cross-track velocity component V_c is caused by the angle $\delta\phi$ (either intentional or due to an error) in applying the descent pulse and results in a change $\delta\psi$ in the final velocity direction. From Figure 5-9, it can be seen that

$$\delta\psi = \tan^{-1}\left(\frac{V_c}{V_o - V_e}\right) \cong \frac{V_c}{V_o - V_e} \tag{5-39}$$

$$\therefore \quad V_c \cong \left(V_o - V_e\right)\delta\psi \tag{5-40}$$

For a 185-km parking orbit, $V_o = 1596$ m/sec, and $V_e = 67$ m/sec, so that

$$V_c = 1529 \ \delta\psi \text{ m/s} \tag{5-41}$$

Substituting equation 5-38 in equation 5-41 there is

$$V_c = 0.88\ \delta\epsilon \tag{5-42}$$

where V_c is in m/s and $\delta\epsilon$ is in km. The cross-track velocity component V_c is related to the angular error $\delta\phi$ in applying the descent pulse as follows:

$$\delta\phi \cong \frac{V_c}{67} \tag{5-43}$$

Then, $\delta\phi$, the angle of the direction of the velocity impulse is related to the cross track error at the target by:

$$\delta\phi = \frac{(0.88)\,(57.3)}{57} = 0.75\ \frac{\text{deg}}{\text{km}} \tag{5-44}$$

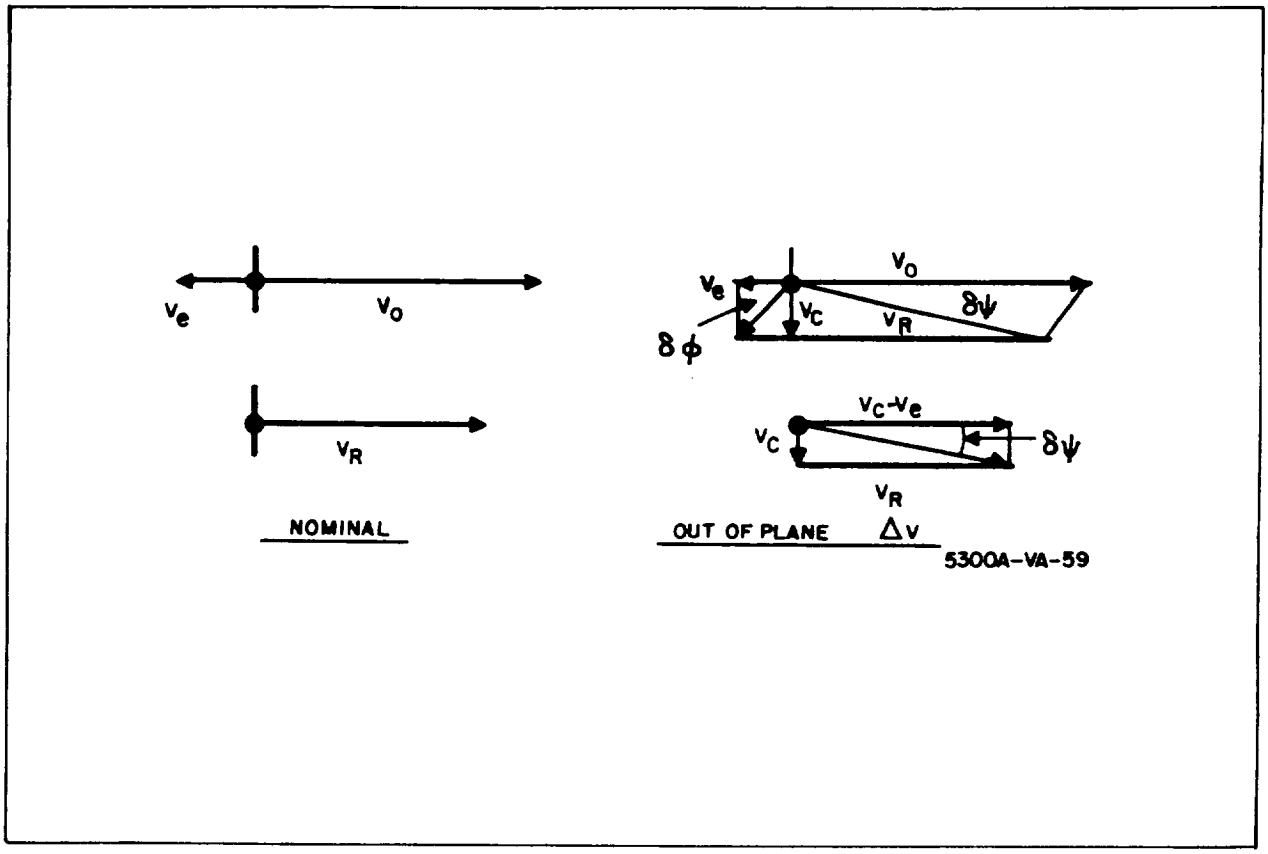

Figure 5-9. Nominal Descent Kick and Out-of-Plane Descent Kick

6. RETROTHRUST APPENDIX

6.1 DEVELOPMENT OF ANALYTICAL MODEL

In this paragraph the analytical model of the overall retrothrust system is developed. There are four major blocks within the system (see figure 2-11): Navigation, Guidance Logic, and Control subsystems, and the dynamic equations of motion. In formulating the analytical models for the subsystems, consideration of actual mechanization is held to a minimum. Certain sources of system error are thus omitted; however, these error sources are not the subject of this study. In addition the idealized models ignore time lags in the actual sensors and control subsystem. It is assumed that the effect of realistic response times on sensor requirements can be treated independently of this study.

6.1.1 State Variables and Equations of Motion

Since a two-dimensional analysis is performed, four state variables are needed to specify vehicle position and velocity. The four selected are defined below and illustrated in figure 2-9.

R is the range (in meters) of the space vehicle from the center of the moon. The initial range, R_i is measured to the point mass represented as A in figure 2-9.

θ is the angular displacement (in radians) of the space vehicle from point A. The central angle is measured clockwise positive from the radius vector at B.

$\dot{R}$ is the range rate (in meters/second) of the space vehicle. The initial radial rate at point A is designated ($\dot{R}_i$).

$\dot{\theta}$ is the rate of angular displacement (in radians/second) of the space vehicle. The initial angular displacement rate at point A is designated $\dot{\theta}_i$.

Thus, the state vector of the space vehicle can be represented as:

$$\left[P\right] = \begin{bmatrix} R \\ \Theta \\ \dot{R} \\ \dot{\Theta} \end{bmatrix} \tag{6-1}$$

The control quantities define the thrust vector of the space vehicle. Two are sufficient because of the restriction to two dimensions. The parameters selected are defined below and illustrated in figure 2-9.

A_F is the magnitude of the applied acceleration (in meters/second^2)

A is the thrust vector angle measured from local horizontal (in radians)

The equations of motion used in this analysis are given below

$$\dot{R} - V_\theta^2/R = A_F \sin A = \mu/R^2 \tag{6-2}$$

$$R\ddot{\Theta} + 2\dot{R}\dot{\Theta} = A_F \cos A \tag{6-3}$$

where

$\dot{R}$ is the time derivative of the space vehicle's range rate (in meter/second^2)

$\ddot{\Theta}$ is the time derivative of the space vehicle's angular displacement rate (in radians/second^2)

V_θ is the horizontal component of vehicle velocity (in meters/second)

Since a constant-thrust rocket model is being assumed, the applied acceleration is

$$A_F(t) = \frac{g_o I_{SP}}{\frac{M_o}{\dot{M}} - t} \tag{6-4}$$

where

g_o is the acceleration due to gravity at the earth's surface

I_{SP} is the fuel specific impulse

M_o is the total initial mass of stages L-I and L-II

$\dot{M}$ is the mass flow rate

These equations are necessary to formulate analytical models of the subsystems in figure 2-11.

6.1.2 Navigation Subsystems

The two candidate navigation subsystems selected for the retrothrust manuever are pure inertial and composite (an altimeter complements the pure inertial subsystem). In this section the inertial navigation (pure) equations are first developed. Then, the necessary modifications for the composite subsystem are indicated.

The magnitude of the applied acceleration can be written as

$$A_F = \frac{F_c + \tilde{f}_c}{M_o - \dot{M}t} \qquad (6\text{-}5)$$

where

F_c is the commanded value of the thrust (in newtons)

$\tilde{f}_c$ is a constant error in measuring the thrust (in newtons)

Thus, the two accelerometers sense*

$$\hat{A}_{F\theta} = A_F \cos (A_c + \tilde{\alpha}_c) + \tilde{a}_{F\theta} \qquad (6\text{-}6)$$

$$\hat{A}_{FR} = A_F \sin (A_c + \tilde{\alpha}_c) + \tilde{a}_{FR} \qquad (6\text{-}7)$$

where

$\hat{A}_{F\theta}$ is the sensed value of A_F along the estimated, local horizontal (in meters/seconds^2)

$\hat{A}_{FR}$ is the sensed value of A_F along the estimated, local vertical (in meters/seconds^2)

A_c is the commanded thrust angle measured from the estimated, local horizontal. The profile is defined by equation 6-28 in paragraph 6.1.3.

*Equations 6-6 and 6-7 are valid in both of the following situations: (1) the platform coordinates are fixed in inertial space and no error is introduced by coordinate transformations; (2) The platform is slaved to the estimated local horizontal with no error.

$\tilde{\alpha}_c$ is a control sensor bias error in measuring the thrust angle

$\tilde{a}_{F\theta}$ is an accelerometer bias error (in meters/second^2)

$\tilde{a}_{FR}$ is an accelerometer bias error (in meters/second^2)

The inertial navigation equations can now be written directly by combining the sensor error models in paragraph 2.1.2.3 with the equations of motion in paragraph 6.1.1.

$$\hat{\ddot{R}} = \hat{A}_{FR} - \mu/\hat{R}^2 + \hat{R}\,\hat{\dot{\theta}}^2 \tag{6-8}$$

$$\hat{\dot{R}} = \int_o^t \hat{\ddot{R}}(\lambda)\,d\lambda + \dot{R}_{Ni} + \dot{r}_i + \tilde{\dot{r}}_i \tag{6-9}$$

$$\hat{R} = \int_o^t \hat{\dot{R}}(\lambda)\,d\lambda + R_{Ni} + r_i + \tilde{r}_i \tag{6-10}$$

$$\hat{\ddot{\theta}} = \left[\hat{A}_{F\theta} - 2\hat{\dot{R}}\,\hat{\dot{\theta}}\right]/\hat{R} \tag{6-11}$$

$$\hat{\dot{\theta}} = \int_o^t \hat{\ddot{\theta}}(\lambda)\,d\lambda + \dot{\theta}_{Ni} + \dot{\theta}_i + \tilde{\dot{\theta}}_i \tag{6-12}$$

$$\hat{\theta} = \int_o^t \hat{\dot{\theta}}(\lambda)\,d\lambda + \theta_{Ni} + \theta_i + \tilde{\theta}_i \tag{6-13}$$

The subscript, i, denotes an initial value. All of the remaining quantities in these equations have been defined previously.

With the exception of equation 6-10, the above relations are also valid for the composite navigation subsystem. The only modification required then is

$$\hat{R} = R + \tilde{r}_h \tag{6-14}$$

where

$\tilde{r}_h$ is the total bias error in estimating range to the center of the moon. It consists of both an altimeter bias error and the uncertainty in the mean lunar radius.

It should be noted that the initial platform misalignment to the estimated local horizontal, $\tilde{\gamma}_i$, does not appear in the navigation equations. This error appears only in the equations defining the actual state of the vehicle*.

6.1.3 Guidance Logic Subsystem

This paragraph presents the explicit guidance logic used during retrothrust into circular orbit. As stated in paragraph 2.1.2.2, the goal was not to develop an optimum guidance scheme but rather one which uses a reasonable amount of fuel. Thus, the approach taken by G. W. Cherry in reference 9, called "E" guidance, was appropriately modified for use.

The guidance equations are used to obtain desired values of the space vehicle's vector velocity and radial position within a given plane. This two-dimensional problem will be treated as two one-dimensional problems. The first one-dimensional problem is controlling the space vehicle's velocity and displacement along the radius vector. The second is controlling the horizontal component of the space vehicle's vector velocity. Controlling these three quantities is sufficient to determine the size and shape of the lunar orbit attained (i.e., the central angle traversed need not be controlled). Thus, the three constraint equations applicable to retrothrust are:

$$\dot{R}_D - \dot{R} = \int_t^{T_B} \ddot{R}(\lambda)\, d\lambda \tag{6-15}$$

$$R_D - R - \dot{R}_i (T_B - t) = \int_t^{T_B} \left[\int_o^t \ddot{R}(\lambda)\, d\lambda \right] dt \tag{6-16}$$

$$V_{\theta D} = V_\theta (T_B) \tag{6-17}$$

where

T_B is the manuever time

*In this analysis the dynamic misalignment to true local vertical is

$$\beta = \tilde{\gamma}_i - (\hat{\theta} - \theta)$$

Quantities having a subscript, D, represent desired terminal values. These constraint equations contain time varying quantities because the guidance equations are recomputed periodically during the maneuver.

It is convenient to define T_{go} as the estimated value of the remaining maneuver time.

$$T_{go} = (T_B - t) \tag{6-18}$$

The time-to-go will appear in all the guidance equations. It is a synchronzing variable for ensuring simultaneous solution of the two one-dimensional problems.

If the number of degrees of freedom of $\ddot{R}$ is limited to two, equations 6-15 and 6-16 are sufficient to determine a solution of the form.

$$\ddot{R}(t) = C_1 P_1(t) + C_2 T_{go} P_1(t) \tag{6-19}$$

where $P_1(t)$ is an integrable function of time; C_1 and C_2 are constants. *

The constants C_1 and C_2 are determined by substituting equation 6-19 into equations 6-15 and 6-16.

$$\dot{R}_D - \dot{R} = f_{11} C_1 + f_{12} C_2 \tag{6-20}$$

$$R_D - R - \dot{R}_i T_{go} = f_{21} C_1 + f_{22} C_2 \tag{6-21}$$

where

$$f_{11} = \int_t^{T_B} P_1(t)\, dt \tag{6-22}$$

$$f_{12} = T_{go} f_{11} \tag{6-23}$$

$$f_{21} = \int_t^{T_B} \left[\int_o^t P_1(\lambda)\, d\lambda \right] dt \tag{6-24}$$

$$f_{22} = T_{go} f_{21} \tag{6-25}$$

*Simulation of the guidance law has shown that the choice of $P_1(t)$ is not critical. A quadratic function of T_{go} is sufficient.

The solution for C_1 and C_2 can now be expressed in matrix form

$$\begin{bmatrix} C_1 \\ C_2 \end{bmatrix} = \begin{bmatrix} e_{11} & e_{12} \\ e_{21} & e_{22} \end{bmatrix} \begin{bmatrix} \dot{R}_D - \dot{R} \\ R_D - R - R_i T_{go} \end{bmatrix} \tag{6-26}$$

where the matrix $E = [e_{ij}]$, is the inverse of the matrix $F = [f_{ij}]$.

A solution for the thrust angle profile can now be found by substituting equation 6-19 into 6-21.

$$\alpha = \sin^{-1} \left[\frac{(C_1 + C_2 T_{go}) P_1(t) + \mu/R^2 - V_\theta^2/R}{A_F} \right] \tag{6-27}$$

Defining the term g_{eff} as the sum of gravitational and centrifugal acceleration, equation 6-27 becomes

$$\alpha = \sin^{-1} \left[\frac{(C_1 + C_2 T_{go}) P_1(t) + g_{eff}}{A_F} \right] \tag{6-28}$$

The determination of the thrust angle profile during retrothrust does not require continuous state information. Periodic updating of equation 6-28 is sufficient, due to the slowly varying nature of g_{eff}.* The value of g_{eff} is assumed constant during the intervals between updating the state.

For any given set of radial boundary conditions, a solution thrust angle profile can be computed for each permissable value of T_B (or its equivalent, T_{go}). The minimum permissible value of the maneuver time is set by the limited ratio of the component of thrust acceleration along the radius vector to the total thrust acceleration. The absolute value of this ratio must be less than one. The maximum permissible value of T_B is set by the space vehicle's fuel capacity. Since the quantity $V_\theta(T_B)$ is a function of the maneuver time, it is reasonable to select a permissible value of T_B such that equation 6-17 is satisfied. This would ensure the simultaneous solution of the three constraint equation at the terminal time.

*Simulation has shown that an updating interval of 1 second is reasonable.

The desired value of T_B is determined by the following iterative procedure. An initial guess at the proper value of T_B is made.* Using the corresponding values of T_{go}, equation 6-28 is used to compute the thrust angle profile which will satisfy equations 6-15 and 6-16 by the estimated time of thrust termination. Sufficient information is now available to predict the terminal horizontal speed which would result. If equation 6-17 is not satisfied, the initial estimate of it is incremented such that the estimate is improved.

$$T_{B\,N+1} = T_{B_N} + K \left[V_\theta (T_B) - V_{\theta D} \right] \tag{6-29}$$

where

K is a positive weighting factor

The iterative procedure is continued until equation 6-17 is satisfied within a suitable error criterion. In a very few passes through the loop this procedure converges to the desired level of accuracy. The desired terminal conditions may be obtained very accurately by applying this procedure each time the state is updated.

Regardless of the choice of $P_1(t)$, the elements of the E-matrix in equation 26 approach infinity as T_{go} vanishes. Consequently, as T_{go} approaches zero, the non-vanishing errors in the boundary conditions cause c_1 and c_2 to increase without bound. This undesirable behavior can be avoided by not recomputing the E matrix in the last few seconds of powered flight.

Because the capability to change the vehicle's radial position diminishes rapidly as T_{go} approaches zero, it is desirable to abandon control of R in the last 30 seconds of flight.** This allows more accurate control of radial rate.

---

*A convenient technique is to assume an impulsive guidance logic for initial estimate of T_B.

**The error introduced in R by this procedure is negligible.

Since only one degree of freedom for $\ddot{R}$ is needed, the constant c_2 is set to zero. The expression for c_1 is then obtained by substituting equation 6-19 to 6-15.

$$c_1 = (R_D - R)/f_{11} \tag{6-30}$$

The terminal value of R is then

$$R(T_B) = R_i + \dot{R}_i T_{go} + C_1 f_{21} \tag{6-31}$$

After simulating this guidance scheme it was found that the iterative procedure for determining T_B could be eliminated. The value of T_B generated by the reference trajectory calculation was used in the guidance equations despite the fact that conditions differed from nominal. This procedure causes $V_\theta(T_B)$ to differ from the desired value since T_B is the synchronizing variable. By using $V_{\theta D}$ as the cutoff criterion rather than nominal T_B, however, this error can be eliminated. It should be noted that a slight fuel penalty may be incurred if $V_{\theta D}$ is used as a cutoff criterion (i.e., terminal time is no longer constrained). The significant reduction in onboard calculations is felt to justify any slight fuel penalty which might be incurred.

6.2 RESULTS USED IN THE INTEGRATION OF ORBITAL MISSION PHASES

As explained in paragraph 2.1.2.3, the following solution is valid if the variational equations applicable during retrothrust is linear.

$$\underline{p}_T = [K_{BT}]\ \underline{p}_i + [K_{\tilde{p}_T}]\ \underline{\tilde{p}}_i + [K_{\tilde{q}_T}]\ \underline{\tilde{q}} \tag{6-32}$$

From a digital simulation of overall guidance and control system, the matrices of sensitivity coefficients, $[K_{BT}]$, $[K_{\tilde{p}_T}]$ and $[K_{\tilde{q}_T}]$ were found to be well defined by equation 6-11 in paragraph 2.1.2.4. These results are not in the proper form, however, for direct use in paragraph 2.6.1 where the error analyses of the various orbital mission phases are integrated. In this section the appropriate coordinate transformations are indicated and the transformed matrices presented.

In paragraph 2.1.6 it is convenient to express the navigation and control sensor errors in a Cartesian coordinate set, X_o, Y_o, Z_o, having its origin at the nominal point of retrothrust initiation (see figure 6-1). Furthermore, vehicle excursion from the nominal at the conclusion of retrothrust are desired in a Cartesian coordinate set, X_1, Y_1, Z_1, having its origin at the nominal point of retrothrust termination. Thus, performing the appropriate transformations from polar coordinates to Cartesian coordinates yields

$$\underline{p}_1 = [S_{p_1 p_o}]\ \underline{p}_o + [S_{p_1 \tilde{p}_o}]\ \tilde{\underline{p}}_o + [S_{p_1 \tilde{q}}]\ \tilde{\underline{q}} \qquad (6\text{-}33)$$

The resulting matrices of sensitivity coefficients are documented below for reference.

$$[S_{p_1 p_o}] = \begin{bmatrix} 6.74(10^{-1}) & 1.0(10^{0}) & -1.17(10^{2}) & 6.60(10^{2}) \\ -1.84(10^{-3}) & 0 & -2.05(10^{-1}) & 0 \\ 0 & 0 & 0 & 0 \\ 0 & 0 & 0 & 0 \end{bmatrix} \qquad (6\text{-}34)$$

$$[S_{p_1 \tilde{p}_o}] = \begin{bmatrix} -6.74(10^{-1}) & 0 & 6.7(10^{1}) & 4.06(10^{2}) \\ 1.09(10^{0}) & 5.56(10^{-4}) & 2.46(10^{2}) & 7.28(10^{1}) \\ -2.7(10^{-4}) & 0 & 4.68(10^{-1}) & -8.84(10^{-1}) \\ 7.23(10^{-4}) & 0 & 9.41(10^{-1}) & 5.36(10^{-1}) \end{bmatrix}$$

$$[S_{p_1 \tilde{q}}] = \begin{bmatrix} 3.56(10^{0}) & 0 & 1.62(10^{4}) & 0 & -9.63(10^{4}) \\ -9.23(10^{-4}) & 2.29(10^{3}) & 1.08(10^{5}) & -3.07(10^{4}) & -5.97(10^{3}) \\ 0 & 0 & 1.51(10^{2}) & 0 & 2.21(10^{2}) \\ 0 & 0 & 8.82(10^{2}) & -2.46(10^{2}) & 0 \end{bmatrix}$$

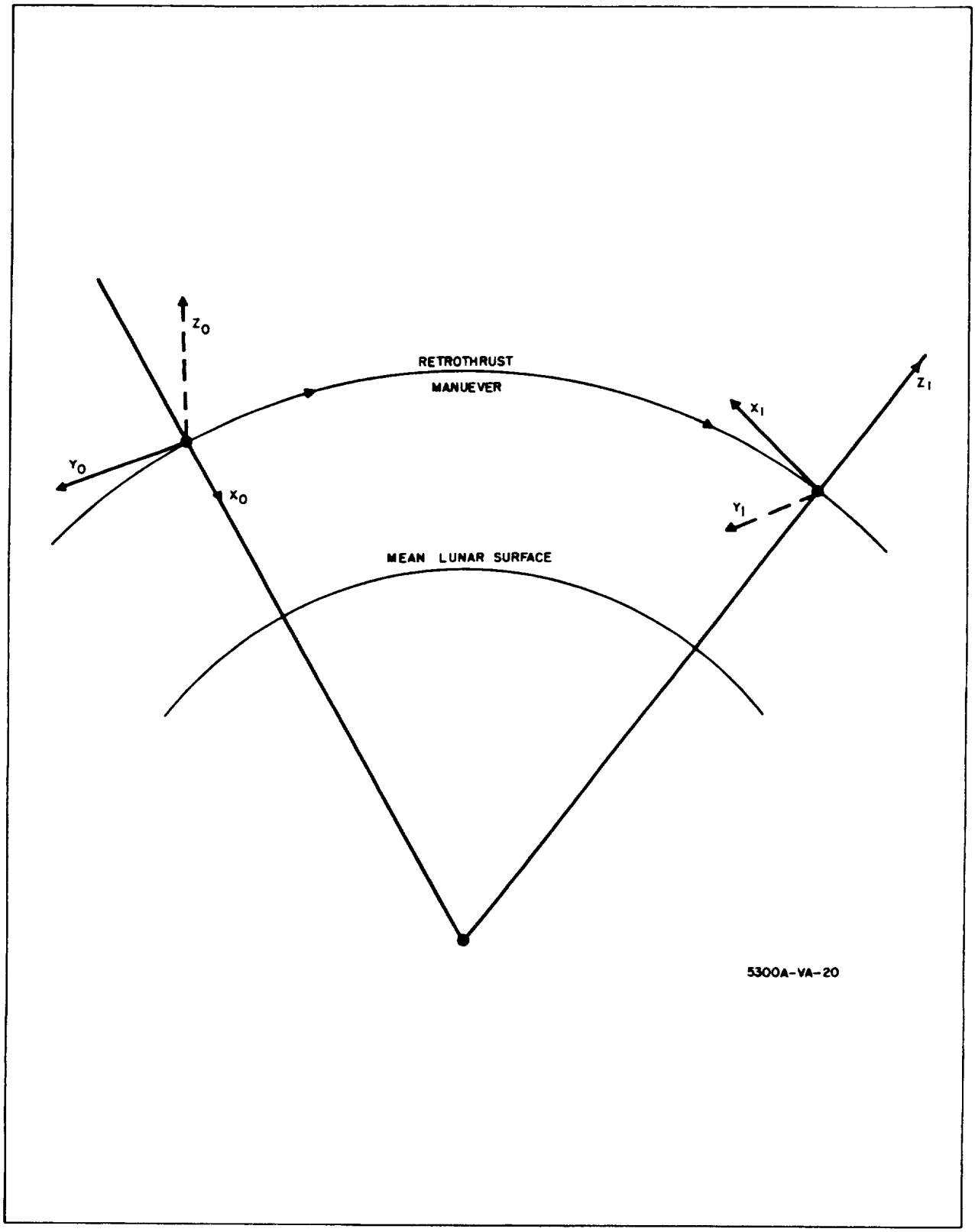

Figure 6-1. Coordinate Sets Used in the Integration of Orbital Mission Phases

7. ORBITAL PHASE APPENDIX

This section discusses the effect of thrust application errors during the descent kick. Immediately prior to application of the descent kick, the vehicle state vector is $\underline{P}_2^-$, the nominal state vector is $\underline{P}_{2n}^-$, and the deviation state vector is $\underline{p}_2^-$, where

$$\underline{p}_2^- = \underline{P}_2^- - \underline{P}_{2n}^- \tag{7-1}$$

During the descent kick maneuver, the vehicle velocity components are changed while the position components remain fixed because of the assumed impulsive nature of the maneuver. Thus, the vector $\underline{P}_2^+$ can be written in the form:

$$\underline{P}_2^+ = \underline{P}_2^- + \underline{\Delta P}_2 \tag{7-2}$$

where

$$\underline{\Delta P}_2 \equiv \begin{bmatrix} 0 \\ 0 \\ 0 \\ \Delta\dot{X}_2 \\ \Delta\dot{Y}_2 \\ \Delta\dot{Z}_2 \end{bmatrix} \tag{7-3}$$

The total change in velocity, denoted $\underline{\Delta V}_2$ is seen to have components $\Delta\dot{X}_2$, $\Delta\dot{Y}_2$, $\Delta\dot{Z}_2$. If the vector $\underline{\Delta V}_2$ is described with respect to the coordinate frame $X_2Y_2Z_2$ by means of its magnitude ΔV_2 and two Euler angles, α and γ as shown in figure 7-1, the following expressions are easily obtained.

$$\Delta\dot{X}_2 = \Delta V_2 \cos\alpha \cos\gamma \tag{7-4}$$

$$\Delta\dot{Y}_2 = \Delta V_2 \sin\gamma \tag{7-5}$$

$$\Delta\dot{Z}_2 = -\Delta V_2 \sin\alpha\cos\gamma \tag{7-6}$$

Note that α represents a rotation about the Y_2 axis, and γ a rotation about the new Z axis (Z_2').

Since the commanded vector $\underline{\Delta V}_2$ is always the nominal one, the actual applied vector will differ from the nominal by the amount of the application errors, denoted δV_2, $\delta\alpha$ and $\delta\gamma$. Thus

$$\Delta V_2 = \Delta V_{2n} + \delta V_2 \tag{7-7}$$

$$\alpha = \alpha_n + \delta\alpha \tag{7-8}$$

$$\gamma = \gamma_n + \delta\gamma \tag{7-9}$$

Thus,

$$\Delta\dot{X}_2 = \Delta\dot{X}_{2n} + \delta\dot{X}_2 = (\Delta V_{2n} + \delta V_2)\cos(\alpha_n + \delta\alpha)\cos(\gamma_n + \delta\gamma) \tag{7-10}$$

$$\Delta\dot{Y}_2 = \Delta\dot{Y}_{2n} + \delta\dot{Y}_2 = (\Delta V_{2n} + \delta V_2)\sin(\gamma_n + \delta\gamma) \tag{7-11}$$

$$\Delta\dot{Z}_2 = \Delta\dot{Z}_{2n} + \delta\dot{Z}_2 = -(\Delta V_{2n} + \delta V_2)\sin(\alpha_n + \delta\alpha)\cos(\gamma_n + \delta\gamma) \tag{7-12}$$

Using the knowledge that $\alpha_n = \gamma_n = 0$, small angle approximations, and dropping second order error terms, yields

$$\delta\dot{X}_2 = \delta V_2 \tag{7-13}$$

$$\delta\dot{Y}_2 = \Delta V_{2n}\,\delta\gamma \tag{7-14}$$

$$\delta\dot{Z}_2 = -\Delta V_{2n}\,\delta\alpha \tag{7-15}$$

Then

$$\underline{\Delta P}_2 = \underline{\Delta P}_{2n} + \underline{\delta P}_2 \tag{7-16}$$

and

$$\underline{P}^+_{2n} + \underline{p}^+_2 = \underline{P}^-_{2n} + \underline{p}^-_2 + \underline{\Delta P}_{2n} + \underline{\delta P}_2 \tag{7-17}$$

which yields

$$\underline{p}^+_2 = \underline{p}^-_2 + \underline{\delta P}_2 \tag{7-18}$$

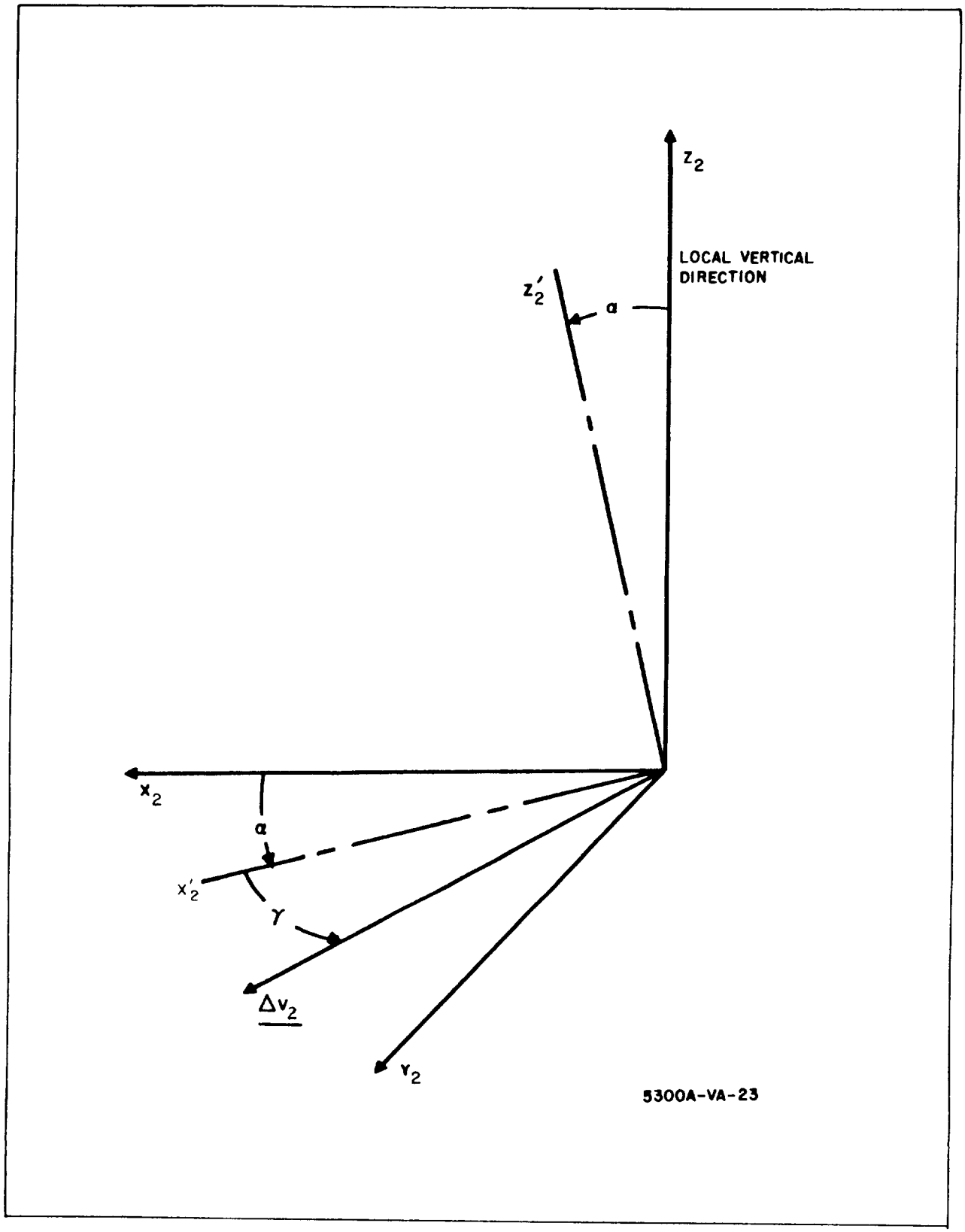

Figure 7-1. Descent Kick Geometry

If we define the vector of descent kick application errors to be

$$\underline{u} \equiv \begin{bmatrix} \delta V_2 \\ \delta \gamma \\ \delta \alpha \end{bmatrix} \tag{7-19}$$

Then it can be seen that $\underline{\delta P}_2$ can be expressed as

$$\underline{\delta P}_2 = \begin{bmatrix} 0 & 0 & 0 \\ 0 & 0 & 0 \\ 0 & 0 & 0 \\ 1 & 0 & 0 \\ 0 & \Delta V_{2n} & 0 \\ 0 & 0 & -\Delta V_{2n} \end{bmatrix} \begin{bmatrix} \delta V_2 \\ \delta \gamma \\ \delta \alpha \end{bmatrix} = [C]\,\underline{u} \tag{7-20}$$

Thus

$$\underline{P}_2^+ = \underline{P}_2^- + [C]\,\underline{u} \tag{7-21}$$

For the mission profile used, $\Delta V_{2n} = 76$ m/sec.

8. MAIN BRAKING PHASE APPENDIX

8.1 NOMINAL TRAJECTORY PROGRAM AND REFERENCE CURVES

The nominal trajectories for the main braking phases of both orbital descent and direct descent were generated in the same way. First, the nominal thrust program was selected (on the basis of references 4 and 5). Then a set of initial conditions consistent with nominal performance of the preceding mission phase and in the neighborhood of the desired nominal initial conditions is specified. These inputs are sufficient to allow integration of the equations of motion. This integration is terminated when the vehicle reaches the desired final velocity. At that time, altitude is compared with desired final altitude, and a new initial altitude is selected on the basis of the comparison. The rest of the initial conditions are adjusted so that the complete set is still consistent with the preceding orbital phase, and another run through the trajectory is made. This procedure leads to rapid convergence on a nominal trajectory with the desired final altitude and vertical velocity, the selected thrust profile, and a set of initial conditions consistent with the preceding mission phase.

The initial and final conditions of the orbital and direct descent main braking phases are presented in paragraphs 2.1.4 and 2.2.5 respectively and will not be repeated here.

The nominal thrust profiles used are:

a. Orbital descent:*

$F = 106,750$ N. = constant

$$\alpha = \begin{cases} 195^\circ; & R > 12.8 \text{ km} \\ 180^\circ; & R \leq 12.8 \text{ km} \end{cases}$$

---

* Taken from reference 4.

b. Direct descent (constant thrust, gravity turn)

$F = 106,750$ N = constant

$\alpha = 180°$ = constant

The angle α is defined in figure 2-14.

It is felt that graphs illustrating the nominal trajectory parameters would contribute little to this report, therefore, this type of information is not included.

It was necessary to generate polynominal approximations for $\dot{R}$ and Γ_{los} as functions of R for use as guidance system reference curves. These were derived by plotting the curves from computer data and curve fitting. The resulting reference curves used in this study are:

a. Orbital descent

(1) $\dot{R}_{ref}$ versus $\hat{R}$ *

For $\hat{R} > 50$ km

$$\dot{R}_{ref} = -39.54 - \left| 6.361\,\hat{R} - 16,713 \right|^{1/2} \text{ m/sec}$$

For 50 km $\geq \hat{R} > 4$ km

$$\dot{R}_{ref} = -49.73 - \left| 5.977\,\hat{R} - 8,370 \right|^{1/2} \text{ m/sec}$$

For 4 km $\geq \hat{R}$

$$\dot{R}_{ref} = -9.195 - \left| 7.669\,\hat{R} - 2,888 \right|^{1/2} \text{ m/sec}$$

(2) $(\Gamma_{los})_{ref}$ versus $\hat{R}$

For $\hat{R} > 37$ km

$$(\Gamma_{los})_{ref} = 0.325 \text{ rad.} = \text{constant}$$

For 37 km $\geq \hat{R} > 14$ km

$$(\Gamma_{los})_{ref} = 0.016 + (8.36 \times 10^{-6})\,\hat{R} \text{ rad}$$

For 14 km $\geq \hat{R} > 5$ km

$$(\Gamma_{los})_{ref} = 0.133 \text{ rad} = \text{constant}$$

---

* $\hat{R}$ is used to indicate that it is the estimated value of R that is used on board to compute the reference values of $\dot{R}$ and Γ_{los}.

For 5 km $\geq \hat{R}$

$$(\Gamma_{los})_{ref} = \frac{1}{-(2.929 \times 10^{-7})\,\hat{R}^2 + (2.980 \times 10^{-3})\,\hat{R} - 0.0757} \text{ rad.}$$

b. Direct descent

(1) $\dot{R}_{ref}$ versus $\hat{R}$

For $\hat{R} > 20$ km

$$\dot{R}_{ref} = -185.3 - [4.380\,\hat{R} - 49,276]^{1/2} \text{ m/sec}$$

For 20 km $\geq \hat{R} > 1.2$ km

$$\dot{R}_{ref} = -19.33 - [6.747\,\hat{R} - 3,080]^{1/2} \text{ m/sec}$$

For 1.2 km $\geq \hat{R}$

$$\dot{R}_{ref} = -5.028 - [8.199\,\hat{R} - 2,714]^{1/2} \text{ m/sec}$$

(2) $(\Gamma_{los})_{ref}$ versus $\hat{R}$

For $\hat{R} > 20$ km

$$(\Gamma_{los})_{ref} = (1.742 \times 10^{-8})\,\hat{R} + 0.0403 \text{ rad}$$

For 20 km $\geq \hat{R} > 1.2$ km

$$(\Gamma_{los})_{ref} = \frac{1}{-(1.020 \times 10^{-7})\,\hat{R}^2 + (3.347 \times 10^{-3})\,\hat{R} + 0.3225} \text{ rad}$$

For $\hat{R} \leq 1.2$ km

$$(\Gamma_{los})_{ref} = \frac{1}{-(5.385 \times 10^{-7})\,\hat{R}^2 + (4.417 \times 10^{-3})\,\hat{R} - 0.3173} \text{ rad}$$

8.2 NONLINEAR SIMULATION PROGRAM

This program, which is used to evaluate the effects of initial deviations from the nominal trajectory and bias components of navigation and control sensor error, is a direct simulation of the two-dimensional navigation, guidance, and control system shown in figure 2-15. The purpose of this paragraph is to show a complete block diagram of the simulation, indicating the manner in which the dynamics and geometry blocks are treated as well as the way in which the various error sources are simulated. The block diagram is shown in figure 8-1.

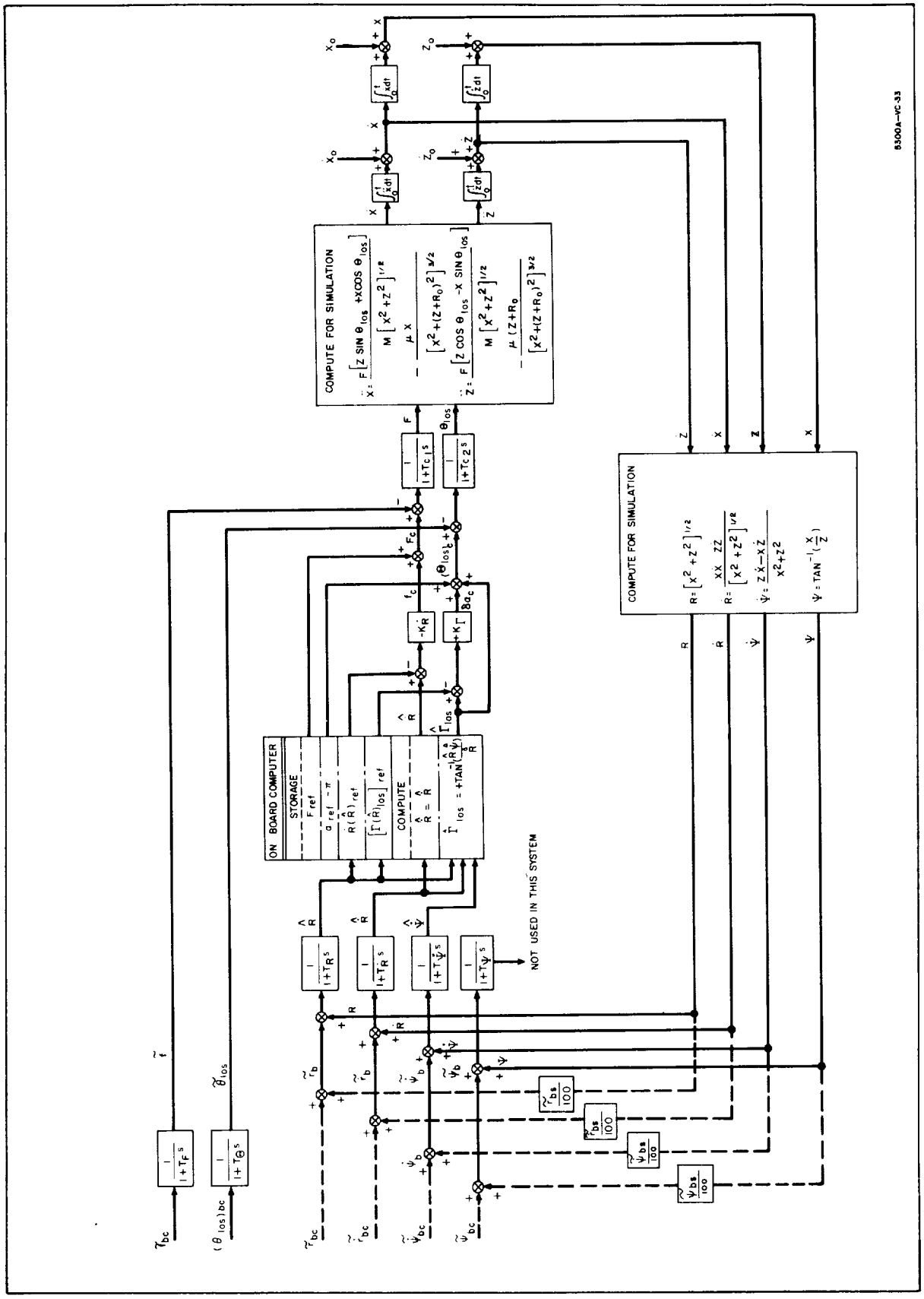

Figure 8-1. Line of Sight Rate System Diagram

It is seen that the equations of motion are written in the beacon centered Cartesian coordinate system (Z is beacon local vertical) shown in figure 2-14. Thus

$$\ddot{X} = \frac{F\left[Z \sin \Theta_{los} + X \cos \Theta_{los}\right]}{M\left[X^2 + Z^2\right]^{1/2}} - \frac{\mu X}{\left[X^2 + (Z + R_o)^2\right]^{3/2}}$$

$$\ddot{Z} = \frac{F\left[Z \cos \Theta_{los} - X \sin \Theta_{los}\right]}{M\left[X^2 + Z^2\right]^{1/2}} - \frac{\mu (Z + R_o)}{\left[X^2 + (Z + R_o)^2\right]^{3/2}}$$

$$M = M_o + \int_o^t \dot{M}\, dt = M_o - \int_o^t \frac{F}{I_{SP}\, g_o}\, dt$$

where

I_{SP} = specified impulse*

μ = lunar gravitational constant = 4.8982×10^{12}

R_o = mean lunar radius = 1738 km

g_o = earth surface gravitational acceleration = 9.80665 m/sec^2

Then

$$\dot{X} = \int_o^t \ddot{X}\, dt + \dot{X}_o$$

$$\dot{Z} = \int_o^t \ddot{Z}\, dt + \dot{Z}_o$$

and

$$X = \int_o^t \dot{X}\, dt + X_o$$

$$Z = \int_o^t \dot{Z}\, dt + Z_o$$

---

* Value used taken from reference 1.

where the initial conditions X_o, Z_o, $\dot{X}_o$, $\dot{Z}_o$ are program inputs. To simulate the effects of initial deviations from the nominal, one sets

$$X_o = X_{on} + x_o$$
$$Z_o = Z_{on} + z_o$$
$$\dot{X}_o = \dot{X}_{on} + \dot{x}_o$$
$$\dot{Z}_o = \dot{Z}_{on} + \dot{z}_o$$

where subscript n denotes the nominal value and x_o, z_o, $\dot{x}_o$, $\dot{z}_o$ are the desired deviations.

The geometry block is represented by the equations expressing the observed quantities R, $\dot{R}$, Ψ and $\dot{\Psi}$ in terms of X, Z, $\dot{X}$ and $\dot{Z}$. Note that the quantity Ψ is computed even though it represents navigation information not actually used.

The expressions used are:

$$R = \left[X^2 + Z^2\right]^{1/2}$$

$$\dot{R} = \frac{X\dot{X} + Z\dot{Z}}{\left[X^2 + Z^2\right]^{1/2}}$$

$$\Psi = \tan^{-1}\left[\frac{X}{Z}\right]$$

$$\dot{\Psi} = \frac{Z\dot{X} - X\dot{Z}}{X^2 + Z^2}$$

The bias error inputs are simulated by degrading the actual value of the appropriate observable by a constant amount plus an amount which is a constant percent of the actual value of the observable. For example, if the observable is R, then the actual input to the block representing range sensor dynamics, denoted R', is:

$$R' = R + \tilde{r}_{bc} + \tilde{r}_{bs}\,\frac{R}{100}$$

The significance of the nomenclature is discussed in paragraph 2.1.4.3. The actual observed value of R is $\hat{R}$ and appears at the output of the range sensor dynamic block.

Note that only constant bias errors and no scale factor bias errors are considered as inputs to the control sensors. The reasons are:

a. $\tilde{f}_{bs}$ is not considered because the main braking thrust level is nearly constant. Hence, a scale factor error and a constant bias error are essentially identical.

b. $(\tilde{\theta}_{los})_{bs}$ is not considered because a scale factor error is not commonly considered to be a component of an angle measurement error.

The constants characterizing the bias error model (e.g., $\tilde{r}_{bc}$, $\tilde{r}_{bs}$, $\tilde{f}_{bc}$) are inputs to the simulator program.

In addition, the time constants of the sensor and control dynamic blocks are program inputs.

Finally, the reference values of F, α, $\dot{R}$, and Γ_{los} are described by functions of the observed range $\hat{R}$. The particular functions used are given in paragraph 8.1 for both orbital and direct descent nominal trajectories.

8.3 ADJOINT SYSTEM SIMULATION

The first step in generating the adjoint simulation used in the investigation of random sensor errors is to linearize the system model described in paragraph 8.2 about the nominal path. Some portions of this model, specifically the sensor dynamics and the state variable integrations, are already linear so that these portions need not be discussed in detail. The discussion here deals with the linearization of guidance equations (including those contained in the guidance computer), the equations of motion, and the geometry equations.

Functionally, the guidance block represents the relationships between $\hat{F}_c$, $(\hat{\theta}_{los})_c$, and the navigation inputs $\hat{R}$, $\dot{\hat{R}}$, $\hat{\Psi}$, $\dot{\hat{\Psi}}$

$$\hat{F}_c = \hat{F}_c(\hat{R}, \dot{\hat{R}}, \hat{\Psi}, \dot{\hat{\Psi}})$$

$$(\hat{\theta}_{los})_c = \hat{\theta}_{los_c}(\hat{R}, \dot{\hat{R}}, \hat{\Psi}, \dot{\hat{\Psi}})$$

The particular functions are easily derived from figure 8-1.

$$\hat{F}_c = F_{ref}(\hat{R}) - K_{\dot{R}}\left[\dot{\hat{R}} - \dot{R}_{ref}(\hat{R})\right]$$

$$(\hat{\theta}_{los})_c = \alpha_{ref}(\hat{R}) - \pi + (1 + K_\Gamma)\hat{\Gamma}_{los} - K_\Gamma\left[\Gamma_{los}(\hat{R})\right]_{ref}$$

After linearization about the nominal, the expressions are written:

$$\hat{f}_c \doteq \left\{\frac{\partial \hat{F}_c}{\partial \hat{R}}\right\}_n \hat{r} + \left\{\frac{\hat{F}_c}{\partial \dot{\hat{R}}}\right\}_n \dot{\hat{r}} + \left\{\frac{\partial \hat{F}_c}{\partial \hat{\Psi}}\right\}_n \hat{\psi} + \left\{\frac{\partial \hat{F}_c}{\partial \dot{\hat{\Psi}}}\right\}_n \dot{\hat{\psi}}$$

$$(\hat{\theta}_{los})_c \doteq \left\{\frac{\partial(\hat{\theta}_{los})_c}{\partial \hat{R}}\right\}_n \hat{r} + \left\{\frac{\partial(\hat{\theta}_{los})_c}{\partial \dot{\hat{R}}}\right\}_n \dot{\hat{r}} + \left\{\frac{\partial(\hat{\theta}_{los})_c}{\partial \hat{\Psi}}\right\}_n \hat{\psi} + \left\{\frac{\partial(\hat{\theta}_{los})_c}{\partial \dot{\hat{\Psi}}}\right\}_n \dot{\hat{\psi}}$$

In this form, the two preceding expressions can be combined into a single matrix equation

$$\begin{bmatrix} \hat{f}_c \\ \hat{\theta}_{los\ c} \end{bmatrix} = \begin{bmatrix} g_{11} & g_{12} & g_{13} & g_{14} \\ g_{21} & g_{22} & g_{23} & g_{24} \end{bmatrix} \begin{bmatrix} \hat{r} \\ \dot{\hat{r}} \\ \hat{\psi} \\ \dot{\hat{\psi}} \end{bmatrix}$$

The definitions of elements g_{jk} can be inferred by comparison. Specifically, the elements are seen to be:

$$g_{11} = \left\{\frac{\partial F_{ref}(\hat{R})}{\partial \hat{R}}\right\}_n + K_{\dot{R}}\left\{\frac{\partial \dot{R}_{ref}(\hat{R})}{\partial \hat{R}}\right\}_n *$$

$$g_{12} = -K_{\dot{R}}$$

$$g_{13} = 0$$

$$g_{14} = 0$$

$$g_{21} = \frac{(1 + K_\Gamma)\dot{R}_n \dot{\Psi}_n}{\dot{R}_n^2 + (R_n \dot{\Psi}_n)^2} - K_\Gamma\left\{\frac{\partial \Gamma_{los}(\hat{R})_{ref}}{\partial \hat{R}}\right\}_n + \left\{\frac{\partial \alpha_{ref}(\hat{R})}{\partial \hat{R}}\right\}_n$$

---

* The specific definitions of $F_{ref}(\hat{R})$, $\alpha_{ref}(\hat{R})$, $\dot{R}_{ref}(\hat{R})$, and $\Gamma_{los}(\hat{R})_{ref}$ are given in paragraph 8.1.

$$g_{22} = - \frac{(1 + K_\Gamma) R_n \dot{\Psi}_n}{\dot{R}_n^2 + (R_n \dot{\Psi}_n)^2}$$

$$g_{23} = 0$$

$$g_{24} = \frac{(1 + K_\Gamma) R_n \dot{R}_n}{\dot{R}_n^2 + (R_n \dot{\Psi}_n)^2}$$

The equations of motion are linearized by starting with the expressions for $\ddot{X}$ and $\ddot{Z}$ as functions of X, Z, $\dot{X}$, $\dot{Z}$, F, and Θ_{los}.

$$\ddot{X} = \frac{F\left[Z \sin \Theta_{los} + X \cos \Theta_{los}\right]}{M\left[X^2 + Z^2\right]^{1/2}} - \frac{\mu X}{\left[X^2 + (Z + R_o)^2\right]^{3/2}}$$

$$\ddot{Z} = \frac{F\left[Z \cos \Theta_{los} - X \sin \Theta_{los}\right]}{M\left[X^2 + Z^2\right]^{1/2}} - \frac{\mu (Z + R_o)}{\left[X^2 + (Z + R_o)^2\right]^{3/2}}$$

In addition, consider the two expressions

$$\dot{X} = \dot{X}$$

$$\dot{Z} = \dot{Z}$$

These identities complete the definition of each of the elements of the time derivative of state vector $\underline{P}$ terms of the elements of $\underline{P}$.

$$\dot{\underline{P}} = \underline{f}(\underline{P}) = \underline{f}(X, Z, \dot{X}, \dot{Z})$$

Linearizing this nonlinear, first order, vector differential equation about the nominal path results in the following matrix differential equation

$$\dot{\underline{p}} = [A]\,\underline{p} + [B]\,\underline{u}$$

where $\underline{u}$ is defined in this instance to be

$$\underline{u} \equiv \begin{bmatrix} f \\ \theta_{los} \end{bmatrix}$$

[A] is a 4 x 4 and [B] a 4 x 2 matrix of partial derivatives evaluated on the nominal path.

$$a_{11} = \left\{\frac{\partial \dot{X}}{\partial X}\right\}_n = 0$$

$$a_{12} = \left\{\frac{\partial \dot{X}}{\partial Z}\right\}_n = 0$$

$$a_{13} = \left\{\frac{\partial \dot{X}}{\partial \dot{X}}\right\}_n = 1$$

$$a_{14} = \left\{\frac{\partial \dot{X}}{\partial \dot{Z}}\right\}_n = 0$$

$$a_{21} = \left\{\frac{\partial \dot{Z}}{\partial X}\right\}_n = 0$$

$$a_{22} = \left\{\frac{\partial \dot{Z}}{\partial Z}\right\}_n = 0$$

$$a_{23} = \left\{\frac{\partial \dot{Z}}{\partial \dot{X}}\right\}_n = 0$$

$$a_{24} = \left\{\frac{\partial \dot{Z}}{\partial \dot{Z}}\right\}_n = 1$$

$$a_{31} = \left\{\frac{\partial \ddot{X}}{\partial X}\right\}_n = \left\{\frac{F\left[Z^2 \cos\Theta_{los} - XZ \sin\Theta_{los}\right]}{M\left[X^2 + Z^2\right]^{3/2}} + \frac{\mu\left[2X^2 - (Z + R_o)^2\right]}{\left[X^2 + (Z + R_o)^2\right]^{5/2}}\right\}_n$$

$$a_{32} = \left\{\frac{\partial \ddot{X}}{\partial Z}\right\}_n = \left\{\frac{F\left[X^2 \sin\Theta_{los} - XZ \cos\Theta_{los}\right]}{M\left[X^2 + Z^2\right]^{3/2}} + \frac{3\mu X (Z + R_o)}{\left[X^2 + (Z + R_o)^2\right]^{5/2}}\right\}_n$$

$$a_{33} = \left\{\frac{\partial \ddot{X}}{\partial \dot{X}}\right\}_n = 0$$

$$a_{34} = \left\{\frac{\partial \ddot{X}}{\partial \dot{Z}}\right\}_n = 0$$

$$a_{41} = \left\{\frac{\partial \ddot{Z}}{\partial X}\right\}_n = \left\{ - \frac{F\left[Z^2 \sin\Theta_{los} + XZ\cos\Theta_{los}\right]}{M\left[X^2 + Z^2\right]^{3/2}} + \frac{3\mu\, X(Z + R_o)}{\left[X^2 + (Z + R_o)^2\right]^{5/2}} \right\}_n$$

$$a_{42} = \left\{\frac{\partial \ddot{Z}}{\partial Z}\right\}_n = \left\{ \frac{F\left[X^2 \cos\Theta_{los} + XZ \sin\Theta_{los}\right]}{M\left[X^2 + Z^2\right]^{3/2}} - \frac{\mu\left[X^2 - 2(Z + R_o)^2\right.}{\left[X^2 + (Z + R_o)^2\right]^{5/2}} \right\}_n$$

$$a_{43} = \left\{\frac{\partial \ddot{Z}}{\partial \dot{X}}\right\}_n = 0$$

$$a_{44} = \left\{\frac{\partial \ddot{Z}}{\partial \dot{Z}}\right\}_n = 0$$

$$b_{11} = \left\{\frac{\partial \dot{X}}{\partial F}\right\}_n = 0 \; ; \quad b_{12} = \left\{\frac{\partial \dot{X}}{\partial \Theta_{los}}\right\}_n = 0$$

$$b_{21} = \left\{\frac{\partial \dot{Z}}{\partial F}\right\}_n = 0 \; ; \quad b_{22} = \left\{\frac{\partial \dot{Z}}{\partial \Theta_{los}}\right\}_n = 0$$

$$b_{31} = \left\{\frac{\partial \ddot{X}}{\partial F}\right\}_n = \left\{ \frac{X\cos\Theta_{los} + Z\sin\Theta_{los}}{M\,(X^2 + Z^2)^{1/2}} \right\}_n$$

$$b_{32} = \left\{\frac{\partial \ddot{X}}{\partial \Theta_{los}}\right\}_n = \left\{ \frac{F\left[Z\cos\Theta_{los} - X\sin\Theta_{los}\right]}{M\,(X^2 + Z^2)^{1/2}} \right\}_n$$

$$b_{41} = \left\{\frac{\partial \ddot{Z}}{\partial F}\right\}_n = \left\{ \frac{Z\cos\Theta_{los} - X\sin\Theta_{los}}{M\,(X^2 + Z^2)^{1/2}} \right\}_n$$

$$b_{42} = \left\{\frac{\partial \ddot{Z}}{\partial \Theta_{los}}\right\}_n = \left\{ \frac{F\left[X\cos\Theta_{los} + Z\sin\Theta_{los}\right]}{M\,(X^2 + Z^2)^{1/2}} \right\}_n$$

In a similar manner, the geometry equations given in paragraph 8.2 are linearized resulting in a perturbation equation.

$$\underline{\dot{q}} \doteq [C]\,\underline{p}$$

where the elements of $[C]$ are:

$$c_{11} = \left\{\frac{\partial R}{\partial X}\right\}_n = \left\{\frac{X}{R}\right\}_n$$

$$c_{12} = \left\{\frac{\partial R}{\partial Z}\right\}_n = \left\{\frac{Z}{R}\right\}_n$$

$$c_{13} = \left\{\frac{\partial R}{\partial \dot{X}}\right\}_n = 0\,; \quad c_{14} = \left\{\frac{\partial R}{\partial \dot{Z}}\right\}_n = 0$$

$$c_{21} = \left\{\frac{\partial \dot{R}}{\partial X}\right\}_n = \left\{\frac{Z\dot{\Psi}}{R}\right\}_n$$

$$c_{22} = \left\{\frac{\partial \dot{R}}{\partial Z}\right\}_n = \left\{-\frac{X\dot{\Psi}}{R}\right\}_n$$

$$c_{23} = \left\{\frac{\partial \dot{R}}{\partial \dot{X}}\right\}_n = \left\{\frac{X}{R}\right\}_n$$

$$c_{24} = \left\{\frac{\partial \dot{R}}{\partial \dot{Z}}\right\}_n = \left\{\frac{Z}{R}\right\}_n$$

$$c_{31} = \left\{\frac{\partial \Psi}{\partial X}\right\}_n = \left\{\frac{Z}{R^2}\right\}_n$$

$$c_{32} = \left\{\frac{\partial \Psi}{\partial Z}\right\}_n = \left\{-\frac{X}{R^2}\right\}_n$$

$$c_{33} = \left\{\frac{\partial \Psi}{\partial \dot{X}}\right\}_n = 0\,; \quad C_{34} = \left\{\frac{\partial \Psi}{\partial \dot{Z}}\right\}_n = 0$$

$$c_{41} = \left\{\frac{\partial \dot{\Psi}}{\partial X}\right\}_n = \left\{-\frac{(R\dot{Z} + 2Z\dot{R})}{R^3}\right\}_n$$

$$c_{42} = \left\{ \frac{\partial \dot{\Psi}}{\partial Z} \right\}_n = \left\{ - \frac{(\dot{X} + 2Z\dot{\Psi})}{R^2} \right\}_n$$

$$c_{43} = \left\{ \frac{\partial \dot{\Psi}}{\partial \dot{X}} \right\}_n = \left\{ \frac{Z}{R} \right\}_n$$

$$c_{44} = \left\{ \frac{\partial \dot{\Psi}}{\partial \dot{Z}} \right\}_n = \left\{ \frac{X}{R^2} \right\}_n$$

Using the matrix representations described above, the linearized system block diagram shown in figure 8-2 is constructed.

The basic adjoint model of the linearized system is directly generated from the block diagram shown in figure 8-2 by applying the following rules (reference 10):

- The inputs and output of all blocks are reversed.
- Summations become branch points.
- Branch points become summations.

In addition, it is to be understood that the time variable in the adjoint model is τ and is equal to $t_{fn} - t$, where t_{fn} is the total time of flight of the nominal main braking maneuver. Thus, integrations in the adjoint model are over the region $\tau = 0$ to $\tau = \tau$. Also, time varying gains, such as the elements of matrix $[A]$, a_{11} for example, are evaluated using parameters of the nominal flight path evaluated at the time corresponding to the value of τ; that is,

$$a_{11}(\tau) = a_{11}(t_{fn} - t)$$

The system block diagram which results is shown in figure 8-3. Note that the data processing blocks used to convert adjoint simulation outputs to sensitivity coefficients are also shown in this diagram.

The theory behind use of the adjoint system model for random error analysis is represented in references 10 and 11 which are readily available;

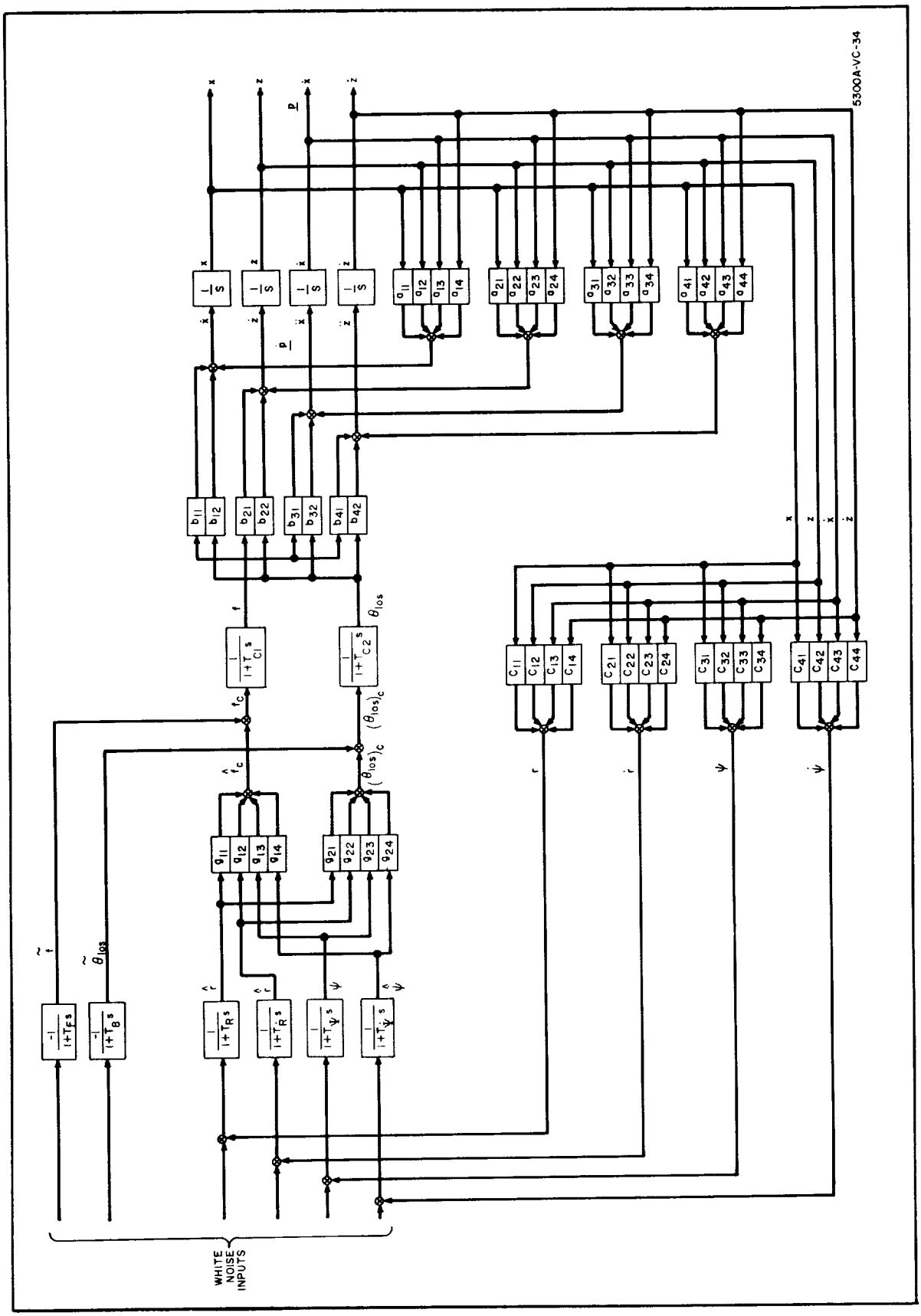

Figure 8-2. Linearized System Model

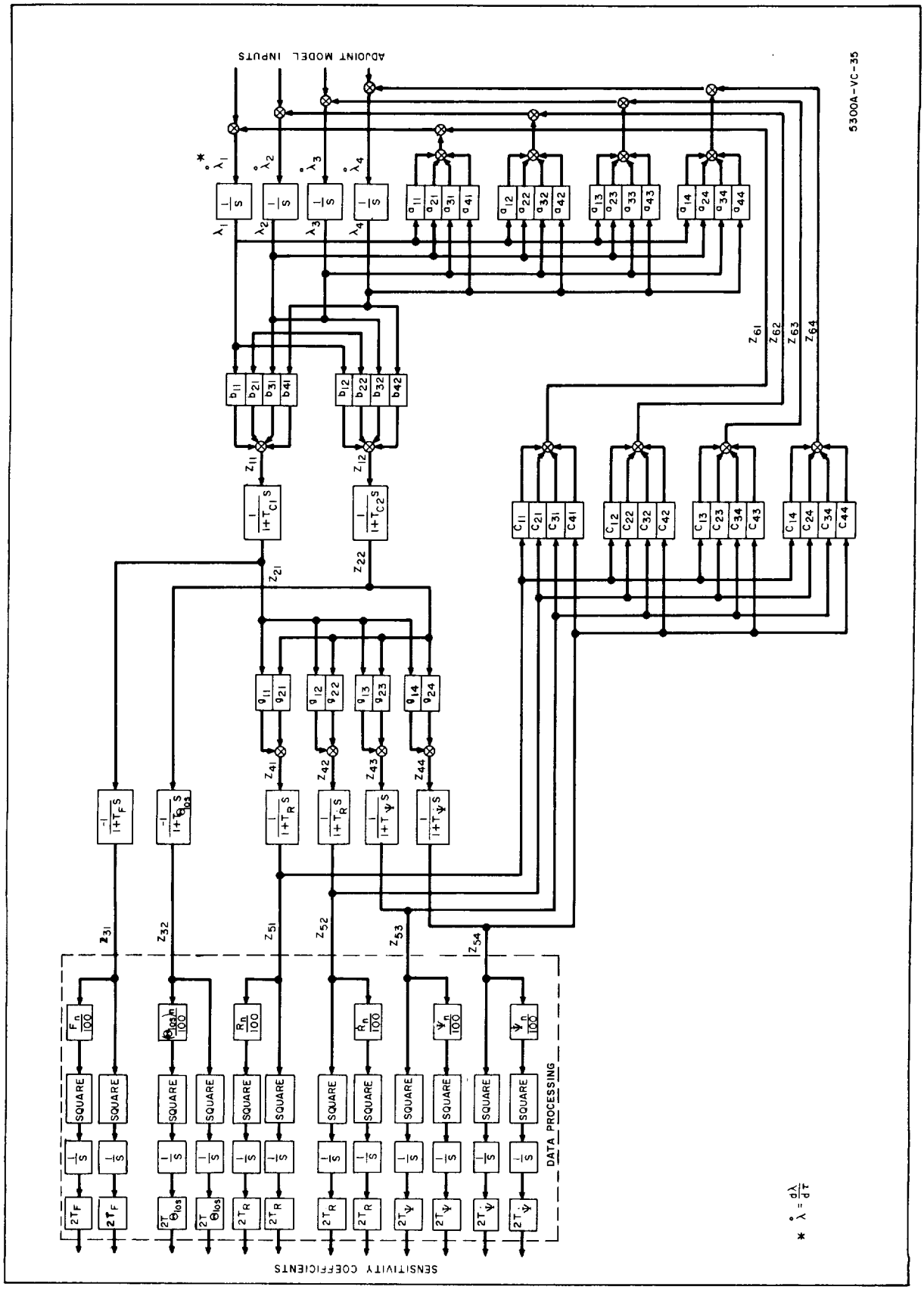

Figure 8-3. Linearized Adjoint System Model

this theory, therefore, is not discussed here. There is one group of blocks in figure 8-3 that are not justified directly by these references. These are multipliers of the form 2T where T is seen to be the time constant of the corresponding sensor dynamic characteristic. To implement the adjoint error analysis, it is necessary to assume that the noise inputs to the original system are white.* In this case, the direct outputs of the adjoint simulation are sensitivity coefficients relating deviations from nominal after the nominal time of flight to the average power spectral densities of the various input white noise sources. It is desired to relate the terminal errors to the mean squared values of the sensor errors measured at the output of the sensor dynamic block. The multiplication blocks under discussion are added to perform this task. As a result, the sensitivity coefficients generated by the adjoint program relate terminal deviations from nominal to the mean squared values of the random error sources, measured at the sensor output.

To provide the necessary nominal trajectory information during adjoint simulation runs, the equations of motion and nominal trajectory thrust program are set up in terms of the variable τ as part of the program. These equations are integrated along with the differential equations describing the adjoint system so that nominal trajectory information is available as it is required to evaluate the matrices, $[A]$, $[B]$, $[C]$, and $[G]$.

The program results are the two matrices $\left[S_{p_f \tilde{q}_{nc}}\right]_{t_{fn}}$ and $\left[S_{p_f \tilde{q}_{ns}}\right]_{t_{fn}}$ where

* If they are known not to be white, noise of the desired form can be generated by passing white noise through a shaping filter. The shaping filter is then included as part of the system and analysis is performed with white noise input. This is one reason for including sensor dynamic characteristics.

$$\begin{bmatrix} \sigma^2_{x\tilde{q}_n} \\ \sigma^2_{z\tilde{q}_n} \\ \sigma^2_{\dot{x}\tilde{q}_n} \\ \sigma^2_{\dot{z}\tilde{q}_n} \end{bmatrix}_{t_{fn}} = \left[S_{p_f \tilde{q}_{nc}} \right]_{t_{fn}} \underline{\sigma}^2_{\tilde{q}_{nc}} + \left[S_{p_f \tilde{q}_{ns}} \right]_{t_{fn}} \underline{\sigma}^2_{\tilde{q}_{ns}}$$

The subscript t_{fn} is used to indicate that this expression estimates the deviations that exist after the nominal time of flight. The two vectors $\underline{\sigma}^2_{\tilde{q}_{nc}}$ and $\sigma^2_{\tilde{q}_{ns}}$ are defined in paragraph 2.1.4.3.

8.4 CONVERSION OF DEVIATIONS AT $t = t_{fn}$ DUE TO RANDOM SENSOR ERRORS TO DEVIATIONS AT Z = 300 M

At the nominal end time of the main braking phase ($t = t_{fn}$), the actual state is $\underline{P}(t_{fn})$. All error sources, except the random sensor errors occurring during main braking, are assumed to be zero. Then, $\underline{p}(t_{fn})$ is given by:

$$\underline{p}(t_{fn}) = \underline{P}(t_{fn}) - \underline{P}_{fn} \tag{8-1}$$

where $\underline{P}_{fn}$ is the nominal terminal state.

The quantity t_f is defined to be the actual time of main braking termination which is the time when the estimated value of Z is 300 meters. To a first approximation, the difference between t_f and t_{fn} can be estimated as:

$$\Delta t \equiv t_f - t_{fn} \doteq - \frac{z(t_{fn})}{\dot{Z}(t_{fn})} \tag{8-2}$$

where

$$z(t_{fn}) = Z(t_{fn}) - Z_{fn} \tag{8-3}$$

Since $\dot{Z}(t_{fn})$ is negative in all cases of practical interest, Δt is positive if the spacecraft is higher than the desired altitude at $t = t_{fn}$ and negative if it is lower.

If $X(t_{fn})$, $\dot{X}(t_{fn})$, $\ddot{X}(t_{fn})$, $Z(t_{fn})$, $\dot{Z}(t_{fn})$, and $\ddot{Z}(t_{fn})$ are the actual position, velocity, and acceleration components of the vehicle at $t = t_{fn}$, then the position and velocity components at $t = t_f$ can be estimated from the following expressions:

$$\dot{X}(t_f) \doteq \dot{X}(t_{fn}) + \Delta t \ \ddot{X}(t_{fn}) \tag{8-4}$$

$$\dot{Z}(t_f) \doteq \dot{Z}(t_{fn}) + \Delta t \ \ddot{Z}(t_{fn}) \tag{8-5}$$

$$X(t_f) \doteq X(t_{fn}) + \Delta t \ \dot{X}(t_{fn}) + \frac{(\Delta t)^2}{2} \ \ddot{X}(t_{fn}) \tag{8-6}$$

$$Z(t_f) \doteq Z(t_{fn}) + \Delta t \ \dot{Z}(t_{fn}) + \frac{(\Delta t)^2}{2} \ \ddot{Z}(t_{fn}) \tag{8-7}$$

The following substitutions are now made

$$\dot{X}(t_f) = \dot{X}_{fn} + \dot{x}(t_f) \tag{8-8}$$

$$\dot{Z}(t_f) = \dot{Z}_{fn} + \dot{z}(t_f) \tag{8-9}$$

$$X(t_f) = X_{fn} + x(t_f) \tag{8-10}$$

$$Z(t_f) = Z_{fn} + z(t_f) \tag{8-11}$$

$$\ddot{X}(t_{fn}) = \ddot{X}_{fn} + \ddot{x}(t_{fn}) \tag{8-12}$$

$$\dot{X}(t_{fn}) = \dot{X}_{fn} + \dot{x}(t_{fn}) \tag{8-13}$$

$$X(t_{fn}) = X_{fn} + x(t_{fn}) \tag{8-14}$$

$$\ddot{Z}(t_{fn}) = \ddot{Z}_{fn} + \ddot{z}(t_{fn}) \tag{8-15}$$

$$\dot{Z}(t_{fn}) = \dot{Z}_{fn} + \dot{z}(t_{fn}) \tag{8-16}$$

$$Z(t_{fn}) = Z_{fn} + z(t_{fn}) \tag{8-17}$$

and the following expressions for the deviations from nominal at $t = t_f$ result.

$$\dot{x}(t_f) \doteq \dot{x}(t_{fn}) + \Delta t \left[\ddot{X}_{fn} + \ddot{x}(t_{fn}) \right] \tag{8-18}$$

$$\dot{z}(t_f) \doteq \dot{z}(t_{fn}) + \Delta t \left[\ddot{Z}_{fn} + \ddot{z}(t_{fn}) \right] \tag{8-19}$$

$$x(t_f) \doteq x(t_{fn}) + \Delta t \left[\dot{X}_{fn} + \dot{x}(t_{fn}) \right] + \frac{(\Delta t)^2}{2} \left[\ddot{X}_{fn} + \ddot{x}(t_{fn}) \right] \tag{8-20}$$

$$z(t_f) \doteq z(t_{fn}) + \Delta t \left[\dot{Z}_{fn} + \dot{z}(t_{fn}) \right] + \frac{(\Delta t)^2}{2} \left[\ddot{Z}_{fn} + \ddot{z}(t_{fn}) \right] \tag{8-21}$$

The quantity Δt can be expressed as follows

$$\Delta t = -\frac{z(t_{fn})}{\dot{Z}(t_{fn})} = \frac{-z(t_{fn})}{\dot{Z}_{fn} + \dot{z}(t_{fn})} = \frac{-z(t_{fn})}{\dot{Z}_{fn}\left[1 + \dfrac{\dot{z}(t_{fn})}{\dot{Z}_{fn}}\right]} \tag{8-22}$$

Since $\dfrac{\dot{z}(t_{fn})}{\dot{Z}_{fn}}$ is generally an order of magnitude less than unity (considering allowed velocity errors), the expression used for Δt is:

$$\Delta t \doteq \frac{-z(t_{fn})}{\dot{Z}_{fn}} \tag{8-23}$$

Substituting this into equations 8-18, 8-19 and 8-20 and retaining only first order deviation terms yields:

$$\dot{x}(t_f) \doteq \dot{x}(t_{fn}) - \frac{z(t_{fn})}{\dot{Z}_{fn}} \ddot{X}_{fn} \tag{8-24}$$

$$\dot{z}(t_f) \doteq \dot{z}(t_{fn}) - \frac{z(t_{fn})}{\dot{Z}_{fn}} \ddot{Z}_{fn} \tag{8-25}$$

$$x(t_f) \doteq x(t_{fn}) - \frac{z(t_{fn})}{\dot{Z}_{fn}} \dot{X}_{fn} \tag{8-26}$$

A similar expression for $z(t_f)$ is obtainable from equation 8-21; however, a better estimate is directly available. By definition, t_f is the time when the estimated value of Z is equal to the nominal final value, Z_{fn}.

Hence:

$$\hat{Z}(t_f) = Z_f + \tilde{z}(t_f) = Z_{fn} + z(t_f) + \tilde{z}(t_f) = Z_{fn} \tag{8-27}$$

which yields:

$$z(t_f) = -\tilde{z}(t_f) \tag{8-28}$$

Estimation error $\tilde{z}(t_f)$ is related to the navigation sensor errors by linearizing the navigation equation:

$$\hat{Z} = \hat{R} \cos \hat{\Psi} \tag{8-29}$$

about the nominal end point.

$$\tilde{z}(t_f) \doteq \left[\tilde{r}_{nc}(t_f) + \tilde{r}_{ns}(t_f) \frac{R_{fn}}{100}\right] \cos \Psi_{fn} - \left[\tilde{\psi}_{nc}(t_f) + \tilde{\psi}_{ns}(t_f) \frac{\Psi}{100}\right] R_{fn} \sin \Psi_{fn} \tag{8-30}$$

Using equations 8-24, 8-25, 8-26, 8-27, and 8-29, the vectors $\underline{\sigma}^2_{p(t_f)} \tilde{q}_{nc}$ and $\underline{\sigma}^2_{p(t_f)} \tilde{q}_{ns}$ are expressed in terms of $\underline{\sigma}^2_{p(t_{fn})} \tilde{q}_{nc}$ and $\sigma^2_{p(t_{fn})} \tilde{q}_{ns}$ (the results obtained from the adjoint system situation) and the vectors $\underline{\sigma}^2_{\tilde{q}_{nc}}$ and $\underline{\sigma}^2_{\tilde{q}_{ns}}$. The relationships are of the form:

$$\underline{\sigma}^2_{p(t_f)} \tilde{q}_{nc} = [A] \underline{\sigma}^2_{p(t_{fn})} \tilde{q}_{nc} + [K_1] \underline{\sigma}^2_{\tilde{q}_{nc}} \tag{8-31}$$

$$\underline{\sigma}^2_{p(t_f)} \tilde{q}_{ns} = [A] \underline{\sigma}^2_{p(t_{fn})} \tilde{q}_{ns} + [K_2] \underline{\sigma}^2_{\tilde{q}_{ns}} \tag{8-32}$$

where

$$[A] \equiv \begin{bmatrix} 1 & \left(\frac{\dot{X}_{fn}}{\dot{Z}_{fn}}\right)^2 & 0 & 0 \\ 0 & 0 & 0 & 0 \\ 0 & \left(\frac{\ddot{X}_{fn}}{\dot{Z}_{fn}}\right)^2 & 1 & 0 \\ 0 & \left(\frac{\ddot{Z}_{fn}}{\dot{Z}_{fn}}\right)^2 & 0 & 1 \end{bmatrix} \tag{8-33}$$

$$[K_1] \equiv \begin{bmatrix} 0 & 0 & 0 & 0 & 0 & 0 \\ \cos^2 \Psi_{fn} & 0 & R_{fn}^2 \sin^2 \Psi_{fn} & 0 & 0 & 0 \\ 0 & 0 & 0 & 0 & 0 & 0 \\ 0 & 0 & 0 & 0 & 0 & 0 \end{bmatrix} \tag{8-34}$$

$$[K_2] = \begin{bmatrix} 0 & 0 & 0 & 0 & 0 & 0 \\ \frac{R_{fn}^2 \cos^2 \Psi_{fn}}{10^4} & 0 & \frac{R_{fn}^2 \Psi_{fn}^2 \sin^2 \Psi_{fn}}{10^4} & 0 & 0 & 0 \\ 0 & 0 & 0 & 0 & 0 & 0 \\ 0 & 0 & 0 & 0 & 0 & 0 \end{bmatrix} \tag{8-35}$$

From the adjoint simulation, sensitivity coefficient matrices $\left[S_{p_f \tilde{q}_{nc}}\right]_{t_{fn}}$ and $\left[S_{p_f \tilde{q}_{ns}}\right]_{t_{fn}}$ are obtained which satisfy the relationships

$$\underline{\sigma}^2_{p(t_{fn})\tilde{q}_{nc}} = \left[S_{p_f\tilde{q}_{nc}}\right]_{t_{fn}} \underline{\sigma}^2_{\tilde{q}_{nc}} \tag{8-36}$$

$$\underline{\sigma}^2_{p(t_{fn})\tilde{q}_{ns}} = \left[S_{p_f\tilde{q}_{ns}}\right]_{t_{fn}} \underline{\sigma}^2_{\tilde{q}_{ns}} \tag{8-37}$$

Substituting these expressions into equations (8-31) and (8-32) yields:

$$\underline{\sigma}^2_{p(t_f)\tilde{q}_{nc}} = \left[S_{p_f\tilde{q}_{nc}}\right] \underline{\sigma}^2_{\tilde{q}_{nc}} = \left\{[A]\left[S_{p_f\tilde{q}_{nc}}\right]_{t_{fn}} + [K_1]\right\} \underline{\sigma}^2_{\tilde{q}_{nc}} \tag{8-38}$$

$$\underline{\sigma}^2_{p(t_f)\tilde{q}_{ns}} = \left[S_{p_f\tilde{q}_{ns}}\right] \underline{\sigma}^2_{\tilde{q}_{ns}} = \left\{[A]\left[S_{p_f\tilde{q}_{ns}}\right]_{t_{fn}} + [K_2]\right\} \underline{\sigma}^2_{\tilde{q}_{ns}} \tag{8-39}$$

Numerical evaluation of $\left[S_{p_f\tilde{q}_{nc}}\right]$ and $\left[S_{p_f\tilde{q}_{ns}}\right]$ is straightforward. From the adjoint system simulation:

$$\left[S_{p_f q_{nc}}\right]_{t_{fn}} = \begin{bmatrix} 1.54\text{x}10^{-2} & 1.38\text{x}10^{0} & 0.0 & 1.16\text{x}10^{9} & 8.54\text{x}10^{-8} & 3.45\text{x}10^{3} \\ 1.42\text{x}10^{-2} & 5.78\text{x}10^{0} & 0.0 & 4.55\text{x}10^{9} & 2.75\text{x}10^{-7} & 6.91\text{x}10^{3} \\ 1.50\text{x}10^{-3} & 5.97\text{x}10^{-2} & 0.0 & 1.01\text{x}10^{6} & 5.46\text{x}10^{-10} & 2.80\text{x}10^{1} \\ 2.06\text{x}10^{-3} & 1.88\text{x}10^{-1} & 0.0 & 1.63\text{x}10^{8} & 6.22\text{x}10^{-9} & 2.47\text{x}10^{2} \end{bmatrix} \tag{8-40}$$

$$\left[S_{p_f\tilde{q}_{ns}}\right]_{t_{fn}} = \begin{bmatrix} 7.60\text{x}10^{0} & 2.59\text{x}10^{1} & 0.0 & 7.22\text{x}10^{-1} & 9.73\text{x}10^{-2} & 7.54\text{x}10^{-2} \\ 2.23\text{x}10^{1} & 7.60\text{x}10^{1} & 0.0 & 1.49\text{x}10^{0} & 3.11\text{x}10^{-1} & 2.10\text{x}10^{-1} \\ 4.36\text{x}10^{-2} & 1.39\text{x}10^{-2} & 0.0 & 1.05\text{x}10^{-2} & 6.25\text{x}10^{-4} & 9.45\text{x}10^{-4} \\ 7.19\text{x}10^{-1} & 2.13\text{x}10^{0} & 0.0 & 5.97\text{x}10^{-2} & 7.06\text{x}10^{-3} & 8.10\text{x}10^{-3} \end{bmatrix} \tag{8-41}$$

To evaluate $[A]$, $[K_1]$, and $[K_2]$ the following nominal terminal conditions are used.

$\dot{X}_{fn} = -9.3$ m/sec
$\dot{Z}_{fn} = -37$ m/sec
$\ddot{X}_{fn} = 1.35$ m/sec^2
$\ddot{Z}_{fn} = 3.72$ m/sec^2
$\Psi_{fn} = 39.8°$
$R_{fn} = 391$ m

Computation yields the following values for $\left[S_{p_f \tilde{q}_{nc}}\right]$ and $\left[S_{p_f \tilde{q}_{ns}}\right]$.

$$\left[S_{p_f \tilde{q}_{nc}}\right] = \begin{bmatrix} 1.64\text{x}10^{-2} & 5.02\text{x}10^{-1} & 0 & 1.44\text{x}10^{9} & 1.04\text{x}10^{-7} & 3.89\text{x}10^{3} \\ 5.90\text{x}10^{-1} & 0 & 6.26\text{x}10^{4} & 0 & 0 & 0 \\ 1.52\text{x}10^{-3} & 6.72\text{x}10^{-2} & 0 & 7.06\text{x}10^{6} & 9.11\text{x}10^{-10} & 3.71\text{x}10^{1} \\ 2.20\text{x}10^{-3} & 2.46\text{x}10^{-1} & 0 & 2.08\text{x}10^{8} & 8.98\text{x}10^{-9} & 3.17\text{x}10^{2} \end{bmatrix} \quad (8\text{-}42)$$

$$\left[S_{p_f \tilde{q}_{ns}}\right] = \begin{bmatrix} 9.01\text{x}10^{0} & 3.07\text{x}10^{1} & 0 & 8.16\text{x}10^{-1} & 1.17\text{x}10^{-1} & 8.85\text{x}10^{-2} \\ 9.03\text{x}10^{0} & 0 & 3.02\text{x}10^{0} & 0 & 0 & 0 \\ 7.32\text{x}10^{-2} & 1.15\text{x}10^{-1} & 0 & 1.25\text{x}10^{-2} & 1.04\text{x}10^{-3} & 1.22\text{x}10^{-3} \\ 9.42\text{x}10^{-1} & 2.89\text{x}10^{0} & 0 & 7.47\text{x}10^{-2} & 1.02\text{x}10^{-2} & 1.02\text{x}10^{-2} \end{bmatrix} \quad (8\text{-}43)$$

These sensitivity coefficient matrices can be used to estimate the mean squared deviations from nominal at the actual time of main braking termination due to random navigation and control sensor error inputs during the main braking maneuver.

8.5 OUT-OF-PLANE ERROR CORRECTION CAPABILITY

To obtain an estimate of the fuel consumption required to correct out-of-plane errors existing at main braking initiation, the following brief investigation is performed. Vehicle motion is described in a beacon centered coordinate system (X, Y, Z) where:

- Z is along beacon local vertical
- X is along beacon horizontal toward the position of the vehicle at main braking initiation
- Y completes the right-handed coordinate set

To perform the analysis, it is assumed that motion in the Y direction is independent of motion in the X and Z directions; that there is no gravity component along the Y axis; and that navigation, guidance, and control are performed without error during main braking.

A simple guidance law is selected that is designed to null the Y components of position and velocity. The form is:

$$\ddot{Y} = -K_1 Y - K_2 \dot{Y} \tag{8-44}$$

where K_1 and K_2 are positive constants.

By virtue of simplifying assumptions, Y direction motion is described by a linear, homogeneous second order differential equation with constant coefficients.

$$\ddot{Y} + K_2 \dot{Y} + K_1 Y = 0 \tag{8-45}$$

The general solution of which has the form

$$Y = C_1 e^{m_1 t} + C_2 e^{m_2 t} \tag{8-46}$$

where

$$m_1 = -\frac{K_2}{2} + \left[\left(\frac{K_2}{2}\right)^2 - K_1\right]^{1/2} \tag{8-47}$$

$$m_2 = -\frac{K_2}{2} - \left[\left(\frac{K_2}{2}\right)^2 - K_1\right]^{1/2} \tag{8-48}$$

and C_1, C_2 are determined by the initial conditions

$$Y_i = 0^* \tag{8-49}$$

$$\dot{Y}_i = \dot{Y}_i \tag{8-50}$$

To satisfy these initial conditions

$$C_1 = -C_2 = \frac{\dot{Y}_i}{m_1 - m_2} = \frac{\dot{Y}_i}{2\left[\left(\frac{K_2}{2}\right)^2 - K_1\right]^{1/2}} \tag{8-51}$$

It was decided to work with the critically damped solution to equation 8-45 which corresponds to the case $m_1 = m_2$ in equation 8-46. It is known

---

* By definition of the coordinate system used, Y is zero initially.

that when $m_1 = m_2$, equation 8-46 is not the proper solution to the differential equation and that the form to be used is:

$$Y = C_1 e^{mt} + C_2 t e^{mt} \tag{8-52}$$

where

$$m = -\frac{K_2}{2} \tag{8-53}$$

Once again, constants C_1 and C_2 are evaluated using the initial conditions.

$$C_1 = 0 \tag{8-54}$$

$$C_2 = \dot{Y}_i \tag{8-55}$$

Thus, in the critically damped case, vehicle motion in the Y direction is given by

$$Y = \dot{Y}_i \, t e^{mt} \tag{8-56}$$

$$\dot{Y} = \dot{Y}_i \, [1 + mt] \, e^{mt} \tag{8-57}$$

$$\ddot{Y} = m\dot{Y}_i \, (2 + mt) \, e^{mt} = - K_2 \dot{Y} - K_1 Y \tag{8-58}$$

The value of m is selected to be (-0.03). This value results in terminal values of Y and $\dot{Y}$ on the order of 1 m and 0.01 m/sec for typical values of $\dot{Y}_i$ (on the order of 50 m/sec.). The terminal values of Y and $\dot{Y}$ referred to in this case are the values after the nominal time of flight (435 seconds for orbital descent.)

From equation 8-53

$$K_2 = - 2m = 0.06 \tag{8-59}$$

and from the expression

$$\left(\frac{K_2}{2}\right)^2 - K_1 = 0 \tag{8-60}$$

which the condition for equal roots in the solution to differential equation 8-45

$$K_1 = 9.0 \times 10^{-4} \tag{8-61}$$

Now estimate ΔV_y, the ΔV required to correct the initial out of plane velocity $\dot{Y}_i$ by integrating the absolute value of $\ddot{Y}$ from t = 0 to t = t_{fn} = 435 sec. Where $|\ddot{Y}|$ is given by

$$|\ddot{Y}| = \left| m\dot{Y}_i (2 + mt)e^{mt} \right| \tag{8-62}$$

With m = -0.03, it can be seen that $\ddot{Y}$ changes sign when -mt = 2 so that the integral giving ΔV_y must be evaluated in two parts

$$\Delta V_y = |\dot{Y}_i| \left\{ -\int_0^{-\frac{2}{m}} m(2 + mt)e^{mt}\, dt + \int_{-\frac{2}{m}}^{t_{fn}} m(2 + mt)e^{mt}\, dt \right\} \tag{8-63}$$

Carrying out the integration yields

$$\Delta V_y = |\dot{Y}_i| \left\{ 2e^{-2} + 1 + [1 + mt_{fn}]\, e^{mt_{fn}} \right\} \tag{8-64}$$

which for m = -0.03 and t_{fn} = 435 sec yields

$$\Delta V_y = 1.27 \left| \dot{Y}_i \right| \tag{8-65}$$

It can be shown that this expression for ΔV_y is very insensitive to a change in parameter m in the region of the operating point selected (m = -0.03).

If the maximum allowable value of ΔV_y is taken to be 5 percent of the nominal main braking ΔV (1900 m/sec), then:

$$(\Delta V_y)_{max} = 95 \text{ m/sec} \tag{8-66}$$

and

$$|\dot{Y}_i|_{max} = 3(\sigma_{\dot{y}_i})_{max} = \frac{95}{1.27} = 75 \text{ m/sec} \tag{8-67}$$

The value of $\dot{Y}_i$ can be related to the cross-track miss of the actual orbital plane by considering the geometry illustrated in figure 8-4.

The angle ϕ is accurately described by the relationship

$$\phi \doteq \sin \phi \doteq \frac{\dot{Y}_i}{V_{in}} = \frac{\dot{Y}_i}{1600} \tag{8-68}$$

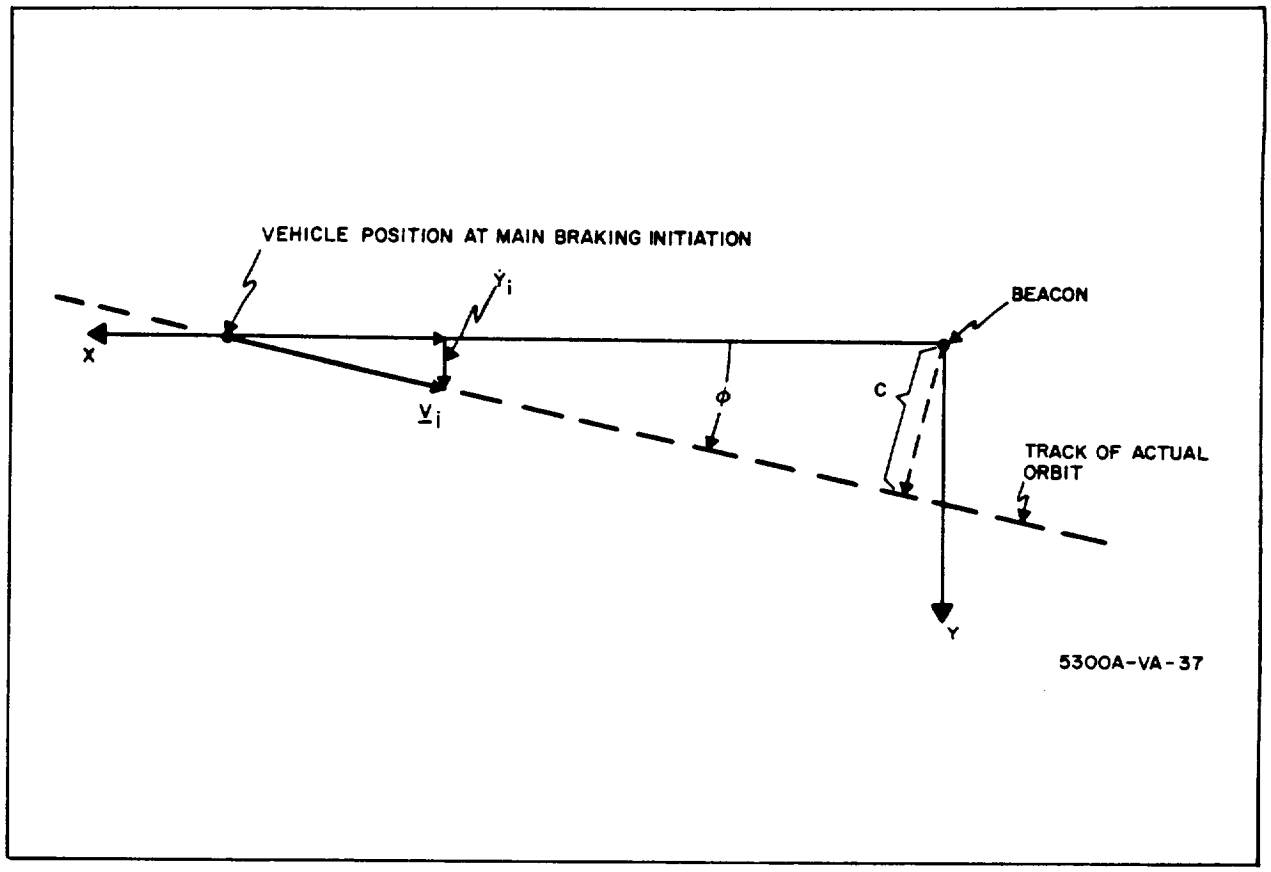

Figure 8-4. Horizontal Plane Geometry

The cross track error (c) is given by

$$c = X_i \sin \phi \doteq X_{in} \phi = \frac{3.4 \times 10^5 \dot{Y}_i}{1.6 \times 10^3} \tag{8-69}$$

Thus, the maximum (3σ) cross track error that can be corrected using 5 percent of the nominal main braking ΔV is:

$$3(\sigma_c)_{max} = (2.1 \times 10^2)\, 3(\sigma_{\dot{y}_i})_{max} = 15.7 \text{ km} \tag{8-70}$$

or

$$(\sigma_c)_{max} = 5.2 \text{ km} \tag{8-71}$$

Since this value is greater than the expected cross-track error as determined in paragraph 2.1.1.4, it is concluded that out-of-plane errors can be allowed to propagate to the start of main braking before corrective action is taken.

9. FINAL TOUCHDOWN ANALYSIS APPENDIX

9.1 DERIVATION OF EXPRESSIONS FOR IMPACT VELOCITY

The final touchdown maneuver system models to be used are given in paragraph 2.1.5. In this paragraph the analysis of the X_v channel is described in some detail terminating in an expression for $\dot{X}_{vI}$, the X_v component of impact velocity, in terms of the error sources $\tilde{\dot{x}}_1$, $\tilde{\ddot{x}}_b$, and ζ defined in paragraph, 2.1.5. Analysis of the Y_v and Z_v channels follow the identical procedure, and therefore only the results are given.

It is assumed that the X_v channel starts in the nonlinear region. That is, the commanded acceleration exceeds the maximum available acceleration. Thus, maximum thrust will be commanded in this direction. Eventually the application of maximum acceleration will drive the vehicle state into the linear region of the respective control loops. It is assumed that system damping is such that the vehicle state will remain in the linear region after this time. Using system conditions at the time of entrance into the linear region as initial conditions, the actual vehicle velocity at impact can be estimated assuming only that there is sufficient time prior to impact, for the control system to reach steady state.

The block diagram of the X_v channel when t is in the interval $t_1 < t \leq t_{2X}$ is shown in figure 2-21a, where t_1 is start time of inertial navigation and t_{2X} is the time when the vehicle dynamical state enters the linear region of the X_v channel guidance and control system. Note that the effect of thrust limiting is to make the system operate in an open loop manner until the

commanded acceleration drops below the maximum available.* If the inputs are considered to be constant over the interval $t_1 < t \leq t_{2X}$, they are expressible in terms of the Laplace variable s, as follows.

$\ddot{X}_{F_{max}}(s) = \frac{\ddot{X}_{F_{max}}}{s}$; $\ddot{X}_{F_{max}}$ is the maximum available X component of thrust acceleration

$\ddot{X}_{vF1}(s) = \frac{\ddot{X}_{vF1}}{s}$; $\ddot{X}_{vF1}$ is the actual value of the X_v component of thrust acceleration at $t = t_1$.

$g_m(s)\,\zeta(s) = \frac{g_m \zeta}{s}$; ζ is the misalignment of Z_v to Z

$\tilde{\ddot{x}}_b(s) = \frac{\tilde{\ddot{x}}_b}{s}$; bias error in the X_v channel acceleration sensor

$\dot{X}_{v1}(s) = \frac{\dot{X}_{v1}}{s}$; $\dot{X}_{v1}$ is the actual value of $\dot{X}_v$ at $t = t_1$

$\hat{\dot{X}}_{v1}(s) = \frac{\hat{\dot{X}}_{v1}}{s}$; $\hat{\dot{X}}_{v1}$ is the estimated value of $\dot{X}_v$ at $t = t_1$

Then the expressions for $\dot{X}_v(s)$ and $\hat{\dot{X}}_v(s)$ are:

$$\dot{X}_v(s) = \frac{\ddot{X}_{F_{max}}}{T_X s^3} + \frac{\ddot{X}_{vF1}}{s^2} + \frac{g_m \zeta}{s^2} + \frac{\dot{X}_{v1}}{s} \qquad (9\text{-}1)$$

$$\hat{\dot{X}}_v(s) = \frac{\ddot{X}_{F_{max}}}{T_X s^3 (1 + T_{\ddot{X}} s)} + \frac{\ddot{X}_{vF1}}{s^2 (1 + T_{\ddot{X}} s)} + \frac{\tilde{\ddot{x}}_b}{s^2 (1 + T_{\ddot{X}} s)} + \frac{\hat{\dot{X}}_{v1}}{s} \qquad (9\text{-}2)$$

---

* Note from figure 2-21a that if $\ddot{X}_{vF1}$ is initially less than $\ddot{X}_{Fmax}$ the system actually starts in the linear control region. This fact has been ignored in the subsequent analysis, but it is felt that this omission will not in any way change the estimated value of $\dot{X}_v(t_{2X}) - \hat{\dot{X}}_v(t_{2X})$ which is the end point of this portion of the analysis. What will change is the actual value of $(t_{2X} - t_1)$ which is not used in the analysis.

The desired result of this portion of the investigation is an estimate of the difference between $\dot{X}_v$ and $\hat{\dot{X}}_v$ at $t = t_{2X}$. Therefore, we work with the expression for $\dot{X}_v(s) - \hat{\dot{X}}_v(s)$

$$\dot{X}_v(s) - \hat{\dot{X}}_v(s) = \frac{T_{\ddot{X}} \ddot{X}_{Fmax}}{T_X s^2 (1 + T_{\ddot{X}} s)} + \frac{T_{\ddot{X}} \ddot{X}_{vF1}}{s(1 + T_{\ddot{X}} s)} + \frac{g_m \zeta}{s^2} - \frac{\tilde{\ddot{x}}_b}{s^2} + \frac{\dot{X}_{v1}}{s} - \frac{\hat{\dot{X}}_{v1}}{s} \tag{9-3}$$

For sufficiently large values of $t_{2X} - t_1$, transients in the response of $\dot{X}_v(t) - \hat{\dot{X}}_v(t)$ to the various inputs are damped out and the value of $\dot{X}_{v2} - \hat{\dot{X}}_{v2}$ is accurately approximated by:*

$$\dot{X}_{v2} - \hat{\dot{X}}_{v2} = -(\tilde{\ddot{x}}_b - g_m \zeta)(t_{2X} - t_1) + \frac{T_{\ddot{X}} \ddot{X}_{Fmax} (t_{2X} - t_1)}{T_X} - \frac{T_{\ddot{X}}^2 \ddot{X}_{Fmax}}{T_X}$$

$$+ T_{\ddot{X}} \ddot{X}_{vF1} + \dot{X}_{v1} - \hat{\dot{X}}_{v1} + T_{\ddot{X}} \tilde{\ddot{x}}_b \tag{9-4}$$

We shall return to this result later.

For t greater than t_{2X}, but less than t_I (impact time) the X_v channel operates in the linear region and the system model is shown in figure 2-20a. The output $\dot{X}_v$ is the actual velocity in the X_v direction while the input $g_m \zeta$ results from misalignment of the X_v, Y_v, Z_v axes to the true local vertical coordinate frame X, Y, Z.

All the inputs are considered to be step functions applied at $t = t_{2X}$, the time that the control system enters the region of linear operation. The inputs, as functions of the Laplace variable s are:

$$\dot{X}_D(s) = \frac{\dot{X}_D}{s}; \quad \text{nominally } \dot{X}_D = 0$$

---

* The damping factor is $\exp(-t/T_{\ddot{X}})$. Typically, $T_{\ddot{X}}$ the acceleration sensor time constant is on the order of 0.01 second so that transients will be damped in a fraction of a second.

$$\ddot{X}_{vF2}(s) = \frac{\ddot{X}_{vF2}}{s}\ ;\ \text{Generally } \ddot{X}_{vF2} \text{ is equal to } \ddot{X}_{F_{max}}$$

$$g_m(s)\,\zeta(s) = \frac{g_m \zeta}{s}$$

$$\tilde{\ddot{x}}_b(s) = \frac{\tilde{\ddot{x}}_b}{s}$$

$$\dot{X}_{v2}(s) = \frac{\dot{X}_{v2}}{s}$$

$$\hat{\dot{X}}_{v2}(s) = \frac{\hat{\dot{X}}_{v2}}{s} = -\frac{\ddot{X}_{F_{max}}}{sK_{\dot{X}}} \quad *$$

Using the block diagram in figure 2-20a as the model, the following transfer function is found to relate $\dot{X}_v$ to the inputs described above.

$$\dot{X}_v(s) = \frac{g_m \zeta}{s^2} + \frac{\dot{X}_{v2}}{s} - \frac{\tilde{\ddot{x}}_b}{s^2} + \frac{\tilde{\ddot{x}}_b}{K_{\dot{X}} s} - \frac{\tilde{\ddot{x}}_b}{s\left[T_X s^2 (1 + T_{\ddot{X}} s) + s + K_{\dot{X}}\right]}$$

$$+ \frac{K_{\dot{X}}(1 + T_{\ddot{X}} s)\dot{X}_D + T_X s(1 + T_{\ddot{X}} s)\ddot{X}_{vF2} - K_{\dot{X}}(1 + T_{\ddot{X}} s)\hat{\dot{X}}_{v2}}{s\left[T_X s^2 (1 + T_{\ddot{X}} s) + s + K_{\dot{X}}\right]}$$

$$- \frac{\left\{T_X T_{\ddot{X}} s^2 + \left[T_X - K_{\dot{X}} T_X T_{\ddot{X}}\right] s + \left[1 - K_{\dot{X}} T_X\right]\right\}\tilde{\ddot{x}}_b}{K_{\dot{X}}\left[T_X s^2 (1 + T_{\ddot{X}} s) + S + K_{\dot{X}}\right]} \qquad (9\text{-}5)$$

To estimate the value of $\dot{X}_{vI}$, (the X_v component of velocity at the time of impact) it is assumed that the time interval $(t_I - t_{2X})$ is sufficiently long such that the control system reaches a steady state condition. For the values of

---

* By definition, at time t_{2X}

$$K_{\dot{X}}\left[\dot{X}_D - \hat{\dot{X}}_{v2}\right] = \ddot{X}_{F_{max}}$$

where $\dot{X}_D$ is zero

T_X, and $T_{\dot{X}}$ which are assumed to be typical in paragraph 2.1.5, the operating time required in the linear region to justify this assumption is on the order of 10 seconds or less. It does not seem unreasonable to expect values of $(t_I - t_{2X})$ of this magnitude. In fact, the nominal velocities and the maximum allowable velocity deviations at the end of the main braking phase can be selected to ensure that this criterion is satisfied. Given this assumption, the value of $\dot{X}_v$ at impact can be estimated from equation 9-5 by using a mixture of inverse Laplace transforms and the final value theorem for estimating steady state response*. Thus,

$$\dot{X}_{vI} \doteq g_m \zeta (t_I - t_{2X}) - \dot{\tilde{x}}_b (t_I - t_{2X}) + \dot{X}_{v2} + \frac{\dot{\tilde{x}}_b}{K_{\dot{X}}}$$

$$+ \lim_{s \to o} \left\{ \frac{K_{\dot{X}} (1 + T_{\dot{X}} s) \dot{X}_D + T_X s (1 + T_{\dot{X}} s) \dot{X}_{vF2} - K_{\dot{X}} (1 + T_{\dot{X}} s) \hat{\dot{X}}_{v2}}{\left[T_X s^2 (1 + T_{\dot{X}} s) + s + K_{\dot{X}} \right]} \right\}$$

$$- \lim_{s \to o} \left\{ \frac{\left[T_X T_{\dot{X}} s^2 + (T_X - K_{\dot{X}} T_X T_{\dot{X}}) s + (1 - K_{\dot{X}} T_X) \right] s \dot{\tilde{x}}_b}{K_{\dot{X}} \left[T_X s^2 (1 + T_{\dot{X}} s) + s + K_{\dot{X}} \right]} \right\}$$

$$- \lim_{s \to o} \left\{ \frac{\dot{\tilde{x}}_b}{\left[T_X s^2 (1 + T_{\dot{X}} s) + s + K_{\dot{X}} \right]} \right\} \qquad (9\text{-}6)$$

This yields

$$\dot{X}_{vI} \doteq -(\dot{\tilde{x}}_b - g_m \zeta) (t_I - t_{2X}) + \dot{X}_{v2} - \hat{\dot{X}}_{v2} + \dot{X}_D \qquad (9\text{-}7)$$

Substituting equation 9-4 for $\dot{X}_{v2} - \hat{\dot{X}}_{v2}$ yields

*The final value theorem states

$$\lim_{t \to \infty} g(t) = \lim_{s \to o} sG(s)$$

$$\dot{X}_{vI} - \dot{X}_D \doteq -(\tilde{\ddot{x}}_b - g_m\zeta)(t_I - t_1) - \tilde{\dot{x}}_1 + \frac{T_{\ddot{X}}\,\ddot{X}_{F_{max}}(t_{2X} - t_1)}{T_X} - \frac{T_{\ddot{X}}^2\,\ddot{X}_{F_{max}}}{T_X} + T_{\ddot{X}}(\ddot{X}_{vF1} + \tilde{\ddot{x}}_b) \tag{9-8}$$

Where

$$\tilde{\dot{x}}_1 = \hat{\dot{X}}_{v1} - \dot{X}_{v1} \tag{9-9}$$

and $\dot{X}_D$ has been subtracted from both sides so that the expression yields an estimate of the deviation of actual impact velocity from desired impact velocity. This completes the derivation of the expression to be used to estimate the actual X_v component of impact velocity.

By similar analysis expressions are derived fro the Y_v and Z_v components of impact velocity:

$$\dot{Y}_{vI} - \dot{Y}_D \doteq -\tilde{\ddot{y}}_b(t_I - t_1) - \tilde{\dot{y}}_1 + \frac{T_{\ddot{Y}}\,\ddot{Y}_{F_{max}}(t_{2Y} - t_1)}{T_Y} - \frac{T_{\ddot{Y}}^2\,\ddot{Y}_{F_{max}}}{T_Y} + T_{\ddot{Y}}(\ddot{Y}_{vF1} + \tilde{\ddot{y}}_b) \tag{9-10}$$

$$\dot{Z}_{vI} - \dot{Z}_D \doteq -\tilde{\ddot{z}}_b(t_I - t_1) - \tilde{\dot{z}}_1 + \frac{T_{\ddot{Z}}\,\ddot{Z}_{F_{max}}(t_{2Z} - t_1)}{T_Z} - \frac{T_{\ddot{Z}}^2\,\ddot{Z}_{F_{max}}}{T_Z} + T_{\ddot{Z}}(\ddot{Z}_{vF1} + g_m + \tilde{\ddot{z}}_b) \tag{9-11}$$

9.2 DETERMINATION OF ALLOWABLE DEVIATIONS FROM NOMINAL AT MAIN BRAKING TERMINATION

To establish criteria which can be used to indicate sensor requirements, limits on the allowable state deviations from nominal at the end of main braking are obtained. Engine limitations and a simplified final touchdown profile provide the basis for determining these limits. In addition, it is

assumed that the final touchdown profile is completed without additional error.

The simplified final touchdown profile is:*

- At $t = t_f$ (time of final touchdown initiation)

  The vertical acceleration required to make $\dot{Z}$ equal to $\dot{Z}_D$ at the time (t_s) when $Z = Z_s$ (some standoff altitude) is computed and implemented.
- For $t > t_s$ thrust acceleration along Z balances gravity and the vehicle moves with constant velocity ($\dot{Z}_D$) until impact.
- Throughout final touchdown, the horizontal guidance logic is simply to null horizontal velocity components. The engine and vehicle limitations that are considered are:

  Maximum thrust: 133,400 N

  Vehicle mass: 19,000 kg (constant)

  Maximum thrust angle** (from local vertical)

  $t_f < t < t_s$ $\quad \Theta_{max} = \Phi_{max} = 15$ degrees

  $t_s < t < t_I$ $\quad \Theta_{max} = \Phi_{max} = 10$ degrees

The equations of motion (9-12 and 9-13) can be solved to give $\ddot{Z}_{Fs}$ (required Z component of thrust acceleration) and t_s in terms of $\dot{Z}_f$, Z_f, g_m, and $\dot{Z}_D$.

$$\dot{Z}_D = \dot{Z}_s = \dot{Z}_f + \ddot{Z}\,(t_s - t_f) \tag{9-12}$$

$$Z_s = Z_f + \dot{Z}_f\,(t_s - t_f) + \frac{\ddot{Z}_s\,(t_s - t_f)^2}{2} \tag{9-13}$$

$$\ddot{Z}_s = \ddot{Z}_s + g_m = \frac{\dot{Z}_f^2 - \dot{Z}_D^2}{2\,(Z_f - Z_s)} + g_m \tag{9-14}$$

---

* The coordinate system used is the beacon X, Y, Z system used in paragraph 2.1.5.

** The allowed thrust angle is reduced during the part of the profile immediately preceding impact because of a restriction on impact attitude given as a study input.

$$t_s - t_f = \frac{-2\,(Z_f - Z_s)}{\dot{Z}_f + \dot{Z}_D} \tag{9-15}$$

From t_s to t_I vertical velocity is constant (implying $\ddot{Z}_F = g_m$) so that the length of the time interval is given by

$$t_I - t_s = -\frac{Z_s}{\dot{Z}_D} \tag{9-16}$$

Substituting

$$(\ddot{Z}_{Fs})_{max} = \frac{133,400}{19,000} = 7.02 \text{ m/sec}^2$$

into equation 9-14 and solving for $\dot{Z}_f^2$ yields an expression for the maximum allowed value of $\dot{Z}_f^2$.

$$(\dot{Z}_f^2)_{max} = 2\,(Z_f - Z_s)\left[(\ddot{Z}_{Fs})_{max} - g_m\right] + (\dot{Z}_D^2)$$

where the negative square root is of most significance since this gives the maximum allowed downward velocity at t_f. The absolute value of the maximum allowed deviation of Z_f from Z_{fn} is then given by the expression:

$$\left|\dot{z}_f\right|_{max} = 3\left(\sigma_{\dot{z}_f}\right)_{max} = \left|(\dot{Z}_f)_{max}\right| - \left|\dot{Z}_{fn}\right| \tag{9-17}$$

Figure 9-1 is a plot of $3\,\sigma_{\dot{z}_f\,max}$ versus Z_s.

The maximum horizontal accelerations are given by the expression:

$$\ddot{Y}_{F\,max} = \ddot{X}_{F\,max} = \begin{cases} \ddot{Z}_{Fs} \sin(15°) & t_f < t < t_s \\ g_m \sin(10°) & t_s < t < t_I \end{cases} \tag{9-18}$$

Thus, the maximum horizontal velocity changes that can occur during final touchdown are given by:

$$\Delta\dot{X}_{max} = \Delta\dot{Y}_{max} = \ddot{Z}_{Fs} \sin(15°)\,(t_s - t_f) + g_m \sin(10°)\,(t_I - t_s) \tag{9-19}$$

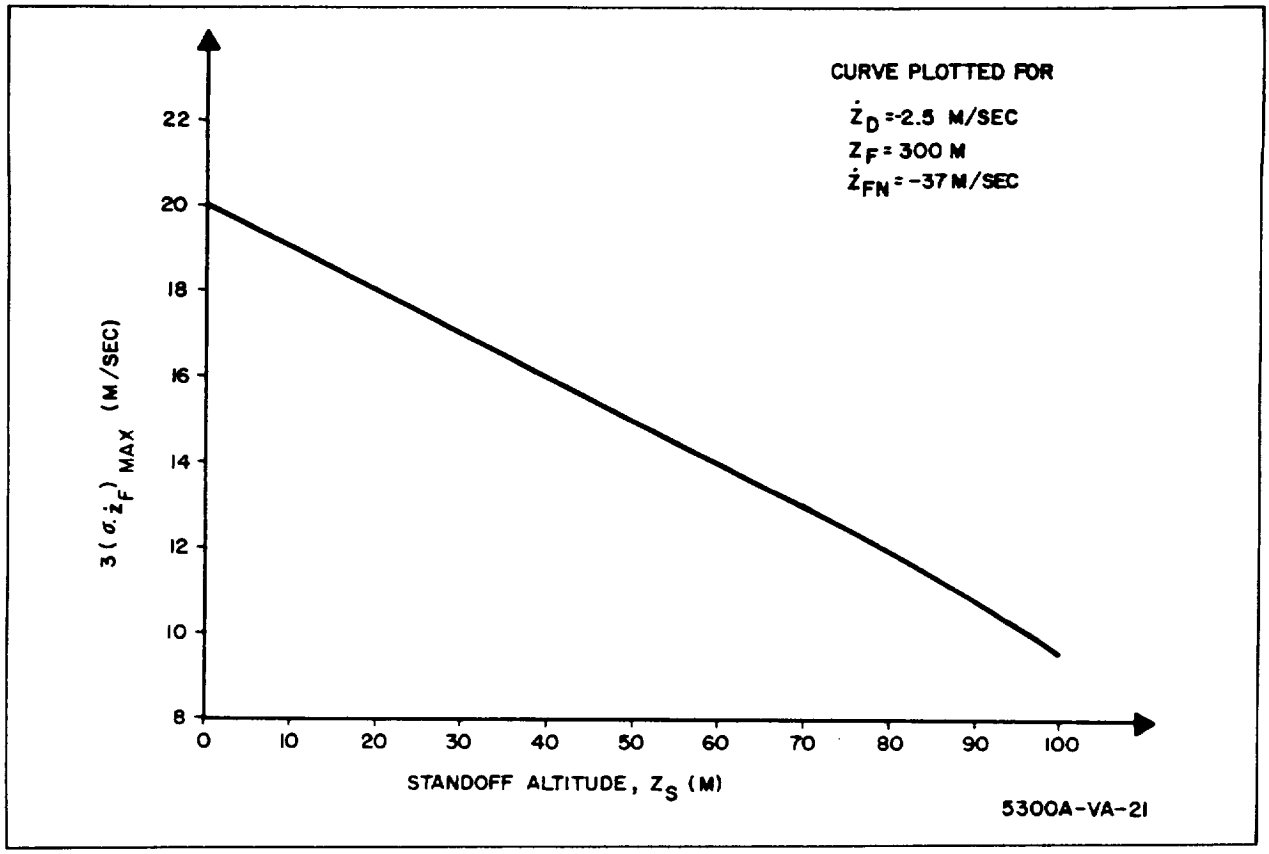

Figure 9-1. Allowable Vertical Velocity Error

If the horizontal velocities at impact are to be zero, the maximum allowed initial horizontal velocities are equal to the maximum velocity change capability given by equation 9-19. Subtracting the magnitude of $\dot{X}_{fn}$ from the magnitude of $(\Delta\dot{X})_{max}$ gives an expression for the magnitude of the maximum allowed initial deviation from nominal.

$$\left|\dot{x}_f\right|_{max} = 3\left(\sigma_{\dot{x}_f}\right)_{max} = \left|\Delta\dot{X}\right|_{max} - \left|\dot{X}_{fn}\right| \qquad (9\text{-}20)$$

Similarly

$$\left|\dot{y}_f\right|_{max} = 3\left(\sigma_{\dot{y}_f}\right)_{max} = \left|\Delta\dot{Y}\right|_{max} - \left|\dot{Y}_{fn}\right| \qquad (9\text{-}21)$$

Quantity $3\left(\sigma_{\dot{x}_f}\right)_{max}$ is plotted versus $\dot{Z}_f$ for various values of Z_s in figure 9-2 with $\dot{Z}_{fn} = -9$ m/sec.*

* Orbital main braking nominal terminal parameter (paragraph 2.1.4.1)

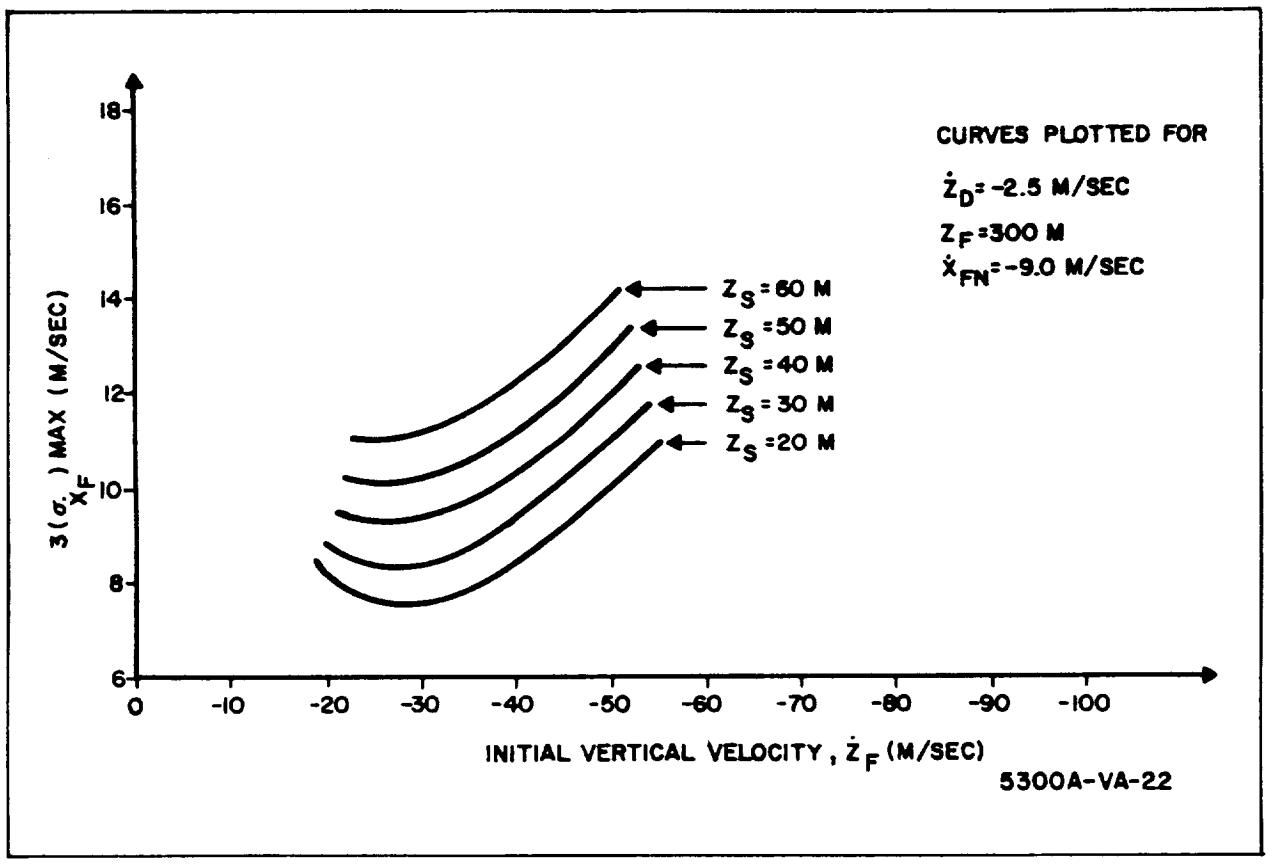

Figure 9-2. Allowable Horizontal Velocity Errors

The value of $3\left(\sigma_{\dot{y}_f}\right)_{max}$ can be obtained from the value of $3\left(\sigma_{\dot{x}_f}\right)_{max}$ by adding 9 m/sec since $\dot{Y}_{fn}$ is zero. The extent of the curves is limited by the maximum and minimum allowed values of $\dot{Z}_f$ determined by $3\left(\sigma_{\dot{z}_f}\right)_{max}$ as a function of Z_s given in figure 9-1.

It can be seen that there is a significant tradeoff between the allowed initial deviations and Z_s. For this study Z_s = 50m has been selected because it seems to offer the most reasonable values of $3\left(\sigma_{\dot{z}_f}\right)_{max}$ and $3\left(\sigma_{\dot{x}_f}\right)_{max}$. The resulting allowable initial velocity deviations are:

$$3\left(\sigma_{\dot{x}_f}\right)_{max} = 10.2 \text{ m/sec}$$

$$3\left(\sigma_{\dot{y}_f}\right)_{max} = 19.2 \text{ m/sec}$$

$$3\left(\sigma_{\dot{z}_f}\right)_{max} = 15 \text{ m/sec}$$

Where the value of $3\left(\sigma_{\dot{x}_f}\right)_{max}$ is the minimum occurring on the $Z_s = 50m$ curve in figure 9-2.

The allowable horizontal position deviation from nominal is not pinned down so easily, especially in the X direction where the nominal velocity at touchdown phase initiation is not zero. This results in the actual impact position being offset from the beacon by more than the 250 meters offset which exists at the end of main braking. This, of course, can be compensated for by altering the main braking profile. For this study we more or less arbitrarily select the allowable 3σ position deviation at the end of main braking to be 120 meters per axis. It is felt that this allows sufficient leeway such that the 3σ error requirement at the impact (essentially 250 meters per axis) can be satisfied without explicit position control during the final touchdown phase.

Summarizing, the 3σ error allowances at the end of main braking (start of final touchdown) are:

$$3\left(\sigma_{x_f}\right)_{max} = 3\left(\sigma_{y_f}\right)_{max} = 120 \text{ m}$$

$$3\left(\sigma_{\dot{x}_f}\right)_{max} = 10.2 \text{ m/sec}$$

$$3\left(\sigma_{\dot{y}_f}\right)_{max} = 19.2 \text{ m/sec}$$

$$3\left(\sigma_{\dot{z}_f}\right)_{max} = 15 \text{ m/sec}$$

10. MISSION INTEGRATION APPENDIX

10.1 EFFECT OF USING ANGLE ESTIMATION TO INITIATE MAIN BRAKING MANEUVER

The objective is to estimate the relationship between $\underline{p}_3'$, the vector of deviations from nominal at the actual time of main braking initiation and $\hat{\underline{p}}_3$, the vector of deviations from nominal at the nominal time of main braking initiation.

The vector of in-plane deviations from the nominal point of main braking initiations at the nominal time of main braking initiation is $\underline{p}_3$ *

$$\underline{p}_3^T = \left[x_3,\ z_3,\ \dot{x}_3,\ \dot{z}_3\right] \tag{10-1}$$

Actual main braking initiation is postulated at the time when the estimated central angle displacement from the landing site is equal to the nominal central angle displacement. This is equivalent to initiating when the estimated value of X_3 is zero. This estimate of central angle is obtainable from beacon tracker measurements referenced to the onboard inertial reference which is aligned to local vertical.

The difference between the nominal time of main braking initiation t_{3n}, and the actual time, t_3 can be estimated (to first order) as the time it takes for the vehicle to travel a distance x_3 at the nominal value of $\dot{X}_3$ which is denoted $\dot{X}_{3n}$.

$$x_3 + \dot{X}_{3n}\,\Delta t = 0 \tag{10-2}$$

where

$$\Delta t \equiv t_3 - t_{3n} \tag{10-3}$$

---

* Coordinate systems used in this section are those defined in paragraph 2.1.3.

Thus,

$$\Delta t \doteq \frac{-x_3}{\dot{X}_{3n}} \tag{10-4}$$

The values of the other components of the deviation from nominal at the actual time of main braking initiation are estimated by the expressions:

$$z'_3 \doteq z_3 + \dot{Z}_3 \Delta t + \ddot{Z}_3 \frac{\Delta t^2}{2} \tag{10-5}$$

$$\dot{x}'_3 \doteq \dot{x}_3 + \ddot{X}_3 \Delta t \tag{10-6}$$

$$\dot{z}'_3 \doteq \dot{z}_3 + \ddot{Z}_3 \Delta t \tag{10-7}$$

While the actual X_3 component of the deviation from nominal is obtained from the fact that the estimated value of X_3 is equal to the nominal value which is zero.

$$0 = \hat{X}_3 = X_{3n} + x'_3 + \tilde{x}_3 \tag{10-8}$$

or

$$x'_3 = -\tilde{x}_3 \tag{10-9}$$

Using the relationships,

$$\dot{Z}_3 = \dot{Z}_{3n} + \dot{z}_3 \tag{10-10}$$

$$\ddot{Z}_3 = \ddot{Z}_{3n} + \ddot{z}_3 \tag{10-11}$$

$$\ddot{X}_3 = \ddot{X}_{3n} + \ddot{x}_3 \tag{10-12}$$

And retaining only the first order terms yields:

$$x'_3 = -\tilde{x}_3 \tag{10-13}$$

$$z'_3 \doteq z_3 - \frac{\dot{Z}_{3n} x_3}{\dot{X}_{3n}} \tag{10-14}$$

$$\dot{x}'_3 \doteq \dot{x}_3 - \frac{\ddot{X}_{3n}}{\dot{X}_{3n}} x_3 \tag{10-15}$$

$$\dot{z}'_3 \doteq \dot{z}_3 - \frac{\ddot{Z}_{3n}}{\dot{X}_{3n}} x_3 \tag{10-16}$$

Thus, in terms of $\underline{p}_3$, $\underline{p}'_3$ is

$$\underline{p}'_3 = \begin{bmatrix} x'_3 \\ z'_3 \\ \dot{x}'_3 \\ \dot{z}'_3 \end{bmatrix} \doteq \begin{bmatrix} 0 & 0 & 0 & 0 \\ -\frac{\dot{Z}_{3n}}{\dot{X}_{3n}} & 1 & 0 & 0 \\ -\frac{\ddot{X}_{3n}}{\dot{X}_{3n}} & 0 & 1 & 0 \\ -\frac{\ddot{Z}_{3n}}{\dot{X}_{3n}} & 0 & 0 & 1 \end{bmatrix} \begin{bmatrix} x_3 \\ z_3 \\ \dot{x}_3 \\ \dot{z}_3 \end{bmatrix} - \begin{bmatrix} \tilde{x}_3 \\ 0 \\ 0 \\ 0 \end{bmatrix} \tag{10-17}$$

$$= [A]\,\underline{p}_3 - \underline{\tilde{x}}_3 \tag{10-18}$$

The values of $\ddot{X}_{3n}$ and $\ddot{Z}_{3n}$ are obtained from the expressions (10-19)

$$\ddot{X}_{3n} = 0$$

$$\ddot{Z}_{3n} = -\frac{\mu}{\left(R_m^2\right)_n} = \frac{-4.9 \times 10^{12}}{(1.84 \times 10^6)^2} = -1.45 \text{ m/sec}^2 \tag{10-20}$$

$R_m \equiv$ range to the center of the moon.

Numerically, $\dot{Z}_{3n}$ is (-100) m/sec and $\dot{X}_{3n}$ is (-1600) m/sec so that the numerical evaluation of $[A]$ is

$$A = \begin{bmatrix} 0 & 0 & 0 & 0 \\ -6.25 \times 10^{-2} & 1 & 0 & 0 \\ 0 & 0 & 1 & 0 \\ -9.05 \times 10^{-4} & 0 & 0 & 1 \end{bmatrix} \tag{10-21}$$

The estimation error $\tilde{x}_3$ is expressible in terms of beacon tracker observation errors as *

$$\tilde{x}_3 \doteq -(R_m)_{in}\,\tilde{\theta}_i \doteq (R_m)_{in}\left\{\frac{\sin(\Theta_a)_{in}}{R_o\cos\Theta_{in}}\,\tilde{r}_i + \frac{R_{in}\cos(\Theta_a)_{in}}{R_o\cos\Theta_{in}}\,(\tilde{\theta}_a)_i\right\} \tag{10-22}$$

For

$(R_m)_{in} = 1.84 \times 10^6$ = range to lunar center

$R_o = 1.738 \times 10^6$ m

$(\Theta_a)_{in} = -67.8$ deg

$\Theta_{in} = 10.6$ degrees

$R_{in} = 3.47 \times 10^5$ m = nominal initial range to beacon

We get

$$\tilde{x}_3 = 0.995\,\tilde{r}_i - 1.41 \times 10^5\,(\tilde{\theta}_a)_i \text{ m}$$

Then the vector $\underline{\tilde{x}}_3$ can be expressed in terms of the vector $\underline{\tilde{q}}_i$ where

$$\underline{\tilde{q}}_i \equiv \begin{bmatrix} \tilde{r}_i \\ (\tilde{\theta}_a)_i \end{bmatrix} \tag{10-23}$$

$$\underline{\tilde{x}}_3 = [B]\underline{\tilde{q}}_i = \begin{bmatrix} 0.995 & -1.41\times10^5 \\ 0 & 0 \\ 0 & 0 \\ 0 & 0 \end{bmatrix} \begin{bmatrix} \tilde{r}_i \\ (\tilde{\theta}_a)_i \end{bmatrix} \tag{10-24}$$

---

* Subscript i indicates quantities evaluated at the point of main braking initiation. Also, angles Θ and Θ_a are illustrated in figure 2-14.

The final expression is then

$$\underline{p}_3' = [A]\,\underline{p}_3 - [B]\,\underline{\tilde{q}}_i \qquad (10\text{-}25)$$

10.2 CONSIDERATION OF CORRELATION BETWEEN STATE DEVIATIONS AND STATE ESTIMATION ERRORS AT MIDCOURSE TERMINATION

In performing the integration of the various mission phases, and deriving an expression for the total covariance matrix of deviations from the nominal point at the end of main braking, it is assumed that no correlations exist between the vector of deviations from nominal at the end of midcourse, $\underline{p}_o$; and the vector of estimation errors at the end of midcourse $\underline{\tilde{p}}_o$. Symbolically it has been assumed that:

$$E\left[\underline{p}_o\,\underline{\tilde{p}}_o^T\right] = [0] = 4 \times 4 \text{ null matrix}$$

In practice, this is not actually true, especially in the case where no navigation is performed subsequent to the second midcourse correction.

This investigation looks at the effects of two likely types of correlation between $\underline{p}_o$ and $\underline{\tilde{p}}_o$ on the contributions to the total error at the end of main braking caused by these sources. The two types of correlation considered are:

a. Case 1: Negative position correlation

b. Case 2: Complete negative correlation

In the following paragraphs, each case is defined; expressions are derived giving the total contribution to $\left[P_f\right]$ caused by $\underline{p}_o$ and $\underline{\tilde{p}}_o$; and a numerical evaluation is performed using input values of $\left[P_o\right]$ and $\left[\tilde{P}_o\right]$ obtained from investigation of the midcourse phase (paragraph 2.1.1) for the following midcourse phase profile:

- Second midcourse correction at 50 hours
- Nominal DSIF errors
- Nominal correction accuracy (0.1 m/sec 1σ)
- No navigation after second midcourse correction.

The results obtained when correlations are taken into account are to be compared with the results presented in paragraph 10.3 where no correlation has been assumed. This result is:

$$\left[P_{fo}\right] \equiv \left[P_{fp_o}\right] + \left[P_{f\tilde{p}_o}\right] = \begin{bmatrix} 5.72\times10^{2} & 0 & -6.79\times10^{1} & 7.07\times10^{1} \\ 0 & 0 & 0 & 0 \\ -6.79\times10^{1} & 0 & 8.00\times10^{0} & -8.36\times10^{0} \\ 7.07\times10^{1} & 0 & -8.36\times10^{0} & 8.74\times10^{0} \end{bmatrix} \tag{10-26}$$

10.2.1 Analysis of Case 1: Negative Position Correlation

The deviation vector $\underline{p}_o$ and the estimation error vector $\underline{\tilde{p}}_o$ in expanded form are:

$$\underline{p}_o^T = \left[x_o,\ y_o,\ \dot{x}_o,\ \dot{y}_o\right] \tag{10-27}$$

$$\underline{p}_o^T = \left[\tilde{x}_o,\ \tilde{y}_o,\ \tilde{\dot{x}}_o,\ \tilde{\dot{y}}_o\right] \tag{10-28}$$

Negative position correlation is defined to mean:

$$x_o = -\tilde{x}_o \tag{10-29}$$

$$y_o = -\tilde{y}_o \tag{10-30}$$

This type of correlation occurs if the best estimate of position at the nominal time of injection maneuver initiation is that it will be the nominal position. With regard to the velocity components, complete independence is assumed for this case; i.e.,

$$E\left\{\dot{x}_o\,\tilde{\dot{x}}_o\right\} = E\left\{\dot{x}_o\,\tilde{\dot{y}}_o\right\} = E\left\{\dot{y}_o\,\tilde{\dot{x}}_o\right\} = E\left\{\dot{y}_o\,\tilde{\dot{y}}_o\right\} = 0 \tag{10-31}$$

From paragraph 2.1.6 the following expression is still applicable:

$$\underline{p}_{f_o} \equiv \underline{p}_{fp_o} + \underline{p}_{f\tilde{p}_o} = \left[S_{p_f p_o}\right] \underline{p}_o + \left[S_{p_f \tilde{p}_o}\right] \underline{\tilde{p}}_o \tag{10-32}$$

Substituting the assumed correlations yields

$$\underline{p}_{f_o} = \underline{p}_{fp_o} + p_{f\tilde{p}_o} = \left[S_{p_f p_o}\right] \begin{bmatrix} x_o \\ y_o \\ \dot{x}_o \\ \dot{y}_o \end{bmatrix} + \left[S_{p_f \tilde{p}_o}\right] \begin{bmatrix} -\tilde{x}_o \\ -y_o \\ \dot{\tilde{x}}_o \\ \dot{\tilde{y}}_o \end{bmatrix} \tag{10-33}$$

$$\underline{p}_{f_o} = \left\{ \left[S_{p_f p_o}\right] + \left[S_{p_f \tilde{p}_o}\right]\left[K_1\right] \begin{bmatrix} x_o \\ y_o \\ \dot{x}_o \\ \dot{y}_o \end{bmatrix} + \left[S_{p_f \tilde{p}_o}\right]\left[K_2\right] \begin{bmatrix} \tilde{x}_o \\ \tilde{y}_o \\ \dot{\tilde{x}}_o \\ \dot{\tilde{y}}_o \end{bmatrix} \right. \tag{10-34}$$

$$= \left[S'_{p_f p_o}\right] \underline{p}_o + \left[S'_{p_f \tilde{p}_o}\right] \tilde{\underline{p}}_o \tag{10-35}$$

where

$$\left[K_1\right] \equiv \begin{bmatrix} -1 & 0 & 0 & 0 \\ 0 & -1 & 0 & 0 \\ 0 & 0 & 0 & 0 \\ 0 & 0 & 0 & 0 \end{bmatrix} \tag{10-36}$$

$$\left[K_2\right] \equiv \begin{bmatrix} 0 & 0 & 0 & 0 \\ 0 & 0 & 0 & 0 \\ 0 & 0 & 1 & 0 \\ 0 & 0 & 0 & 1 \end{bmatrix} \tag{10-37}$$

Then, the covariance matrix of $\underline{p}_{f_o}$ is $\left[P_{f_o}\right]$:

$$\left[P_{f_o}\right] \equiv E\left[\underline{p}_{f_o}\ \underline{p}_{f_o}^T\right] = \left[S'_{p_f p_o}\right]\left[P_o\right]\left[S'_{p_f p_o}\right]^T + \left[S_{p_f p_o}\right]\left[\tilde{P}_o\right]\left[S'_{p_f \tilde{p}_o}\right]^T$$

$$+ \left[S'_{p_f p_o}\right]\left\{E\left[\underline{p}_o \tilde{\underline{p}}_o^{\,T}\right]\right\}\left[S'_{p_f \tilde{p}_o}\right]^T \qquad (10\text{-}38)$$

$$+ \left[S'_{p_f \tilde{p}_o}\right]\left\{E\left[\tilde{\underline{p}}_o \underline{p}_o^{\,T}\right]\right\}\left[S'_{p_f p_o}\right]^T$$

Matrices

$$\left[P_o\right] \equiv E\left[\underline{p}_o \underline{p}_o^{\,T}\right]$$
$$\left[\tilde{P}_o\right] \equiv E\left[\tilde{\underline{p}}_o \tilde{\underline{p}}_o^{\,T}\right] \qquad (10\text{-}39)$$

are obtained as results of the midcourse phase analyses. Expanding yields

$$E\left[\underline{p}_o \tilde{\underline{p}}_o^{\,T}\right] = E\left\{\begin{bmatrix} x_o\tilde{x}_o & x_o\tilde{y}_o & x_o\dot{\tilde{x}}_o & x_o\dot{\tilde{y}}_o \\ y_o\tilde{x}_o & y_o\tilde{y}_o & y_o\dot{\tilde{x}}_o & y_o\dot{\tilde{y}}_o \\ \dot{x}_o\tilde{x}_o & \dot{x}_o\tilde{y}_o & \dot{x}_o\dot{\tilde{x}}_o & \dot{x}_o\dot{\tilde{y}}_o \\ \dot{y}_o\tilde{x}_o & \dot{y}_o\tilde{y}_o & \dot{y}_o\dot{\tilde{x}}_o & \dot{y}_o\dot{\tilde{y}}_o \end{bmatrix}\right\} \qquad (10\text{-}40)$$

Substituting

$$x_o = -\tilde{x}_o \qquad (10\text{-}41)$$

$$y_o = -\tilde{y}_o \qquad (10\text{-}42)$$

yields

$$E\left[\underline{p}_o \tilde{\underline{p}}_o^{\,T}\right] = E\left\{\begin{bmatrix} x_o x_o & x_o y_o & \tilde{x}_o\dot{\tilde{x}}_o & \tilde{x}_o\dot{\tilde{y}}_o \\ y_o x_o & y_o y_o & \tilde{y}_o\dot{\tilde{x}}_o & \tilde{y}_o\dot{\tilde{y}}_o \\ \dot{x}_o x_o & \dot{x}_o y_o & \dot{x}_o\dot{\tilde{x}}_o & \dot{x}_o\dot{\tilde{y}}_o \\ \dot{y}_o x_o & \dot{y}_o y_o & \dot{y}_o\dot{\tilde{x}}_o & \dot{y}_o\dot{\tilde{y}}_o \end{bmatrix}\right\} \qquad (10\text{-}43)$$

It is seen that the terms contained in $E\left[\underline{p}_o \tilde{\underline{p}}_o^{\,T}\right]$ are negatives of terms taken from matrices $\left[P_o\right]$ and $\left[\tilde{P}_o\right]$. Hence, these terms are known.

Then, it is noted that

$$E\left[\tilde{\underline{p}}_o \underline{p}_o^T\right] = E\left[\underline{p}_o \tilde{\underline{p}}_o^T\right]^T \tag{10-44}$$

Thus, all the information required to evaluate $\left[P_{f_o}\right]$ is available.

Numerical evaluation for the selected sample case yields

$$\left[P_{f_o}\right] = \begin{bmatrix} 3.4\times10^{2} & 0 & -3.8\times10^{1} & 4.0\times10^{1} \\ 0 & 0 & 0 & 0 \\ -3.8\times10^{1} & 0 & 4.6\times10^{0} & -4.7\times10^{0} \\ 4.0\times10^{1} & 0 & -4.7\times10^{0} & 5.0\times10^{0} \end{bmatrix} \tag{10-45}$$

10.2.2 Case 2: Complete Negative Correlations

By complete negative correlations it is meant

$$\underline{p}_o = -\tilde{\underline{p}}_o \tag{10-46}$$

which occurs if the estimated state at injection maneuver initiation is equal to the nominal state.

Then

$$\underline{p}_{f_o} \equiv \underline{p}_{f p_o} + \underline{p}_{f \tilde{p}_o} = \left[S_{p_f p_o}\right]\underline{p}_o + \left[S_{p_f \tilde{p}_o}\right]\tilde{\underline{p}}_o \tag{10-47}$$

$$= \left\{\left[S_{p_f p_o}\right] - \left[S_{p_f \tilde{p}_o}\right]\right\}\underline{p}_o \tag{10-48}$$

$$= \left[S''_{p_f p_o}\right]\underline{p}_o \tag{10-49}$$

and

$$\left[P_{f_o}\right] = \left[S''_{p_f p_o}\right]\left[P_o\right]\left[S''_{p_f p_o}\right]^T \tag{10-50}$$

Matrix $\left[P_o\right]$ is available from the midcourse analysis. For the particular sample case chosen, the numerical evaluation of $\left[P_{f_o}\right]$ is

$$\left[P_{f_o}\right] = \begin{bmatrix} 2.00 \times 10^{2} & 0 & -2.37 \times 10^{1} & 2.47 \times 10^{1} \\ 0 & 0 & 0 & 0 \\ -2.37 \times 10^{1} & 0 & 2.80 \times 10^{0} & -2.92 \times 10^{0} \\ 2.47 \times 10^{1} & 0 & -2.92 \times 10^{0} & 3.04 \times 10^{0} \end{bmatrix} \quad (10\text{-}51)$$

Table 10-1 compares the three cases considered; no correlation, negative position correlation, and complete negative correlation.

TABLE 10-1

COMPARISON OF RMS CONTRIBUTIONS TO $\underline{p}_f$ FOR THREE LEVELS OF CORRELATION BETWEEN $\underline{p}_o$ AND $\tilde{\underline{p}}_o$

Case	RMS Contribution to:		
	σ_{x_f} (m)	$\sigma_{\dot{x}_f}$ (m/s)	$\sigma_{\dot{z}_f}$ (m/s)
No Correlation	24.0	2.83	2.96
Negative Position Correlation	18.5	2.14	2.24
Complete Negative Correlation	14.1	1.67	1.74

It can be seen that the effects of the type of negative correlations considered is to reduce the error caused by deviations and estimation errors at the end of midcourse. In general, whatever correlations exist between deviations and estimation errors are expected to be negative, with the actual situation lying somewhere between the negative position correlation case and complete negative correlation when no navigation is done after the second midcourse correction. When navigation is performed, the true situation is expected to be essentially the no correlation case.

Since good information is not available describing the true nature of correlations between deviations and estimation errors at the end of midcourse, independence has been assumed. Thus, results obtained with respect to

mission profiles postulating no navigation after the second midcourse correction are probably pessimistic.

10.3 CONTRIBUTIONS OF ERROR SOURCES TO $[P_f]$

In this paragraph, numerical evaluation of the terms composing $[P_f]$ is performed. For the terms reflecting the performance of the midcourse navigation and guidance system, contributions resulting from several navigation and guidance concept are evaluated. For the other contributing terms, sample error levels are assumed for the purpose of defining an input covariance matrix and the resulting contribution to $[P_f]$ evaluated. The numerical results obtained here are used as a starting point for defining navigation and guidance requirements.

10.3.1 Contribution Due To Actual Deviations From Nominal $[P_o]$

Only two different midcourse guidance concepts are considered. One postulates second midcourse correction 50 hours after injection into the earth-moon transfer orbit, while the second approach makes this correction after 66 hours. In both approaches, DSIF navigation is assumed at least up until the time of second midcourse correction. Based on assumed error covariance matrices at the time of second midcourse correction, the resulting covariance matrices of the actual deviations from nominal time of midcourse periselenum are given below.* These are taken from results given in paragraph 2.1.1.4, but it should be noted that the length unit has been changed from kilometers to meters resulting in a factor of 10^6 difference between the following matrices and those in paragraph 2.1.1.4 and paragraph 5.2.

---

* All covariance matrices $[P_o]$ and $[\tilde{P}_o]$ used in paragraph 10.3 are two dimensional, retaining only the in-plane elements of the 3-dimensional (6 x 6) matrices given in paragraph 2.1.1.4.

a. Second midcourse correction at 50 hours. Nominal DSIF accuracy (Run 126)

$$[P_o] = \begin{bmatrix} 2.39 \times 10^{7} & -1.64 \times 10^{7} & 1.46 \times 10^{4} & -1.28 \times 10^{4} \\ -1.64 \times 10^{7} & 1.10 \times 10^{8} & -6.26 \times 10^{4} & 8.97 \times 10^{3} \\ 1.46 \times 10^{4} & -6.26 \times 10^{4} & 3.91 \times 10^{1} & -7.48 \times 10^{0} \\ -1.28 \times 10^{4} & 8.97 \times 10^{3} & -7.48 \times 10^{0} & 6.92 \times 10^{0} \end{bmatrix}$$

b. Second midcourse correction at 50 hours. Degraded DSIF accuracy (Run 135)

$$[P_o] = \begin{bmatrix} 2.55 \times 10^{8} & -5.00 \times 10^{8} & 3.26 \times 10^{5} & -1.36 \times 10^{5} \\ -5.00 \times 10^{8} & 3.17 \times 10^{9} & -1.81 \times 10^{6} & 2.69 \times 10^{5} \\ 3.26 \times 10^{5} & -1.81 \times 10^{6} & 1.15 \times 10^{3} & -1.55 \times 10^{2} \\ -1.36 \times 10^{5} & 2.69 \times 10^{5} & -1.55 \times 10^{2} & 8.44 \times 10^{1} \end{bmatrix}$$

c. Second midcourse correction at 66 hours. Nominal DSIF accuracy (Run 108)

$$[P_o] = \begin{bmatrix} 5.64 \times 10^{6} & -4.37 \times 10^{6} & 3.79 \times 10^{3} & -2.99 \times 10^{3} \\ -4.37 \times 10^{6} & 2.08 \times 10^{7} & -1.21 \times 10^{4} & 2.40 \times 10^{3} \\ 3.79 \times 10^{3} & -1.21 \times 10^{4} & 2.93 \times 10^{1} & 3.00 \times 10^{0} \\ -2.99 \times 10^{3} & 2.40 \times 10^{3} & 3.00 \times 10^{0} & 3.42 \times 10^{0} \end{bmatrix}$$

d. Second midcourse correction at 66 hours. Degraded DSIF accuracy (Run 146)

$$[P_o] = \begin{bmatrix} 2.30 \times 10^{8} & -4.38 \times 10^{8} & 2.87 \times 10^{5} & -1.23 \times 10^{5} \\ -4.38 \times 10^{8} & 2.22 \times 10^{9} & -1.29 \times 10^{6} & 2.35 \times 10^{5} \\ 2.87 \times 10^{5} & -1.29 \times 10^{6} & 1.81 \times 10^{3} & 1.20 \times 10^{2} \\ -1.23 \times 10^{5} & 2.35 \times 10^{5} & 1.20 \times 10^{2} & 2.49 \times 10^{2} \end{bmatrix}$$

The resulting contributions to $[P_f]$ are obtained by evaluating the expression

$$[P_{f_{P_o}}] = [S_{P_f P_o}] [P_o] [S_{P_f P_o}]^T$$

for each of the input matrices.

a. • Second midcourse correction at 50 hours

• Nominal DSIF accuracy

$$\left[P_{fp_o}\right] = \begin{bmatrix} 8.24 \times 10^{1} & 0 & -9.78 \times 10^{0} & 1.02 \times 10^{1} \\ 0 & 0 & 0 & 0 \\ -9.78 \times 10^{0} & 0 & 1.16 \times 10^{0} & -1.21 \times 10^{0} \\ 1.02 \times 10^{1} & 0 & -1.21 \times 10^{0} & 1.26 \times 10^{0} \end{bmatrix}$$

b. • Second midcourse correction at 50 hours

• Degraded DSIF accuracy

$$\begin{bmatrix} 2.36 \times 10^{3} & 0 & -2.79 \times 10^{2} & 2.91 \times 10^{2} \\ 0 & 0 & 0 & 0 \\ -2.79 \times 10^{2} & 0 & 3.29 \times 10^{1} & -3.43 \times 10^{1} \\ 2.91 \times 10^{2} & 0 & -3.43 \times 10^{1} & 3.58 \times 10^{1} \end{bmatrix}$$

c. • Second midcourse correction at 66 hours

• Nominal DSIF accuracy

$$\left[P_{fp_o}\right] = \begin{bmatrix} 1.55 \times 10^{1} & 0 & -1.83 \times 10^{0} & 1.91 \times 10^{0} \\ 0 & 0 & 0 & 0 \\ -1.83 \times 10^{0} & 0 & 2.17 \times 10^{-1} & -2.26 \times 10^{-1} \\ 1.91 \times 10^{0} & 0 & -2.26 \times 10^{-1} & 2.36 \times 10^{-1} \end{bmatrix}$$

d. • Second midcourse correction at 66 hours

• Degraded DSIF accuracy

$$\left[P_{fp_o}\right] = \begin{bmatrix} 1.65 \times 10^{3} & 0 & -1.95 \times 10^{2} & 2.04 \times 10^{2} \\ 0 & 0 & 0 & 0 \\ -1.95 \times 10^{2} & 0 & 2.31 \times 10^{1} & -2.41 \times 10^{1} \\ 2.04 \times 10^{2} & 0 & -2.40 \times 10^{1} & 2.51 \times 10^{1} \end{bmatrix}$$

The resulting mean squared contributions to the deviations from nominal at the end of main braking are summarized in table 10-2.

TABLE 10-2

MEAN SQUARED ERRORS AT MAIN BRAKING TERMINATION CAUSED BY DEVIATIONS FROM NOMINAL AT MIDCOURSE TERMINATION

Midcourse Guidance Scheme	$\sigma^2_{x_f P_o}$ $(m)^2$	$\sigma^2_{\dot{x}_f P_o}$ $(m/sec)^2$	$\sigma^2_{\dot{z}_f P_o}$ $(m/sec)^2$
Second midcourse correction at 50 hours; nominal initial uncertainties	82.4	1.16	1.26
Second midcourse correction at 50 hours; degraded initial uncertainties	2360	32.9	35.8
Second midcourse correction at 66 hours; nominal initial uncertainties	15.5	0.217	0.236
Second midcourse correction at 66 hours; degraded initial uncertainties	1650	23.1	25.1

10.3.2 Contributions Due to State Estimation Errors at Initiation of Injection Maneuver $\left[\tilde{P}_o\right]$

The covariance matrix of estimation errors at midcourse perselenum depends on the time of the second midcourse correction, the accuracy of navigation prior to the second correction, the accuracy of information about the magnitude of the second correction, and the type and accuracy of navigation performed in the interval between the second midcourse correction and injection initiation.

Several combinations of the influencing factors mentioned above have been treated by means of the midcourse phase analysis program. For each combination, the analysis results in a numerical evaluation of the covariance matrix of estimation errors at the nominal time of injection initiation. These results and the contributions they make to the final covariance matrix $\left[P_f\right]$ are summarized below:

a. Concept 1

- Second correction at 50 hours
- Monitoring accuracy 0.1 m/sec (1σ)
- No subsequent navigation
- Nominal DSIF accuracy
- Covariance matrix of estimation errors (Run 126):

$$\left[\tilde{P}_o\right] = \begin{bmatrix} 2.39 \times 10^{7} & -1.64 \times 10^{7} & 1.46 \times 10^{4} & -1.28 \times 10^{4} \\ -1.64 \times 10^{7} & 1.10 \times 10^{8} & -6.26 \times 10^{4} & 8.97 \times 10^{3} \\ 1.46 \times 10^{4} & -6.26 \times 10^{4} & 3.68 \times 10^{1} & -7.91 \times 10^{0} \\ -1.28 \times 10^{4} & 8.97 \times 10^{3} & -7.91 \times 10^{0} & 6.79 \times 10^{0} \end{bmatrix}$$

- Contribution to $\left[P_f\right]$:

$$\left[P_f \tilde{P}_o\right] = \begin{bmatrix} 4.90 \times 10^{2} & 0 & -5.81 \times 10^{1} & 6.05 \times 10^{1} \\ 0 & 0 & 0 & 0 \\ -5.81 \times 10^{1} & 0 & 6.84 \times 10^{0} & -7.15 \times 10^{0} \\ 6.05 \times 10^{1} & 0 & -7.15 \times 10^{0} & 7.48 \times 10^{0} \end{bmatrix}$$

b. Concept 2

- Second correction at 66 hours
- Monitoring accuracy 0.1 m/sec (1σ)
- No subsequent navigation
- Nominal DSIF accuracy
- Covariance matrix of estimation errors (Run 108):

$$\left[\tilde{P}_o\right] = \begin{bmatrix} 5.64 \times 10^{6} & -4.37 \times 10^{6} & 3.79 \times 10^{3} & -2.99 \times 10^{3} \\ -4.37 \times 10^{6} & 2.08 \times 10^{7} & -1.21 \times 10^{4} & 2.40 \times 10^{3} \\ 3.79 \times 10^{3} & -1.21 \times 10^{4} & 7.41 \times 10^{0} & -2.05 \times 10^{0} \\ -2.99 \times 10^{3} & 2.40 \times 10^{3} & -2.05 \times 10^{0} & 1.59 \times 10^{0} \end{bmatrix}$$

- Contribution to $\left[P_f\right]$

$$\left[P_{f\tilde{p}_o}\right] = \begin{bmatrix} 8.79 \times 10^{1} & 0 & -1.04 \times 10^{1} & 1.08 \times 10^{1} \\ 0 & 0 & 0 & 0 \\ -1.04 \times 10^{1} & 0 & 1.23 \times 10^{0} & -1.28 \times 10^{0} \\ 1.08 \times 10^{1} & 0 & -1.28 \times 10^{0} & 1.34 \times 10^{0} \end{bmatrix}$$

c. Concept 3

- Second midcourse correction at 66 hours
- Monitoring accuracy 0.1 m/sec (1σ)
- No subsequent navigation prior to injection
- Degraded DSIF accuracy
- Covariance matrix of estimation errors (Run 146):

$$\left[\tilde{P}_o\right] = \begin{bmatrix} 2.30 \times 10^{8} & -4.38 \times 10^{8} & 2.87 \times 10^{5} & -1.23 \times 10^{5} \\ -4.38 \times 10^{8} & 2.22 \times 10^{9} & -1.29 \times 10^{6} & 2.35 \times 10^{5} \\ 2.87 \times 10^{5} & -1.29 \times 10^{6} & 7.55 \times 10^{2} & -1.54 \times 10^{2} \\ -1.23 \times 10^{5} & 2.35 \times 10^{5} & -1.54 \times 10^{2} & 6.59 \times 10^{1} \end{bmatrix}$$

- Contribution to $[P_f]$

$$[P_{f\tilde{p}_o}] = \begin{bmatrix} 8.12 \times 10^3 & 0 & -9.62 \times 10^2 & 1.01 \times 10^3 \\ 0 & 0 & 0 & 0 \\ -9.62 \times 10^2 & 0 & 1.14 \times 10^2 & -1.19 \times 10^2 \\ 1.01 \times 10^3 & 0 & -1.19 \times 10^2 & 1.25 \times 10^2 \end{bmatrix}$$

d. Concept 4

- Second midcourse correction at 50 hours
- Monitoring accuracy 0.1 m/sec (1σ)
- Degraded DSIF accuracy
- Navigation after second midcourse correction using local vertical angle. 2 mrad (1σ) measurement accuracy
- Covariance matrix of estimation errors (Run 111):

$$[\tilde{P}_Q] = \begin{bmatrix} 1.03 \times 10^7 & -1.65 \times 10^7 & 1.13 \times 10^4 & -5.50 \times 10^3 \\ -1.65 \times 10^7 & 3.79 \times 10^7 & -2.42 \times 10^4 & 8.84 \times 10^3 \\ 1.13 \times 10^4 & -2.42 \times 10^4 & 1.56 \times 10^1 & -6.04 \times 10^0 \\ -5.50 \times 10^3 & 8.84 \times 10^3 & -6.04 \times 10^0 & 2.94 \times 10^0 \end{bmatrix}$$

- Contribution to $[P_f]$:

$$[P_{f\tilde{p}_o}] = \begin{bmatrix} 8.41 \times 10^1 & 0 & -9.96 \times 10^0 & 1.05 \times 10^1 \\ 0 & 0 & 0 & 0 \\ -9.96 \times 10^0 & 0 & 1.18 \times 10^0 & -1.24 \times 10^0 \\ 1.05 \times 10^1 & 0 & -1.24 \times 10^0 & 1.30 \times 10^0 \end{bmatrix}$$

e. Concept 5

- Second midcourse correction at 66 hours
- Monitoring accuracy 0.1 m/sec (1σ)
- Degraded DSIF accuracy
- Navigation after second midcourse correction using local vertical angle. 2mrad (1σ) measurement accuracy
- Covariance matrix of estimation errors (Run 121):

$$\left[\tilde{P}_o\right] = \begin{bmatrix} 1.15 \times 10^7 & -1.78 \times 10^7 & 1.26 \times 10^4 & -6.08 \times 10^3 \\ -1.78 \times 10^7 & 3.92 \times 10^7 & -2.55 \times 10^4 & 9.46 \times 10^3 \\ 1.26 \times 10^4 & -2.55 \times 10^4 & 1.70 \times 10^1 & -6.66 \times 10^0 \\ -6.08 \times 10^3 & 9.46 \times 10^3 & -6.66 \times 10^0 & 3.23 \times 10^0 \end{bmatrix}$$

- Contribution to $\left[P_f\right]$:

$$\left[P_f \tilde{p}_o\right] = \begin{bmatrix} 8.55 \times 10^1 & 0 & -1.01 \times 10^1 & 1.06 \times 10^1 \\ 0 & 0 & 0 & 0 \\ -1.01 \times 10^1 & 0 & 1.20 \times 10^0 & -1.26 \times 10^0 \\ 1.06 \times 10^1 & 0 & -1.26 \times 10^0 & 1.34 \times 10^0 \end{bmatrix}$$

f. Concept 6

- Second midcourse correction at 50 hours
- Monitoring accuracy 0.1 m/sec (1σ)
- Degraded DSIF accuracy
- Navigation after second midcourse correction using 1000 K, altimeter. 3 measurements, 2 km (1σ) accuracy.
- Covariance matrix of estimation errors (Run 135):

$$\left[\tilde{P}_o\right] = \begin{bmatrix} 5.84 \times 10^6 & 9.09 \times 10^6 & -3.51 \times 10^3 & -3.11 \times 10^3 \\ 9.09 \times 10^6 & 2.51 \times 10^7 & -1.14 \times 10^4 & -4.84 \times 10^3 \\ -3.51 \times 10^3 & -1.14 \times 10^4 & 5.32 \times 10^0 & 1.87 \times 10^0 \\ -3.11 \times 10^3 & -4.84 \times 10^3 & 1.87 \times 10^0 & 1.66 \times 10^0 \end{bmatrix}$$

- Contribution to $\left[P_f\right]$:

$$\left[P_f \tilde{p}_o\right] = \begin{bmatrix} 2.29 \times 10^2 & 0 & -2.70 \times 10^1 & 2.82 \times 10^1 \\ 0 & 0 & 0 & 0 \\ -2.70 \times 10^1 & 0 & 3.20 \times 10^0 & -3.33 \times 10^0 \\ 2.82 \times 10^1 & 0 & -3.33 \times 10^0 & 3.47 \times 10^0 \end{bmatrix}$$

g. Concept 7

- Second midcourse correction at 50 hours
- Monitoring accuracy 0.1 m/sec (1σ)
- Degraded DSIF accuracy

- Navigation after second midcourse correction using 1000 km altimeter, 3 measurements, 4 km (1σ) measurement accuracy
- Covariance matrix of estimation errors (Run 136):

$$\left[\tilde{P}_o\right] = \begin{bmatrix} 2.00 \times 10^7 & 3.01 \times 10^7 & -1.15 \times 10^4 & -1.07 \times 10^4 \\ 3.01 \times 10^7 & 8.84 \times 10^7 & -4.03 \times 10^4 & -1.60 \times 10^4 \\ -1.15 \times 10^4 & -4.03 \times 10^4 & 1.90 \times 10^1 & 6.11 \times 10^0 \\ -1.07 \times 10^4 & -1.60 \times 10^4 & 6.11 \times 10^0 & 5.69 \times 10^0 \end{bmatrix}$$

- Contribution to $\left[P_f\right]$:

$$\left[P_{f\tilde{p}_o}\right] = \begin{bmatrix} 7.78 \times 10^2 & 0 & -9.22 \times 10^1 & 9.55 \times 10^1 \\ 0 & 0 & 0 & 0 \\ -9.22 \times 10^1 & 0 & 1.09 \times 10^1 & -1.13 \times 10^1 \\ 9.55 \times 10^1 & 0 & -1.13 \times 10^1 & 1.17 \times 10^1 \end{bmatrix}$$

The resulting mean squared contributions to the deviations from nominal at main braking termination are summarized in table 10-3.

10.3.3 Contribution to $\left[P_f\right]$ Caused by Sensor Errors During Retrothrust

As stated previously, an initial estimate of the contributions due to the covariance matrix $\left[\tilde{Q}\right]$ is obtained by assuming sample values for the elements of $\left[\tilde{Q}\right]$. Since $\left[\tilde{Q}\right]$ is assumed to be diagonal, this is equivalent to specifying typical RMS values for the elements of the vector $\tilde{q}$.

The values assumed are:

$\sigma_{\tilde{q}_1} = \sigma_{\tilde{f}_c} = 1000$ Newtons

$\sigma_{\tilde{q}_2} = \sigma_{\tilde{\alpha}_c} = 0.01$ rad

$\sigma_{\tilde{q}_3} = \sigma_{\tilde{\gamma}_i} = 0.002$ rad

$\sigma_{\tilde{q}_4} = \sigma_{\tilde{a}_{FR}} = 0.002$ m/sec^2

$\sigma_{\tilde{q}_5} = \sigma_{\tilde{a}_{F\theta}} = 0.002$ m/sec^2

TABLE 10-3

MEAN SQUARED DEVIATIONS AT MAIN BRAKING TERMINATION CAUSED BY ESTIMATION ERRORS AT MIDCOURSE PERISELENUM

Midcourse Navigation Concept	Measurement Accuracy	2nd correction time	DSIF Accuracy		$\sigma^2_{\tilde{x}_f p_o}$ $(m)^2$	$\sigma^2_{\dot{\tilde{x}}_f p_o}$ $(m/s)^2$	$\sigma^2_{\dot{\tilde{z}}_f p_o}$ $(m/s)^2$
			Nominal	Degraded			
No Navigation	N/A	50 hours	X		490	6.84	7.48
	N/A	66 hours	X		87.9	1.23	1.34
	N/A	66 hours		X	8120	114	125
Use Horizon scanner to measure local vertical angle with respect to inertial reference	2 m rad (1σ)	50 hours		X	84.1	1.18	1.30
	2 m rad (1σ)	66 hours		X	85.5	1.20	1.34
Use altimeter to estimate range to the center of the moon (Max alt = 1000 km total of 3 measurements)	2 km (1σ)	50 hours		X	229	3.20	3.47
	4 km (1σ)	50 hours		X	778	10.9	11.7

Then the covariance matrix $[\tilde{Q}]$ is:

$$[\tilde{Q}] = \begin{bmatrix} 1.0 \times 10^{6} & 0 & 0 & 0 & 0 \\ 0 & 1.0 \times 10^{-4} & 0 & 0 & 0 \\ 0 & 0 & 4.0 \times 10^{-6} & 0 & 0 \\ 0 & 0 & 0 & 4.0 \times 10^{-6} & 0 \\ 0 & 0 & 0 & 0 & 4.0 \times 10^{-6} \end{bmatrix}$$

and the resulting contribution to $[P_f]$ is

$$\left[P_{f\tilde{q}}\right] = \begin{bmatrix} 4.28 \times 10^{1} & 0 & -5.11 \times 10^{0} & 5.36 \times 10^{0} \\ 0 & 0 & 0 & 0 \\ -5.11 \times 10^{0} & 0 & 6.05 \times 10^{-1} & -6.33 \times 10^{-1} \\ 5.36 \times 10^{0} & 0 & -6.33 \times 10^{-1} & 6.63 \times 10^{-1} \end{bmatrix}$$

Because of the diagonal nature of $[\tilde{Q}]$, the contributions of each of the error sources represented by $\tilde{q}$ to the mean squared value of each of the elements of p_f can be identified. These contributions are tabulated in table 10-4 for the sample input error levels.

10.3.4 Contribution to $[P_f]$ Caused by Control Errors During Descent Kick Application

The procedure here is exactly the same as that used in evaluating the sample values of navigation errors during the injection maneuver. The sample control errors in applying the descent kick are:*

$$\sigma_{u_1} = \sigma_{\delta V_2} = 0.5 \text{ m/sec}$$

$$\sigma_{u_2} = \sigma_{\delta\alpha} = 0.02 \text{ rad}$$

Then, the covariance matrix $[U]$ is

$$[U] = \begin{bmatrix} 2.5 \times 10^{-1} & 0 \\ 0 & 4 \times 10^{-4} \end{bmatrix}$$

* The error source $\delta\gamma$ does not contribute to the in-plane error and is therefore not included in this discussion.

TABLE 10-4

SAMPLE COMPUTATION RESULTS

Error Source	Sample RMS Value	Contribution To:		
		$\sigma^2_{x_f}$ $(m)^2$	$\sigma^2_{\dot{x}_f}$ $(m/sec)^2$	$\sigma^2_{\dot{z}_f}$ $(m/sec)^2$
Thrust Magnitude: $\tilde{f}_c$	1000 Newt.	9.00	0.126	0.137
Thrust Pointing: $\tilde{\alpha}_c$	0.01 rad	0.0180	0.000250	0.000272
Initial Platform Misalignment: $\tilde{\gamma}_i$	0.002 rad	13.4	0.187	0.206
Radial Direction Accelerometer: $\tilde{a}_{FR}$	0.002 m/sec^2	0.0390	0.000538	0.000615
Transverse Direction Accelerometer: $\tilde{a}_{F\theta}$	0.002 m/sec^2	20.79	0.292	0.319
Total Mean Squared Contributions		42.8 $(m)^2$	0.605 $(m/sec)^2$	0.663 $(m/sec)^2$
Total RMS Contributions		6.54 m	0.777 m/sec	0.815 m/sec

and the resulting contribution to $[P_f]$ is:

$$[P_{fu}] = \begin{bmatrix} 1.02 \times 10^{1} & 0 & -1.36 \times 10^{0} & 1.42 \times 10^{0} \\ 0 & 0 & 0 & 0 \\ -1.36 \times 10^{0} & 0 & 1.81 \times 10^{-1} & -1.89 \times 10^{-1} \\ 1.42 \times 10^{0} & 0 & -1.89 \times 10^{-1} & 1.98 \times 10^{-1} \end{bmatrix}$$

The individual contributions to the mean squared terminal deviations are tabulated in table 10-5.

10.3.5 Contribution to $[P_f]$ Caused by Main Braking Initiation Error

The assumed sample RMS errors are:

$$\sigma_{\tilde{q}_{i1}} = \sigma_{\tilde{r}_i} = 3.5 \text{ km}$$

$$\sigma_{\tilde{q}_{i2}} = \sigma_{(\tilde{\theta}_a)_i} = 0.005 \text{ rad}$$

The matrix $[\tilde{Q}_i]$ is

$$[\tilde{Q}_i] = \begin{bmatrix} 1.225 \times 10^{7} & 0 \\ 0 & 2.5 \times 10^{-5} \end{bmatrix}$$

The resulting contribution to $[P_f]$ is

$$[P_{f\tilde{q}_i}] = \begin{bmatrix} 2.20 \times 10^{0} & 0 & -2.62 \times 10^{-1} & 2.67 \times 10^{-1} \\ 0 & 0 & 0 & 0 \\ -2.62 \times 10^{-1} & 0 & 3.11 \times 10^{-2} & -3.18 \times 10^{-2} \\ 2.67 \times 10^{-1} & 0 & -3.18 \times 10^{-2} & 3.25 \times 10^{-2} \end{bmatrix}$$

The mean squared contributions to terminal deviations from nominal caused by the error in estimating initial central angle to the beacon are summarized in table 10-6.

TABLE 10-5

SAMPLE COMPUTATION RESULTS

Error Source	Sample RMS Value	Contribution To:		
		$\sigma^2_{x_f}$ $(m)^2$	$\sigma^2_{\dot{x}_f}$ $(m/sec)^2$	$\sigma^2_{\dot{z}_f}$ $(m/sec)^2$
Descent Kick magnitude: δv_2	0.5 m/sec	2.59	0.0365	0.0380
Descent Kick Direction: $\delta\alpha$ (in-plane)	0.02 rad	7.62	0.144	0.160
Total mean squared contribution		10.2 $(m)^2$	0.181 (m/sec)	0.198 $(m/sec)^2$
Total RMS Contributions		3.2 (m)	0.425 (m/sec)	0.445 (m/sec)

TABLE 10-6

SAMPLE COMPUTATION RESULTS

Error Source	Sample RMS Value	$\sigma^2_{x_f}$ $(m)^2$	Contribution To:	
			$\sigma^2_{\dot{x}_f}$ $(m/sec)^2$	$\sigma^2_{\dot{z}_f}$ $(m/sec)^2$
Initial range Estimation	$\sigma_{\tilde{r}_i}$ 3.5×10^3 m	2.11	0.0299	0.0312
Initial Angle Estimation	$\sigma_{(\tilde{\theta}_{a_1})}$ 0.005 rad.	0.0864	0.00122	0.00128
Total Mean squared contribution		2.20	0.0311	0.0325
Total RMS contributions		1.48 m	0.176 m/sec	0.180 m/sec

10.3.6 Contributions to $[P_f]$ Caused by Constant Sensor Bias Errors During Main Braking

The assumed sample RMS (average over ensemble missions) input error levels are:*

$$\sigma_{(\tilde{q}_{bc})_1} = \sigma_{\tilde{r}_{bc}} = 2.0 \text{ m}$$

$$\sigma_{(\tilde{q}_{bc})_2} = \sigma_{\dot{\tilde{r}}_{bc}} = 0.1 \text{ m/sec}$$

$$\sigma_{(\tilde{q}_{bc})_3} = \sigma_{\tilde{\psi}_{bc}} = 1.0 \times 10^{-3} \text{ rad}$$

$$\sigma_{(\tilde{q}_{bc})_4} = \sigma_{\dot{\tilde{\psi}}_{bc}} = 1.0 \times 10^{-4} \text{ rad/sec}$$

$$\sigma_{(\tilde{q}_{bc})_5} = \sigma_{\tilde{f}_{bc}} = 1000 \text{ Newtons}$$

$$\sigma_{(\tilde{q}_{bc})_6} = \sigma_{(\tilde{\theta}_{los})_{bc}} = 0.01 \text{ rad}$$

The corresponding input covariance matrix $[\tilde{Q}_{bc}]$ is

$$[\tilde{Q}_{bc}] = \begin{bmatrix} 4.00\times10^{0} & 0 & 0 & 0 & 0 & 0 \\ 0 & 1.00\times10^{-2} & 0 & 0 & 0 & 0 \\ 0 & 0 & 1.00\times10^{-6} & 0 & 0 & 0 \\ 0 & 0 & 0 & 1.00\times10^{-8} & 0 & 0 \\ 0 & 0 & 0 & 0 & 1.00\times10^{6} & 0 \\ 0 & 0 & 0 & 0 & 0 & 1.00\times10^{-4} \end{bmatrix}$$

and the resulting contribution to $[P_f]$ is:

$$[P_{f\tilde{q}_{bc}}] = \begin{bmatrix} 1.24\times10^{3} & -2.32\times10^{0} & -1.47\times10^{2} & 1.48\times10^{2} \\ -2.32\times10^{0} & 2.43\times10^{0} & -.127\times10^{-1} & 1.52\times10^{-1} \\ -1.47\times10^{2} & -1.27\times10^{-1} & 1.76\times10^{1} & -1.76\times10^{1} \\ 1.48\times10^{2} & 1.52\times10^{-1} & -1.76\times10^{1} & 1.80\times10^{1} \end{bmatrix}$$

---

* Note that these are (1σ) error levels

The individual contributions of each error source to the mean squared terminal deviations are tabulated in table 10-7.

10.3.7 Contributions to $[P_f]$ Caused by Scale Factor Sensor Bias Errors During Main Braking

The assumed RMS input error levels are:

$$\sigma_{(\tilde{q}_{bs})_1} = \sigma_{\tilde{r}_{bs}} = 1.0 \text{ percent}$$

$$\sigma_{(\tilde{q}_{bs})_2} = \sigma_{\dot{\tilde{r}}_{bs}} = 0.1 \text{ percent}$$

$$\sigma_{(\tilde{q}_{bs})_3} = \sigma_{\tilde{\psi}_{bs}} = 0^{*}$$

$$\sigma_{(\tilde{q}_{bs})_4} = \sigma_{\dot{\tilde{\psi}}_{bs}} = 1.0 \text{ percent}$$

$$\sigma_{(\tilde{q}_{bs})_5} = \sigma_{\tilde{f}_{bs}} = 0^{**}$$

$$\sigma_{(\tilde{q}_{bs})_6} = \sigma_{(\tilde{\theta}_{los})_{bs}} = 0^{*}$$

The corresponding input covariance matrix $\left[\tilde{Q}_{bs}\right]$ is

$$\left[\tilde{Q}_{bs}\right] = \begin{bmatrix} 1.00\times10^{0} & 0 & 0 & 0 & 0 & 0 \\ 0 & 1.0\times10^{-2} & 0 & 0 & 0 & 0 \\ 0 & 0 & 0 & 0 & 0 & 0 \\ 0 & 0 & 0 & 1.0\times10^{0} & 0 & 0 \\ 0 & 0 & 0 & 0 & 0 & 0 \\ 0 & 0 & 0 & 0 & 0 & 0 \end{bmatrix}$$

---

* Scale factor errors are not usually considered as part of the error model of an angle sensor.

** Thrust is essentially constant throughout the landing maneuver so that a scale factor error is equivalent to a constant error and need not be considered separately.

TABLE 10-7

SAMPLE COMPUTATION RESULTS

Error Source	Sample RMS Value	Contribution To:			
		$\sigma^2_{x_f}$ $(m)^2$	$\sigma^2_{z_f}$ $(m)^2$	$\sigma^2_{\dot{x}_f}$ $(m/sec)^2$	$\sigma^2_{\dot{z}_f}$ $(m/sec)^2$
Range Observation	$\sigma_{\tilde{r}_{bc}}$ = 1.0 m	2.26	2.37	0.00678	0.00970
Range Rate Observation	$\sigma_{\dot{\tilde{r}}_{bc}}$ = 0.1 m/sec	0.266	0	0.00000864	0.00870
Angle Observation	$\sigma_{\tilde{\psi}_{bc}}$ = 0.001 rad	0	0.0625	0	0
Angle Rate Observation	$\sigma_{\dot{\tilde{\psi}}_{bc}}$ = 0.0001 rad/sec	1150	0	16.8	16.2
Thrust Magnitude Observation	$\sigma_{\tilde{f}_{bc}}$ = 1000 N	0.188	0	0.00290	0.1498
Thrust Direction Observation	$\sigma_{(\tilde{\theta}_{los})_{bc}}$ 0.01 rad	85.8	0	0.812	1.64
Total mean squared contributions		1240 $(m)^2$	2.43 $(m)^2$	17.6 $(m/s)^2$	18.0 $(m/s)^2$
Total RMS contributions		35.2 m	1.56 m	4.20 m/s	4.25 m/sec

and the resulting contribution to $\left[P_f\right]$ is

$$\left[P_{f\tilde{q}_{bs}}\right] = \begin{bmatrix} 2.76 \times 10^{2} & -3.45 \times 10^{1} & -1.84 \times 10^{1} & 3.00 \times 10^{1} \\ -3.45 \times 10^{1} & 9.00 \times 10^{0} & 1.97 \times 10^{0} & -2.36 \times 10^{0} \\ -1.84 \times 10^{1} & 1.97 \times 10^{0} & 1.25 \times 10^{0} & -2.09 \times 10^{0} \\ 3.00 \times 10^{1} & -2.36 \times 10^{0} & -2.09 \times 10^{0} & 3.68 \times 10^{0} \end{bmatrix}$$

The individual contributions of each error source to the mean squared terminal deviations are tabulated in table 10-8.

10.3.8 Contributions to $\left[P_f\right]$ Caused by Random Navigation and Control Sensor Errors During Main Braking

From previous work

$$\underline{\sigma}^2_{p_f\tilde{q}_n} = \left[S_{p_f\tilde{q}_{nc}}\right] \underline{\sigma}^2_{\tilde{q}_{nc}} + \left[S_{p_f\tilde{q}_{ns}}\right] \underline{\sigma}^2_{\tilde{q}_{ns}}$$

where

$$\left[S_{p_f\tilde{q}_{nc}}\right] = \begin{bmatrix} 5.21\text{x}10^{-3} & 1.60\text{x}10^{-1} & 0 & 4.60\text{x}10^{8} & 3.32\text{x}10^{-8} & 1.24\text{x}10^{3} \\ 5.90\text{x}10^{-1} & 0 & 6.26\text{x}10^{4} & 0 & 0 & 0 \\ 4.83\text{x}10^{-4} & 2.14\text{x}10^{-2} & 0 & 2.25\text{x}10^{6} & 2.90\text{x}10^{-10} & 1.18\text{x}10^{1} \\ 7.02\text{x}10^{-4} & 7.85\text{x}10^{-2} & 0 & 6.64\text{x}10^{7} & 2.86\text{x}10^{-9} & 1.01\text{x}10^{2} \end{bmatrix}$$

and

$$\left[S_{p_f\tilde{q}_{ns}}\right] = \begin{bmatrix} 2.87\text{x}10^{0} & 9.79\text{x}10^{0} & 0 & 2.60\text{x}10^{-1} & 3.72\text{x}10^{-2} & 2.82\text{x}10^{-2} \\ 9.03\text{x}10^{0} & 0 & 3.02\text{x}10^{0} & 0 & 0 & 0 \\ 2.33\text{x}10^{-2} & 3.66\text{x}10^{-2} & 0 & 3.97\text{x}10^{-3} & 3.31\text{x}10^{-4} & 3.90\text{x}10^{-4} \\ 3.00\text{x}10^{-1} & 9.21\text{x}10^{-1} & 0 & 2.38\text{x}10^{-2} & 3.25\text{x}10^{-3} & 3.26\text{x}10^{-3} \end{bmatrix}$$

The assumed typical rms values defining the components of vectors $\underline{\sigma}^2_{\tilde{q}_{nc}}$ and $\underline{\sigma}^2_{\tilde{q}_{ns}}$ are

a. Sample elements of $\underline{\sigma}^2_{\tilde{q}_{nc}}$

$$\sigma_{(\tilde{q}_{nc})_1} = \sigma_{\tilde{r}_{nc}} = 2.0 \text{ m}$$

$$\sigma_{(\tilde{q}_{nc})_2} = \sigma_{\dot{\tilde{r}}_{nc}} = 0.2 \text{ m sec}$$

TABLE 10-8

SAMPLE COMPUTATION RESULTS

Error Source	Sample rms Value	Contribution To:			
		$\sigma^2_{x_f}$ $(m)^2$	$\sigma^2_{z_f}$ $(m)^2$	$\sigma^2_{\dot{x}_f}$ $(m/sec)^2$	$\sigma^2_{\dot{z}_f}$ $(m/sec)^2$
Range Observation	$\sigma_{\tilde{r}_{bs}}$ = 1.0 percent	132	1.97	0.430	0.618
Range Rate Observation	$\sigma_{\dot{\tilde{r}}_{bs}}$ = 0.1 percent	0.380	0	0.00279	0.0000672
Angle Observation	$\sigma_{\tilde{\psi}_{bs}}$ = 0	0	0	0	0
Angle Rate Observation	$\sigma_{\dot{\tilde{\psi}}_{bs}}$ = 1.0 percent	144	0	0.814	3.06
Thrust Magnitude Observation	$\sigma_{\tilde{f}_{bs}}$	0	0	0	0
Thrust Direction Observation	$\sigma_{(\tilde{\theta}_{los})_{bs}}$ = 0	0	0	0	0
Total Mean Squared Contributions		277 $(m)^2$	1.97 $(m)^2$	1.25 $(m/sec)^2$	3.68 $(m/sec)^2$
Total RMS Contributions		16.6 m	1.40 m	1.12 m/s	1.92 m/sec

$$\sigma_{(\tilde{q}_{nc})_3} = \sigma_{\tilde{\psi}_{nc}} = 1 \times 10^{-3} \text{ rad}$$

$$\sigma_{(\tilde{q}_{nc})_4} = \sigma_{\dot{\tilde{\psi}}_{nc}} = 1 \times 10^{-4} \text{ rad/sec}$$

$$\sigma_{(\tilde{q}_{nc})_5} = \sigma_{\tilde{f}_{nc}} = 1000 \text{ Newtons}$$

$$\sigma_{(\tilde{q}_{nc})_6} = \sigma_{(\tilde{\theta}_{los})_{nc}} = 1 \times 10^{-3} \text{ rad}$$

b. Sample elements of $\underline{\sigma}^2_{\tilde{q}_{ns}}$

$$\sigma_{(\tilde{q}_{ns})_1} = \sigma_{\tilde{r}_{ns}} = 0.5 \text{ percent}$$

$$\sigma_{(\tilde{q}_{ns})_2} = \sigma_{\dot{\tilde{r}}_{ns}} = 0.2 \text{ percent}$$

$$\sigma_{(\tilde{q}_{ns})_3} = \sigma_{\tilde{\psi}_{ns}} = 0^*$$

$$\sigma_{(\tilde{q}_{ns})_4} = \sigma_{\dot{\tilde{\psi}}_{ns}} = 1.0 \text{ percent}$$

$$\sigma_{(\tilde{q}_{ns})_5} = \sigma_{\tilde{f}_{ns}} = 0^{**}$$

$$\sigma_{(\tilde{q}_{ns})_6} = \sigma_{(\tilde{\theta}_{los})_{ns}} = 0^*$$

The resulting contribution to $[P_f]$, denoted $[P_{f_{\tilde{q}_n}}]$ is a diagonal matrix composed from the elements of the vector $\underline{\sigma}^2_{p_f \tilde{q}_n}$.

---

* Scale factor errors are not usually considered as part of the error model of an angle sensor.

** Thrust is essentially constant throughout the landing maneuver so that a scale factor error is equivalent to a constant error and need not be considered separately.

$$\left[P_{f\tilde{q}_n}\right] \begin{bmatrix} 6.03 \times 10^{0} & 0 & 0 & 0 \\ 0 & 4.68 \times 10^{0} & 0 & 0 \\ 0 & 0 & 3.68 \times 10^{-2} & 0 \\ 0 & 0 & 0 & 8.08 \times 10^{-1} \end{bmatrix}$$

The contributions to the mean squared deviations from nominal at main braking termination caused by each input sensor error using the sample error levels are tabulated in table 10-9.

TABLE 10-9

SAMPLE COMPUTATION RESULTS

Error Source	Sample rms Value	Resulting Contribution to:			
		$\sigma^2_{x_f}$ $(m)^2$	$\sigma^2_{z_f}$ $(m)^2$	$\sigma^2_{\dot{x}_f}$ $(m/sec)^2$	$\sigma^2_{\dot{z}_f}$ $(m/sec)^2$
Range Observation	$\sigma_{\tilde{r}_{nc}}$ = 2.0m	0.0653	2.36	0.00605	0.00850
	$\sigma_{\tilde{r}_{ns}}$ = 0.5 percent	2.25	2.26	0.0183	0.236
Range Rate Observation	$\sigma_{\dot{\tilde{r}}_{nc}}$ = 0.2 m/sec	0.0201	0.0	0.00268	0.00985
	$\sigma_{\dot{\tilde{r}}_{ns}}$ = 0.2 percent	1.23	0.0	0.00459	0.116
Angle Observation	$\sigma_{\tilde{\psi}_{nc}}$ = 0.001 rad	0.0	0.0626	0.0	0.0
	$\sigma_{\tilde{\psi}_{ns}}$ = 0	0.0	0.0	0.0	0.0
Angle Rate Observation	$\sigma_{\dot{\tilde{\psi}}_{nc}}$ = 0.0001 rad/s	14.5	0.0	0.0706	2.08
	$\sigma_{\dot{\tilde{\psi}}_{ns}}$ = 1.0 percent	0.815	0.0	0.0125	0.0747
Thrust Magnitude Observation	$\sigma_{\tilde{f}_{nc}}$ = 1000 N	0.104	0.0	0.00091	0.00897
	$\sigma_{\tilde{f}_{ns}}$ = 0	0.0	0.0	0.0	0.0
Thrust Angle Observation	$\sigma_{(\tilde{\theta}_{los})_{nc}}$ = 0.001 rad	0.00389	0.0	0.000037	0.00032
	$\sigma_{(\theta_{los})_{ns}}$ = 0	0.0	0.0	0.0	0.0
Total Mean Squared Contributions		18.9 $(m)^2$	4.68 $(m)^2$	0.116 $(m/sec)^2$	2.54 $(m/sec)^2$

11. LUNAR RADAR BEACON ANALYSIS APPENDIX

This section examines the feasibility and limitations of a lunar surface radar beacon system using solid-state components subject to the restriction that the surface system be transportable and of less than 55 kg earth weight.

Conclusions are that:

a. A cooperative type radar utilizing a transponder should be used to provide an onboard guidance and navigation capability for the LLV in preference to a two-way radar utilizing a passive type reflector.

b. The frequency of operation of the system should be in the X-band frequency region, primarily in order to minimize the effects of rocket flame attenuation.

c. Solid-state techniques can provide a small reliable radar system for the lunar landing mission. However, because of the relatively low peak powers which can be generated using solid-state techniques, long pulses will be required in order to transmit sufficient power. Therefore, in order to obtain sufficient range accuracy some technique such as a pseudonoise coded radar, FM-CW radar, etc, is required.

d. For the maximum range considered (2×10^4 km) a vehicle antenna diameter of 1.52 meters should be sufficient to provide a range accuracy of approximately 1 km, assuming peak power capabilities of 1 to 2 watts estimated for future solid-state components in the X-band frequency region and a transponder antenna with hemispherical coverage.

e. Typically, the total surface transponder system weight and volume, including the power supply, power source, and antenna, are estimated to be 23 kg and 9300 cubic centimeters respectively. The vehicle radar system weight, excluding the power source, is estimated to be approximately 36 kg.

The radar volume, excluding the antenna and power source, is estimated to be 9850 cubic centimeters.

11.1 COMPARISON OF RADAR-TRANSPONDER WITH RADAR-CORNER REFLECTOR

For a signal transmitted by a lunar surface beacon and received at the vehicle, the signal power can be expressed in terms of the vehicle antenna diameter as

$$S = (P_T D_v^2) \frac{G_B \rho_a}{16R^2} \tag{11-1}$$

where the subscript B indicates the gain of the beacon or transponder antenna and D_v the diameter of the vehicle antenna. The term ρ_a is the antenna aperture efficiency with a typical value of about 0.6. Equation 11-1 applies to transmission in either direction because of the principle of reciprocity.

For a two-way system utilizing a corner reflector on the lunar surface the signal received at the vehicle can be written as

$$S = (P_T D_v^4) \frac{\pi \sigma_T \rho_a^2}{64 \lambda^2 R^4} \tag{11-2}$$

where σ_T is the radar cross section of the corner reflector and λ is the transmitted wavelength.

Taking the ratio of equations 11-2 and 11-1,

$$\frac{S_2}{S_1} = \frac{P_{T_2} D_v^2}{P_{T_1} R^2} \quad \frac{\pi \sigma_T \rho_a}{4 \lambda^2 G_B} \tag{11-3}$$

where the subscript 1 denotes the cooperative or one-way system and the subscript 2 denotes the two-way system. The augmentation possible with a corner reflector is limited by the largest size reflector that can be constructed while maintaining accurate dimensions, and by logistic considerations on the surface of the moon. A displacement of the outer edge of the

corner from its ideal position by $\lambda/2$ results in a loss of return signal of 3 db (reference 14). Assuming that this tolerance can be maintained for a corner reflector dimension a of 2 meters (where a is the edge of the corner) and a transmitted wavelength of 3 centimeters, the maximum cross section, as given by the expression

$$\sigma_{T_{max}} = \frac{4 \pi a^4}{3 \lambda^2} \qquad (11\text{-}4)$$

is 7.45×10^4 square meters. Figure 11-1 illustrates the ratio of signal strengths for the two-way and one-way systems given by equation 11-3 (for the above value of σ_T and other parameters as noted on the figure) as a function of range and peak powers. It is apparent that at appreciable ranges, the use of a two-way radar and a passive reflector on the moon would require so much higher peak powers aboard the LLV than would the cooperative radar, that solid-state techniques with their advantages (e.g., weight savings and reliability), would not be feasible for the time period of interest. These considerations help to cancel the obvious advantages of the passive reflector; i.e., simplicity and reliability.

In the following sections equal transmitted power and receiver sensitivity will be assumed for the vehicle radar and the transponder. No advantage in saving power would be derived by using a very low noise level receiver in the vehicle radar since it must look directly at the surface of the moon; this is discussed further in paragraph 11-2.

There are several additional advantages attendant with using the cooperative type radar:

a. The use of a time delay at the transponder permits zero range measurement.

b. The echo center for a transponder is well defined with resulting improved angular accuracy.

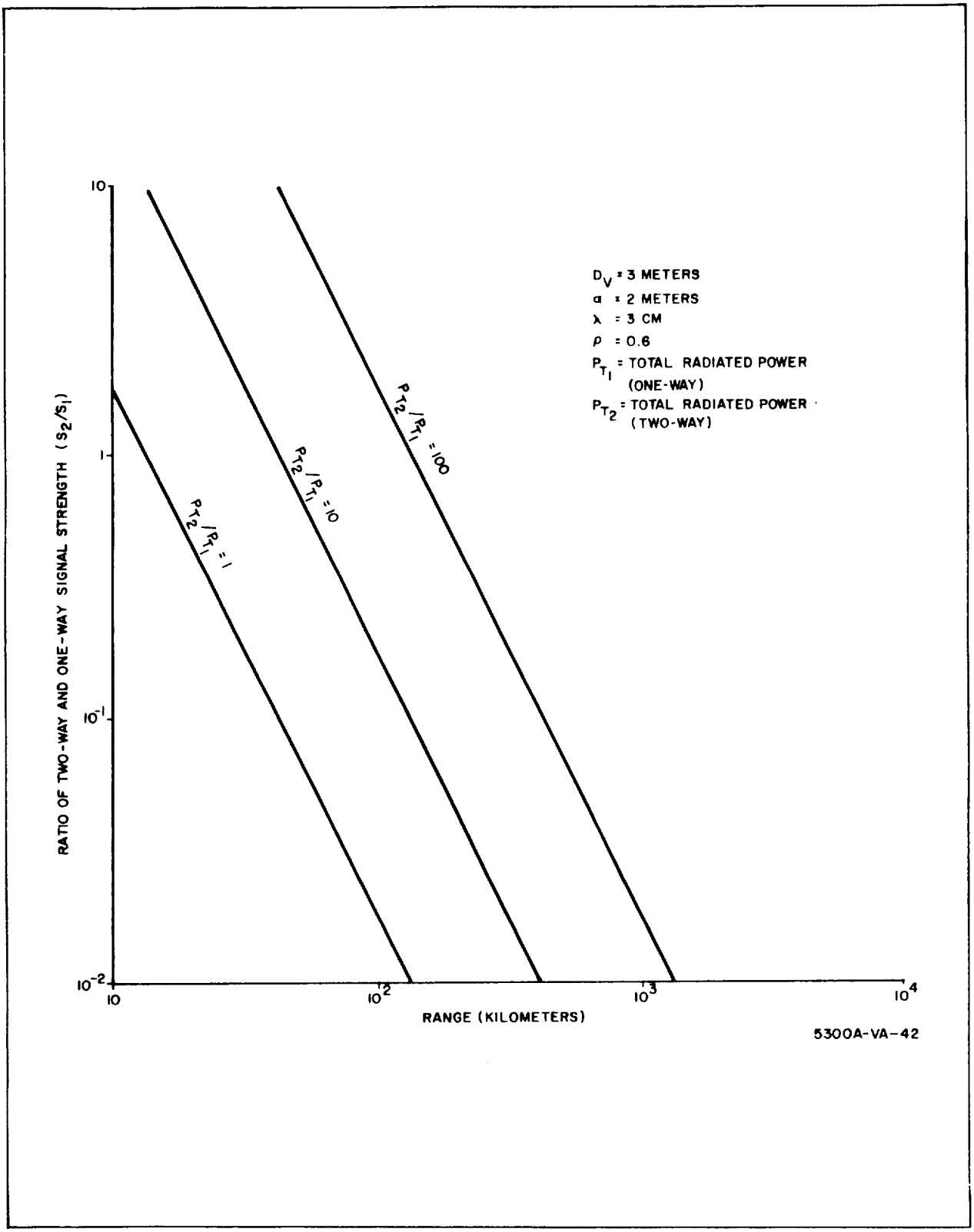

Figure 11-1. Ratio of Two-Way and One-Way Signal Strengths

c. There is a smaller dynamic range of signals with fewer resulting AGC problems.

11.2 OPERATING FREQUENCY

The selection of frequency for the vehicle radar and transponder depends to a large extent on the frequency characteristics of the expected environmental interferences, such as galactic and extra galactic or cosmic, and discrete sources such as the sun, moon, and stars.

The overall system noise power may be expressed by:

$$\text{Noise power} = KB\,(T_A + T_e) \qquad (11\text{-}5)$$

where

K = Boltzmann's constant

B = receiver bandwidth

T_A = equivalent noise temperature of the antenna, which involves the superposition of noise temperatures from the sources discussed above

T_e = receiver equivalent noise temperature

Figure 11-2 illustrates the maximum and minimum cosmic noise levels as a function of frequency. It is apparent that in terms of cosmic noise considerations, a frequency of 2-3 gc/sec or higher would be desirable. Cosmic noise becomes of increasing concern as receivers with lower equivalent temperatures become available. The noise level from the sun is such that the only solution is to not point the antenna in the direction of the sun. The noise temperature of the moon is between 200 and 300° K (reference 15). The actual contribution of the moon to the system temperature will depend upon the beamwidth of the vehicle antenna and the distance to the moon, or the ratio of the angular diameter of the moon to the antenna beamwidth. For beamwidths (between the 3 db points) from 1 to about 40 times the subtended diameter of the moon, the temperature increment is given by

$$T = \frac{75}{\theta^2} \qquad (11\text{-}6)$$

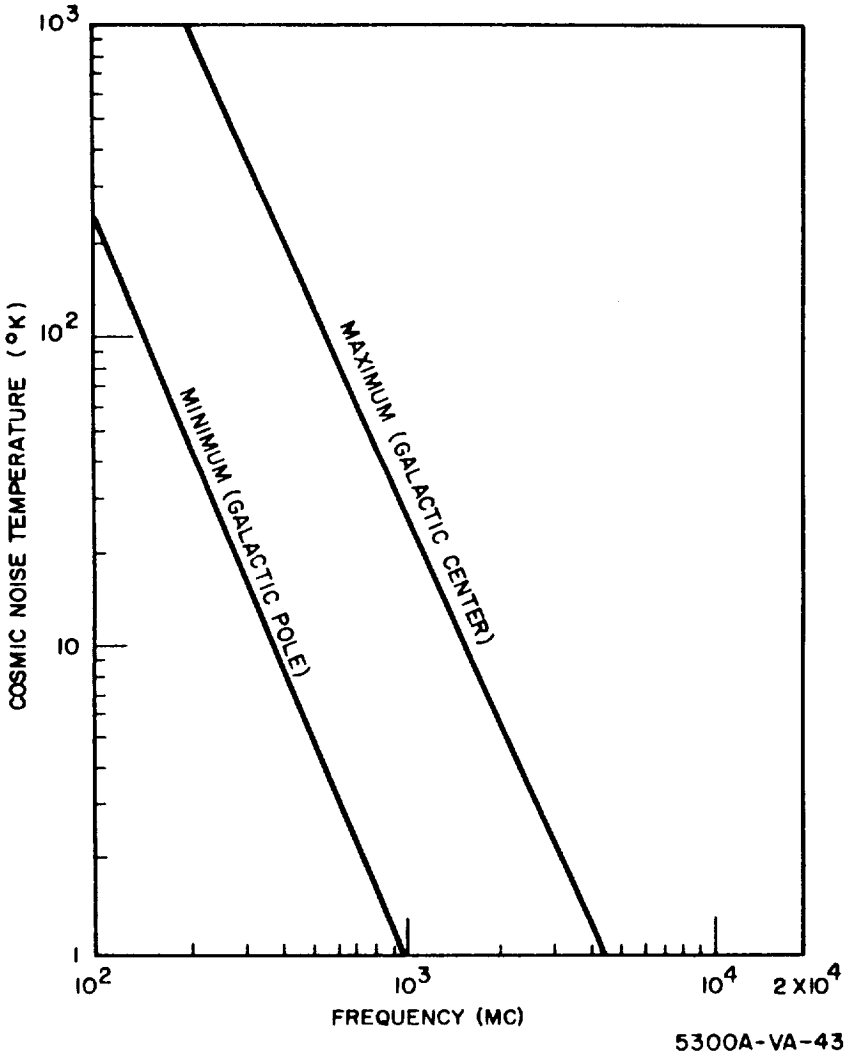

Figure 11-2. External Noise Versus Frequency

where θ is the beamwidth and it is assumed that the moon is in the center of the beam (reference 15). For smaller beamwidths the temperature is given by the temperature of the moon (300° K). It is to be noted that as a result of the requirement for the vehicle radar to point directly at the moon the advantages to be derived from using a very low noise level receiver, (that is, with a noise figure of less than 3 db), would not be realized, as indicated by equation 10-5. For example, the equivalent noise temperature of a maser, which is typically 10° K or less, represents a very small fraction of the equivalent noise temperature of the antenna which arises from the moon.

Another consideration regarding the choice of system frequency results from the attenuation that occurs when the RF energy passes through the rocket flame or plume, which may occur during the terminal or descent phase of the mission. In general, the exhaust gasses behave as a weakly ionized plasma (reference 16), ω_p, a constant of the plasma medium, can be expressed as a function of the electron density by (reference 17)

$$\omega_p = \left[\frac{e^2 N}{M \epsilon}\right]^{1/2} \qquad (11\text{-}7)$$

where

- e = electron charge
- M = electron mass
- N = electron density
- ϵ = dielectric constant of free space

As the signal frequency approaches the plasma frequency the signal phase constant undergoes large variations and the attenuation drops sharply as shown in figure 11-3. The extent to which attenuation occurs is a function of the type of rocket engine and fuel, the angle of transmission through the flame, frequency of the RF energy, location of the antenna, etc, so that specific estimates of the amount of attenuation to be expected requires knowledge of the specific configuration. As an example, measurements for

one particular case have indicated attenuations of 18 db at L-band, 4.5 db at S-band, and 0.5 db at X-band (reference 16). It is apparent that microwave propagation through rocket flames will be improved at higher frequencies where the attenuation is less than it is at lower frequencies.

An additional consideration in the choice of frequency involves the peak power which can be generated at a given frequency using solid-state components; the power levels attainable decrease with increasing frequency. (In paragraph 11.5, it will be seen that for practical antenna sizes the future power levels expected in the X-band frequency region should be sufficient to provide useful information at ranges up to 2×10^4 kilometers.)

11.3 SYSTEM CONSIDERATIONS

The signal-to-noise ratio, S/N, a most useful measure of range performance, can be written for the one-way case, using equations 11-1 and 11-5, as

$$S/N = \frac{P_T D_v^2 G_B \rho_a}{16 R^2 K T_o \overline{NF} BL} \tag{11-8}$$

where noise power has been expressed in terms of the receiver noise figure $\overline{NF}$ which is based on the standard temperature T_o (290° K). An additional loss factor L has been included to account for miscellaneous system losses. While S/N may be improved by increasing peak power, P_T, the power levels obtained with solid-state components are limited, as noted in paragraph 2.1. S/N may be improved by narrowing receiver bandwidth at the expense of a longer pulse, assuming the optimum relationship, $B\tau \approx 1$. Then, as shown in reference 18, the error in the measurement of the time delay, δT_R, of a pulse edge is given by

$$\delta T_R = \left(\frac{\tau}{2 BE/N_o}\right)^{1/2} \tag{11-9}$$

where E is the signal energy, N_o the noise power per unit bandwidth and τ the pulsewidth, so that range measurement error increases with increasing pulsewidth.

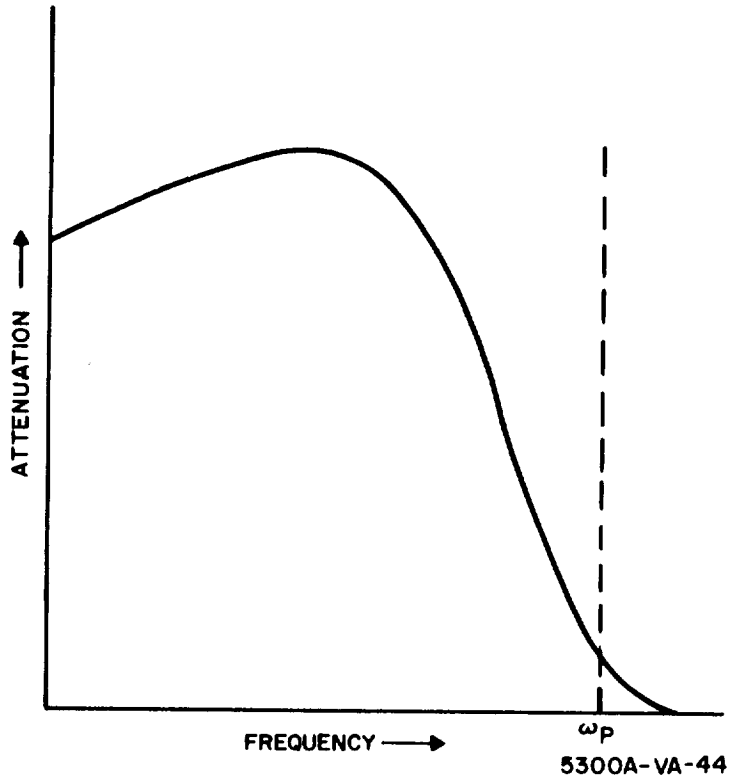

Figure 11-3. RF Attenuation in a Plasma as a Function of Frequency

Equation 11-8 may be rewritten in terms of average power to show that benefit is gained by increasing pulse repetition rate, but a requirement for unambiguous range measurement limits this.

There are several techniques which circumvent these problems and which permit the measurement of range using CW or long pulse systems. One such technique (FM-CW) involves the modulation of the transmitted frequency as a function of time in a known manner. The phase of the transmitted signal provides a time reference and thus a measurement of range. Another technique (multiple frequency CW radar) involves the use of multiple CW frequencies to provide a measure of range by measurement of the variation of phase with frequency. A third technique is to automatically control the widths of the transmitted pulses from the radar and transponder to be equal to the range transmission time. As this relationship is maintained, a measurement of the pulsewidths or pulse repetition frequency provides a measure of range. A solid state operating model of this system has been built by Westinghouse to demonstrate possible performance. A fourth technique involves the phase modulation of long pulses to obtain a range measurement of high accuracy. It is designed to combine a long pulse and its associated advantages of low peak power and narrow bandwidth with high range accuracy. This system is referred to here as a pulse pseudonoise radar.

Although the preceding types of systems will differ somewhat in complexity and performance, they will have approximately the same weight, size, and power, especially when designed to use all solid-state components. Since it is the purpose of this analysis to consider the feasibility of using a solid-state radar, a comparison of the various mechanized systems is not considered here. However, in order to indicate typical values of weight, size, and performance of a solid-state radar and transponder, the last mentioned system was examined in detail.

11.4 PULSE PSEUDONOISE RADAR SYSTEMS*

11.4.1 System Description

This radar utilizes a wide pulsewidth; however, as pointed out, the range accuracy of any radar system is inversely proportional to the signal bandwidth. Therefore, in the proposed system a wideband signal must exist somewhere in the system in order to determine range accurately. This is accomplished in the transmitter and in the receiver before signal extraction.

The wide bandwidth signal is generated by phase coding within the carrier frequency pulse in discrete steps of 0 or 180 degrees in accordance with a binary code. The binary code is generated by a shift register whose output is a series of binary "1's" and "0's" in accordance with a flip-flop that is used as an output stage. These 1's and 0's are arranged in a random fashion within a code length, thus having a noise like appearance. The binary code generator generates this code repetitively. If certain shift register stages are fed back into a Module-2 adder (half adder) and injected into the first stage, the code generator (shift register) will produce the longest code that it is capable of generating without repeating any given sequence. This is called a pseudorandom (or noise) code. The exact PN code produced by the shift register is fixed by the wired in feedback connections.

One bit time within the code is defined as the smallest pulsewidth, T_b that is capable of being generated or resolved and is equal to the reciprocal of the clock frequency ($1/f_c$), which is used to step the shift register. The length of the particular code is determined by

$$N = 2^s - 1 \qquad (11\text{-}10)$$

where N equals the number of bits in the code and s is the number of stages in the shift register.

The code is used to modulate the transmission in such a manner that a "0" permits transmission of the RF, and a "1" causes a phase shift of

*The description of this radar system is adapted from reference 19.

180 degrees. When this coded signal is matched exactly against itself in the receiver (as in a decoder), and both signals appear at the same time, a maximum signal is present at the output. As one signal varies in time with respect to the other signal the output of the decoder falls off rapidly. This characteristic (the correlation function) permits accurate range measuring by causing a large decoder output signal variation for a small time deviation. The width of the base of the correlation function is two bit widths. Range measurement accuracy can be increased by increasing the clock frequency. The bandwidth (RF or IF) of the transmitted and received pulses is approximately equal to $2 f_c$, while that of the correlated signal is $2/\tau$, where τ is the pulsewidth.

11.4.2 General Theory of Operation

Figures 11-4 and 11-5 are simplified block diagrams of the radar and transponder. Initially the radar transmits an unmodulated CW signal. The transponder phase-locks to this frequency, and retransmits a CW signal which is offset from the radar transmitter frequency by an amount equal to the radar IF. Thus, the transmitter frequencies in both the radar and the transmitter are used as local oscillators. The radar then phase locks to the CW signal from the transponder and tracks the doppler frequency in a doppler track loop. Phase coherence is thereby maintained from the radar to the transponder and back to the radar.

After phase lockup has been completed, the radar begins to transmit pulse-modulated CW. (The pulsewidth is approximately 14.3 milliseconds, and the PRF is approximately 14 cps.) The transponder senses the pulse modulation, closes a PRF phase track loop thereby positioning a gate over the received signal, and begins to pulse modulate its transmitted signal. The radar closes a range track loop and begins to range track the wide pulse from the transponder. The transponder will transmit a pulse at a given time delay after reception while the radar transmits at a fixed PRF.

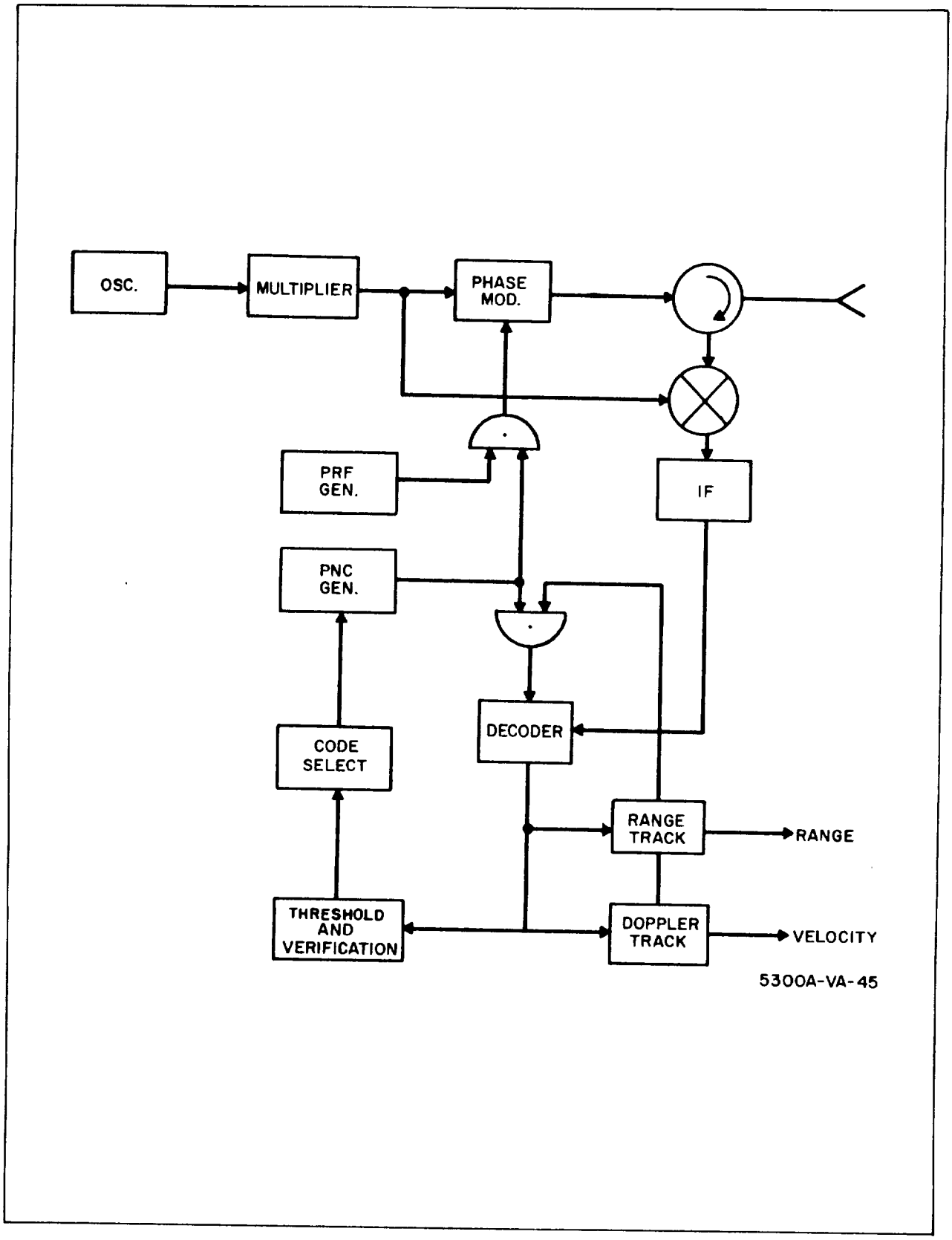

Figure 11-4. Simplified Block Diagram of Radar

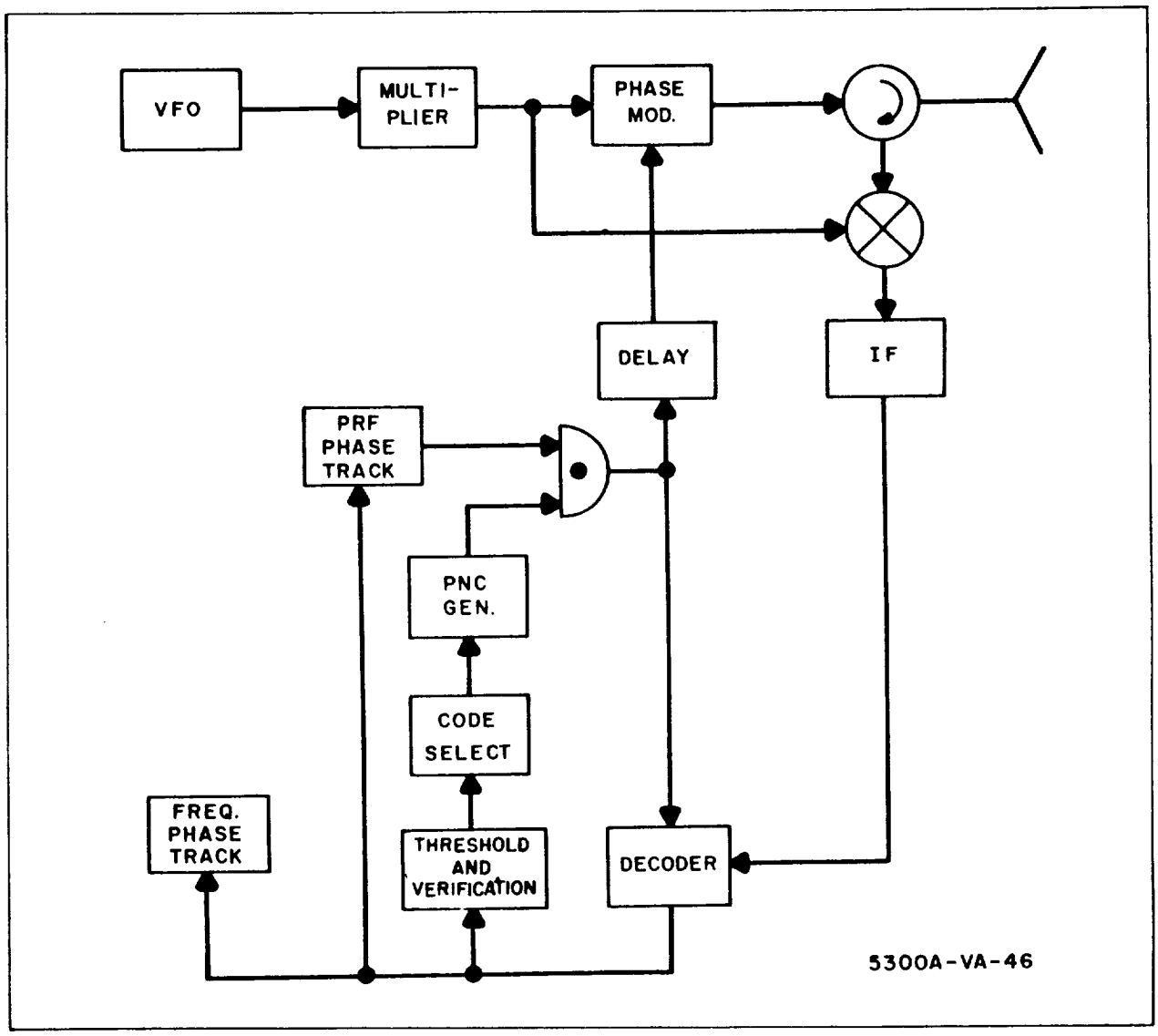

Figure 11-5. Simplified Block Diagram of Transponder

When the range track error in the radar reaches a given low level, the radar begins to phase modulate its transmitted signal by means of a coarse code from a pseudonoise code generator. The total transmitted pulsewidth remains approximately the same, but the bit widths in the code are chosen slightly wider than the maximum range error expected in range tracking the wide pulse. The transponder senses the coding on the incoming signal and begins to correlate the incoming signal with the output of a transponder PNC generator. The transponder PNC generator supplies the same coarse code as that began generated by the PNC generator in the radar. The transponder

then begins to phase modulate its transmission from the transponder and correlates this signal with the coarse code output of its PNC generator in a decoder. The range track error signal is derived after the decoder, and the total range aperture is then equal to two bit widths.

The range track loop in the radar minimizes the range error, and the entire sequence described above is repeated twice more, with the radar and transponder switching first to a medium code and finally to a fine code. The bit widths in each succeeding code are chosen slightly wider than the maximum range error expected while tracking in the previous code. In each instance, the total transmitted pulsewidth remains approximately the same. In this manner, the radar realizes the advantages of transmitting a long pulse of low peak power while at the same time achieving the high range accuracy and resolution of a narrow pulse. Also, by proper choice of the code change steps, the range tracking uncertainty is always encompassed by the next code bit width and the range track system will never have to search in time, but will merely pull in the range uncertainty.

11.4.3 Acquisition Range

The acquisition sequence occurs in series, with doppler and angle lockup occurring first in the CW mode. Range lockup is then accomplished by progressing through uncoded pulses, coarse coded pulses, medium coded pulses, to fine coded pulse operation.

The acquisition range has been calculated using the techniques of Marcum for CW systems as outlined in reference 20. Figure 11-6 gives the calculated detection range as a function of peak power for several radar antenna sizes. The parameters assumed are given in table 11-1.

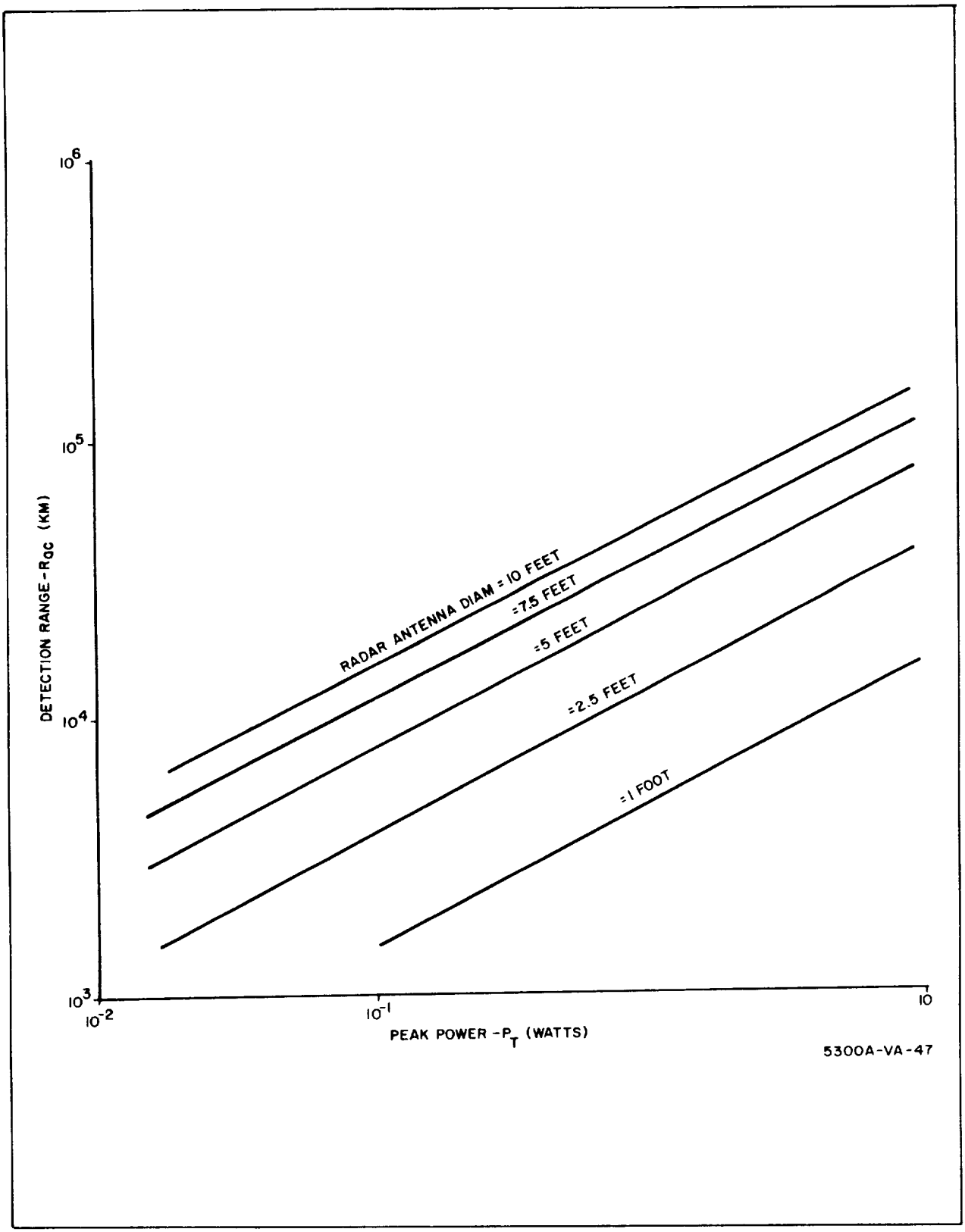

Figure 11-6. Radar Acquisition Range

TABLE 11-1

ASSUMED RADAR PARAMETERS

Operating frequency	X-band
Transponder antenna gain	3 db
Radar antenna efficiency factor	0.6
System temperature, T_o	290°K
Receiver noise figure	10 db
Receiver bandwidth	400 cps
System losses	4 db
False alarm number	10^8

From figure 11-6, it is seen that the peak powers required to achieve an acquisition range of about 2×10^4 kilometers will be in the approximate range of several hundred milliwatts to a watt or so, depending on the radar antenna size. For the terminal case where a range of 1000 km has been assumed, it is apparent that for the same level of power an antenna of the order of a foot should be adequate. A relatively small antenna is desirable for this phase, not only because of size and weight considerations but because the antenna must be capable of scanning; this will require some form of gimbal system if a parabolic type of antenna is used. The range of power levels expected for solid-state systems at X-band by 1970 may be such as to permit the use of an antenna small enough that it can track at the rates required for the terminal phase and also provide sufficient gain for the midcourse phase, should this be required.

11.4.4 Accuracy Considerations

Predictable bias errors arise from the dynamic response characteristics of the measuring equipment; while they may be fixed for a given equipment they can have a distribution over an ensemble of equipments. Random errors arise from several sources such as the measurement uncertainties caused by the basic limitations of the measuring device and system noise.

The total system error can be expressed as a function of the various error sources by the expression (reference 21)

$$\text{Total system error} = \Sigma \Delta X_i + \left[\Sigma (\sigma_{X_i})^2 \right]^{1/2} \qquad (11\text{-}11)$$

where

ΔX_i = summation of predictable bias errors

$\left[\Sigma(\sigma_{X_i})^2\right]^{1/2}$ = standard deviation of the total random error

11.4.4.1 Error Levels Calculated for the PNC Radar

11.4.4.1.1 Range - In the range tracking mechanization of the system described in reference 19 the three major sources of range error are:

a. Transponder delay variation

b. Quantization error

c. Error due to noise

Transponder delay, the delay between the reception of the signal by the transponder and the retransmission, is necessary to permit range measurements at very short ranges. This error is due to a slight variation in the basic oscillator frequency from which the delay is derived. Reference 19 gives an rms value for this error of 1.1 feet or 0.34 meter. The only quantization error present is that in the radar digital range track loop reference 19. The magnitude of this error is calculated to be 1.89 feet (rms) or 0.58 meter (rms). The major contribution to the dynamic tracking error is the noise variation. This can be calculated from the expression (reference 22).

$$\sigma^2 = \frac{\tau^2}{\frac{8 f_r}{2 f_s} \left(\frac{(S/N)^2}{1 + 2\, S/N} \right)} \qquad (11\text{-}12)$$

where

σ = rms range track jitter due to noise

τ = pulsewidth (bit width in coded case)

f_r = pulse repetition frequency

f_s = range track servo bandwidth

Before this quantity can be calculated several system parameters must be determined.

The pulse repetition frequency, f_r, will be determined by the maximum unambiguous range required. For a range of 2×10^4 kilometers the required PRF is about 7 pps. Assuming range gate dither at $f_r/2$ this becomes 14 cps. Assuming a duty cycle of 20 percent the required pulsewidth is 14.3 milliseconds. If a 2047 bit code (11 stage shift register) is assumed the bit width is

$$\tau_b = \frac{\tau}{N} = \frac{1.43 \times 10^{-2}}{2047} = 6.97\ \mu\text{sec}$$

and the clock frequency is

$$f_c = \frac{1}{\tau_b} = 143.5\ \text{kc}$$

The signal-to-noise ratio can be determined using the equation

$$\frac{S}{N} = \frac{P_T G_B D_v^2 f}{16 R^2 K T \Delta f L \overline{NF}} \qquad (11\text{-}13)$$

where the various quantities have been defined previously.

The system parameters assumed are listed in table 11-1 plus a range track servo bandwidth of 1 cps, a pulsewidth of 6.97 microseconds, and a PRF of 7 sec^{-1}. Figure 11-7 illustrates the variation of the rms two-way tracking error σ as a function of signal-to-noise ratio. Figure 11-8 illustrates the signal-to-noise rate as a function of peak power at a range of 2×10^4 kilometers and for several radar antenna diameters. It was stated previously that the desired range accuracy is about 1 kilometer. If this is taken as the 3σ value it is seen from figure 11-7 that this requires a S/N of about 10 db. Referring then to figure 11-8, it is seen that a S/N of 10 db would require a peak power of several hundred milliwatts up to a watt or more depending on

the antenna size. However, experience has shown in general that a S/N of perhaps as much as 15 db would be desirable. Thus, the power requirement would range from slightly less than a watt to several watts.

Figure 11-9 gives the S/N at a range of 1000 kilometers as a function of peak power for several radar antenna diameters. A comparison of this figure with figure 11-8 indicates that for the same conditions the range error will be much smaller at the shorter range. For example, assuming an antenna diameter of 5 feet and a peak power of 1 watt, the dynamic range error is approximately 10 meters (rms) at 1000 km or 0.001 percent. As range decreases, the dynamic error decreases and the total range error approaches 0.67 meter (rms).

11.4.4.1.2 Range Rate - The velocity track loop as described in reference 19 is a type II servo loop with a loop noise bandwidth of 400 cps in order to match the range channel filter and eliminate the need for filter switching when transferring from CW to the pulse mode of operation. It will produce a zero error in its output for a constant velocity input and has a constant error for a constant acceleration input. The range rate measurement accuracy quoted in reference 19 for the PNC radar is 1 percent or 1 foot/sec; these values will be assumed here.

11.5 SYSTEM DESIGN CONSIDERATIONS

This paragraph considers the antenna size necessary to achieve the specified range and range accuracy in terms of expected future power capabilities and size and weight limitations.

11.5.1 Solid-State Power Capabilities

The current approximate peak power output capability of solid-state frequency multipliers and amplifiers is shown by the solid curve of figure 11-10. It is estimated that in the next few years multipliers and amplifiers can be developed which are capable of peak power outputs of 1 to 2 watts in the X-band frequency region; this estimate is reflected by the dashed curve of figure 11-10.

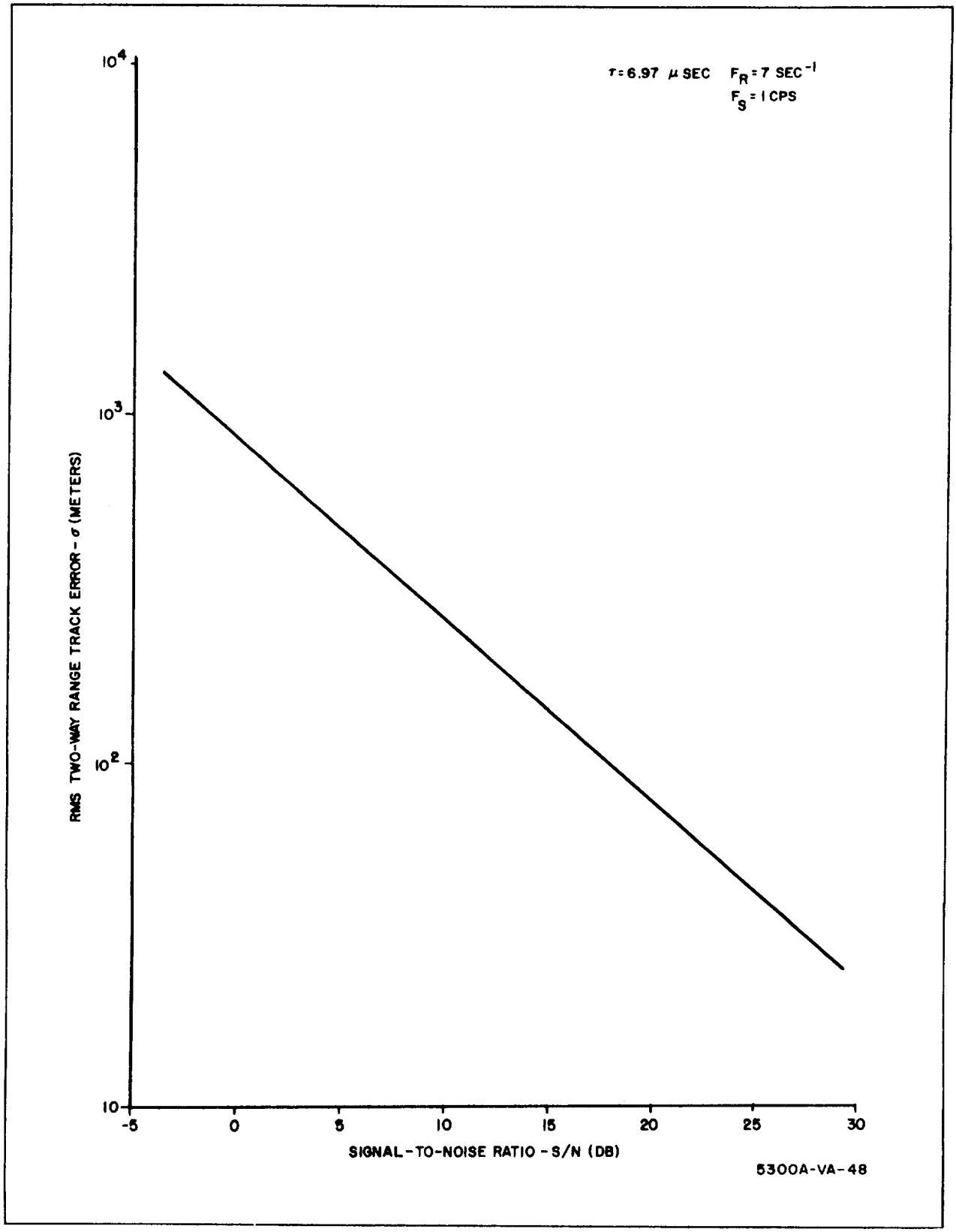

Figure 11-7. Range Track Error Versus Signal-to-Noise Ratio

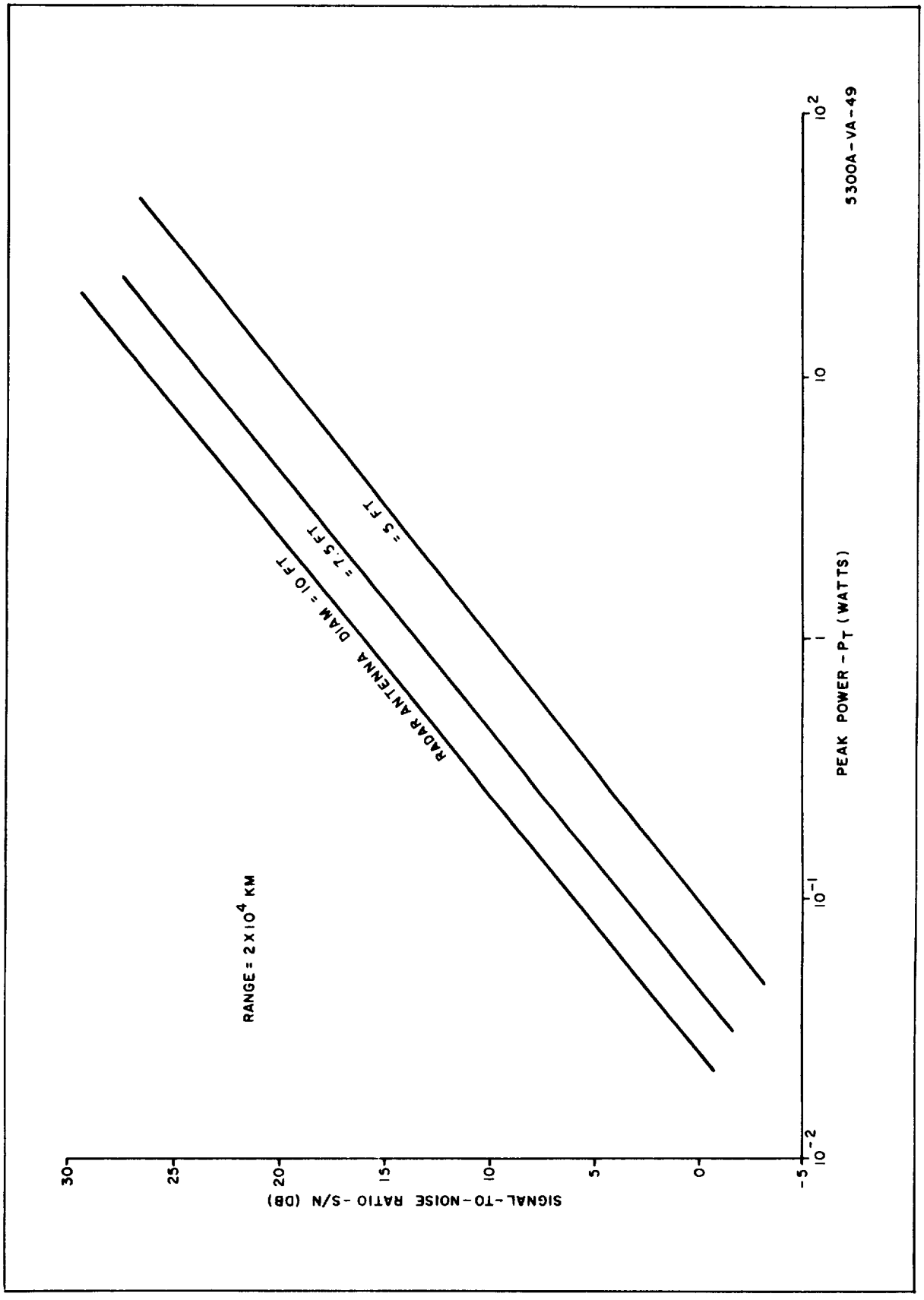

Figure 11-8. Signal-to-Noise Ratio Versus Peak Power

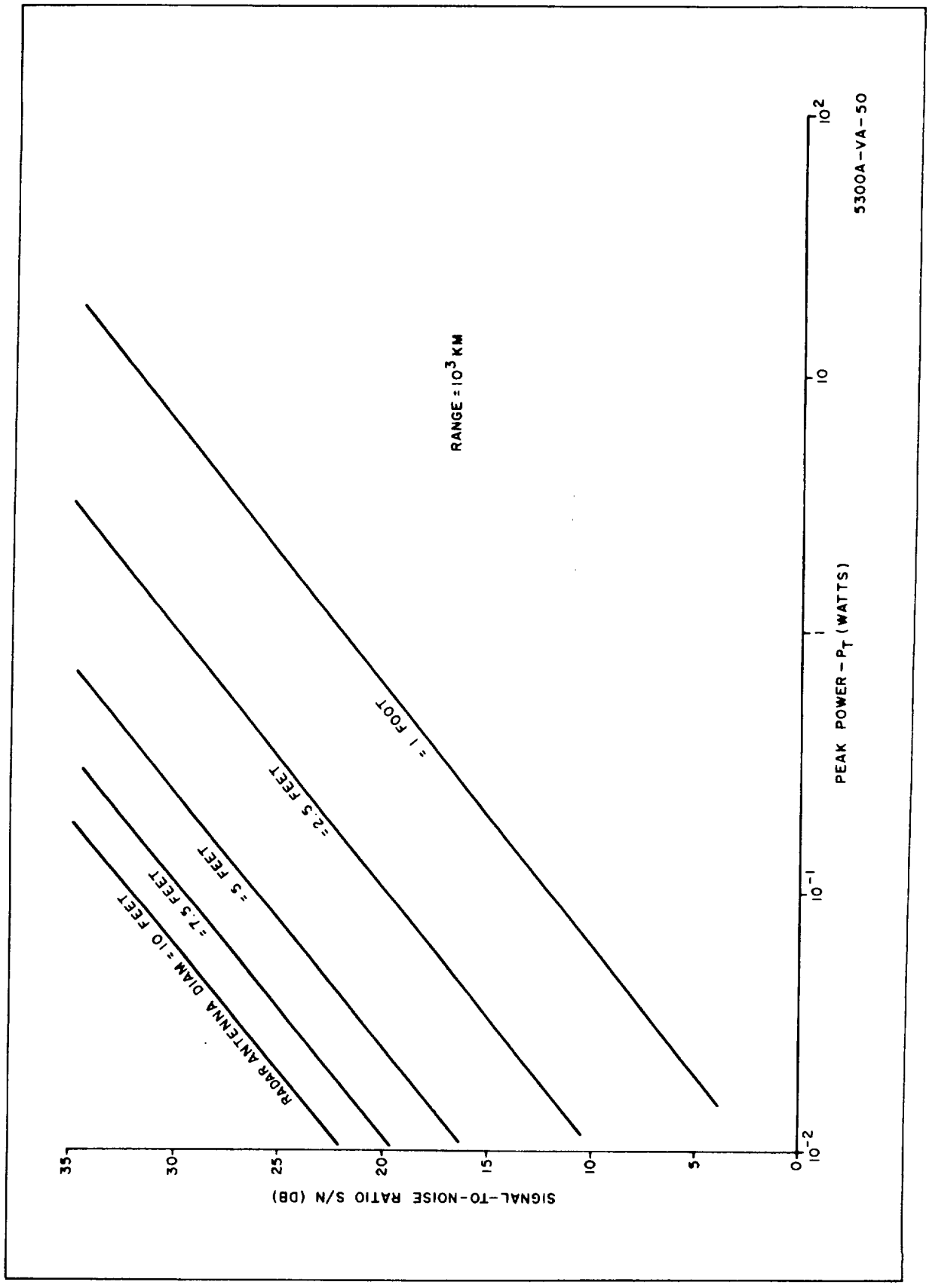

Figure 11-9. Signal-to-Noise Ratio Versus Peak Power

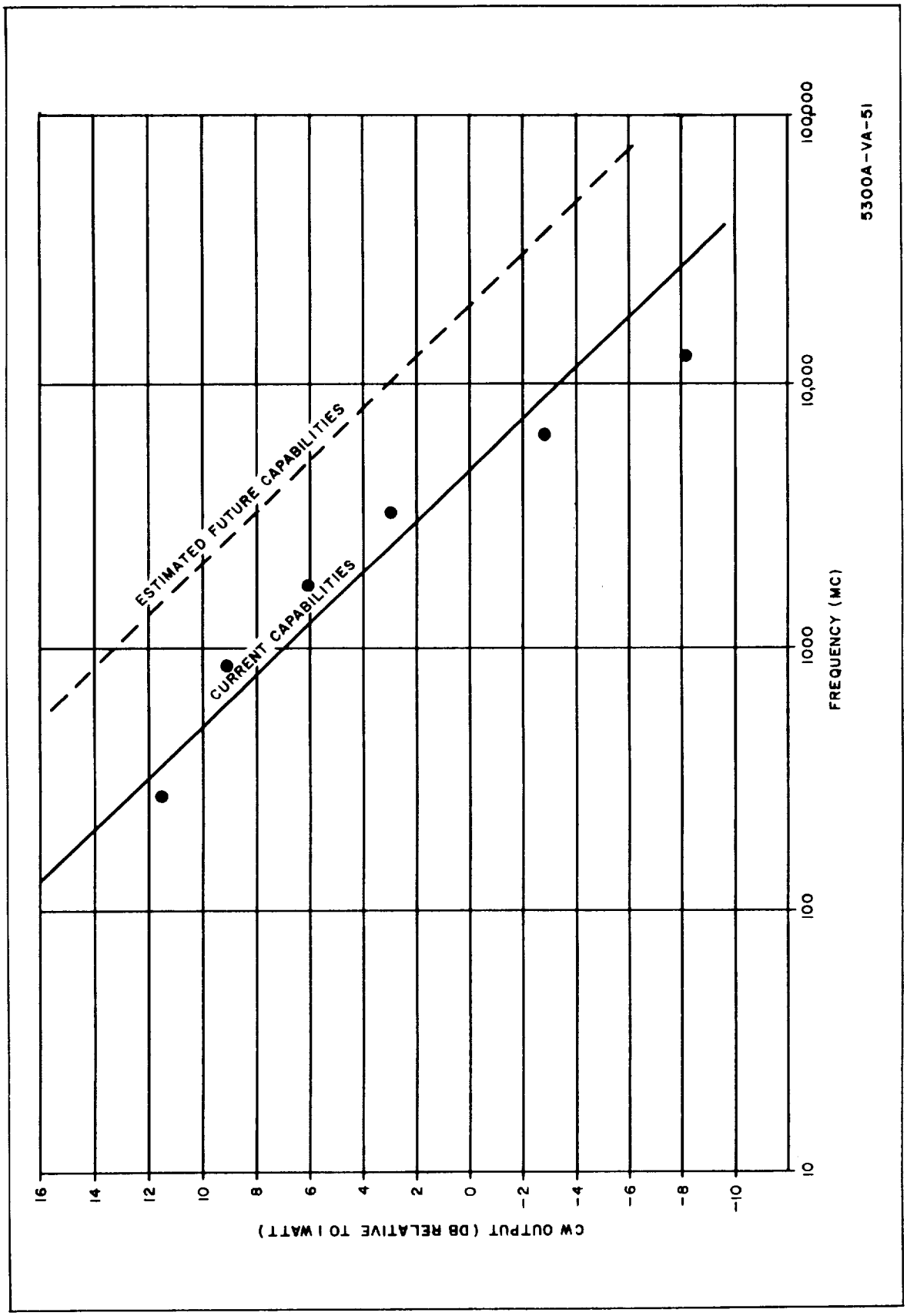

Figure 11-10. Current and Estimated Future Power Output Capabilities of Solid State Frequency Multipliers and Amplifiers

11.5.2 Antenna Size Requirements*

Examination of the curves of figure 11-6 indicates that for a peak power level of 2 watts, an antenna diameter of 5 feet should be adequate to provide a detection range of 2×10^4 kilometers. Examination of figures 11-7 and 11-8 indicates that this power level and antenna size should be adequate also to provide a 3σ range accuracy somewhat better than 1 kilometer at a range of 2×10^4 kilometers.

11.5.3 Power System Requirements

The overall power consumption given for the radar in reference 19 is 69 watts and for the transponder 32 watts for a peak power output of 100 mw. For the increased power output of 2 watts the power consumption for the radar will be estimated as 80 watts and for the transponder 43 watts.

The overall power plant weight required to supply the above power requirements will depend upon the type of power system selected. The selection of the power source in turn will also depend upon the considerations of reliability, length of mission, and specific mass or weight per kilowatt produced. Figure 11-11 illustrates the power capabilities of various chemical power systems in terms of specific mass plotted against duration (reference 23). All chemical systems become prohibitively heavy when durations exceed a few weeks. Figure 11-12, also from reference 23, compares solar and nuclear-energy power systems on the basis of specific mass plotted against electric power level. These systems, in contrast to the chemical systems, find application whenever mission duration exceeds a month. In the power range up to a few kilowatts the competing power plants include solar cells, solar collectors with thermionic converters, radioisotope power cells with either thermoelectric or therionic converters, and nuclear reactor thermoelectric systems. The solar systems basically weigh less than 200 lb/kw. However, because of varying periods of darkness or peak power demands,

*The use of a single antenna with hemispherical coverage is assumed here for the transponder.

which depend on the mission, either thermal-storage provisions or supplemental battery power must be charged to the overall system weight. These systems masses then vary over the rather broad range from about 200 lb/kw to over 1000 lb/kw. Variation of the other system types is evident from the figure.

The Westinghouse Astronuclear Laboratory currently is developing an isotopic thermoelectric power source. This source is described in a proposal for a feasibility study and design of an integrated power unit for lunar applications recently submitted to NASA Manned Spacecraft Center (reference 24). The source, which is in the form of a cylinder with three equally spaced fins, has the following characteristics:

Power Output	50 watts at 28 volts
Weight	22.7 lb (2.2 w/lb)
Cylinder dimensions	
Diameter	2.55 inches
Length	12 inches
Overall diameter (including fins)	10 inches
Fin Length	11.5 inches

This device is expected to have a degradation of 5 percent or less in power output after 4000 hours of operation. It is seen that the output capability of the isotopic thermoelectric power source described is sufficient to supply the estimated power requirement of 43 watts for the transponder. The power requirements for the radar would presumably be supplied from the overall vehicle power supply. Therefore, size and weight estimates for the radar power source will not be considered here.

11.5.4 System Weight and Size Estimates

Weight estimates given in reference 19 indicate a weight of 23 pounds for the radar minus the antenna and 18 pounds for the transponder minus the antenna. This estimate is based upon a peak power of 100 milliwatts. For a

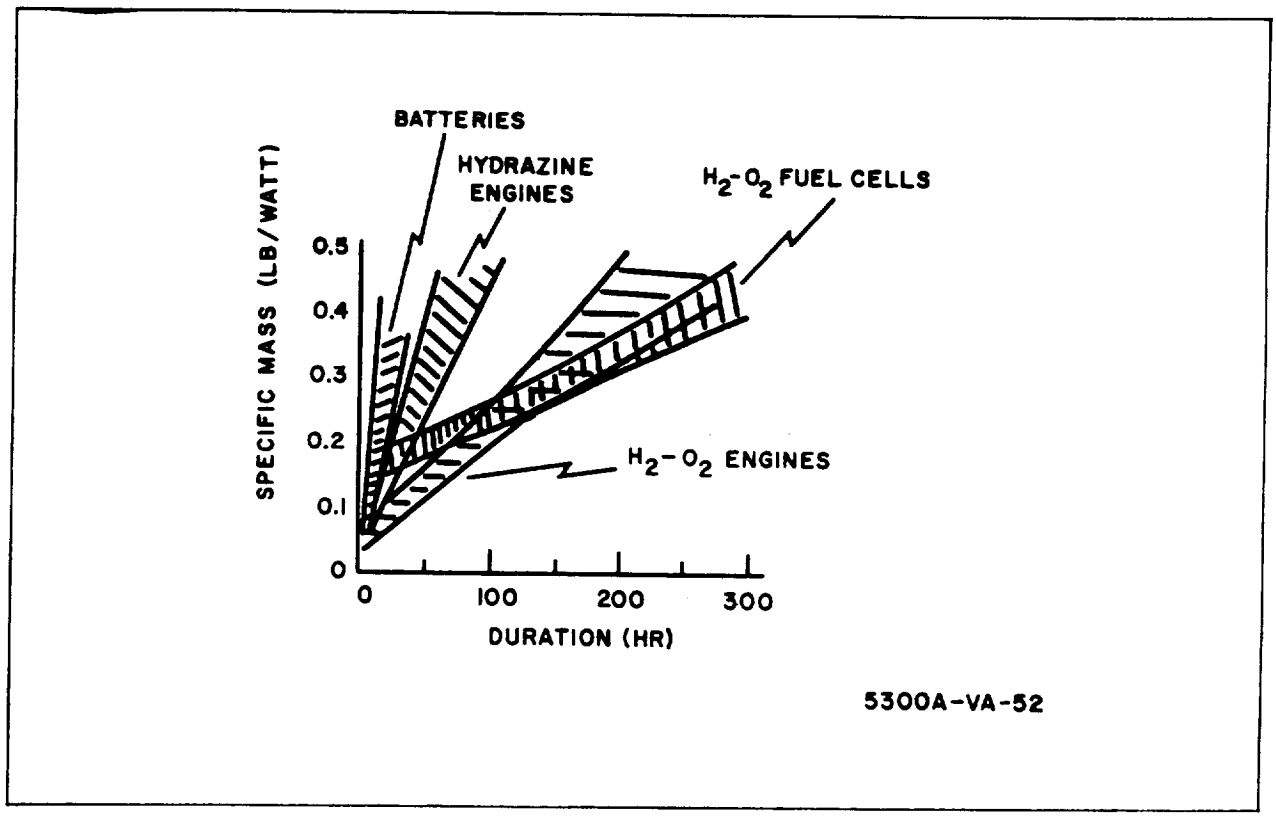

Figure 11-11. Chemical Power System Mass

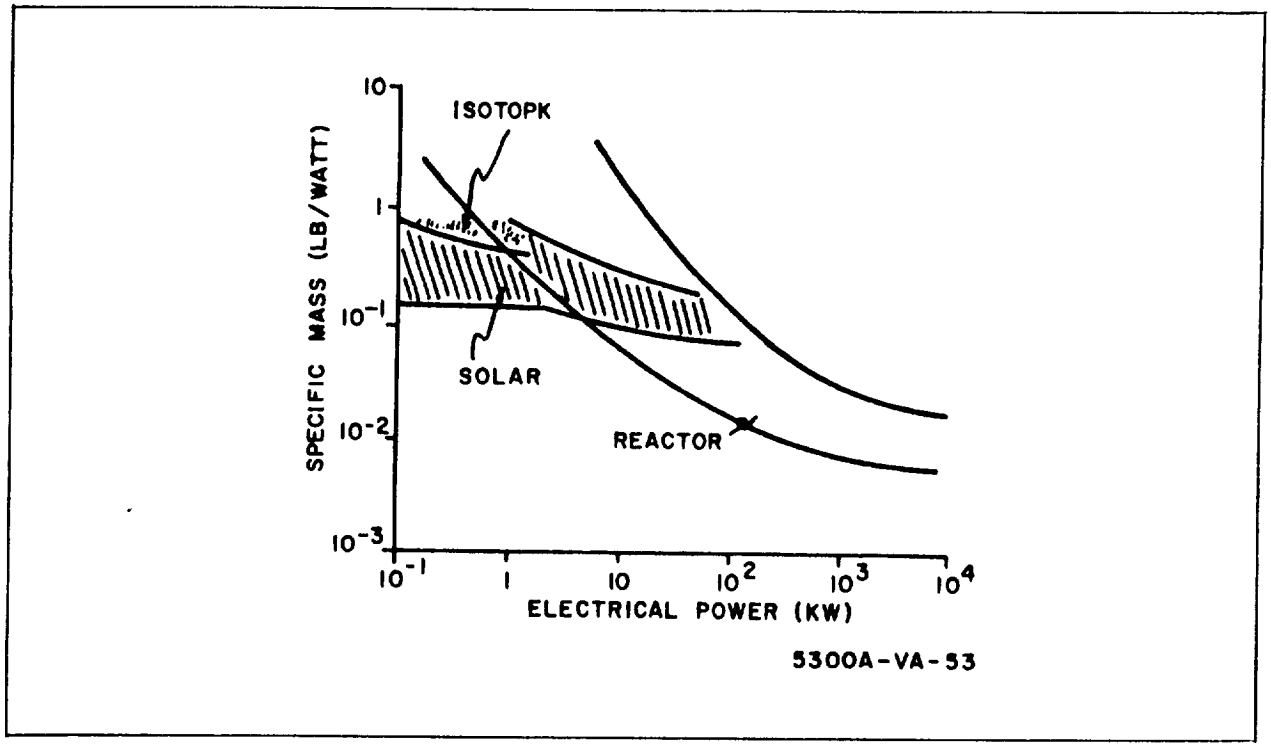

Figure 11-12. Solar and Nuclear Power System Mass

power output of approximately 2 watts, the system weight for the radar and transponder will be increased somewhat due primarily to the multiplier-amplifier and the power supply. Weights of 30 and 25 pounds will be estimated for the radar and transponder respectively. Including an isotopic power source with an estimated weight of approximately 23 pounds and a conical spiral antenna with an estimated weight of approximately 2 pounds, the total system weight for the transponder should be about 50 pounds. Estimating a weight of approximately 50 pounds for the radar antenna (this assumes a solid-structure 5-foot antenna capable of scanning through an angle of ±60 degrees) the radar system weight, excluding the power source, should be approximately 80 pounds.

Volume estimates for the radar and transponder given in reference 19 are 524 cubic inches for the radar minus the antenna and 428 cubic inches for the transponder minus the antenna. For the transponder with the increased power output a total system volume of approximately 565 cubic inches is estimated; this includes an estimate of 500 cubic inches for the transponder, 61 cubic inches for the isotopic power source, excluding the cooling fins, and 3 cubic inches for the antenna. A volume of 600 cubic inches is estimated for the radar, excluding the antenna and power source.

12. GYROCOMPASSING ANALYSIS APPENDIX

This section presents an analysis of a gyrocompass heading reference for the Lunar Landing Vehicle (LLV) in orbit. In practice, the vehicle's heading relative to the orbit plane can be measured by a body-mounted rate gyro whose input axis is nominally in the plane of the orbit. This sensor, however, is additionally sensitive to attitude motion of the vehicle about its input axis. Thus, the heading indication is dynamically inexact.

The desired property of dynamic exactness can be obtained by using a fully gimbaled platform in the gyrocompassing mode. To make this mode possible, the vector orbital rate must be imparted to the platform. This rate is obtained by tracking the lunar local vertical as measured by a horizon scanner.

12.1 ALIGNMENT GEOMETRY AND DYNAMICS

The objective of the gyrocompassing mode is to align the platform coordinates to the reference triad shown in figure 12-1. Reference coordinates are defined by the true, local vertical, and the vector orbital rate. Since gyrocompassing alignment time will be measured in minutes, the time of response of each platform servo can be neglected in this study of alignment dynamics. Thus, the platform axes (X_p, Y_p and Z_p) are always exactly aligned with the input axes of the gyros.

The dynamic relations of interest during alignment are the torque balances on the output axis of each gyro. These consist of a gyroscopic torque, an uncertainty torque, and a control torque.

The gyroscopic torque is $\underline{H} \times \underline{\Omega}_T$, in which $\underline{H}$ is the spin angular momentum of the gyro, and $\underline{\Omega}_T$ is the angular velocity of the platform in inertial space. Assuming an X, Y, Z sequence, the three components of this angular rate are defined by an Euler transformation.

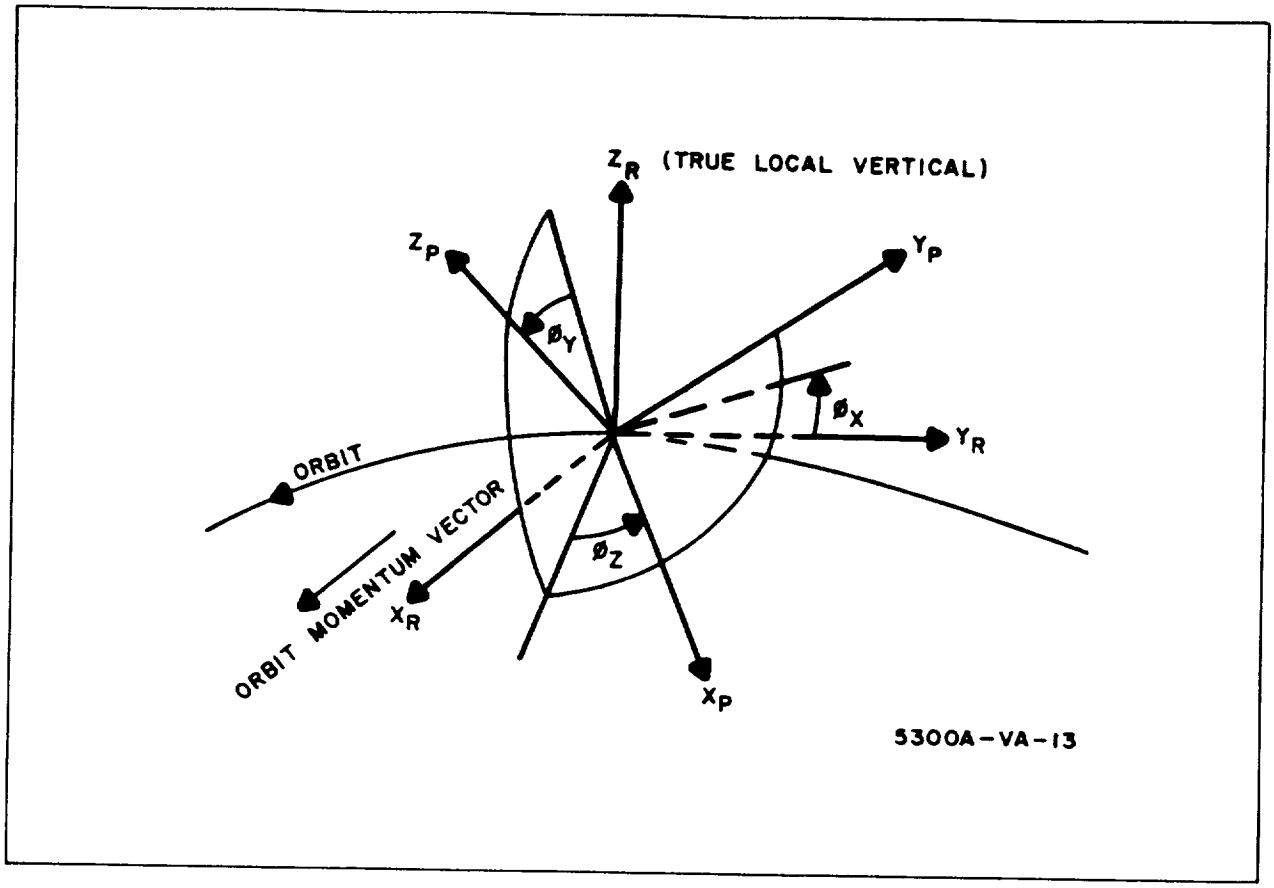

Figure 12-1. Alignment Geometry

$$\begin{bmatrix} \dot{\phi}_{X_T} \\ \dot{\phi}_{Y_T} \\ \dot{\phi}_{Z_T} \end{bmatrix} = \begin{bmatrix} \phi_Z \end{bmatrix} \begin{bmatrix} \phi_Y \end{bmatrix} \begin{bmatrix} \Omega_o + \dot{\phi}_X \\ 0 \\ 0 \end{bmatrix} + \begin{bmatrix} \phi_Z \end{bmatrix} \begin{bmatrix} 0 \\ \dot{\phi}_Y \\ 0 \end{bmatrix} + \begin{bmatrix} I \end{bmatrix} \begin{bmatrix} 0 \\ 0 \\ \dot{\phi}_Z \end{bmatrix} \quad (12\text{-}1)$$

where Ω_o is the orbital rate and ϕ_X, ϕ_Y, and ϕ_Z are Euler angles representing alignment errors. For small angle deflections, the rotation matrices are:

$$\begin{bmatrix} \phi_Z \end{bmatrix} = \begin{bmatrix} 1 & \phi_Z & 0 \\ -\phi_Z & 1 & 0 \\ 0 & 0 & 1 \end{bmatrix} ; \quad \begin{bmatrix} \phi_Y \end{bmatrix} = \begin{bmatrix} 1 & 0 & -\phi_Y \\ 0 & 1 & 0 \\ \phi_Y & 0 & 1 \end{bmatrix} \quad (12\text{-}2)$$

Substituting these matrices into equation 12-1 yields the three components of $\underline{\Omega}_T$.

$$\dot{\phi}_{X_T} = \Omega_o + \dot{\phi}_X + \phi_Z \dot{\phi}_Y \tag{12-3}$$

$$\dot{\phi}_{Y_T} = -\phi_Z \Omega_o + \dot{\phi}_Y - \phi_Z \dot{\phi}_X \tag{12-4}$$

$$\dot{\phi}_{Z_T} = \phi_Y \Omega_o + \dot{\phi}_Z + \phi_Y \dot{\phi}_X \tag{12-5}$$

Since the term $\phi_Z \dot{\phi}_Y$ in equation 12-3 is negligible, alignment about the X_p axis is almost independent of alignment about Y_p and Z_p. Furthermore, alignment about X_p involves seeking the vertical only (no gyrocompassing) and can be accomplished very rapidly. It is therefore reasonable to assume that $\dot{\phi}_X = 0$ during the gyrocompassing mode. By these assumptions, the components of $\underline{\Omega}_T$ are

$$\dot{\phi}_{X_T} = \Omega_o \tag{12-6}$$

$$\dot{\phi}_{Y_T} = -\phi_Z \Omega_o + \dot{\phi}_Y \tag{12-7}$$

$$\dot{\phi}_{Z_T} = \phi_Y \Omega_o + \dot{\phi}_Z \tag{12-8}$$

The torque balances on the output axes of the gyros can now be determined.

$$H(\dot{\phi}_Y - \phi_Z \Omega_o) = T_Y + D_Y \tag{12-9}$$

$$H(\dot{\phi}_Z + \phi_Y \Omega_o) = T_Z + D_Z \tag{12-10}$$

where T_Y and T_Z are control torques; D_Y and D_Z are uncertainty torques. Dividing these equations by the spin angular momentum yields

$$\dot{\phi}_Y - \phi_Z \Omega_o = \Omega_Y + \delta_Y \tag{12-11}$$

$$\dot{\phi}_Z + \phi_Y \Omega_o = \Omega_Z + \delta_Z \tag{12-12}$$

where Ω_Y and Ω_Z are controlled rates, δ_Y and δ_Z are gyro drift rates. Equations 12-11 and 12-12 represent the alignment dynamics of an inertial platform in the gyrocompassing mode.

12.2 SYSTEM CONFIGURATION

12.2.1 Absolute Stability

The alignment errors ϕ_Y and ϕ_X are detected by a horizon scanner whose axes are assumed to be coincident with $X_p - Y_p - Z_p$ (i.e., a fully gimbaled configuration is assumed). Since the Y_p gyro senses a rate proportional to the heading error, it is reasonable to use the vertical error as an indication of heading error. Thus, the stiffness of the gyrocompass loop is provided by

$$\Omega_Z = - K_Z (\phi_Y + \epsilon_y) \tag{12-13}$$

where

K_Z is a constant gain

ϵ_y is the noise output of the horizon scanner

Such a loop is undamped, however, and will not settle. Due to the noise content of horizon scanner measurements, rate damping is not feasible. For this reason proportional damping is used in the form:

$$\Omega_Y = - K_y (\phi_Y + \epsilon_y) \tag{12-14}$$

where K_y is a constant gain.

Substituting these control relations into equations 12-11 and 12-12 yields:

$$\dot{\phi}_Y - \phi_Z \Omega_o = - K_y (\phi_Y + \epsilon_y) + \delta_y \tag{12-15}$$

$$\dot{\phi}_Z + \phi_Y \Omega_o = - K_Z (\phi_Y + \epsilon_y) + \delta_Z \tag{12-16}$$

Since the vehicle is in a near circular orbit during gyrocompass alignment, the orbital rate is treated as a constant in the analysis.* By this assumption, the dynamic equations can be separated and expressed in Laplace notation.

$$\phi_Z(s) = \frac{(s + K_y)\left[(\phi_{Z_o} + \delta_Z(s)\right] - (K_Z + \Omega_o)\left[(\phi_{Y_o} + \delta_y(s)\right] - (K_Z s - K_y \Omega_o)\epsilon_y(s)}{s(s + K_y) + \Omega_o (K_Z + \Omega_o)} \tag{12-17}$$

$$\phi_Y(s) = \frac{S\left[\phi_{Y_o} + \delta_y(s)\right] + \Omega_o\left[(\phi_{Z_o} + \delta_Z(s)\right] - (K_y s + K_Z \Omega_o)\epsilon_y(s)}{s(s + K_y) + \Omega_o (K_Z + \Omega_o)} \tag{12-18}$$

where ϕ_{Z_o} and ϕ_{Y_o} are impulses representing initial alignment errors.

A mathematical model of the gyrocompass loop derived from these equations is shown in figure 12-2.

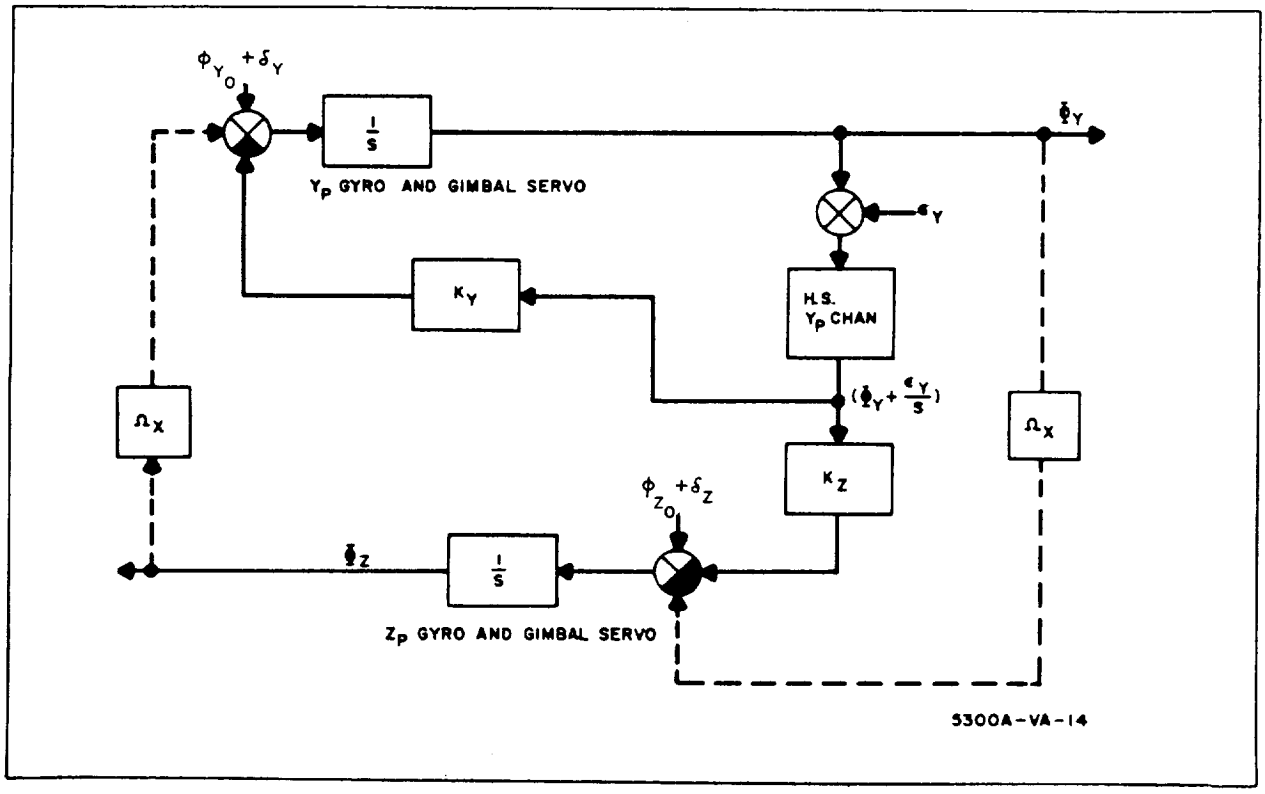

Figure 12-2. Mathematic Model of Gyrocompass Loop

* Dynamic perturbations such as those caused by lunar oblateness are negligible.

12.2.2 Relative Stability

It will be shown later that initial alignment errors are small enough to warrant treating the gyrocompass loop as settled in four time constants. Since the allowable settling time for the gyrocompass loop is 46 minutes, the maximum system time constant is*

$$\tau_{maximum} = 11.5 \text{ minutes} \tag{12-19}$$

From equations 12-17 and 12-18, the characteristic equation of the dynamic loop is:

$$s^2 + K_y s + \Omega_o (K_Z + \Omega_o) \tag{12-20}$$

So that

$$K_y = 2/\tau = 10.45 \frac{\text{radians}}{\text{hour}} \tag{12-21}$$

Selection of the system natural frequency was based on the frequency response of alignment errors to the vertical sensor error, ϵ_y.** It was found that system natural frequencies lower than orbital frequency tend to amplify low-frequency horizon scanner error inputs. Furthermore, natural frequencies considerably higher than orbital frequency extend the bandwidth response to these errors. To obtain good settling and well-behaved responses to a variety of input errors, the system natural frequency was set equal to 7.46 rad/hr. The resulting frequency responses of the alignment errors appear in figure 12-3. Note that this choice of natural frequency yields a near optimum damping factor of 0.7.

From equation 12-20, the relation of the loop gain, K_Z, to system natural frequency can be written as

$$K_Z = \frac{\omega_N^2}{\Omega_o} - \Omega_o \tag{12-22}$$

---

* After 46 minutes in orbit, the vehicle will execute a brief, powered maneuver.

** Horizon scanner error is the most significant component error.

where

ω_N is the system natural frequency

Since the nominal value of Ω_o is 2.99 rad/hr, equation 12-22 yields:

$$K_Z = 15.66 \text{ rad/hr} \tag{12-23}$$

With these system parameters specified, the dynamic responses of the alignment errors are completely defined by equations 12-17 and 12-18.

12.3 ERROR ANALYSIS

The mean-squared values of the alignment errors are related to their power spectral density functions by

$$\overline{\phi_Z^2} = \frac{1}{2\pi} \int_o^\infty \bar{P}_{\phi_Z}(f)\, d\omega \tag{12-24}$$

and

$$\overline{\phi_Y^2} = \frac{1}{2\pi} \int_o^\infty \bar{P}_{\phi_Y}(f)\, d\omega \tag{12-25}$$

where $\bar{P}_{\phi_Z}(f)$ and $\bar{P}_{\phi_Y}(f)$ are one-sided, power spectral density functions. The bar symbol represents an averaging process.

Using the system parameters selected in paragraph 12.2.2, the power spectral density functions of the alignment errors are approximately

$$\bar{P}_{\phi_Z}(f) \doteq \frac{\omega^2 + 109}{\omega^4 + 3100} \bar{P}_{\delta_Z}(f) + \frac{3475}{\omega^4 + 3100} \bar{P}_{\delta_Y}(f) + \frac{245(\omega^2 + 39.7)}{\omega^4 + 3100} \bar{P}_{\epsilon_y}(f)$$

and (12-26)

$$\bar{P}_{\phi_Y}(f) \doteq \frac{\omega^2}{\omega^4 + 3100} P'_{\delta_Y}(f) + \frac{8.9}{\omega^4 + 3100} \bar{P}_{\delta_Z}(f) + \frac{109(\omega^2 + 20)}{\omega^4 + 3100} \bar{P}_{\epsilon_y}(f)$$

(12-27)

where

$\bar{P}_{\delta_Z}(f)$ is a one-sided power spectral density function of the drift rate for the Z_p gyro

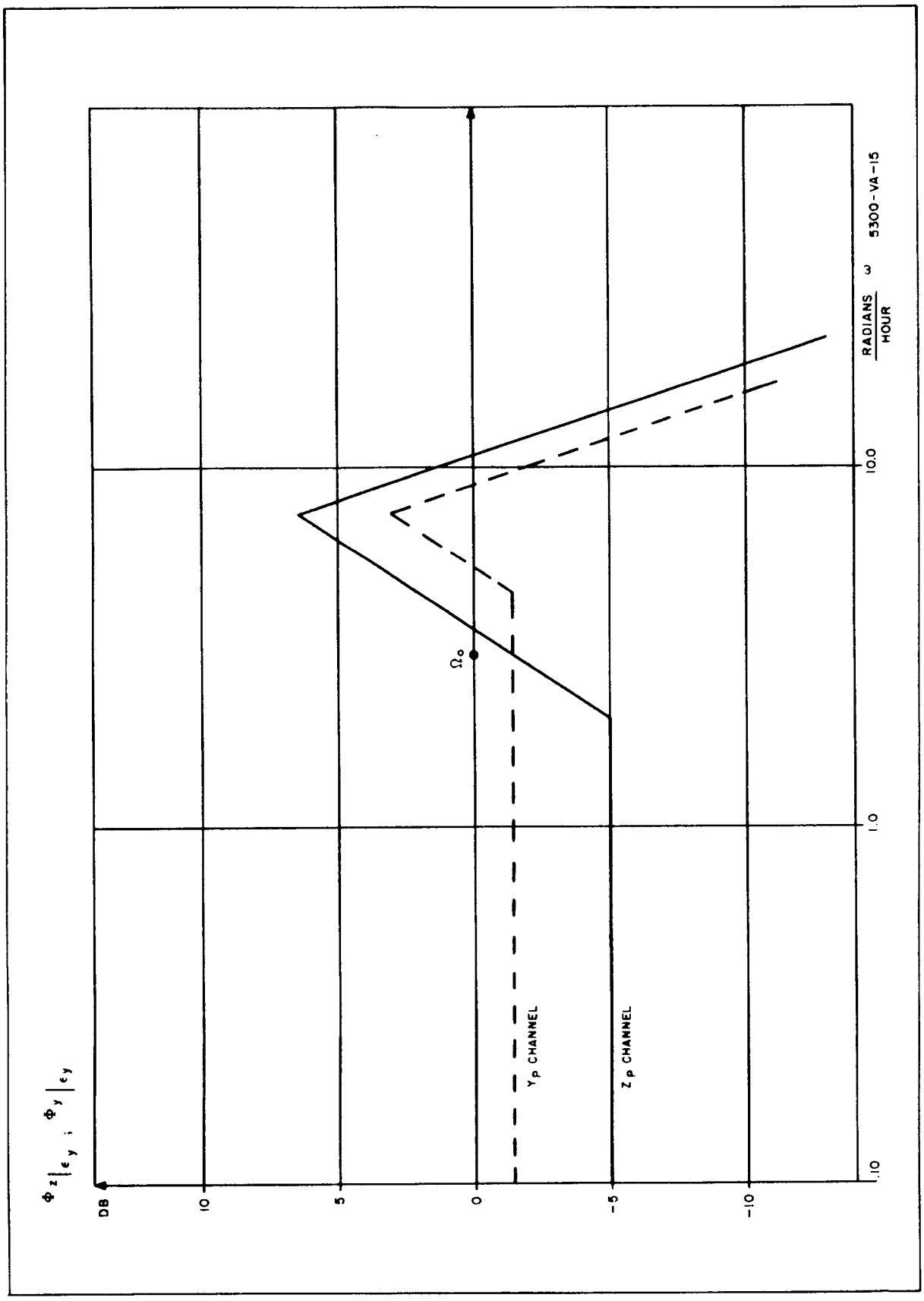

Figure 12-3. Frequency Responses of Alignment Errors to Vertical Sensor Error

$\bar{P}_{\delta_Y}(f)$ is a one-sided power spectral density function of the drift rate for the Y_p gyro

$\bar{P}_{\epsilon_y}(f)$ is a one-sided power spectral density function of the angular error in the horizon scanner measurements

$\bar{P}'_{\delta_y}(f)$ is a one-sided power spectral density function of the random drift rate for the Y_p gyro.

In this analysis, the power spectral density functions of the gyros are assumed to be equal and approximately representable by ***

$$\bar{P}_{\delta_Z}(f) = \bar{P}_{\delta_y}(f) \doteq 4\pi B^2 \delta(\omega) + \frac{4C^2 T_g}{1 + \omega^2 T_g^2} \quad \omega \geq 0 \qquad (12\text{-}28)$$

where

B is the rms value of the bias drift rate

C is the rms value of the random drift rate

T_g is the correlation time. In this analysis, its value is 2 hours

$\delta(\omega)$ is the dirac delta function

The power spectral density function of the angular error in the horizon scanner measurements is representable as:

$$\bar{P}_{\epsilon_y}(f) = 4\pi \epsilon_B^2 \delta(\omega) + \epsilon_R^2 \qquad (12\text{-}29)$$

where

ϵ_B is the rms value of the bias error in the measurement

ϵ_R^2 is the amplitude of the power spectral density function of the random angular error.

Using these power spectral density functions, the mean-squared values of the alignment errors are:

*** Reference 6

$$\overline{\phi_Z^2} = \left[0.148\,B^2 + 0.312\,\epsilon_B^2\right] + \left[0.16\,C^2 + 3.43\,\epsilon_R^2\right] \qquad (12\text{-}30)$$

$$\overline{\phi_Y^2} = \left[0.003\,B^2 + 0.703\,\epsilon_B^2\right] + \left[0.004\,C^2 + 14.95\,\epsilon_R^2\right] \qquad (12\text{-}31)$$

It can also be shown that the alignment error about X_p is approximately:

$$\overline{\phi_X^2} \doteq \overline{\mu_X^2} \qquad (12\text{-}32)$$

where

$\overline{\mu_X^2}$ is the mean-squared value of the random portion of the horizon scanner error.

For typical sensor accuracies, the largest contributor to the alignment errors is the random error in the horizon scanner measurements.

12.4 ALIGNMENT REQUIREMENTS

As indicated in paragraph 12.2.2, the vehicle will execute a brief powered maneuver (descent kick) after 46 minutes in the circular parking orbit. This maneuver, which is nominally planar, places the vehicle at aposelenum of a descent ellipse with eccentricity of 0.082. The elliptical trajectory is followed in a coasting mode until initiation of the main braking phase, some 15 minutes after aposelenum. The main braking maneuver then places the vehicle on the lunar surface in the vicinity of the target beacon, which lies in the Kepler-Copernicus-Lansberg triangle.

The most stringent alignment requirements occur at the start of the main braking phase rather than the descent kick. At this time, the reference triad will be used to establish both the vehicle's heading relative to the target beacon and a beacon, local-vertical triad. From analyses of the main braking phase, the allowable values (rms) of the alignment errors are

$$\phi_Z \leqq 0.065^\circ \text{ (rms)} \qquad (12\text{-}33)$$

$$\phi_Y \leqq 0.01^\circ \text{ (rms)} \qquad (12\text{-}34)$$

$$\phi_X \leqq 0.1^\circ \text{ (rms)} \qquad (12\text{-}35)$$

It is appropriate at this point to note that the orbital rate is a slowly varying function of time along the descent ellipse. Furthermore, the net change in magnitude is very small. Thus, equations 12-30, 12-31 and 12-32 are still valid at the start of main braking.

12.5 NUMERICAL RESULTS

To evaluate the performance of the gyrocompass heading reference at the start of main braking, three different sets of component errors were considered. In case A, state-of-the-art component errors were assumed. Cases B and C represent degraded sensor performance. The numerical values are listed in table 12-1.

TABLE 12-1

RANGE OF COMPONENT ERRORS CONSIDERED FOR GYROCOMPASS LOOP (RMS)

Case A	Case B	Case C
$B = 0.18\ (10^{-3})$ rad/hr	$B = 1.8\ (10^{-3})$ rad/hr	$B = 0.18\ (10^{-3})$ rad/hr
$C = 0.18\ (10^{-3})$ rad/hr	$C = 1.8\ (10^{-3})$ rad/hr	$C = 0.18\ (10^{-3})$ rad/hr
$\epsilon_B = 0.36\ (10^{-3})$ radians	$\epsilon_B = 0.36\ (10^{-3})$ radians	$\epsilon_B = 1.8\ (10^{-3})$ radians
$\epsilon_R^2 = 5.4\ (10^{-8})\ \frac{\text{radians}^2}{\text{cy/hr}}$	$\epsilon_R^2 = 5.4\ (10^{-8})\ \frac{\text{radians}^2}{\text{cy/hr}}$	$\epsilon_R^2 = 5.4\ (10^{-8})\ \frac{\text{radians}^2}{\text{cy/hr}}$

In all cases, the root-mean-square value of the random error in the horizon scanner measurements was equal to 0.1 degree. This is the maximum allowable value as determined by equations 12-32 and 12-35. Substituting the component errors tabulated above into equations 12-30, 12-31, and 12-32 yields the alignment errors (rms) listed in table 12-2.

TABLE 12-2

ERROR BUDGET FOR GYROCOMPASS HEADING REFERENCE (RMS)

Case A	Case B	Case C
$\phi_X = 0.1^\circ$	$\phi_X = 0.1^\circ$	$\phi_X = 0.1^\circ$
$\phi_Y = 0.053^\circ$	$\phi_Y = 0.053^\circ$	$\phi_Y = 0.1^\circ$
$\phi_Z = 0.027^\circ$	$\phi_Z = 0.062^\circ$	$\phi_Z = 0.061^\circ$

The prime conclusions drawn from this error budget are:

- Alignment to the lunar local vertical is essentially independent of the quality of the gyros.* Furthermore, the verticality requirement can be met when the horizon scanner instrument error (bias) is degraded by an order of magnitude.
- Alignment to the orbit plane is highly dependent on the quality of both the gyros and horizon scanner. With high quality components, the desired heading accuracy is easily achieved; however, degradation of either sensor by an order of magnitude yields marginal performance.

The final choice of the sensor accuracies depends on the overall mission requirements and mechanization considerations, which are not discussed here.

12.6 HEADING REFERENCE DURING MIDCOURSE APPROACH

The vehicle approaches the moon along an approximately hyperbolic trajectory. Near the point of periselenum, the engines are activated to inject the vehicle into a retrograde, circular orbit as described in paragraph 2.1.2. During this maneuver, it is desired that the inertial platform be aligned to the reference triad defined in paragraph 12.1. In order to satisfy the overall mission requirements, the alignment errors in vertical and heading should not exceed 0.1 degree (rms). This section demonstrates the need for gyrocompassing to achieve these alignment accuracies.

---

* The gyro errors B and C are negligible until increased beyond 0.1 degree/hour.

If gyrocompassing techniques are not employed, the platform must be aligned to the orbit plane as defined by the vehicle's velocity vector and the lunar local vertical (measured). Assuming perfect knowledge of the velocity vector, the error in alignment to the approach plane normal is approximately:

$$\phi \doteq \frac{1}{\sin\theta}\ \gamma \qquad (12\text{-}36)$$

where

γ is the rms alignment error to the measured, lunar local vertical

θ is the angular separation between the velocity vector and the lunar local vertical

In this analysis, the value of γ is assumed to be 0.1 degree (rms). Unless θ equals 90 degrees, then the value of ϕ exceeds its allowable value. In actual practice, alignment must begin approximately 1 hour prior to injection. At this time, however, the value of ϕ is approximately three times its allowable value.

To avoid this alignment problem, the inertial platform can be placed in a gyrocompassing mode approximately 1.0 hour prior to the start of retrothrust. The alignment errors at the start of retrothrust will be approximately the same as Case A in table 12-2, which are in the allowable region.*

* Since Ω_o is a rapidly varying function of time during approach, the dynamic error responses are no longer well defined by equations 12-17 and 12-18.

13. REFERENCES

1. "Lunar Logistic System", Volume II, "Vehicle Design Aspects", MTP-M-63-1; NASA, Marshall SFC, Huntsville, Ala.; March 15, 1963 (Confidential).

2. "Lunar Logistic System", Volume VI; "Tracking and Mission Control", MTP-M-63-1; NASA, Marshall Space Flight Center; March 15, 1963 (Confidential).

3. "Study of Lunar Guidance Techniques for Saturn V", 8662-6009-RC-001, Contract NAS8-2635, Space Tech Labs, Redondo Beach, California, December 6, 1963 (Confidential).

4. "Studies of Guidance Systems for Future Space Vehicles", Final Report, Martin Co., Baltimore, Md.; ER 13193; Contract No. NAS8-85410, November, 1963.

5. McCrone, C.R.; "Lunar Descent Guidance Studies"; Astrionics Research and Development Report No. 2; NASA TMX-53044; Marshall SFC, Huntsville, Ala.; May 1, 1964.

6. Gordon, Robert L., "An Orbital Gyrocompass Heading Reference for Satellite Vehicles", AIAA Paper No. 64-238, July 2, 1964.

7. Compilation Report for Advanced Spaceborne Detection, Tracking, and Navigation Systems Study and Analysis. NAS8-11205, Westinghouse Defense and Space Center, July, 1964.

8. G. L. Smith and E. V. Harper, "Midcourse Guidance Using Radar Tracking and Onboard Observation Data", NASA TN D-2238, April, 1964.

9. Cherry, George W., "A General, Explicit, Optimizing Guidance Law for Rocket-Propelled Spaceflight", AIAA Paper No. 64-638, August 26, 1964.

10. Laning, J. H. and Battin, R. H.; "Random Processes in Automatic Control"; McGraw-Hill Book Co., Inc.; New York; 1956.

11. Peterson, E.L.; "Statistical Analysis and Optimization of Systems"; John Wiley & Sons, Inc.; New York; 1961.

12. S. Pines, H. Wolf, D. Woolston and R. Squires; "Goddard Minimum Variance Orbit Determination Program"; GSFC Report No. X-640-62-191.

13. V. C. Clarke, Jr., "Constants and Related Data Used in Trajectory Calculations at the Jet Propulsion Laboratory"; Tech Report No. 32-273; JPL Pasadena, California; May 1, 1962.

14. Ridenour, L. N., Radar System Engineering, McGraw-Hill Book Co., 1947.

15. Rechtin, Eberhardt, Space Communications, Tech. Release No. 34-68, Jet Propulsion Laboratory, May 1, 1960.

16. The Electromagnetics of the Rocket Exhaust, Rept. GM-TM-0165-00397, Space Technology Laboratory, June 15, 1958, (Confidential).

17. Krassner, G.N. and Michaels, J.V., Introduction to Space Communication Systems, McGraw-Hill Book Co., 1964.

18. Skolnik, M.I., Introduction to Radar Systems, McGraw-Hill Book Co., 1962.

19. Gaheen, A.F., Jr. and Bragg, S.L., A Phase Coded Radar and Communication System Radar Development Tech. Memo #34, Westinghouse Electric Corporation, Aerospace Division, January 27, 1964.

20. Marcum, J.I., A Statistical Theory of Target Detection by Pulsed Radar, Rand Corporation, RM-754, April 25, 1952.

21. Povejsil, D.J., Raven, R.S. and Waterman, Peter; Airborne Radar, D. Van Nostrand Co., 1961.

22. Swerling, P., Some Factors Affecting the Performance of a Tracking Radar, Rand Corporation, RM-989-1, September 27, 1954.

23. Bernatowicz, D.T., Guentert, D.C., and Klann, J.L., Space Powerplant Needs and Selection, Astronautics and Aerospace Engineering, May 1963.

24. Proposal to MSC, NASA, Electrical Power Supply MSC 64-1349P, submitted by Westinghouse Electric Corporation, Astronuclear Laboratory, August 21, 1964.

REFERENCES NOT CITED

Cannon, Robert H., Jr.; "Alignment of Inertial Guidance Systems by Gyrocompassing--Linear Theory", Journal of Aerospace Sciences, pp. 885-895, November, 1961.

Fernandez, Manuel, Macombek, George R., Inertial Guidance Engineering, Prentice-Hall, Inc., Englewood Clitts, New Jersey, 1962.

"Advanced Spaceborne Detection, Tracking, and Navigation Systems Study and Analysis", Part II, Volume III, Analytical Solution, Westinghouse Electric Corporation, Performed Under Contract NASw-460, April, 1963.

Akridge, Charles M. and Harlin, Sam H., "Parametric Performance Analysis for Lunar Orbit Braking and Descent", G.C.M.S.F.C., NASA TN.D-2643, February, 1965.